Fire Island Inlet to Montauk Point

Final General Reevaluation Report

APPENDIX A1

BASELINE CONDITIONS: STORM SURGE MODELING AND STAGE FREQUENCY GENERATION

U.S. Army Corps of Engineers
New York District

February 2020
Updated April 2020

EXECUTIVE SUMMARY

The US Army Engineer District, New York (CENAN) is currently conducting a reformulation study of the shore protection and storm damage reduction project for the south shore of Long Island, New York. Exposure to Atlantic Ocean storms such as hurricanes and nor'easters subjects the project area to higher than normal water levels and wave heights. These storms generate higher water levels (storm stage), larger waves, and stronger currents. The further inshore these effects are projected, the greater the risk of damage to property, infrastructure, and natural resources. In order to determine the likelihood and size of a justified federal project to reduce the magnitude, frequency, and risk of these damages, engineering studies are being conducted to provide coastal processes analyses and design input. Numerical modeling of physical coastal processes, in support of these analyses and designs, has been undertaken for the full extent of the project area. Formulating a long-term solution to storm damage reduction will identify alternatives that optimize mainland and barrier beach benefits by reducing economic losses while preserving important human and ecological habitats.

The numerical modeling strategy for FIMP addresses a comprehensive list of physical processes (wind conditions, barometric pressure, astronomic tide, wave conditions, and morphologic response, and localized wind and wave setup) by merging hydrodynamic, wave, and sediment transport models. The result is a description of storm surge elevations throughout the project for input into the economic analyses, coastal engineering design, environmental studies, and final alternative selection.

The modeling method consisted of four (4) process models: 1) WAVAD (i.e., WISWAVE) was applied to determine extreme storm wave conditions; 2) ADCIRC simulated the ocean and nearshore, outside the surf zone, storm water levels; 3) SBEACH was used to estimate pre-inundation dune lowering; and 4) the Delft3D model suite was used to compute the bay water levels under storm conditions, taking into account the contribution of storm surge, waves, winds and the contribution of overwash and/or breaching.

Both hydrodynamic models, ADCIRC and Delft3D, underwent extensive calibration before the models were used to simulate historical storm events. The ADCIRC model was calibrated to match measured tidal water levels by simulating a 30-day record and comparing model output with measurements at four NOAA stations and one Long Island SHORE (LISHORE) station. To match measured tidal water levels in ADCIRC, the bottom friction values were adjusted within reasonable ranges. Ocean storm surge modeling with ADCIRC requires wind stress and barometric pressure for each node within the grid as well as tidal constituent forcing. Significant efforts were put forth to ensure that the wind and pressure inputs were the best available. In addition, research into the drag coefficient formulation for wind stress calculation led to changes from the default ADCIRC drag coefficients, which resulted in better water level comparisons to available measured data. To assess ADCIRC's calibration for storm surge due to wind and barometric pressure, 12 historical tropical and extratropical events were modeled, and the results were compared with NOAA measured hydrographs at four nearshore

locations: Sandy Hook, NJ; The Battery, NY; Montauk Fort Pond, NY; and Newport, RI. This rigorous calibration verified that ADCIRC reliably and accurately simulates both tide and storm surges over a regional domain that spans from New Jersey to Rhode Island.

As with the ocean tidal calibration, the Delft3D model was calibrated for bay tide by simulating a 30-day record and comparing model output with measurements at 13 measurement locations (6 in Great South Bay, 4 in Moriches Bay, and 3 in Shinnecock Bay). To match measured tidal water levels in Delft3D, the bottom friction values in this model were also adjusted within reasonable ranges. A February 2003 field investigation, including water level gages at six locations in Great South and Moriches Bays, provided reliable information for calibration of the Delft3D suite in the bays under storm conditions. The simulation water levels were compared with the measured water levels at the six bay locations and simulated results compare well with measured, showing that Delft3D performs well for this small winter storm.

Before proceeding with the simulation of the production run (final) set of storms under Baseline Conditions barrier island topography (LIDAR 2000), the Delft3D model skill was assessed by comparing model results with available high water marks (HWM) and overwash and breaching data for two of the most significant storms of record: the September 1938 Hurricane and the December 1992 Nor'easters. The intent of the test was specifically to qualitatively validate the ability of the model to reproduce observed overwash and breaching. Overall, the model simulations for these historic storms provide very realistic results, particularly when considering the uncertainty in the input hydrodynamic conditions and, more importantly, the pre-storm topography. The simulation results are particularly realistic in the case of the 1938 storm, for which more comprehensive topographic data in the vicinity of some of the damaged areas were available. The agreement between simulated peak water levels for both storms and the reported measurements can be considered excellent considering the uncertainty associated with this type of data.

Under With Project Conditions, the hydrodynamics of the inlets will not change. The flow contributions through then inlets during storm events are significant, even under Baseline Conditions that are susceptible to barrier island breaching and overwash during severe events. Tidal and surge propagation into the bays depends strongly on the hydraulic efficiency of the existing inlets and also bay hydrographic conditions. Ocean tide range is reduced by 25% in Shinnecock Bay and by more than 60% in Moriches Bay. In Great South Bay, observed tidal range reduction varies, with distance from Fire Island Inlet, from about 40% to 75%. Moriches Bay is smaller than Great South Bay and Moriches Inlet is more efficient than Fire Island Inlet. Consequently, Moriches Bay fills more rapidly with storm surge flows than Great South Bay, disrupting the normal tidal flood and ebb flow and producing a continued flow westward from west Moriches Bay through Narrow Bay into eastern Great South Bay. Shinnecock Inlet is the most efficient of the three inlets. During storm conditions the peak water levels observed at Shinnecock Bay are close to the same magnitude as peak water levels in the open ocean. During

storm conditions a significant exchange in water level is observed between Moriches and Shinnecock Bays, particularly affecting Quantuck Bay.

To develop stage-frequency relationships, the one-dimensional Empirical Simulation Technique (EST) was employed. In addition, this method was improved to account for other, equally probable, astronomical tide timings relative to each individual storm's timing. In order to implement this EST method, several supplemental storms were also selected for numerical modeling. The final stage-frequency curves demonstrate gradual alongshore variability in ocean station peak water levels, at all return periods, as a result of accounting for variation in astronomical tide scenarios. Peak combined (tropical and extratropical) ocean water levels[1] associated with the 50-year and 100-year return period vary from about 7.5 ft to 10 ft and 9 ft to 11 ft, respectively, from Sandy Hook, NJ to Montauk Point. At ocean stations, contribution to peak water level from wave setup may add as much as 4 ft to these stage-frequency values. Both the stage-frequency values and wave setup values will be included in FIMP economic analyses.

Stage-frequency relationships within each of the three bays reflect spatial variations that are consistent with each bay's geometry and inlet configuration as well as with each bay's corresponding ocean stage-frequency relationship. Peak water levels in Great South Bay are approximately 4 ft to 5 ft and 4 ft to 6 ft for the 50- and 100-year return periods, respectively. Peak water levels in Moriches and Shinnecock Bays are somewhat higher. In Moriches Bay, peak water levels are approximately 6 ft to 7 ft and 6.5 ft to 7.5 ft for the 50- and 100-year return periods, respectively. In Shinnecock Bay, peak water levels are approximately 7 ft to 8 ft and 7.5 ft to 8.5 ft for the 50- and 100-year return periods, respectively.

[1] Peak water levels for stage-frequency in this report do not include local wave setup contributions. All peak stage-frequency water levels are referenced to NGVD29 and adjusted for sea level rise in the year 2000.

TECHNICAL REVIEW PANEL ROLE AND FINAL COMMENTS

By Henry Bokuniewicz, Technical Review Panel Chairman

For the Fire Island Inlet to Montauk Point Reformulation Study (FIMP), the New York District had and needed to continue to utilize numerical models to predict the breaching of the barrier islands and the magnitude of storm surges in the bays along Long Island's south shore. The storm surge modeling is the cornerstone of the FIMP reformulation study, since the model output is used to generate ocean and bay stage-frequency curves for input into economic analyses, coastal engineering design, environmental processes, and final alternative selection.

In addition, from preliminary economic evaluations, the storm damage estimates seem relatively sensitive to surge elevation. An increase in surge elevation of 0.5 feet (15 cm) doubles the amount of annualized damages in some locations.

Despite noble, initial efforts between 1995 and 2001, by the summer of 2002, the development of ocean and bay stage frequency relationships had come to a point where new methodologies where needed to rigorously incorporate the likelihood of barrier island overwash and breaching in a technically robust and defensible manner. Within the District and with other parties, such as the New York State DEC and DOS, Department of Interior and the Coastal and Hydraulics Laboratory in the summer of 2002, there was considerable amounts of discussion on the numerical modeling strategy to continue the FIMP study. Required was a complete updating of the hydrodynamic storm surge modeling, and new state-of-the–art numerical modeling of storm induced barrier island morphology, including overwashing and breaching. A new tool, the Delft3D modeling system was being considered for use in the prediction of barrier island breaching and storm-induced changes in bay water levels. Although ADCIRC is the U.S. standard for hydrodynamic forecasts, Delft3D had the advantage of providing a sediment transport module for calculating the formation and impacts of new breaches. The District and its consultants wanted to ensure that they were proceeding on the modeling with sound technical judgment. Approaches that were somewhat new and untested needed outside review and steering in methodology, assumptions and descriptions of modeling limitations. The FIMP PDT embraced the concept of a technical review panel.

A list of potential members of the panel were generated by soliciting opinions of many consultants, academics, and other coastal processes professionals in sister Federal and state agencies. Guidance on the members and conduct of the panel was also sought from Corps Headquarters. The District was seeking a balanced panel with experience in hydrodynamic modeling, barrier island breaching processes, and sediment transport modeling. To make the panel a coherent, cohesive group, a maximum of four members were sought, including a local coastal expert, a member of the Corps' Coastal Engineering Research Board (CERB), someone from academia, and a member from a sister federal agency. Twenty-two potential candidates for the TRP were identified, and from that list, with the consensus again from a large group of experts, Henry Bokuniewicz, Professor of Oceanography, Marine Science Research Center at Stony Brook University was selected as the chairman of the panel. Bruce Taylor, Chief

Executive Officer of Taylor Engineering and CERB member, David Basco, Director of the Coastal Engineering Center at Old Dominion University, and S. Jeffress Williams, Senior Coastal Geologist, United States Geological Survey were asked and graciously agreed to form the Technical Review Panel. As a group, the Panel was thoroughly familiar with model applications, specifically ADCIRC and SBEACH; they also embodied considerable site-specific experiences.

A contract was put in place for attendance at and participation in three meetings, and the review of reports and documents. The technical review panel was to provide specific technical comments and guidance on all aspects of the numerical modeling of storm surge and barrier island breaching, including data gathering, model input and assumptions, parameters of modeling such as grid size and time step and insight into modeling results. The panel members were to provide written comments to the District through the panel chairman, on the reports, documents, and meeting proceedings presented to the panel. All review comments and recommendations were considered by the New York District to improve and clarify the storm surge and breaching numerical modeling.

The contract identified three initial concerns that were to be addressed specifically by the Technical Review Panel: (1) An updated circulation model (ADCIRC) which would incorporate the latest bathymetry and topography of the barrier islands, inlets and back bays and be calibrate and validate to match water levels and surges for a full range of storm events, (2) the inclusion of wave set-up, wave run-up, and dune erosion of the barrier island through either modeling of storm-induced erosion with the standard tool (SBEACH) or new development in the Delft3D modeling system; and (3) prediction of flooding of the interior bays to include not only storm surge through the inlets, but also overtopping of the dunes and flow through newly created inlets.

Three meetings were held over a twenty-month period. These were on December 12 and 13, 2002; May 27 and 28, 2003; and January 12 and 13, 2004. Over thirty formal recommendations were made in the course of these meetings. The principal foci of the panel's recommendations are summarized, however, in four general topics:

First, the panel considered the Corps' plan to meld three existing models (ADCIRC, SBEACH and Delft3D) and agreed with an approach that would best match the individual strengths of these numerical tools. In brief, ADCIRC was recalibrated and used to produce the regional storm-surge simulations. ADCIRC provided the boundary conditions to Delft3D, which was used to simulate the bay water levels and breaching of the barrier islands. The Delft3D numerical model was calibrated successfully to simulate multiple, simultaneous, inundation and breaching events over the study area. The recommended comparison of ADCIRC results to Delft3D results under the same conditions was excellent. There was little difference between the two models providing a high level of confidence to the results. The SBEACH application is discussed below.

Second, the panel advised a 30-day, synoptic, water level measurement program in the bays. Sufficient funds were made available to support a 30-day field measurement

campaign to verify the model results. During the field program, storm conditions were captured in February 2003. The predicted water elevations were in excellent agreement with the observed observations. The level of agreement substantially added to the level of confidence in the approach. In addition, the comparison established the importance of (a) wave set-up in the ocean propagating through the inlets to increase water levels in the bays and (b) the sensitivity of coastal winds in the set-up within the bays themselves.

Third, dune elevations are clearly key factors in controlling storm overwash inundation and breaching. At the second meeting, the panel advised the use of recent, densely spaced LIDAR coverage to establish initial conditions. LIDAR measurements of dune/beach geometry coupled with multiple SBEACH simulations have provided better initial conditions for the Delft3D computations. In addition, there was considerable discussion of the best applications of SBEACH to impose pre-breach conditioning and technical suggestions for its use in this case. This recommendation was implemented greatly expanding the application of SBEACH in establishing the initial conditions for the Delft3D/ADCIRC production run. Prior to breaching, lowering of the dune due to wave action was calculated on LIDAR profiles using SBEACH and incorporated into the initial conditions for Delft3D. The panel agreed that the water volume of overtopping before inundation could be ignored in the final analysis although the change in dune geomorphology could not. The earlier Corps calculation of overtopping appears to be a substantial overestimate when compared to recent, laboratory-calibrated methods. Lowering of the dune crest before overtopping could, however, be a deciding factor in breaching.

Fourth, the panel reviewed the model simulations of the historical storms of September 1938 and December 1992 that were based on actual pre-storm topography and called "realism" tests. The "realisms" examples were useful and the panel considered that further documentation was warranted. A "realism" test of the infamous Ash Wednesday storm (March 1962) was recommended for both technical and political reasons, even though the quality of the available data was not as good as that for other events (marginal, even). Some attempt at recreating this particular storm was deemed important because it was a memorable one and many will expect to be able to compare their experience with the calculations.

In conclusion, the panel was impressed by these results and compliments the investigators. This is an exceptional body of work and at the cutting-edge of our technical ability. It is probably the most comprehensive treatment of this phenomenon in the country.

Submitted by Henry Bokuniewicz, Technical Review Panel Chairman

TABLE OF CONTENTS

LIST OF FIGURES

LIST OF TABLES

IMPORTANT DEFINITIONS

Barrier Island Processes

A ***hurricane*** is an intense tropical cyclone in which winds tend to spiral inward toward a core of low pressure, with maximum surface wind velocities that equal or exceed 74 mph (33 m/sec or 64 knots) for several minutes or longer at some points. Tropical storm is the term applied if maximum winds are less than 74 mph. Tropical storms are typically fast moving and compact. Therefore, surge hydrographs peak rapidly, within a few hours, and surge varies along the coast depending on the location of landfall.

A ***Northeaster***, or ***Nor'easter***, is a large-scale storm formed by Artic cold fronts mixing with warm low pressure fronts from the Gulf of Mexico that are pulled up the Northeast coast by the northeast winds. These storms generally occur in fall, winter, and spring. The predominant wind direction during these storms is from the northeast. These storms generally are characterized by widespread area of influence and elevated surge levels lasting over one tidal cycle or more.

The severity of flooding along the mainland shoreline in the FIMP bays (Great South Bay, Moriches Bay and Shinnecock Bay) is a function of open coast ***storm surge***, defined as the rise above normal water level due to wind-induced surface shear stress and/or atmospheric pressure reduction propagation through the inlets, storm surge in the bay (i.e., local wind and pressure effects), and barrier island overwash and breaching. These three effects plus astronomical tides combine to produce the net bay ***storm stage***, defined as the level of the quasi-steady state water surface above a given datum at a given location. The following definitions were adopted for this study:

Overwash is "(a) a mass of water representing the part of the uprush that runs over the berm crest (or other structure) without flowing directly back to the sea or lake and (b) the flow of water in restricted areas over low parts of barriers or spits, especially during high tides or storms," (Glossary of Geology, American Geological Institute, 1978). Overwash tends to erode or flatten dunes during a storm with an attendant deposition of eroded sediment on the landward side of the barrier island (***washover***). This terminology is commonly used in most of the relevant research in the area of barrier island morphodynamics (e.g., Leatherman, 1981) and in reports of large storm damage available in the literature (e.g., Wilby et al., 1939). More importantly, a similar terminology has been adopted in previous reports and studies relating to FIMP (e.g., USACE, 1995).

Note, however, that engineers and researchers sometimes use the term overwash to refer specifically to the intermittent volume of water that overtops the dune due solely to ***wave runup***, defined as the peak elevation of ***wave uprush*** above still-water level. ***Wave uprush*** consists of two components: super elevation of the mean water level due to wave action (***wave setup***) and fluctuations about that mean (***swash***) (USACE, 2002). This intermittent flow occurs only when the ***total water level*** (tide + storm surge + wave setup) remains below the dune crest elevation. Others use the term ***overtopping*** instead to refer to this intermittent water flow and the term overwash to refer to the sediment transport

associated with it. For the purposes of this study the intermittent flow due to runup will be referred to as ***overtopping***, whereas the continuous flow that occurs after the dune is inundated by setup will be denoted as ***overflow***. Overwash will be used according to the more general definition provided in the previous paragraph, which could include both overtopping and overflow.

The term ***overwash*** (or ***overwash area***) will also be used in this report to denote the resulting storm-induced barrier island response (topographic change) to water moving over the barrier island by overwash and overflow processes (Figure ID-1). In this report, the term ***overwash*** when referring to storm-induced morphological change will indicate lowering of the barrier island, between its pre-storm elevation and the Mean High Water (MHW) datum. An ***overwash*** area only allows exchange of ocean and bay waters through a portion of the spring tidal cycle. While the formation of a full breach during spring-tide conditions following a storm event is possible, it is much less likely than if the same barrier island location was cut to a lower elevation and during the storm.

Breaching refers to the condition where overflow cuts a channel across the island that permits the exchange of ocean and bay waters under normal tidal conditions. For this report, two degrees of morphological response to breaching will be used (Figure ID-1). A ***partial breach*** is a storm-induced barrier island cut that has a scoured depth between MHW and Mean Low Water (MLW) while a ***full breach*** is a storm-induced barrier island cut that has a scoured depth at or below Mean Low Water (MLW). A partial breach will allow for water to exchange between the ocean and bay during a portion of

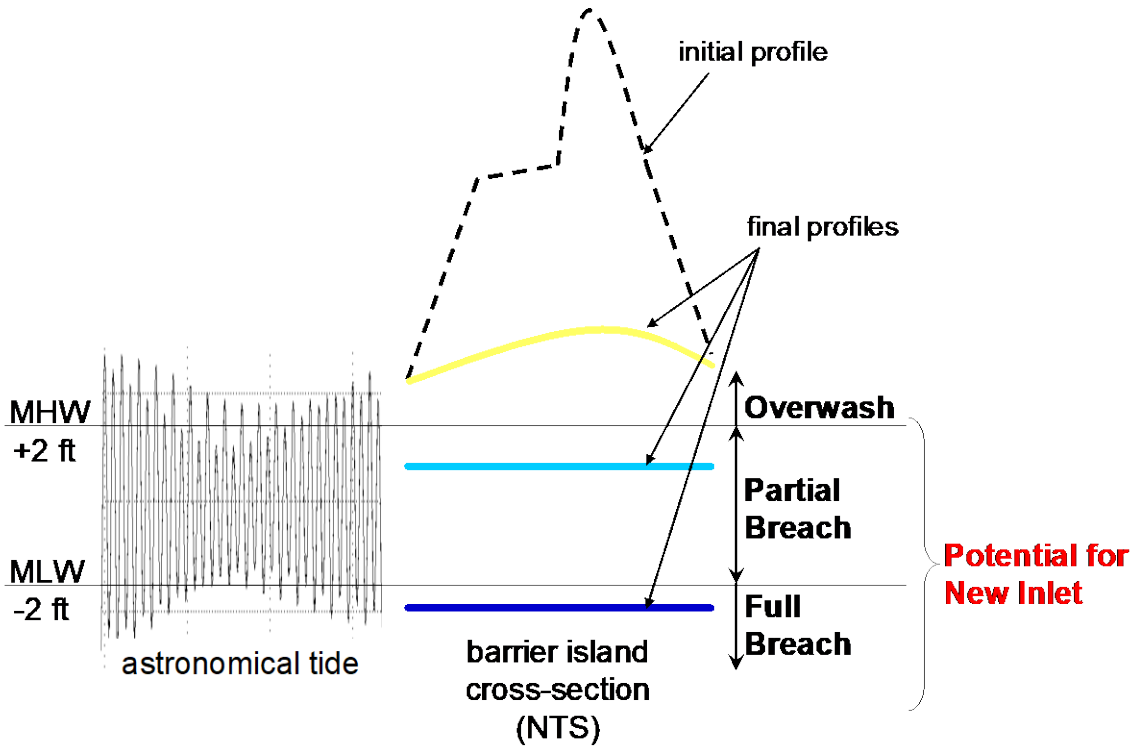

Figure ID-1. Definition of morphological responses used in this report.

the normal tidal cycle while a full breach will allow water exchange during the complete tidal cycle. A partial or full breach may potentially develop into a permanent breach during normal tide conditions following a storm.

Overwashing and breaching are interrelated. For example, severe overwashing can lead to breaching. The breach or overwash area may be temporary or permanent (i.e., a new inlet) depending on the size of the breach, adjacent bay water depths, potential tidal prism, littoral drift, etc.

Overwash, and particularly breaching, during a storm may contribute significantly to the storm stage in the bays and therefore the modeling approach should be capable of simulating these effects as well as open coast surge propagation through the inlets and bay storm surge.

Vertical Datums

Collected bathymetric and topographic data for the study area were referenced to various different vertical datums including Mean Sea Level (MSL), Mean Low Water (MLW), and National Geodetic Vertical Datum 1929 (NGVD29). However, for this study The New York District has adopted feet NGVD29 as the vertical datum for design elements and reporting. Further complicating matters is the fact that hydrodynamic model inputs must be relative to meters in mean sea level (MSL). Therefore, all available data were converted to meters, MSL. For those data sets referenced to MLW, conversions were applied based on the nearest tidal benchmark information developed from long-term water level measurements. These included a number of NOAA tidal benchmark sheets (1960-1978 tidal epoch) nearby and throughout the study area along with several LISHORE measurements offshore and within Shinnecock and Moriches Bays. Generally, available tidal benchmark information within or near the study area does not include vertical reference to NGVD29. Further, the limited information regarding NGVD29-to-MSL conversions show that conversions vary widely throughout the study area: NGVD29 is below MSL by 0.59 ft (0.18 m), 0.50 ft (0.15 m), and 0.75 ft (0.23 m), at Shinnecock, Moriches, and Fire Island Coast Guard Stations, respectively. This presented a challenge for converting measured data referenced to NGVD29 to MSL. For this study, the following conversion between NGVD29 and MSL was adopted:

$$\text{Elevation}_{\text{NGVD29}} = \text{Elevation}_{\text{MSL}} + 0.5\ \text{ft}\ (0.15\ \text{m})$$

This conversion was based upon that used for past New York District studies for the south shore of Long Island and approximates the average of the known conversions within the study area. Fortunately, water level predictions by hydrodynamic models are not overly sensitive to small bathymetric changes (on the order of 0.2 ft (0.1 m)). Therefore, using one conversion for the entire project is expected to have a negligible impact on the final water level simulations.

The conversion given by the equation above is also used to convert simulated peak water levels from MSL to NGVD29 for stage-frequency development and reporting. In this

report, all water level comparisons between simulate storm water levels and measured water levels are presented relative to MSL. However, all stage-frequency results and comparisons are presented in NGVD29, as this is the datum required for this study.

Tidal Constituents

Tidal constituents are components of the astronomic tidal time series computed by performing a harmonic analysis. This analysis decomposes the tide signal into diurnal (K1, O1, Q1, etc.) and semidiurnal (M2, N2, S2, K2, etc.) components, where each component is itself a sine wave defined by amplitude, phase, and speed. The most dominant tidal constituent will have the largest amplitude. In the FIMP area, the largest-amplitude constituent is M2, a semidiurnal constituent.

Observed and Measured Peak Water Levels

Two types of information exist that document historical storm water levels within the FIMP area. ***High Water Marks (HWM)*** are indirect measurements of high water level. These are namely post-storm observations of the high water line, typically on a permanent structure, and are oftentimes represented by the debris line. The HWM includes the effects of astronomical tide, storm surge, localized wave setup, and the impact of individual waves (including wave runup). Figure ID-2 illustrates these contributions to the HWM.

Another type of peak water level measurements are ***Water Level Gage (WLG)*** measurements. These are direct measurements of water surface elevation, and they are generally more accurate and more reliable than HWM observations. A peak WLG measurement includes the effects of all quasi-steady state contributions to water level. Specifically, the WLG measures the water level contributions from astronomical tide, storm surge, and localized wave setup (Figure ID-2). These measurements do not include the effects of individual waves; therefore, they better reflect the quasi-steady state water level conditions experienced during storm events.

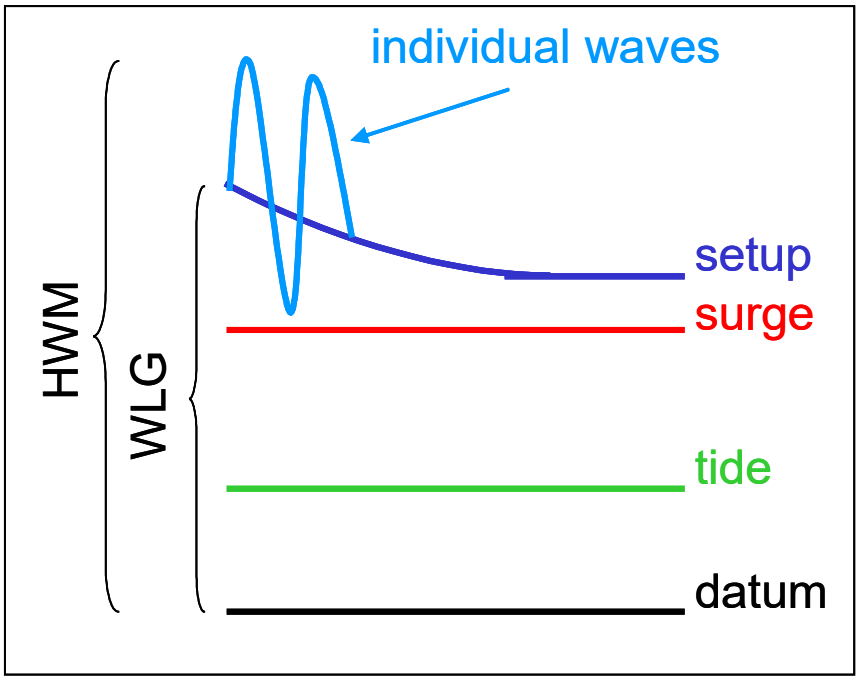

Figure ID-2. Water level contributions to HWM and WLG peak water level records.

1. Introduction and Project Background

The US Army Engineer District, New York (CENAN) is currently conducting a reformulation study of the shore protection and storm damage reduction project for the south shore of Long Island, New York. The study area, shown in Figure 1-1, extends approximately 83 miles (130 km) from Fire Island to Montauk Point (FIMP) and includes the barrier islands, Atlantic Ocean shorelines, and adjacent back-bay areas. The three bays of concern are, from west to east, Great South Bay, Moriches Bay, and Shinnecock Bay and are connected to the Atlantic Ocean by Fire Island, Moriches, and Shinnecock Inlets respectively. The area is primarily low-lying and as such, subject to flooding by storm surge from the Atlantic Ocean, surge propagation through tidal inlets, wave setup and runup, and barrier island overwash and breaching. In 1995, in order to protect property from storm surge, wave attack, and storm-induced erosion, this reformulation was initiated as a multi-year, multi-task effort to identify and evaluate long-term solutions for both the barrier islands and back-bay mainland. Structural (beachfill, groins, revetments, and bulkheads) and non-structural solutions are the primary focus of the alternative engineering designs to be evaluated as part of the study. However, there is also an environmental restoration portion to the study to investigate methods for restoring natural processes and increasing sustainable and valuable habitat for native flora and fauna.

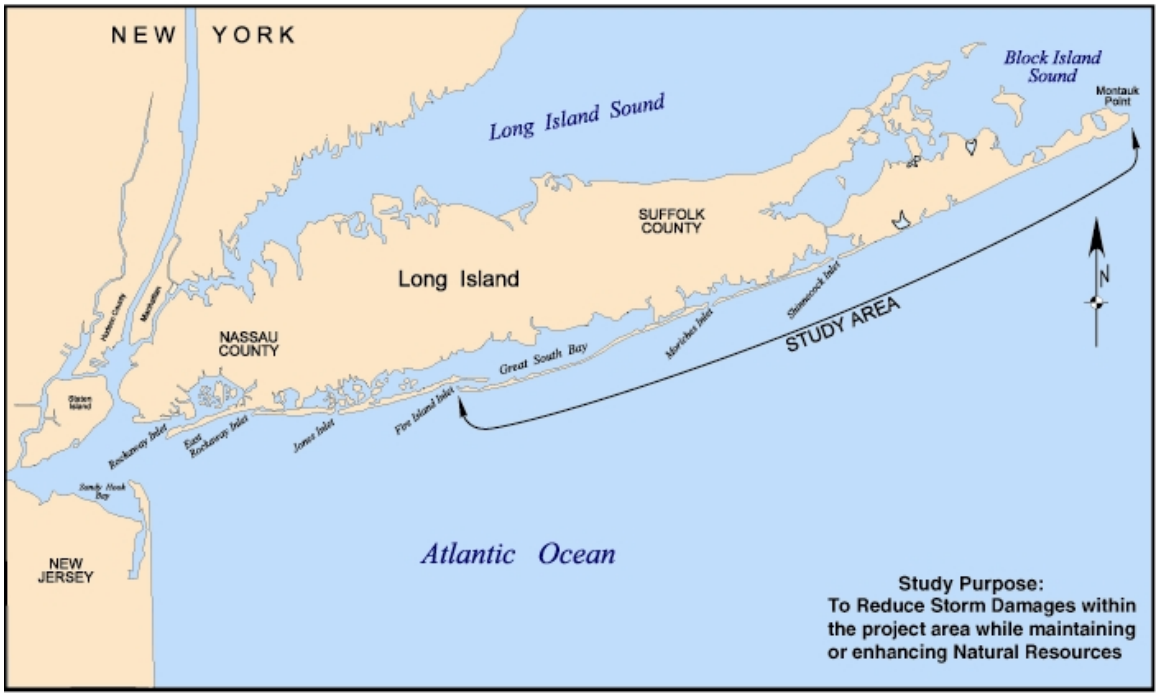

Figure 1-1: Fire Island to Montauk Point (FIMP) Project Area.

1.1 Project Area

The project area is located entirely in Suffolk County, Long Island, along the Atlantic and the bay shores of the towns of Babylon, Islip, Brookhaven, Southampton, and East Hampton. The overall study area is approximately 83 miles long and includes three large estuarial bays: Great South Bay (connected to the ocean by Fire Island Inlet), Moriches Bay (connected to the ocean by Moriches Inlet), and Shinnecock Bay (connected to the ocean by Shinnecock Inlet). The westernmost portion of the overall study area, the Nassau/Suffolk County border at Great South Bay, is located about 47 miles east of The Battery, NY.

1.2 Project Background and Goals

The original study was initiated in 1981 in response to decades long erosion due to seasonal storms and their affects on dune systems, shoreline orientation, nearshore and back-bay bathymetry, and inlet orientation and cross-sectional geometry. This reformulation study was initiated in 1995 because significant erosion after 1981 could have affected storm surge propagation and subsequently the possibility of overtopping, breaching, and back-bay flooding (Scheffner and Wise, 2001). To achieve the goal of determining the likelihood and size of a justified federal project, engineering studies are being conducted to provide coastal processes analyses and design input. Numerical modeling of physical, coastal processes in support of these analyses and designs has been undertaken for the full extent of the project area. Shoreline change models (GENESIS), littoral transport sediment budgets, beach profile erosion models (SBEACH), wave models (STWAVE and HISWA), and storm surge models (ADCIRC and Delft3D) have and will continue to be used. This report summarizes the use of several of these models in combination to simulate storm surge within the project.

By merging hydrodynamic, wave, and sediment transport models, accurate surge levels can be determined throughout the project. The storm surge modeling is the cornerstone of the FIMP study, since the model output is used to generate ocean (ADCIRC) and bay (Delft3D) stage-frequency curves for input into the economic analyses, coastal engineering design, environmental studies, and final alternative selection. Chapter 3 of this report provides details about the different models, how they were used, and the methodology behind their integration.

In general, compared to studies in the 1980's and mid-1990's, this recent study employs more advanced numerical models that include wave effects and morphological response in an integrated manner. This study is also based on improved historical storm wind and pressure fields, an improved tidal database, an expanded historical storm set, improved stage-frequency methodology, and rigorous calibration and comparison with measured data. This recent study is compared with past studies in Chapter 0.

The baseline conditions presented in this report are the basis for formulating a long-term solution to storm damage reduction within the FIMP area. This formulation study will identify alternatives that can optimize benefits by reducing economic loss to the mainland and barrier beaches, while preserving important human and ecological habitats. Furthermore, the Reformulation Study will reevaluate the Authorized Plan (House Document 1960) based on existing study area conditions and in accordance with current Corps of Engineers' policies and study criteria.

2. Storm Surge Modeling Methodology

Coastal storm water levels are governed by a number of complex physical processes: wind conditions, barometric pressure, astronomic tide, wave conditions, and morphologic response. Further, storm water levels in estuarial bays and sounds are highly dependent on tidal inlet and bay geometry and barrier island condition prior to the storm. In particular, back bay water levels are driven by flow through the tidal inlets, flow over the barrier island as a result of overwash and breaching, and localized wind and wave setup (Figure 2-1). Ocean and nearshore (offshore of the surf zone) storm water levels are dominated by meteorological conditions and astronomic tide.

The numerical modeling strategy for FIMP addresses all of these processes by combining a number of numerical models, some with external communication and others with integrated dynamic communication. The strategy also employs state-of-the-art meteorological methods and uses recent high-resolution lidar surveys to describe tidal inlet and barrier island geometry. Figure 2-2 illustrates the complexity of the numerical modeling strategy. The numerical models and methods used for this project are:

- Planetary Boundary Layer model (PBL)
- Kinematic Reanalysis
- ADvanced CIRCulation model (ADCIRC)
- WISWAVE
- Storm-induced BEAch CHange model (SBEACH)
- Delft3D-FLOW
- Delft3D-WAVE (HISWA)
- Delft3D-MOR
- SWAN
- Empirical Simulation Technique (EST)

A description of Baseline Conditions, output locations for subsequent stage-frequency development, and details of each numerical modeling component are described in this chapter. The Empirical Simulation Technique (EST) used to develop stage-frequency relationships is detailed in Chapter 1.

2.1 Baseline Conditions

Baseline Conditions for the storm water level modeling effort were developed based on the most up-to-date and reliable topography and bathymetry for the project area. This Baseline Condition is representative of the FIMP area's condition in 2000. Table 2-1 shows the data source for each area.

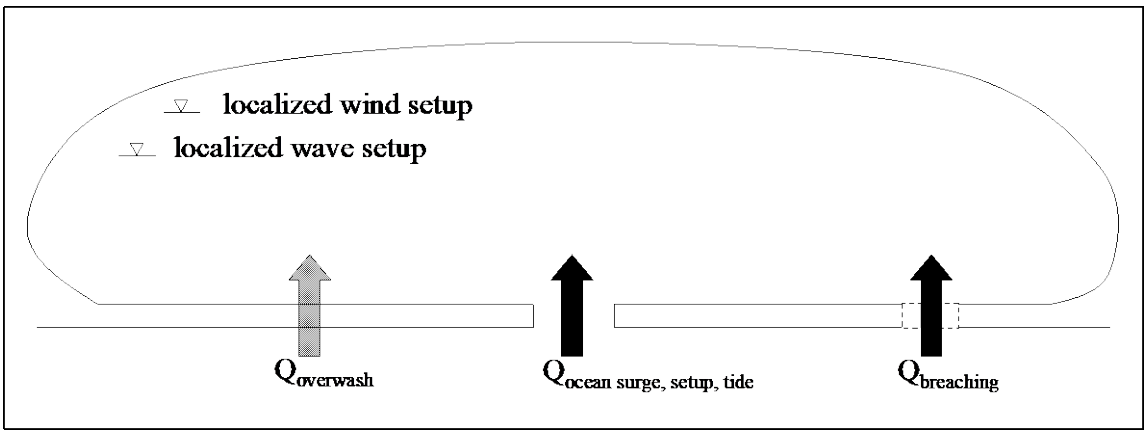

Figure 2-1: Contributions to bay storm water level.

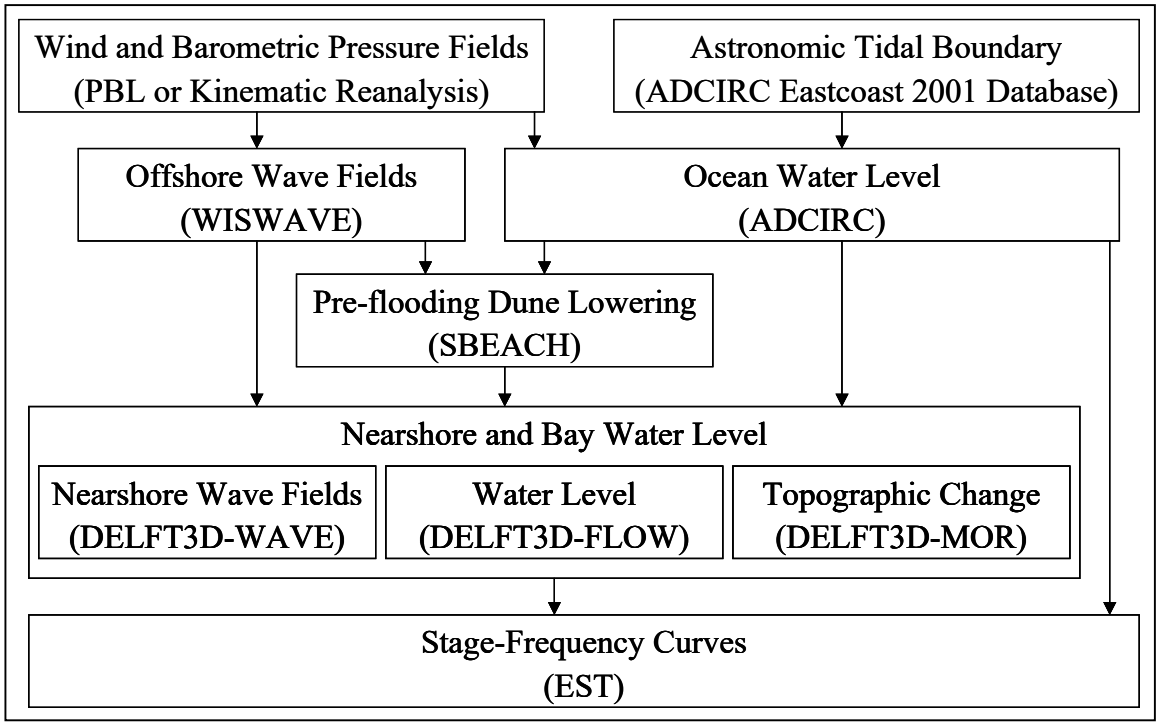

Figure 2-2: FIMP storm water level modeling and stage-frequency methodology.

Because tidal inlet geometry and barrier island topography are critical elements for accurate modeling of water level and morphological processes, extra care was given to ensure the numerical grids and profiles adequately reflect Baseline Conditions. Subaerial barrier island topography is based on a 1995 topographic survey complemented with the high-resolution topographic LIDAR data (Sallenger *et al*., 2001) collected by NOAA in September 2000 that covers the area between Fire Island Inlet and Southampton. The LIDAR data only covers the barrier islands therefore all the subaerial coastal areas along the northern bay shorelines are based on the 1995 data. Submerged profiles were described using beach profiles collected in 2001. High-resolution bathymetric LIDAR

data (Lillycrop *et al*., 1996), from 2000 and 1998, were used to describe both Moriches and Shinnecock Inlets, respectively. Finally, composite hydrographic survey data from 2001 were used to describe Fire Island Inlet (Moffatt and Nichol, 2005).

Outside of the FIMP area, tidal inlet bathymetry was based on surveys performed in 1998. Morphological impacts to the barrier islands outside the FIMP area were not included in this modeling effort.

For numerical modeling purposes, all survey data were converted to Mean Sea Level (MSL) based on available published NOAA (National Oceanic and Atmospheric Administration) benchmark sheets for the 1960-1978 tidal epoch and values used historically for FIMP. Vertical conversions for each data set are presented in Table 2-1.

2.1.1 Verification and Processing of LIDAR 2000 Data

Raw LIDAR 2000 data was processed using an automatic classification of the data points into three types: error, ground and no-ground points based on distance and slope among neighboring points. For example when the slope between two points separated by a relatively short distance is close to 90^{o} the higher of the two points will likely be classified as a no-ground (e.g., a building) point. After points have been classified in the aforementioned three categories, all the remaining points are classified as vegetation. An additional manual check is finally performed to ensure the validity of the automatic classification. A cross check comparison of profiles obtained from the raw LIDAR 2000 data and the processed LIDAR 2000 against profiles from the Atlantic Coast of New York Monitoring Program (ACNYMP) spring 2001 survey show reasonable agreement. The comparison of four profiles is presented in Figure 2-3. The figure illustrates typical differences between raw and processed LIDAR 2000 data. Spikes in the data corresponding to buildings and vegetation were removed from profile F19.

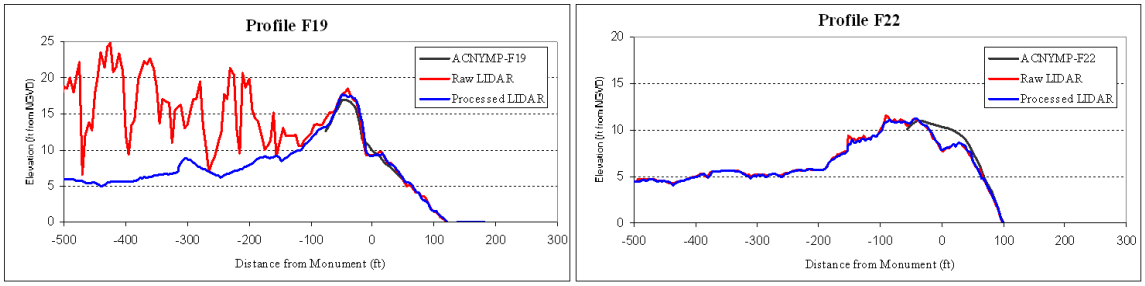

Figure 2-3: Comparison of LIDAR extracted profiles before and after processing with ACNYMP profiles – (Baseline Conditions).

Table 2-1: Baseline Conditions bathymetry and topography data sources and conversions for FIMP area.

Project Area	Data Source	Horizontal Datum	Vertical Datum	Vertical Conversion Source	Vertical Conversion[2]
Nearshore: Jones Inlet to Montauk Point	GEODAS	Geographic NAD27 (deg)	MLW	LISHORE P1	0.53 m (1.73 ft)
South Oyster, Great South, Narrow Bays	GEODAS	Geographic NAD27 (deg)	MLW	LISHORE P7	0.19 m (0.62 ft)
Moriches Bay	GEODAS	Geographic NAD27 (deg)	MLW	LISHORE P6	0.35 m (1.14 ft)
North shore of Montauk	GEODAS	Geographic NAD27 (deg)	MLW	NOAA Benchmark	0.37 m (1.2 ft)
Great Peconic Bay	GEODAS	Geographic NAD27 (deg)	MLW	NOAA Benchmark	0.10 m (0.32 ft)
Moriches Inlet	1998 SHOALS	LI, NY State Plane NAD83 (ft)	NGVD29	Previous FIMP	0.15 m (0.50 ft)
Fire Island Inlet	2001 surveys	LI, NY State Plane NAD83 (ft)	NGVD29	Previous FIMP	0.15 m (0.50 ft)
Shinnecock Inlet	1998 SHOALS	Geographic NAD27 (deg)	MSL	not required	
Shinnecock Bay	1998 Multibeam (SUNY)	Geographic NAD27 (deg)	MSL	not required	
Subaerial (east of Wantach Pkwy to Montauk Point)	USGS Topography	UTM NAD83 Zones 18 & 19 (m)	NGVD29	Previous FIMP	0.15 m (0.50 ft)
All Other Subaerial	2000 USGS LIDAR Topography	Geographic NAD83 (deg)	NGVD29	Previous FIMP	0.15 m (0.50 ft)

2.1.2 Barrier Island Vulnerability to Overwash

The filtered LIDAR data was used to develop the barrier island topography in the Delft3D model grid. Particular consideration was given to adequately representing areas previously identified as vulnerable to breaching and overwash. A preliminary analysis of areas that would require increased resolution was performed based on available topographic data, the breaching risk analysis presented in the Breach Contingency Plan (Moffatt & Nichol, 1995), and estimates of overwashing/breaching potential based on previous SBEACH simulations performed by CHL. Specifically, SBEACH results suggest that areas of the barrier island with a dune elevation of less than 15 ft (4.6 m) NGVD would be subject to significant overwashing, dune lowering and potential breaching under severe storm conditions. This limit is consistent with available estimates

[2] MSL = Vertical Datum + Vertical Conversion; all conversions based on NOAA benchmark sheets for the 1960-1978 tidal epoch.

of peak total water levels[3] (4.3 m or 14 ft NGVD) and dune lowering due to wave-induced runup[4] (3 ft or 0.9 m). Note that this initial dune lowering means that even a dune with a relatively high crest elevation of 17 ft (5.2 m) NGVD may be subject to full inundation and potential breaching, albeit to a lesser extent than low lying areas.

This analysis is also consistent with the limited information available from previous significant storms such as the 1938 Hurricane. Specifically, USACE (1947) notes that areas where dune crest height exceeded 18 feet above mean sea level remained relatively intact during this storm.

Figure 2-4 and Figure 2-5 show maximum barrier island elevation (typically the dune crest) along the length of the FIMP project area based on the 1995 topographic data and the filtered 2000 LIDAR data. The figures suggest that most areas identified as vulnerable for the 1995 data are also vulnerable for the 2000 data. The most significant differences between the two datasets are due to recent beach fill projects in Fire Island Pines (1997, 2002), Water Island/Barrett Beach (1996), Cupsogue Beach and Pikes Beach (Westhampton Interim, 1996-97, 2000-01), as well as other, smaller, dune rebuilding efforts (e.g., beach scraping at Kismet and Water Island/Barratt Beach). The 2000 Baseline Condition, in general, shows that the barrier island system is generally more robust than in 1995. This is indicative of the natural short-term variability in this barrier island system.

Table 2-2 summarizes the characteristics of each of these areas. As noted in sections below, Baseline-Condition model simulations have not suggested significant overwash or breaching outside these areas. Nonetheless, numerical simulations for Future Without-Project Conditions may lead to overflow and breaching in other areas, thus requiring that areas of increased resolution in the model be expanded.

Locations in Table 2-2 were identified on basis of dune elevation only, and not other considerations such as barrier island width, adjacent back-bay water depth, proximity to an inlet, potential tidal prism, etc. Although these additional factors would also affect the development of a breach, they are explicitly included in the model, and no prior screening based on these factors was considered. As such, model simulations suggest that some of these areas (e.g., the dune cut at the Wilderness Area or relatively small dune cuts in Southampton) do not contribute significant water volumes to the bay. Therefore, high resolution may not be required for some of the future storm simulations.

Table 2-2 does not include several locations along the barrier with relatively small "cuts" in the dune for beach access roads, etc. These small cuts are generally less than 30 ft (10 m) wide and are not expected to contribute significantly to peak storm water levels in the bays.

[3] Peak total water level is computed as the sum of the ocean surge (2.3 m or 7.5 ft, corresponding to hurricane Gloria), spring tide (0.8 m or 2.6 ft NGVD), and setup (1.2 m or 3.9 ft, based on 20% of a 6 m or 20 ft, incident wave).

[4] Dune lowering due to wave runup and prior to wave setup inundation. Based on available SBEACH simulations.

Table 2-2: Vulnerable areas and LIDAR profiles.

Name	Description	Location	Approximate Length of Reach		Minimum Dune Elevation (NGVD)		Number of LIDAR Profiles
			ft	m	ft	m	
Western FI Communities	Kismet to Point O' Woods	Kismet to Point O' Woods	23,500	7200	10	3.0	44
Central FI Communities	Fire Island Pines to Water Island	Sailor's Haven	200	60	12	3.7	30
		Fire Island Pines (West)	3000	900	8	2.4	
		Fire Island Pines (East)	1000	300	9	2.7	
		Barrett Beach/Water Island	5000	1500	12	3.7	
Davis Park	Davis Park to Watch Hill	Davis Park	1000	300	12	3.7	21
Dune Cut	Localized dune cut in Otis Pike Wilderness area	Dune cut in Wilderness Area	300	90	11	3.4	9
Old Inlet	Eastern part of Otis Pike Wilderness area	Old Inlet	8000	2400	6	1.8	40
Smith Point County Park	Central part of Smith Point County Park	Smith Point County Park	8000	2400	10	3.0	32
Tiana Beach	Western and central part of Tiana Beach	Tiana Beach (West)	5500	1700	9	2.7	57
		Tiana Beach (East)	1000	300	7	2.1	
West of Shinnecock Inlet	Localized area just west of Shinnecock Inlet	West of Shinnecock	3000	900	11	3.4	6
Southampton	Localized area just east of Shinnecock Inlet	Southampton	5000	1500	7	2.1	13

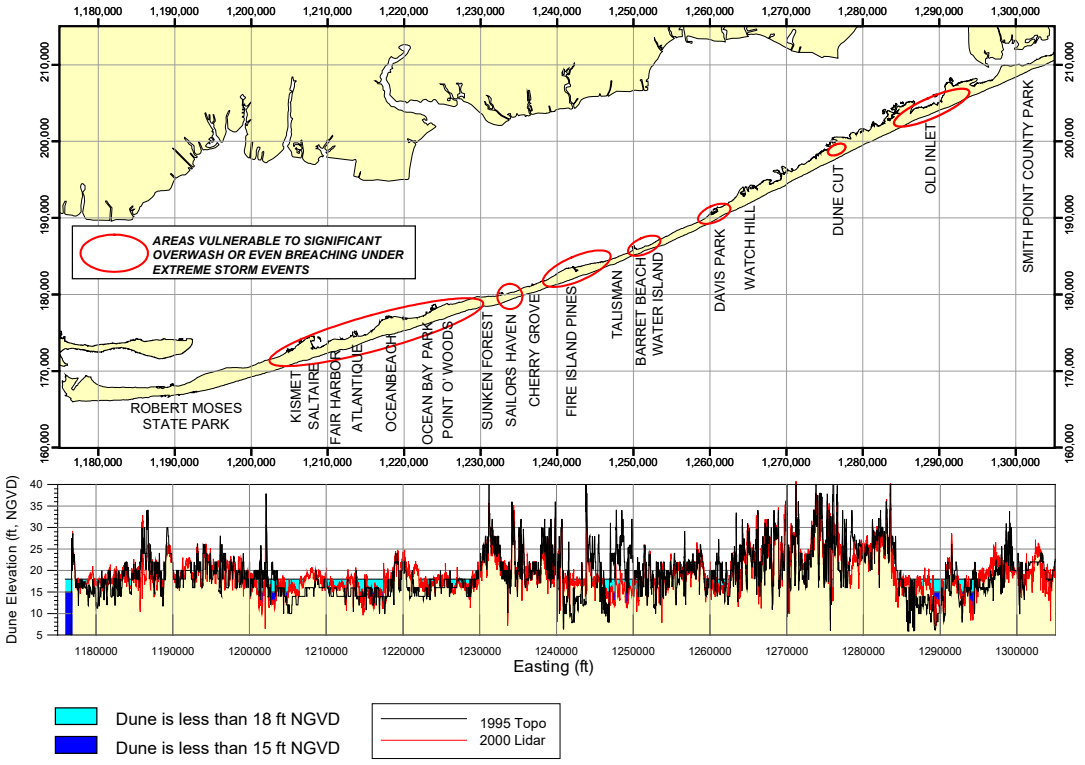

Figure 2-4: Maximum dune elevation: Fire Island Inlet to Smith Point.

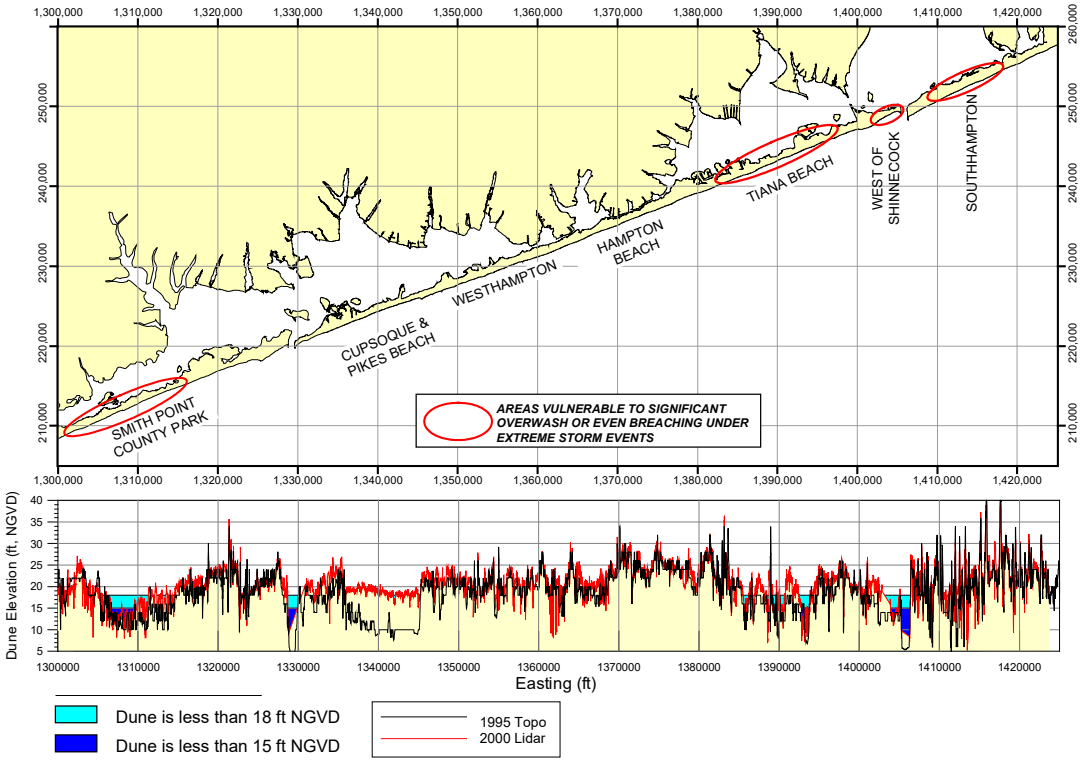

Figure 2-5: Maximum dune elevation: Smith Point to Southampton.

2.2 Historical Storm Set Selection

2.2.1 Tropical Storms

Historical tropical storms were selected by evaluating the National Hurricane Center's (NHC) hurricane Atlantic tracks database and NOAA water level measurements at Sandy Hook, NJ; Montauk Fort Pond, NY; and Newport, RI. Of the three NOAA measurement locations, Newport dates back the farthest to 1 January 1930. All tropical storms from 1930 through 2001 whose tracks came within 500 nautical miles of Long Island were considered. Of these storms, only those with peak surges (measured water level less NOAA predicted tide) greater than 2.23 ft (0.68 m), at Sandy Hook, Montauk Fort Pond, or Newport, were selected for storm surge modeling. In addition, the September 1954 hurricane was added because Harris (1963) reports a peak surge over 3.3 ft (1 m) at Montauk. Although Hurricane Sandy was not included in the storm set, it was determined that the existing storm set captured storms the represent the Hurricane Sandy condition in the project area.

Table 2-3: Historical storms selected for FIMP training set.

Tropical Events (1930 – 2001)			**Extratropical Events (1950 – 1998)**	
Name	**Start Date (based on NHC database)**	**Duration** (hours)**	**Start Date**	**Duration** (hours)**
not named	10-Sep-1938*	15	22-Nov-1950	34
not named	9-Sep-1944	10	04-Nov-1953	26
Carol	25-Aug-1954	5	11-Oct-1955	43
Edna	2-Sep-1954	7	25-Sep-1956	34
Hazel	5-Oct-1954	6	03-Mar-1962*	56
Connie	3-Aug-1955	0	05-Nov-1977	28
Donna	29-Aug-1960*	13	17-Jan-1978	16
Esther	10-Sep-1961	14	04-Feb-1978	27
Doria	20-Aug-1971	2	22-Jan-1979	19
Agnes	14-Jun-1972	18	22-Oct-1980*	17
Belle	6-Aug-1976*	7	26-Mar-1984	31
Gloria	16-Sep-1985*	5	09-Feb-1985	17
Bob	16-Aug-1991*	4	28-Oct-1991	50+
Floyd	7-Sep-1999*	3	01-Jan-1992	18
			08-Dec-1992*	78
			02-Mar-1993	12
			10-Mar-1993*	25
			28-Feb-1994*	22
			21-Dec-1994*	23
			05-Jan-1996	25
			6-Oct-1996	12
			02-Feb-1998	24

* Indicates storm is included in the calibration set.

** Storm durations represent duration that storm surge exceeded 1 ft (0.3 m), based

on ADCIRC simulations at Station 31.

+ Storm duration for this storm based on measured storm surge at Sandy Hook, NJ.

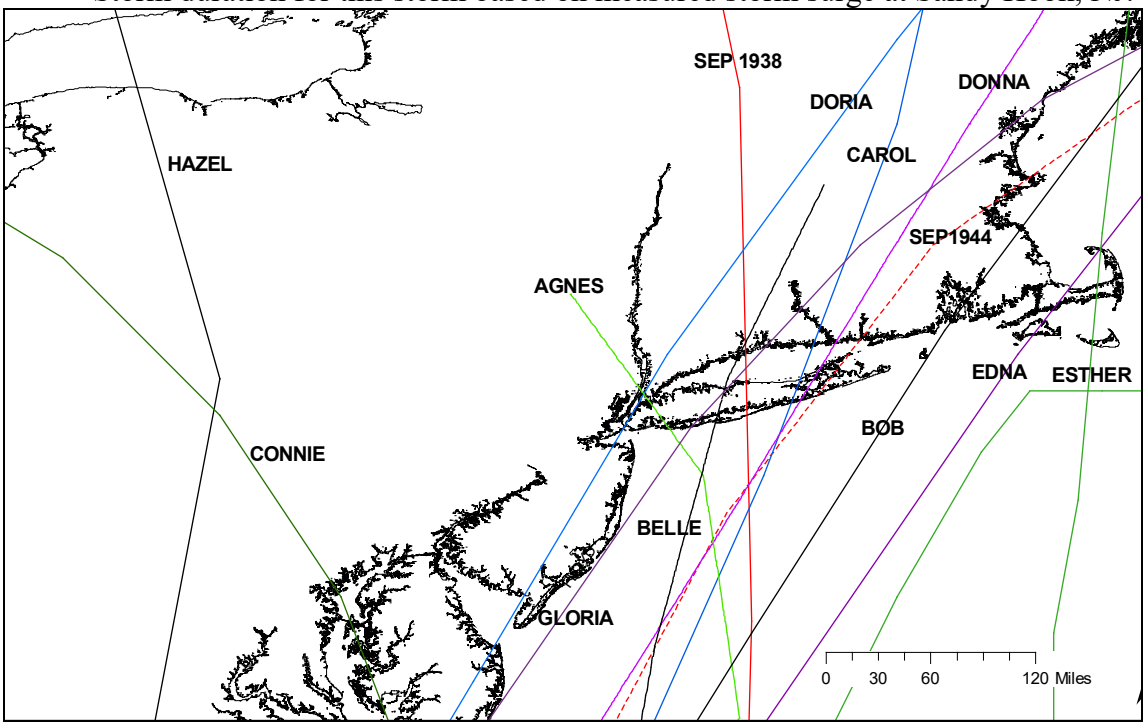

Figure 2-6. Tracks of tropical storms impacting Long Island.

During wind field development, Oceanweather Inc. reclassified the September 1956 and October 1996 events as extratropical events. These two events are now included in the Nor'easter storm set (note that both storms exceed the 3.3 ft (1-m) surge cutoff for extratropical events). There are a total of 14 historical storms in the final tropical storm training set (Table 2-3). Storm tracks for these 14 historical storms are illustrated in Figure 2-6.

2.2.2 Extratropical Storms

Historic extratropical events were selected by evaluating the prior FIMP surge modeling storm set plus the four additional storms used for prior FIMP SBEACH modeling. Additionally, storm selected for the recently completed NAN Asharoken/Bayville study were also evaluated. All storms with a peak surge greater than 3.3 ft (1 m) at Sandy Hook, Montauk, or Newport were included in the FIMP extratropical storm training set. The 22 selected storms, between 1950 and 1998, are listed in Table 2-3.

2.3 Supplemental Surge Modeling Simulations

To develop stage-frequency relationships, several supplemental storms were selected for numerical modeling. These included variation in the timing of major historical events

such that different astronomical tide scenarios could be considered. Table 2-4 lists the storms selected for supplemental simulations. For each of these storms, the maximum

Table 2-4: Storm selected for supplemental simulations.

Storm Date
Sep-38
Sep-44
Aug-54
Sep-60
Aug-76
Sep-85
Nov-50
Nov-53
Mar-62
Oct-80
Dec-92
9-Mar-93

high-spring-tide scenario was simulated. A full discussion of the reasoning for, selection of, and implementation of alternate tide scenarios for stage-frequency development is given in Chapter 10.2.2.

2.4 Storm Water Level Output Locations

For input to stage-frequency development, peak storm water level for each storm was extracted at 80 locations, 49 of which fall within the FIMP area. The 49 stations within the FIMP area were selected to capture the variability in storm water levels along the open coast and within the three bays. The remaining stations were selected to support other New York District coastal and ecosystems projects. Table 2-5 and Figure 2-7 through Figure 2-10 give the location of these output stations. In the figures, stations using Delft3D simulated results for water levels (Great South, Moriches, and Shinnecock Bays) are distinguished, by color, from those using ADCIRC simulated results (all others).

2.5 Wind and Barometric Pressure Fields

Since the study area is affected by intense tropical and extratropical storm events, wind and pressure fields are needed in addition to tidal forcing in order to drive the storm surge models. The need for accurate model results requires wind and pressure fields to be specified at higher temporal and spatial resolutions than typically available from public domain sources and previous hindcast studies. For that reason, NAN contracted with OCTI/Oceanweather, Inc. to provide wind and pressure fields for all the historical storms in the FIMP set. Storm winds and barometric pressure were modeled by introducing

wind stress and pressure (in m of water) at each grid node at uniform temporal intervals: every hour for tropical events and every 3 hours for extratropical events.

Table 2-5: Storm water level output stations.

Station Number	Latitude (deg)	Longitude (deg)	Location Description
1	-73.4288736260	40.6550903730	Unqua Point
2	-73.4614488710	40.6317107990	South Oyster Bay
3	-73.2269947500	40.7144234420	Great Cove
4	-73.1581093300	40.6525715130	Ocean Beach
5	-73.1239263700	40.7222901470	Connetquot River
6	-72.9890471930	40.6963460930	Watch Hill
7	-73.0111938060	40.7452313470	Patchogue
8	-72.8909393410	40.7570645950	Long/Sandy Point
9	-72.8946815280	40.7176628460	Old Inlet (ocean)
10	-72.8424683520	40.7500541100	Mastic Beach
11	-72.7477013760	40.7989795920	Hart Cove
12	-72.7267709190	40.8070857950	Seatuck Cove
13	-72.6696602340	40.8009574760	Apacuck Point
14	-72.5827236370	40.8185131460	Quogue Canal
15	-72.5367418400	40.8579335080	Tiana Bay
16	-72.4921723890	40.8797241020	Cormorant Point
17	-73.3121000000	40.6816000000	Sampawams Point
18	-73.3100000000	40.6300000000	Fire Island Mouth
19	-73.2700000000	40.6300000000	Fire Island Bridge
20	-73.1868000000	40.6986000000	Heckshire State Park
21	-73.0736000000	40.7162000000	Brown Point
22	-73.0728000000	40.6754000000	Great South Beach (bay)
23	-73.0707000000	40.6564000000	Great South Beach (ocean)
24	-72.9477000000	40.7313000000	Narrow Bay
25	-72.8849000000	40.7383000000	Smith Point
26	-72.8040000000	40.7778000000	Masury Point
27	-72.7533000000	40.7699000000	Moriches Inlet (bay)
28	-72.7556000000	40.7620000000	Moriches Inlet (ocean)
29	-72.7484000000	40.7846000000	Moriches CGS
30	-72.7000000000	40.7950000000	Westhampton Beach
31	-72.5900000000	40.8000000000	Post Lane
32	-72.5553000000	40.8392000000	Pine Neck Point
33	-72.5200000000	40.8500000000	Shinnecock CGS
34	-72.5000000000	40.8420000000	Shinnecock Bridge
35	-72.4770000000	40.8355000000	Shinnecock Inlet (ocean)
36	-72.4789000000	40.8479000000	Shinnecock Inlet (bay)
37	-72.4423085900	40.8707413300	Shinnecock Indian Reservation
38	-72.2069981610	40.9279511080	Apaquogue (ocean)
39	-71.9135552390	41.0334139410	Ditch Plains (ocean)
40	-71.9342158830	41.0741126610	Montauk Harbor
41	-73.1905700000	40.6295300000	Great South Beach (ocean)
42	-73.3581600000	40.6561300000	Great South Bay
43	-72.8045800000	40.7705000000	Moriches Bay
44	-72.6851100000	40.7893200000	Moriches Bay (Gunning Point)
45	-72.5342900000	40.8292500000	Shinnecock Bay (opposite Tiana Beach)
46	-74.0136700000	40.5735800000	Coney Island Lighthouse
47	-73.9469200000	40.5731200000	Manhattan Beach Park
48	-73.8850900000	40.6176400000	Island Channel (Jamaica Bay)
49	-73.8358300000	40.6428100000	Channel Bridge (Jamaica Bay)
50	-73.7964500000	40.6324100000	Grassy Bay (JFK airport)

Station Number	Latitude (deg)	Longitude (deg)	Location Description
51	-73.8849200000	40.5735300000	Marine Parkway Bridge
52	-73.8359600000	40.5735500000	Rockaway Park (ocean)
53	-73.7567300000	40.5879000000	East Rockaway Inlet (ocean)
54	-73.5802400000	40.5783200000	Jones Inlet (ocean)
55	-73.6673900000	40.5794900000	Long Beach (ocean)
56	-73.5685000000	40.5926800000	Jones Inlet (bay)
57	-73.4565400000	40.5986400000	Tobay Beach (ocean)
58	-74.0084400000	40.5836300000	Gravesend Bay Entrance (Rockaway Point)
59	-73.9230500000	40.5470900000	Rockaway Beach (ocean)
60	-73.7861300000	40.6067700000	Grass Hassock Channel
61	-73.8199000000	40.5926300000	Cross Bay Bridge
62	-73.6724700000	40.5946200000	Reynolds Channel (Long Beach)
63	-72.3429900000	40.8817900000	Watermill Beach (ocean)
64	-72.0528200000	40.9868200000	Napeaque Beach (ocean)
65	-71.8483500000	41.0745500000	Montauk Point (ocean)
66	-73.2994000000	40.6167000000	Fire Island - Democrat Point (ocean)
67	-74.0176460000	40.4628330000	Sandy Hook, NJ (also NOAA)
68	-74.0214290000	40.6991740000	The Battery, NY (also NOAA)
405	-73.8046779576	40.5978451856	Jamaica Bay (kad 1)
407	-73.7741085619	40.6151637767	Jamaica Bay (kad 3)
426	-73.8783340000	40.6310540000	Jamaica Bay (kad 6a and 7a)
429	-73.8705460000	40.6323550000	Jamaica Bay (kad 6b and 7b)
435	-73.8845624808	40.6283545569	Jamaica Bay (kad 8)
436	-73.8904190000	40.6165130000	Jamaica Bay (kad 9a and 10a)
442	-73.8910250000	40.6222360000	Jamaica Bay (kad 9a and 10a)
446	-73.9068350000	40.5843110000	Jamaica Bay (kad 11)
452	-73.9036478695	40.5866923940	Jamaica Bay (kad 12)
453	-74.0826343800	40.5027055600	Sandy Hook/Raritan Bays (cr 1)
454	-74.1679275400	40.4742975100	Sandy Hook/Raritan Bays (cr 2)
520	-74.2708333300	40.4900000000	Raritan Bay (Stu)

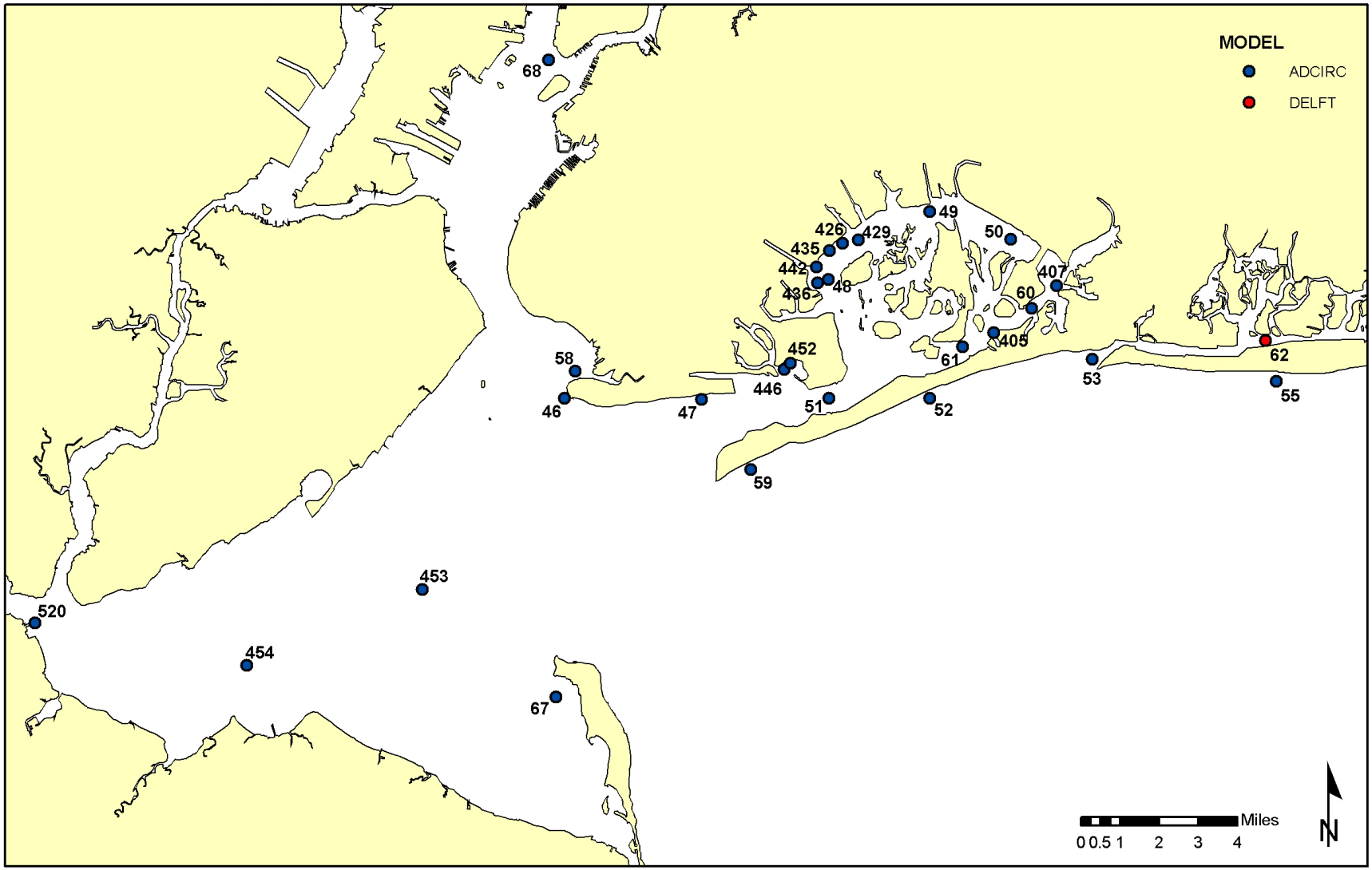

Figure 2-7: Storm water level output stations.

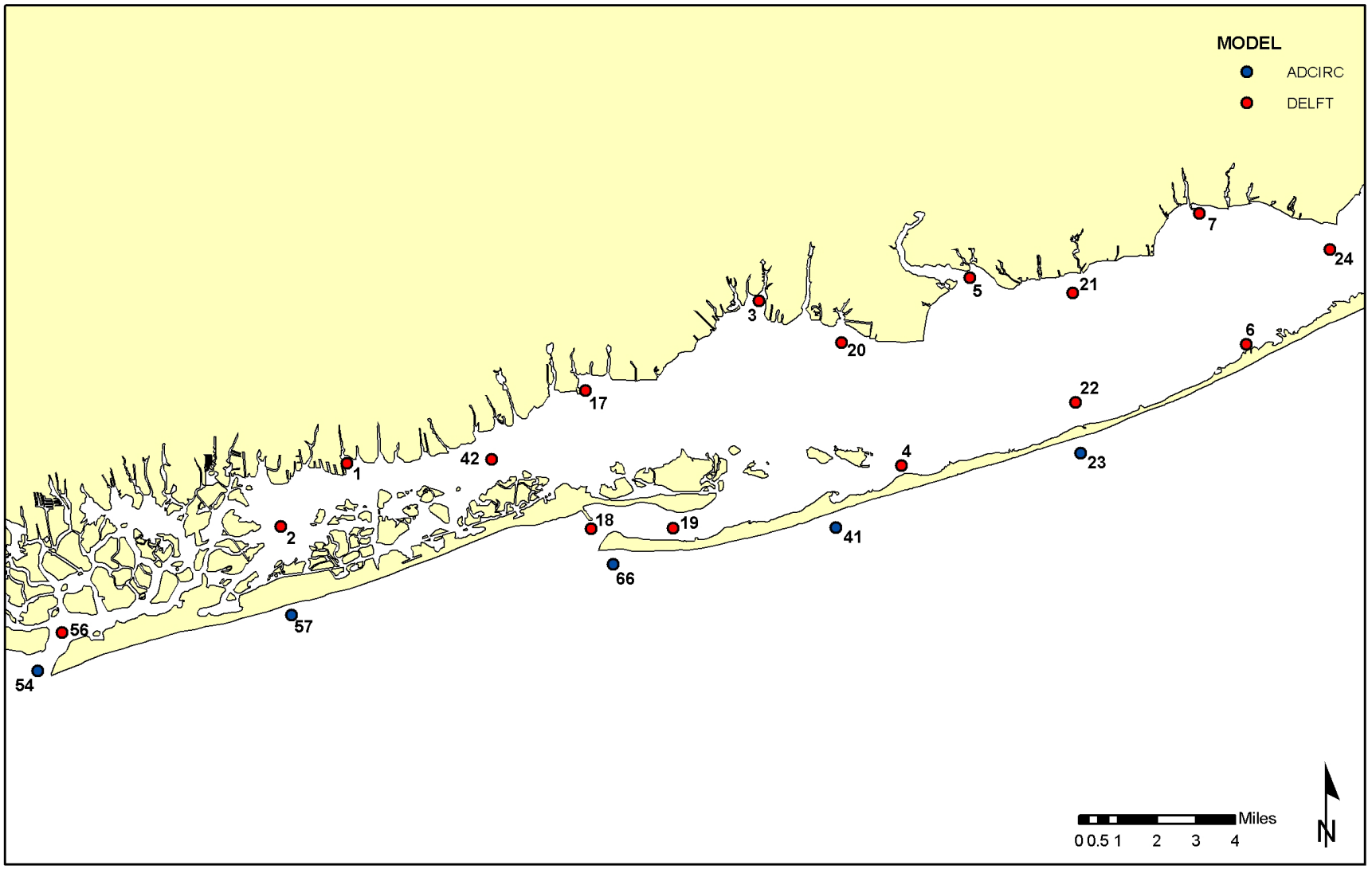

Figure 2-8: Storm water level output stations (continued).

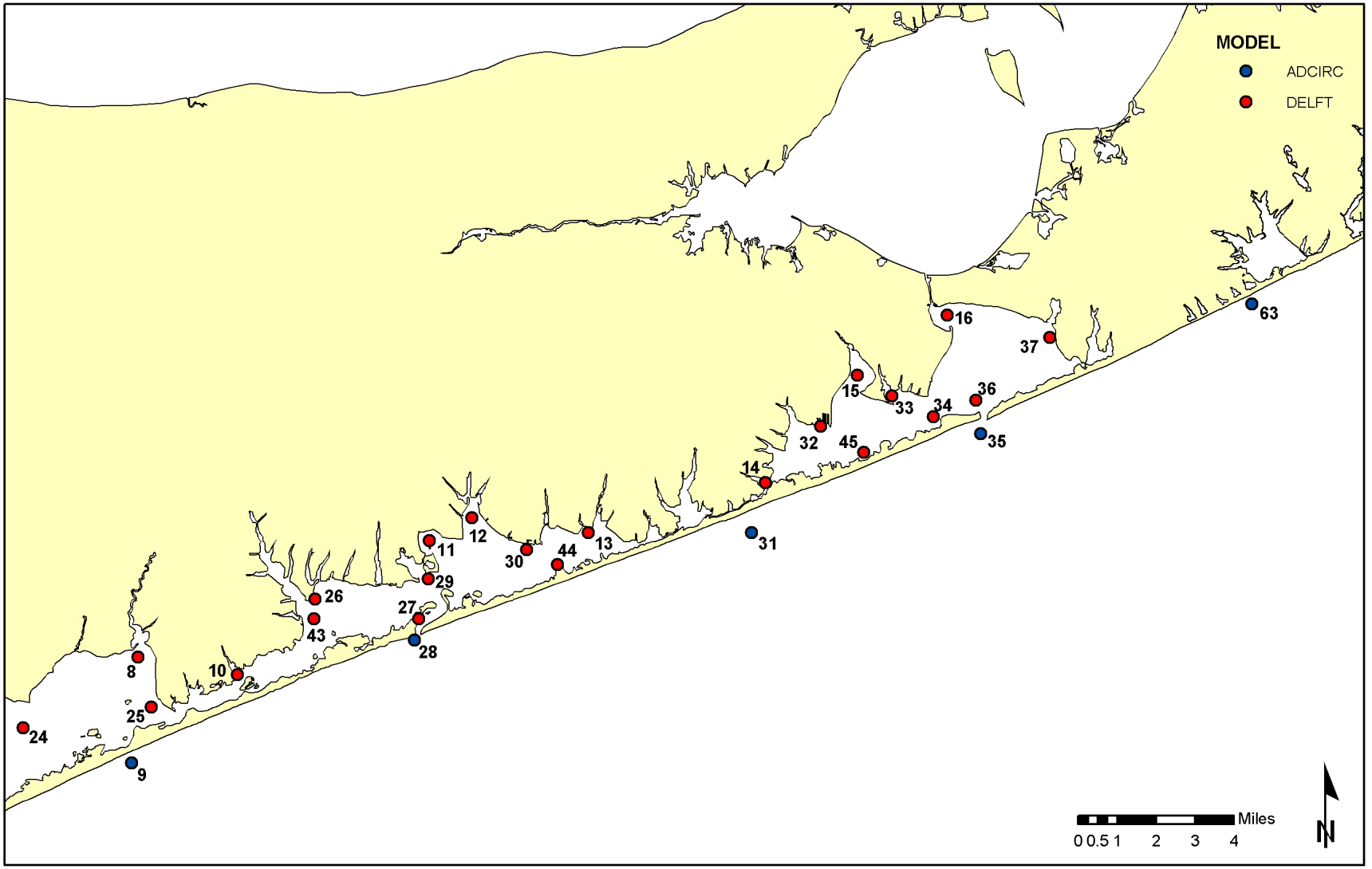

Figure 2-9: Storm water level output stations (continued).

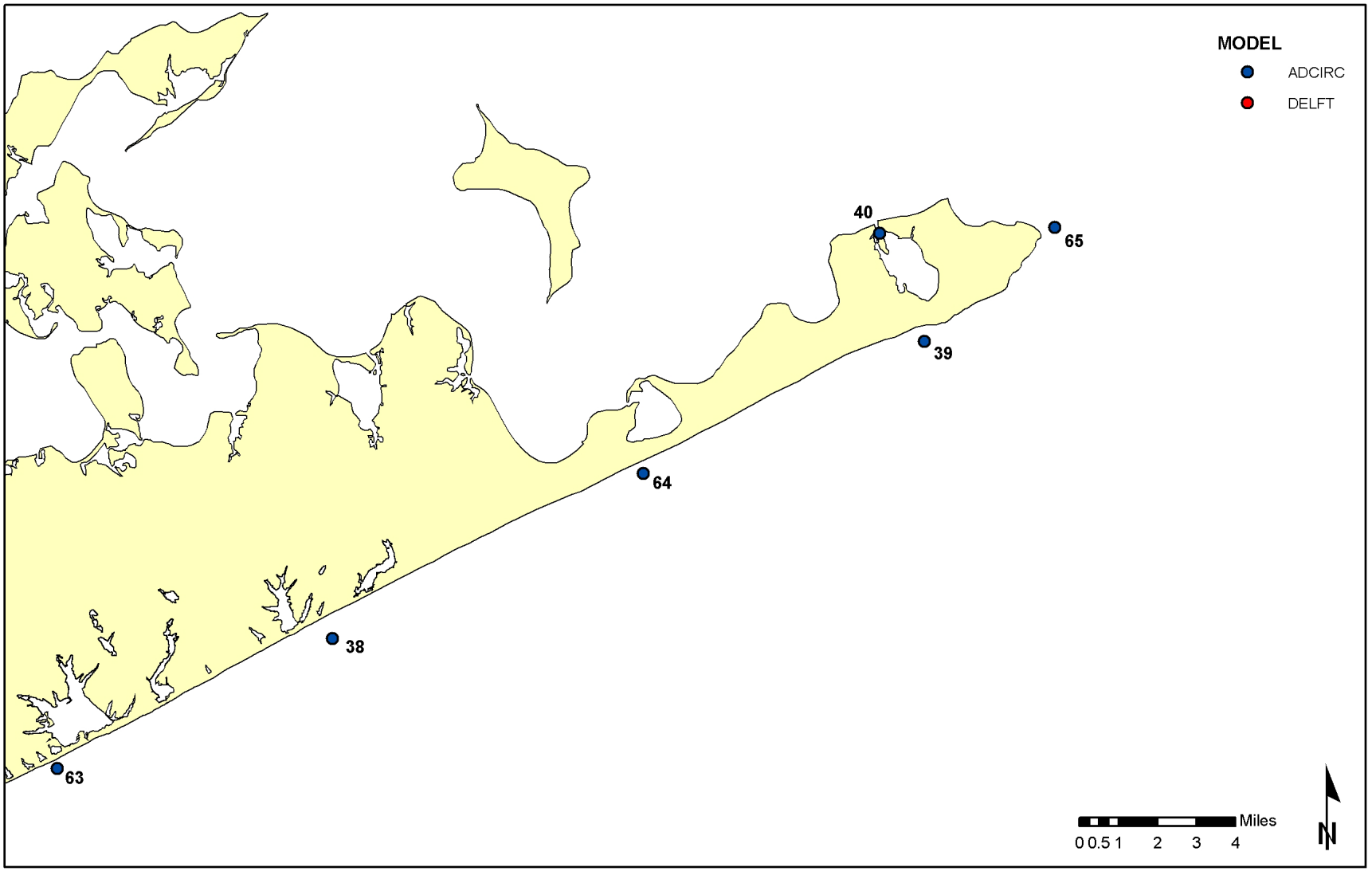

Figure 2-10: Storm water level output stations (continued).

2.5.1 Tropical Wind and Pressure

OCTI/Oceanweather, Inc. developed wind velocity fields (10-m (33-ft) above the water surface) and barometric pressure fields for tropical storm events using their Planetary Boundary Layer (PBL) model. The wind and pressure fields were produced on a grid domain extending from 30° N to 47° N and from 64° W to 82° W with grid spacing of 0.0625° latitude by 0.0625° longitude (about 7 km) at 1-hour intervals. Wind fields were not produced outside this domain for tropical storms. Specifically, the tropical storms were hindcast using Oceanweather Inc.'s (OWI) PBL tropical cyclone wind model, which was mainly driven by existing historical storm parameters including storm track, scale radius of the storm, and radial pressure profile. High-resolution surface wind fields for all tropical cyclones were specified by the PBL, a proven tropical cyclone boundary layer model (Thompson and Cardone, 1996). The model is driven by the specification of a relatively few parameters that describe the vortex pressure field and other parameters that describe the pressure field of the environment in which the cyclone is embedded. Briefly, the track and initial estimates of intensity of an historical North Atlantic basin tropical storm to be analyzed are taken, with modification, from the NOAA Tropical Prediction Center's database. The radial distribution of the vortex pressure field, which mainly determines the radius of max wind, is one of the storm input variables and is incorporated using a pressure profile fit to available surface observations and aircraft reconnaissance data. Surface winds generated from the model are then imported into a graphical interface called WindWorkstation (WWS) at 6-hourly intervals and evaluated against available surface data and aircraft reconnaissance wind observations adjusted to the surface as described by Powell and Black (1989). The whole process is iterated until a solution for the surface wind fields that is most consistent with all of the available data is achieved. The final wind field is this best fit model solution.

2.5.2 Extratropical Wind and Pressure

OCTI/OWI also developed wind fields for extratropical storm events using data assimilation methods. Barometric pressure fields for extratropical events were taken directly from NOAA's NCEP (National Centers for Environmental Prediction) database (www.ncep.noaa.gov). The wind fields were delivered on the same grid domain and spacing as the tropical storms, but with a temporal resolution of 3-hours. The difference is that outside this grid and for the domain covering the entire North Atlantic Ocean, wind fields from the NOAA/NCEP Global Reanalysis Project (NRA) were interpolated in space and time and delivered at 3-hourly resolution on a grid of spacing 0.625° latitude by 0.833° longitude. For extratropical storms and within the fine resolution domain, the wind fields were developed by OWI's Interactive Kinematic Objective Analysis (IOKA) method. The benefits of IOKA enhancement to the skill of ocean response modeling over wind fields produced by strictly automated methods for extratropical storms are well established (e.g., Cardone et al., 1995). The method starts from a first-guess "background" wind field and then proceeds to assimilate observations of surface winds from ships, buoys, coastal stations, and remote sensing sources. The analyst interactively affects and controls the analysis on the WWS and may impose the constraints of a classical kinematic analysis. For storms within the NRA period, the background winds

are taken from the AES40 (Swail and Cox, 1999) hindcast. However, if the extratropical storm occurred within the decade of the 1980s or 1990s the background winds are specified at 0.25 degree and 3-hourly resolution from wind fields produced by OWI in support of the ERDC CHL WIS update study (made available to this project with permission of WES/ERDC, Vicksburg). As a part of the quality control process, the final winds were compared to measured winds from NOAA NDBC data buoys within the areas of interest, mainly buoy #44025 located just south of Shinnecock Inlet (OCTI/OWI, 2002). These comparisons are presented in Chapter 5.

2.6 WISWAVE – Offshore Wave Fields

In an effort to determine extreme storm wave conditions during the training set of 36 storms (14 tropical and 22 extratropical), a directional spectral, temporally sensitive wave model WAVAD (also known as WISWAVE) was applied.

2.6.1 Model Input and Output Parameters

The wave model was driven by the wind fields developed for the wind hindcast, described in Chapter 2.5. The wind fields were interpolated onto the wave grid domains for each level of nesting. Input parameters for the model included the model time step, (30 seconds for the finest grid), the 15 wave frequencies over which the wave spectrum was computed (0.03 to 0.31 Hz with an increment of 0.02 Hz), and the discretization increment for the directional spectrum (22.5 degrees). Output included bulk parameters (zero-moment wave height, peak wave period, peak wave direction) and full two-dimensional wave spectra. Storm simulations were reported at output locations on an hourly basis.

2.6.2 Computational Grid

Open ocean bathymetry was obtained from NOAA nautical charts, with the New York Bight area resolved from chart 12300, “Approaches to New York” and from chart 12352, “Shinnecock Bay to East Rockaway Inlet.” Five levels of nesting were used to generate the wave data:

- A 1.0-degree grid extending from 50 degrees to 80 degrees west longitude and from 20 to 45 degrees north latitude.
- A 0.25-degree grid extending from 67.75 degrees to 74.25 degrees west longitude and from 36.75 to 42.25 degrees north latitude.
- A 0.08333-degree grid extending from 69.50 degrees to 74.083 degrees west longitude and from 40.1666 to 41.3333 degrees north latitude (Figure 2-11).
- A 0.01667-degree (approximately 1 nautical mile) grid extending from 70.750 degrees to 74.083 degrees west longitude and from 40.417 degrees to 41.000 degrees north latitude (Figure 2-11).
- A 0.008333-degree (approximately 0.5 nautical mile) grid extending from 72.08333 degrees to 73.5000 degrees west longitude and from 40.500 degrees to 40.833 degrees north latitude (Figure 2-11).

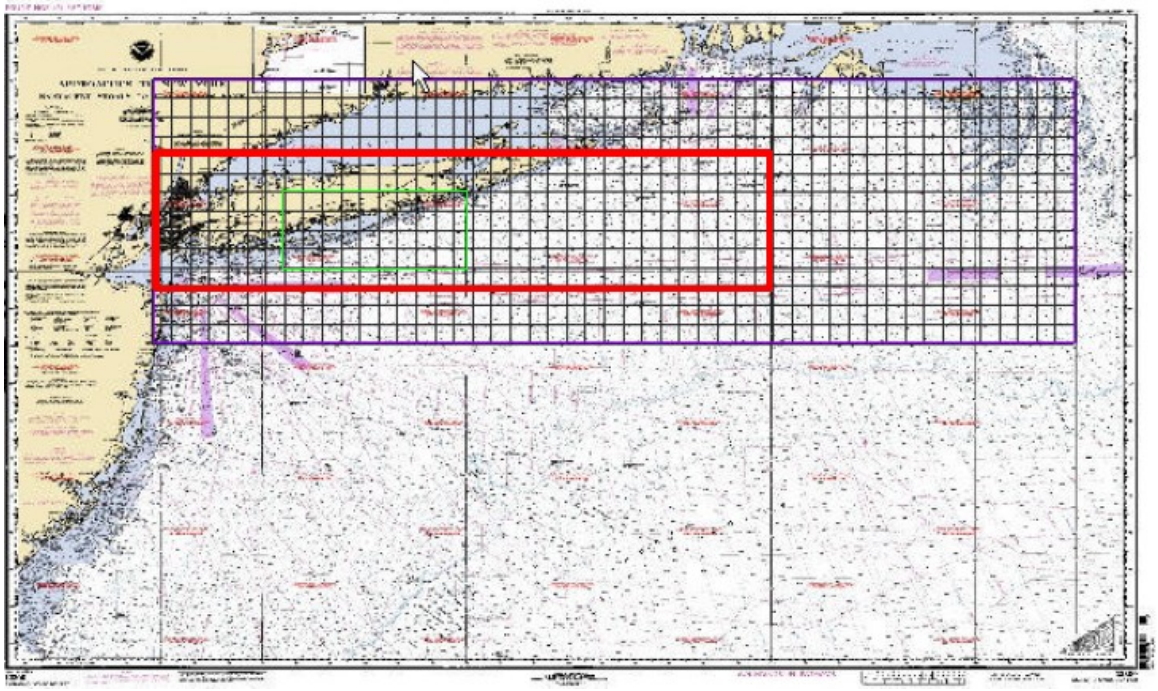

Figure 2-11: Map depicting the 5-min model grid. (The red box bounds the area modeled at 1-min resolution. The green box bounds the area modeled at 0.5 –min resolution.)

2.7 ADCIRC – Nearshore Water Levels

Ocean and nearshore, outside the surf zone, storm water levels are simulated with ADCIRC Version 43.02 (ADvanced CIRculation model; Luettich *et al*., 1992). ADCIRC is a long-wave hydrodynamic numerical model that simulates water surface elevations and currents from astronomic tides, wind, and barometric pressure. ADCIRC solves the two-dimensional, depth-integrated momentum and continuity equations on a finite element grid in spherical coordinates.

2.7.1 Computational Grid

For the FIMP study, the numerical grid covers a large computational domain, spanning the northeastern Atlantic Ocean, to fully capture large-scale wind and pressure effects during storm events (Figure 2-12). In addition, the numerical grid has high resolution at inshore areas, such as the tidal inlets and bays, to fully capture the complexity of the hydrodynamics in these areas. The subaerial portions of the barrier islands are not included in the computational domain. Instead the shorelines are represented with shoreline boundary conditions. In total, the computational domain includes 44329 nodes. Model bathymetry is based on several data sources. At the three FIMP tidal inlets and in Shinnecock Bay, recent high-resolution SHOALS LIDAR or multibeam survey data was used. In Moriches and Great South Bays and in the nearshore areas of FIMP, data from

the GEODAS (GEOphysical DAta System) database, supplemented with data provided on NOAA charts, was employed. In all other areas, the bathymetry is based on that compiled for developing the East Coast 2001 Tidal Constituents Database (Mukai et al., 2002). This data set was developed using the ETOPO5, Digital Nautical Charts, and National Ocean Service raw sounding databases.

2.7.2 Model Forcing

The ADCIRC model is forced:

- On its offshore boundaries with astronomic tidal constituents from the ADCIRC East Coast 2001 Tidal Constituent Database for seven main tidal constituents (Mukai et al., 2002; Table 2-6).
- Throughout the computational domain with simulated wind and barometric pressure fields (see Chapter 2.5).

2.7.3 Model Setup

For each storm simulation, time series of simulated water level are output from the model every 6 minutes (real-time) at 42 of the 80 reporting stations for stage-frequency analyses (see Figure 2-7 through Figure 2-10). The remaining 38 stations are outside of the FIMP project boundaries and were included for the benefit of other New York District projects. In addition, time series are recorded at 8 stations approximately 2.25 miles (3.6 km) offshore of the FIMP area at an approximate depth of 65 ft (20 m). These 8 stations are used to force subsequent SBEACH and Delft3D simulations.

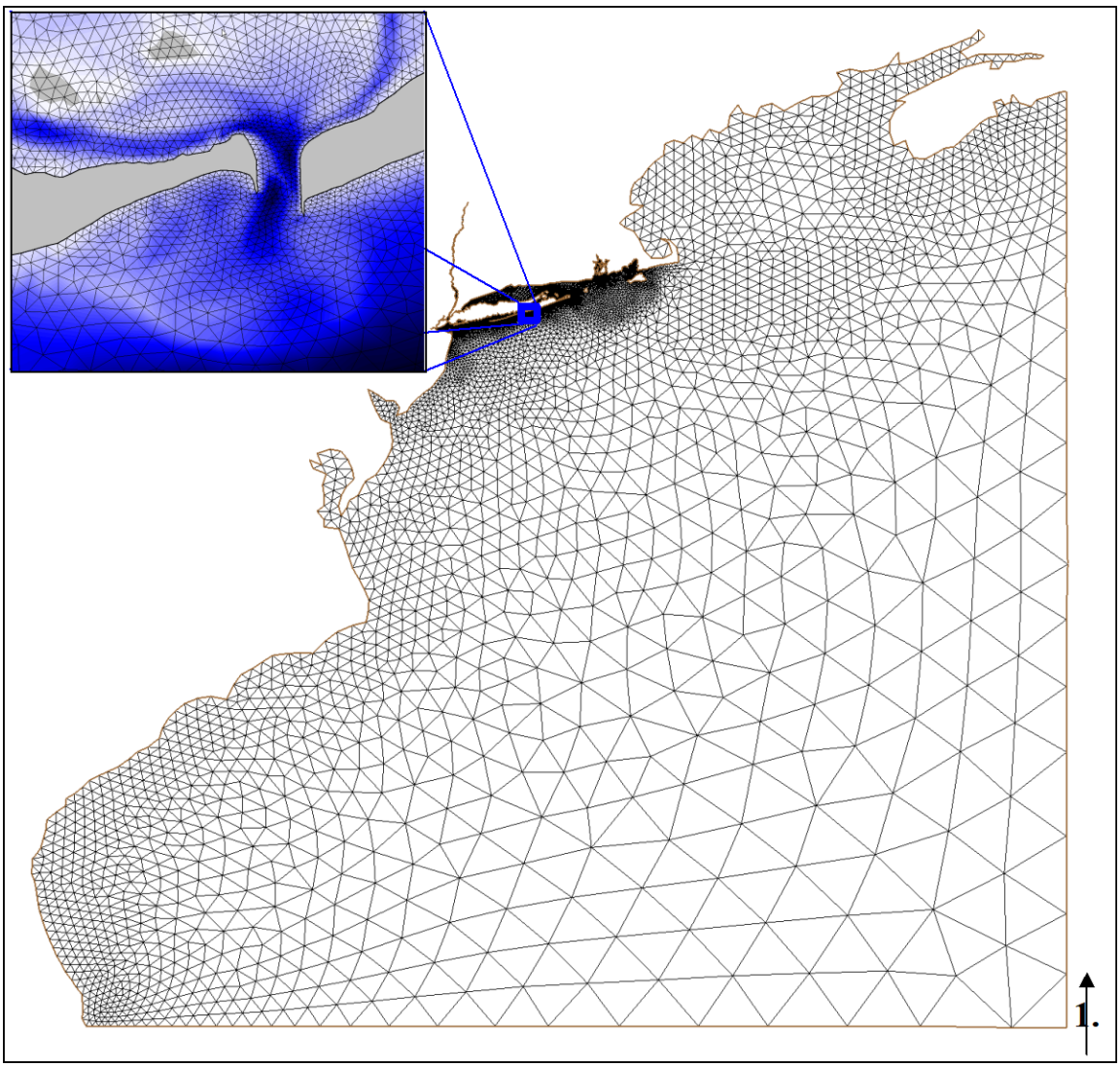

Figure 2-12: ADCIRC computational domain (insert illustrates higher resolution inshore at Shinnecock Inlet).

Table 2-6: Astronomic tidal constituents.

Tidal Constituent	NOAA Measured Amplitude (ft (m))	
	Sandy Hook, NJ (west of FIMP)	Montauk Fort Pond, NY (eastern FIMP)
M2	2.258 (0.688)	0.992 (0.302)
N2	0.518 (0.158)	0.260 (0.079)
S2	0.438 (0.134)	0.213 (0.065)
K2	0.126 (0.038)	0.061 (0.019)
K1	0.338 (0.103)	0.244 (0.074)
O1	0.176 (0.054)	0.176 (0.054)
Q1	0.037 (0.011)	0.049 (0.015)

2.8 SBEACH – Pre-inundation Dune Lowering and Ocean Wave Setup

2.8.1 Pre-inundation Dune Lowering

The SBEACH (**S**torm-induced **BEA**ch **CH**ange) model was used to estimate pre-inundation dune lowering along the study area. The overall objective of this modeling task was to estimate changes in existing barrier island topography prior to inundation. These estimates are required to pre-condition the Delft3D-MOR topography grid to account for wave runup and overtopping processes not included in that modeling technology and to improve estimates related to overwash processes and potential barrier island breaching. Dune lowering is caused by wave runup and overtopping of waves in conjunction with storm-elevated water levels and encroaching on the more vulnerable dunes, causing collapse and/or landward retreat of the dune crest. Lowering of dune crests results in increased risk of profile inundation and potential for breaching. All vulnerable sections (those areas where overtopping and breaching are considered possible) of the study area were modeled. Recent high-resolution LIDAR surveys provided subaerial profiles in nine identified vulnerable areas (Table 2-2). LIDAR profiles were coupled with updated submerged profiles derived from repeated conventional surveys along established ACNYMP profile lines over the period April 1995 through March 2002. Additional detail on the methodology is provided in the following paragraphs.

SBEACH (Larson and Kraus 1989a; Larson, Kraus, and Byrnes 1990) is a numerical simulation model for predicting beach, berm, and dune erosion due to storm waves and water levels. A basic assumption of the SBEACH model is that profile change is produced solely by cross-shore processes, resulting in a redistribution of sediment across the profile with no net gain or loss of material. Longshore transport processes are assumed to be uniform and therefore can be neglected in the calculation of beach profile change. These assumptions are expected to be valid for short-term storm-induced profile responses on open coasts sufficiently removed from the influence of tidal inlets and coastal structures. SBEACH was initially formulated using data from prototype-scale laboratory experiments and further developed and verified based on field measurements and sensitivity testing from four sites (CHL's Field Research Facility (FRF) at Duck, North Carolina; Manasquan and Point Pleasant Beach, New Jersey; and Torrey Pines, California).

SBEACH is an empirically-based model of beach profile change developed to replicate dynamics of dune and berm erosion using standard data (topography, beach profiles, etc.) available in most engineering applications. In model simulations, the beach profile progresses to an equilibrium state as a function of the initial profile condition (including median grain size and shoreward boundary conditions) and storm conditions (wave height, period, and direction; wind speed and direction; and water level). The model predicts profile response to storms including wave over-topping and dune lowering (Kraus and Wise 1993, Wise and Kraus 1993). Model improvements including the implementation of a random wave model for wave transformation and sediment transport and the dune overwash algorithm are documented in SBEACH Report 4 (Wise, Smith,

and Larson 1996) together with extensive model validation with data collected in both the laboratory and the field.

SBEACH simulations were performed for all LIDAR profiles from the nine vulnerable areas (see Chapter 2.1.2) and a set of storms identified as capable of producing inundation (when tide plus surge plus wave setup exceeds the remnant dune crest elevation) for at least one profile. Storms consisted of 36 historical events, both tropical and extratropical storms, and 21 variations of historical events to account for alternate astronomical tide occurrences. Selection of the storm training set is discussed in Chapter 2.2. Dune crest elevation change just prior to inundation was extracted from the SBEACH simulation results to identify most vulnerable profile behavior and to pre-condition the Delft3D-MOR topography grid to improve estimates of potential breaching and overwash processes. Following inundation, the Delft3D model simulates the overwash and breaching processes. For profile and storm combinations in which inundation was not predicted, dune crest elevation change at the end of the simulation was extracted. Figure 2-13 shows an example of initial and final profile from SBEACH simulation of a severe tropical storm. Dune volume change between the initial and final SBEACH profiles was also extracted and evaluated. The procedure for calculating dune volume change was the same as used in an earlier phase of the FIMP study to produce response vectors for EST analysis, including eroded volume above 0 ft NGVD and eroded volume above 9.8 ft (+3 m) NGVD.

The LIDAR profiles provide a wide range of profile characteristics within the vulnerable areas. Thus, the SBEACH results indicate the range of responses that could be expected in each area and help to identify a most vulnerable section in each vulnerable area. Profile vulnerability to inundation was found to depend on a combined effect of dune crest elevation, dune crest distance from the shore, and dune volume. For example, dune crest elevations and distance from shore for the 57 LIDAR profiles at Tiana Beach are shown in Figure 2-14 and Figure 2-15 respectively. Profiles which experienced inundation in at least one storm are circled in red. Most inundated profiles have dune crest elevations less than 15 ft. Exceptions (inundation cases with dune crest elevation higher than 15 ft and non-inundation cases with dune crest elevation lower than 15 ft) can be explained with consideration of dune crest distance from shore (berm width) and/or dune volume.

2.8.2 Ocean Wave Setup

To assess oceanfront damages, the SBEACH model was applied representative profiles for all 36 historical events. This effort will be detailed in a subsequent report. However, the application of SBEACH for this purpose will be summarized here since ocean wave setup computed with SBEACH contributes to the total water level for subsequent economic analyses.

Ocean wave setup is an important physical process for simulating storm water level and barrier island morphology during storm events. The additional contribution to total water

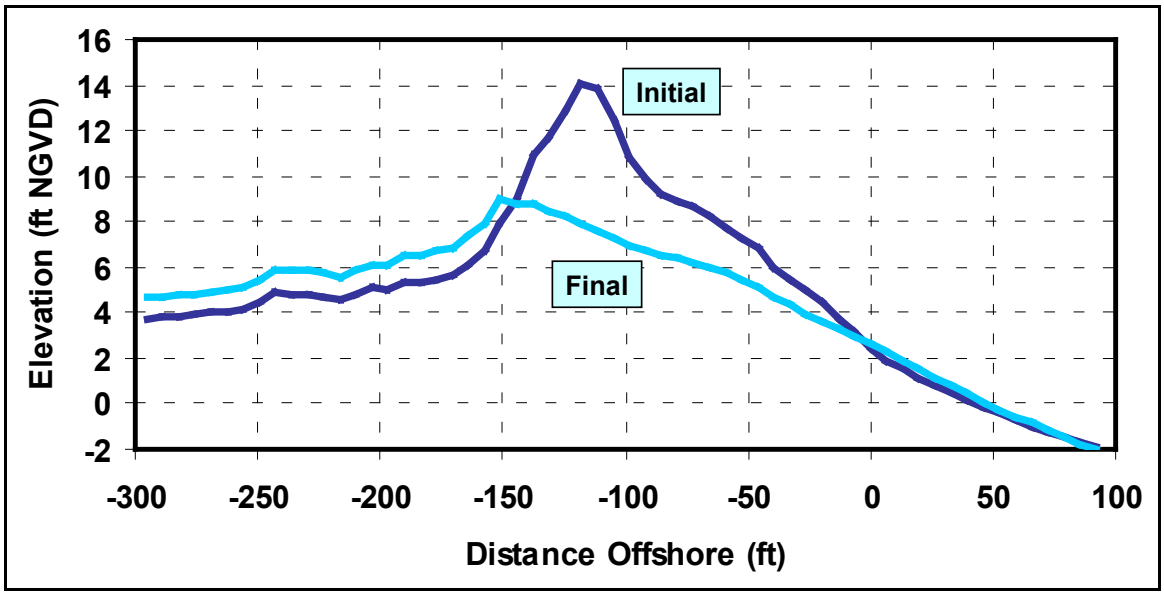

Figure 2-13: Initial and final Tiana Beach LIDAR profile #35 from SBEACH simulation of Sep 60 hurricane.

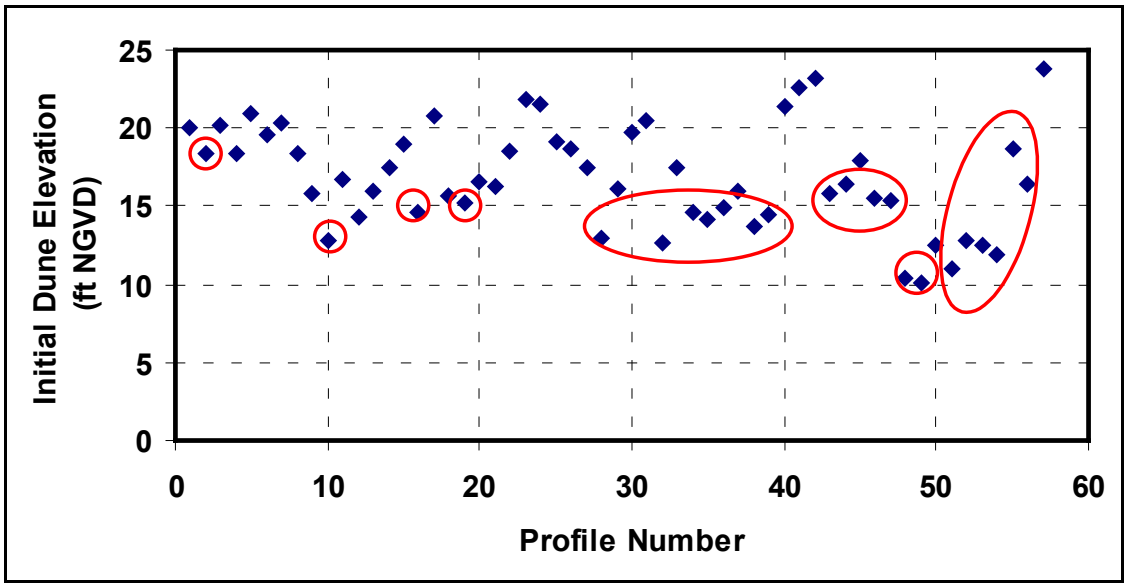

Figure 2-14: Initial dune crest elevation for Tiana Beach LIDAR profiles; circles identify profiles inundated in at least one storm.

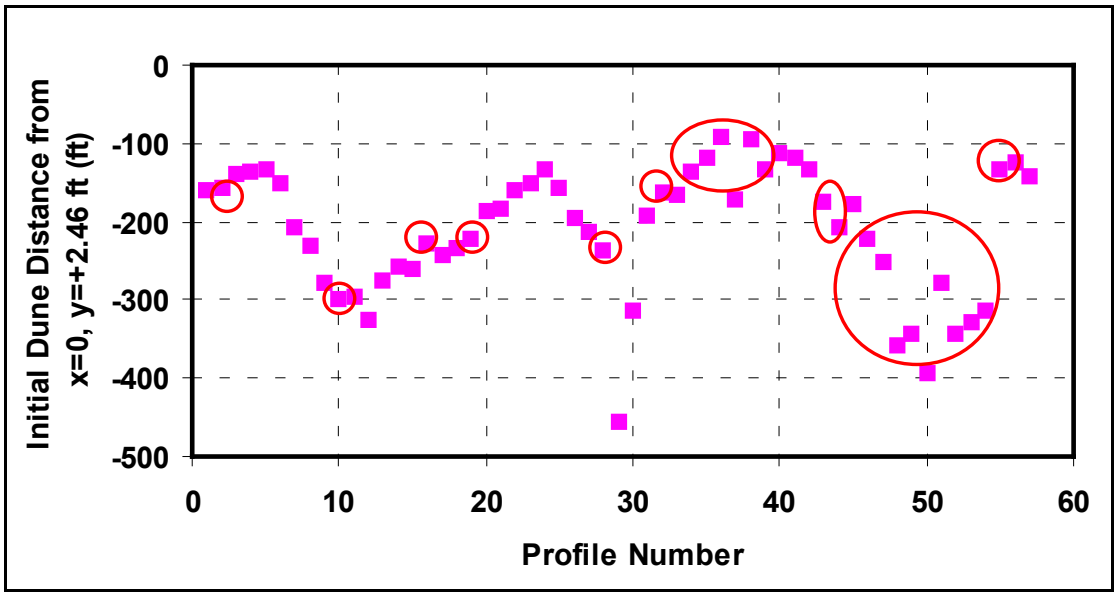

Figure 2-15: Initial dune distance from shore for Tiana Beach LIDAR profiles; circles identify profiles inundated in at least one storm.

level at the shoreline from wave setup is on the order of 20% of the nearshore wave height. This additional contribution is sizable for major storms impacting the south shore of Long Island.

For FIMP, ocean wave setup was computed using two methods: SBEACH and Delft3D. In SBEACH, detailed cross-shore resolution allows an accurate depiction of wave setup across the surf zone. In Delft3D, the two-dimensional HISWA wave model and hydrodynamic model allow accurate depiction of the two-dimensional distribution of wave setup and its impacts on nearshore circulation and barrier island morphology. The HISWA model is described in the following section.

While SBEACH simulations for baseline conditions profile response will be presented in a separate report, a summary of ocean wave setup findings from the SBEACH simulations for dune lowering are presented here because wave setup is a sizable total water level contribution.

SBEACH employs a random wave modeling approach developed by Larson (1995), and this approach is detailed in USACE (1996). The random wave model applies a technique similar to Monte Carlo simulation but uses statistical relationships such that only one representative wave height is required. The representative wave is transformed across shore, and the statistical relationships determine the fractions of the random wave field that break or reform. In SBEACH, the sea is assumed to be narrow-banded in both frequency and direction, and surf-zone wave decay follows Dally et al. (1985). Finally, SBEACH solves for wave setup by using the cross-shore momentum equation and linear theory to find radiation stress.

Variation of Wave Setup Alongshore

Because wave setup varies with profile shape, the peak wave setup at the instantaneous shoreline for a particular storm varies with alongshore location. As such, two values of wave setup will be presented for discussion: nearshore and shoreline (Figure 2-16). The nearshore wave setup value represents the cross-shore location for which little variation, due to profile shape, in wave setup alongshore is observed from the SBEACH results. As shown on the figure, this nearshore location is just seaward of the berm. The shoreline wave setup value indicates the peak wave setup at the instantaneous shoreline. This shoreline value varies somewhat from profile to profile.

Wave Setup Simulations for Major Historic Storms

To assess the influence of wave setup on total ocean water level, SBEACH simulations of wave setup for 10 major historic storms were analyzed. The historic storms considered here include five hurricanes and five Nor'easters:

Hurricanes
- September 1938
- September 1944
- September 1960 (Donna)
- June 1972 (Agnes)
- September 1985 (Gloria)

Nor'easters
- November 1950
- November 1953
- March 1962
- December 1992
- 9 March 1993

Wave setup information was extracted from the SBEACH simulations for the 252 profiles used to calculate pre-inundation dune lowering (see Chapter 2). For comparisons with ocean water level output stations, widely-spaced as shown in Figure 2-7 and Figure 2-9, the 252 more closely-spaced profiles were grouped based on proximity to stations 41 (Great South Beach), 23 (Great South Beach), 9 (Old Inlet), 28 (Moriches Inlet), and 35 (Shinnecock Inlet) (see Figure 2-8)[5]. At least 30 profiles are associated with each station.

Based on the profiles assigned to each station, mean nearshore and shoreline wave setup values were calculated for each storm. In addition, standard deviation in shoreline wave setup was calculated. Because the cross-shore location for extracting the nearshore wave setup value was such that variation was small, no standard deviation is presented here. Figure 2-17and Figure 2-21 show total water level contributions offshore (ADCIRC), wave setup at the nearshore location, and additional wave setup at the shoreline. The error bars on the figures represent one standard deviation around the mean setup result.

On average, ocean wave setup increases total water level at the nearshore location by 40 to 50 percent and at the instantaneous shoreline by 65 to 75 percent, relative to offshore (surge plus tide) water level. For the ten major storms presented, mean wave setup at the instantaneous shoreline is at least 3 feet at all stations. The most extreme hurricanes, September 1938 and September 1985 (Gloria), produce mean wave setup in excess of 4 feet at the instantaneous shoreline.

[5] Note that no vulnerable profiles are closest to station 31 (Post Lane).

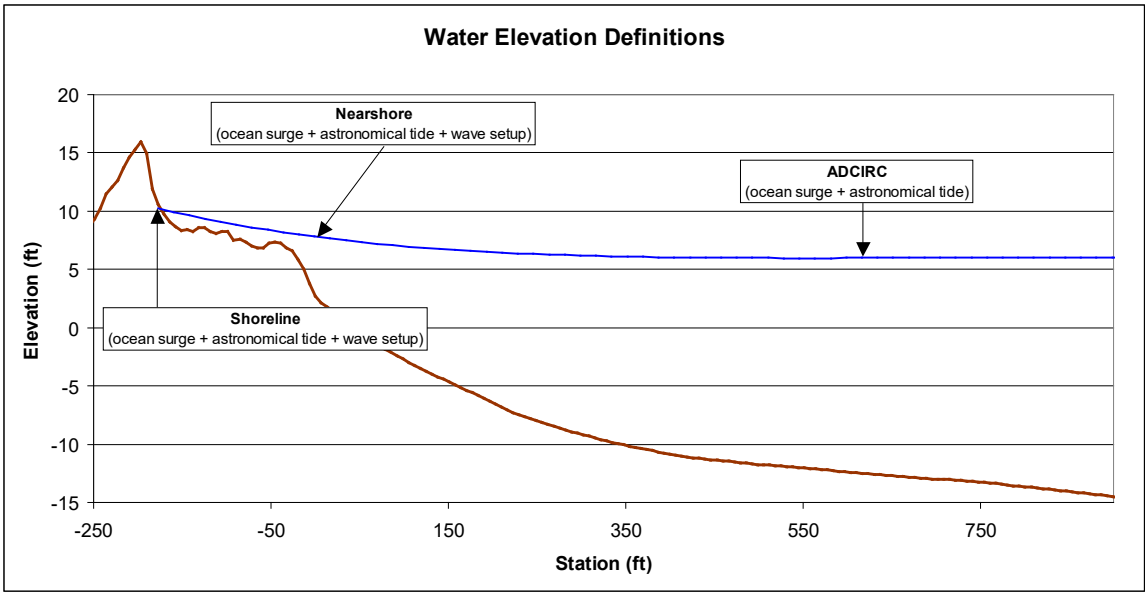

Figure 2-16. Definition of total water level at shoreline, nearshore, and offshore locations.

Impact of Ocean Wave Setup on FIMP Economic Analyses

In performing the assessment of economic damages along the oceanfront for FIMP, total water level from SBEACH life-cycle simulations will be used. Consequently, the values used for economic analyses will inherently include the influence of wave setup as computed at the instantaneous shoreline.

As discussed in Chapter 2, ADCIRC time series, representing ocean surge plus astronomical tide, and transformed WISWAVE wave parameter time series were input along the offshore boundary for all SBEACH simulations. Then, SBEACH was used to simulate total water level at the shoreline as the sum of ocean surge, astronomical tide and shoreline wave setup. These total water levels, including ocean surge, astronomical tide, and shoreline wave setup, are used to develop life-cycle simulations of total water level. It is these life cycles that are ultimately incorporated into the oceanfront economic analyses for FIMP.

Therefore, the influencing water level for oceanfront economic damage assessment is better reflected by the SBEACH-simulated total water levels than by the EST stage-frequency curves presented in Chapter 12, since these curves represent ocean surge and astronomical tide only. Figure 2-22 presents the EST stage-frequency relationship for station 9, Old Inlet, and illustrates this difference. Using the ADCIRC water levels, return periods were interpolated for each of the 10 storms presented in this Chapter. Superimposed on the stage-frequency relationship in Figure 2-22 are the total water levels, including nearshore (circles) and shoreline (stars) wave setup, plotted at each storm's corresponding return period. As this figure indicates, the total water level employed for economic analyses (stars) is 3.5 to 4.0 feet higher than the EST stage-frequency curve. Note that the superimposed individual storm results including wave

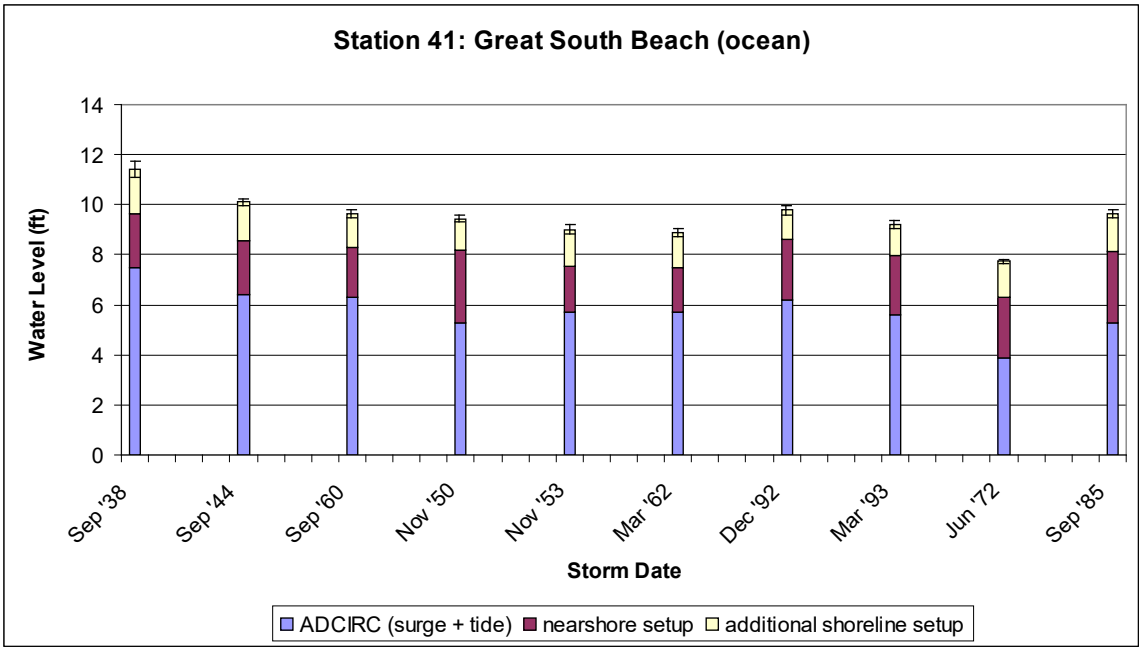

Figure 2-17. Simulated total water level contributions at Station 41.

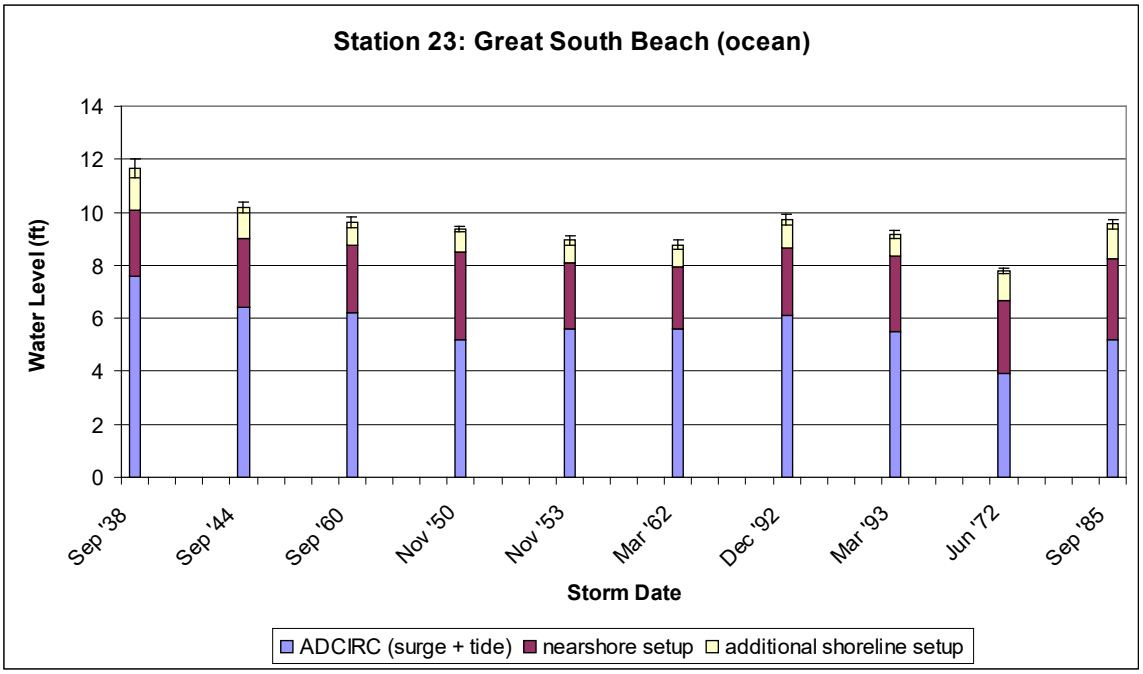

Figure 2-18. Simulated total water level contributions at Station 23.

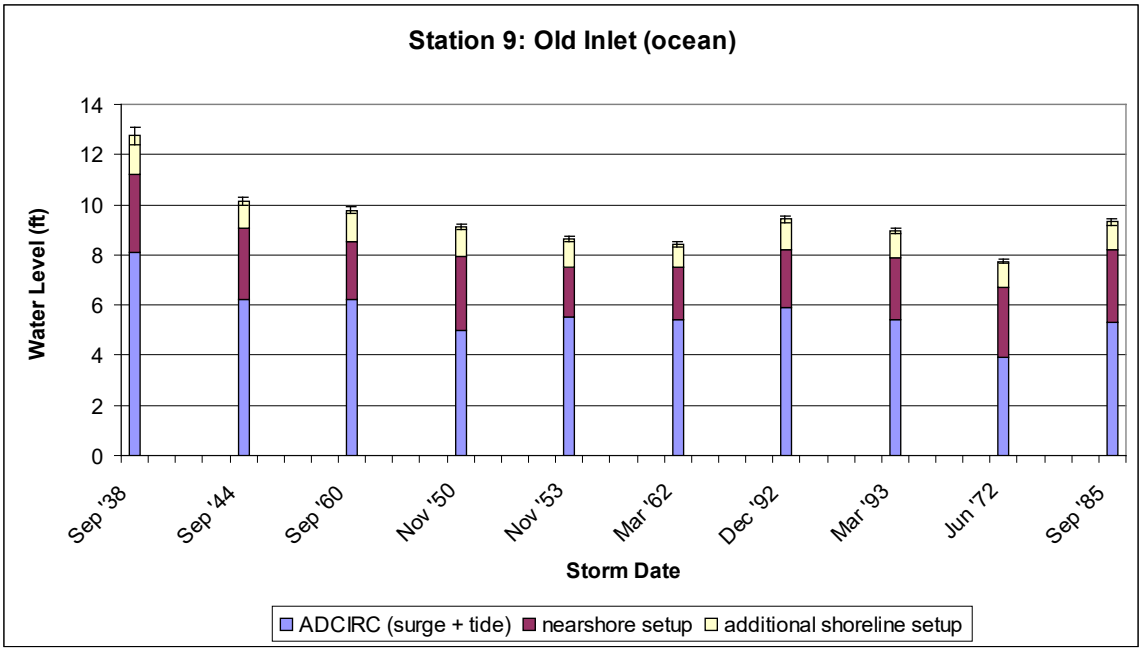

Figure 2-19. Simulated total water level contributions at Station 9.

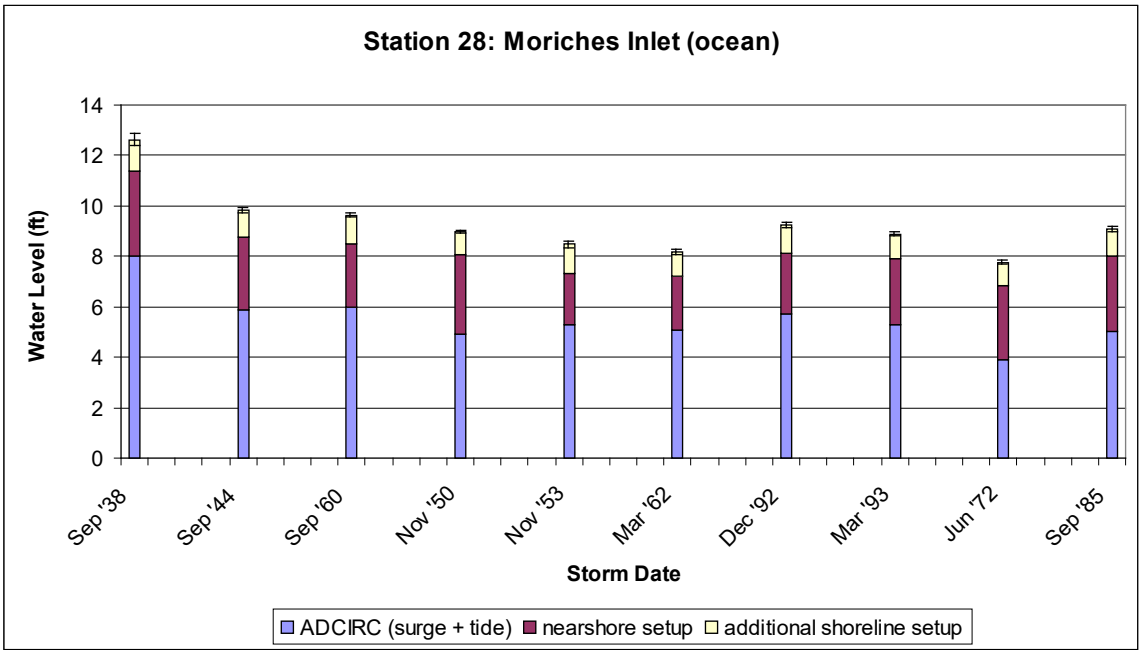

Figure 2-20. Simulated total water level contributions at Station 28.

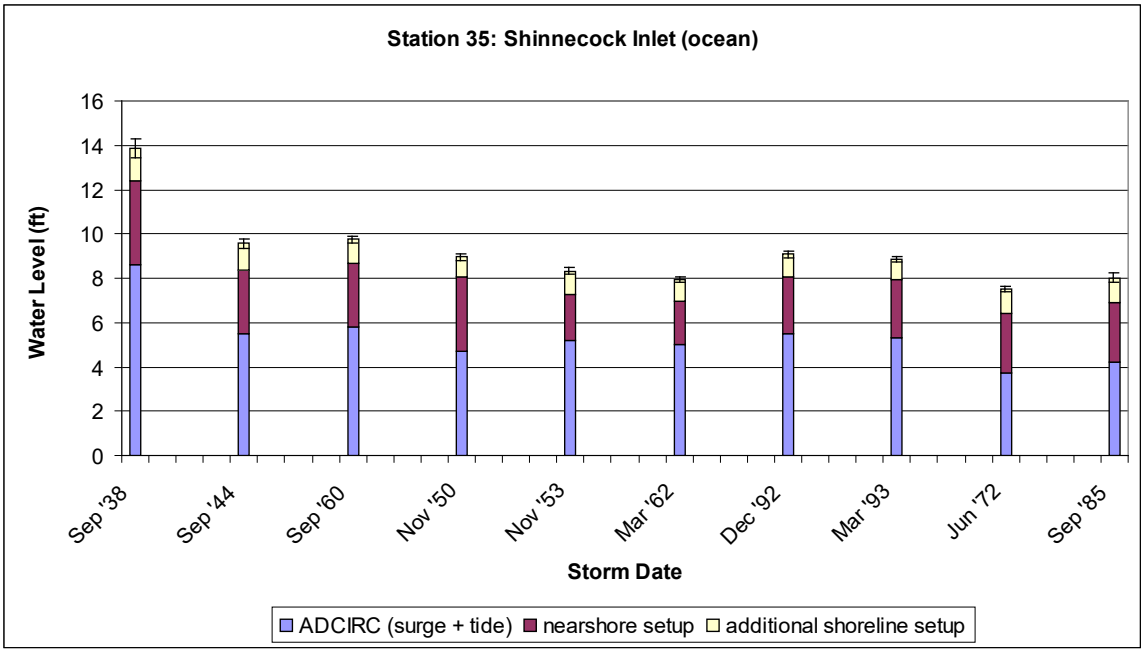

Figure 2-21. Simulated total water level contributions at Station 35.

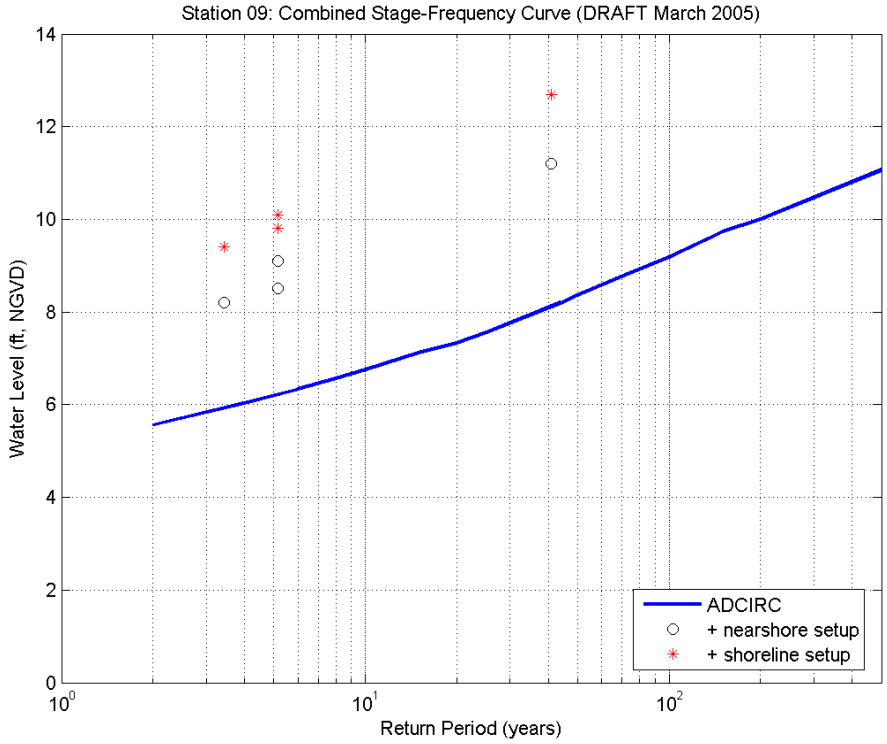

Figure 2-22. EST stage-frequency curve based on ocean surge and astronomical tide (solid line) with individual historic storm water level results that include the additional effects of wave setup. . Note that the superimposed individual historical storm results including wave setup presented here are for illustrative purposes only; they do not represent formal stage-frequency results.

setup in Figure 2-22 are for illustrative purposes only and that they do not represent formal stage-frequency results.

As the FIMP simulations illustrate, ocean wave setup is an important process for determining total water level at the shoreline. Ocean wave setup not only directly impacts the total water level at the ocean shoreline, but also influences morphological profile response, barrier island overwash, barrier island breaching, and water flow through the tidal inlets. Since the simulations presented above show that ocean wave setup increases total water level by as much as 75 percent, it is essential that this phenomenon be included throughout the surge modeling process, as described in Chapter 2, and in subsequent economic analyses.
An additional set of stage-frequency curves will be developed that include the contributions of wave setup to the total water level. These curves will be presented in a subsequent report.

2.9 Delft3D – Bay Water Levels and Bay Wave Setup

The activity presented in this section integrates the results from the previously presented wind, wave (WISWAVE), circulation (ADCIRC), and morphology (SBEACH) modeling efforts into a single numerical model to compute the bay water levels under storm conditions taking into account the contribution of storm surge, waves, winds and the contribution of overwash and/or breaching. Use of the Delft3D modeling suite allows fully-integrated, simultaneous simulation of wave fields, morphological change, and hydrodynamics. Capturing these phenomena in an integrated manner is necessary since storm-induced breaching and overwash historically occurred during a number of storm events included in the FIMP training set.

2.9.1 Numerical Model Description (Delft3D)

The Nearshore and Bay Water Level model of FIMP is a fully morphological model developed using the general Delft3D modeling system. The Delft3D system fully integrates the effects of waves, currents and sediment transport on morphological evolution. The different components of the Delft3D system applied in this study are presented in the following sections.

Hydrodynamic Model

The hydrodynamic module, Delft3D-FLOW, simulates two-dimensional (2D, depth averaged) or three-dimensional (3D) unsteady flow and transport phenomena resulting from tidal and/or meteorological forcing, including the effect of density differences due to a non-uniform temperature and salinity distribution (density-driven flow). This model can be used to predict the flow in shallow seas, coastal areas, estuaries, lagoons, rivers and lakes. Three-dimensional modeling is of particular interest in transport problems where the horizontal flow field shows significant variation in the vertical direction. This variation may be generated by wind forcing, bed stress, Coriolis force, bed topography, and/or density differences. When the fluid is vertically homogeneous, as is the case for this study, a depth-averaged approach is appropriate. In that case, Delft3D-FLOW is run

in two-dimensional mode (one computational layer), which corresponds to solving the depth-averaged equations.

Delft3D-FLOW solves the Navier Stokes equations for an incompressible fluid, under the shallow water and the Boussinesq assumptions. In the vertical momentum equation the vertical accelerations are neglected, which leads to the hydrostatic pressure equation. Delft3D-FLOW's system of equations consists of the horizontal equations of motion, the continuity equation, and the transport equations for conservative constituents. The equations are formulated in orthogonal curvilinear co-ordinates. In curvilinear co-ordinates the free surface level and bathymetry are related to a flat horizontal plane of reference. The flow is forced by water levels or velocities at the open boundaries, wind stress at the free water surface, and pressure gradients due to free surface gradients (barotropic) or density gradients (baroclinic). In addition, results from the wave model are included in Delft3D-FLOW resulting in a surf zone longshore current and a cross-shore set up generated by the variation in the radiation stresses and also an enhancement of the bed shear-stress. Source and sink terms may be included in the equations to model the discharge and withdrawal of water.

Sediment Transport model

Three-dimensional transport of suspended sediment is calculated in Delft3D by solving the three-dimensional advection-diffusion (mass-balance) equation for the suspended sediment. The local flow velocities and eddy diffusivities are based on the results of the hydrodynamic computations. Computationally, the three-dimensional transport of sediment is computed in exactly the same way as the transport of any other conservative constituent, such as salinity and heat. However, there are a number of important differences between sediment and other constituents, including the exchange of sediment between the bed and the flow and the settling velocity of sediment under the action of gravity. These additional processes for sediment are obviously of critical importance. Other processes such as the effect that sediment has on the local mixture density, and hence on turbulence damping, can also be taken into account. In addition, if a net flux of sediment from the bed to the flow, or vice versa, occurs then the resulting change in the bathymetry should influence subsequent hydrodynamic calculations. The formulation of several of these processes are sediment-type specific, this especially applies for sand and mud. The sediment transport computation of Delft3D allows the combined use of cohesive and non-cohesive sediment. For cohesive sediment fractions the fluxes between the water phase and the bed are calculated with the well-known Partheniades-Krone formulations (Partheniades, 1965). For the transport of non-cohesive sediment the Van Rijn (1993) formulation is used, which accounts for the effect of waves.

The elevation of the bed is dynamically updated at each computational time-step. This is one of the distinct advantages of the model as the hydrodynamic flow calculations are always carried out using the correct bathymetry. At each time-step, the change in the mass of bottom sediment that has occurred as a result of the sediment sink and source terms is calculated. This change in mass is then translated into a change in thickness of the bottom sediment layer using the density of the bed material. This change in thickness

is equivalent to a change in bed elevation, which is applied to the depth values stored at computational points.

The hydrodynamic model implementation used in the sediment transport and morphology model includes the effects of the waves on both nearshore hydrodynamics (i.e., longshore currents and wave setup) and sediment transport (i.e., increased bottom shear stresses and turbulence). It should be noted, however, that the model does not include all of the physics affecting beach profile changes during storm conditions, such as the three-dimensional wave and hydrodynamic processes that generate undertow and offshore sand transport. Nonetheless, this model implementation is particularly suitable for simulating barrier island inundation and sediment overwash processes.

HISWA Wave Model

The stationary wave model HISWA was used within the storm surge modeling framework to compute nearshore waves during the morphological simulations. HISWA (Holthuijsen et al., 1989) is a second generation wave model that computes wave propagation, wave generation by wind, non-linear wave-wave interactions and dissipation for a given bottom topography and stationary wind, water level and current field in waters of deep, intermediate and finite depth. The model accounts for the following physics: Wave refraction over a bottom of variable depth and/or spatially varying ambient current; depth and current induced shoaling; wave generation by wind; dissipation by depth-induced breaking and/or bottom friction; and wave blocking by strong counter currents. Since the model does not account for pure diffraction effects the wave field computed will generally not be accurate in the immediate vicinity of obstacles and in harbors.

HISWA is based on the action balance equation and wave propagation is based on linear wave theory (including the effect of currents). HISWA wave computations are carried out on a rectangular grid. The results obtained in this rectangular grid are automatically transferred to the hydrodynamic module, which simulates the flow on a curvilinear grid. Non-stationary conditions are simulated with HISWA as quasi-stationary with repeated model runs, i.e. as the flow model progresses in time a stationary wave computation is performed at intermediate time steps. Such stationary wave computations are usually considered to be acceptable since the travel time of the waves from the seaward boundary to the coast is mostly relatively small compared to the time scale of variations in incoming wave field, the wind or tidal induced variations in depth and currents.

The HISWA model also has a dynamic interaction with Delft3D-FLOW (i.e., two way wave-current interaction). By this the effect of waves on current (via forcing, enhanced turbulence and enhanced bed shear stress) and the effect of flow on waves (via set-up, current refraction and enhanced bottom friction) are accounted for if the HISWA model is applied within Delft3D.

Applicability of Delft3D to the Simulation of Breaches

The simulation of breaching using the Delft3D modeling system was validated by Van Kessel and Roelvink (2002) who presented a comparison between model simulations and

breaching data from laboratory experiments conducted by Visser (1998). The model skill was further assessed by comparing model results with available measurements from the 1994 field experiment at Zwin Channel (Visser, 1998).

Model Resolution

The Delft3D morphological model grid extents from 1.9 miles west of the East Rockaway Inlet to 4.3 miles east of Shinnecock Inlet. From East to West it includes Shinnecock Bay, Moriches Bay, Great South Bay, South Oyster Bay, East Bay, Middle Bay and Hempstead Bay. The model also includes Shinnecock, Moriches, Fire Island, Jones and East Rockaway inlets. The distance between the ocean shoreline and the offshore model boundary varies between 1.9 to 3.1 miles. The maximum depth at the offshore model boundary is on the order of 77 ft (23.5 m), offshore of Moriches Inlet. The minimum depth, on the order of 54 ft (16.5 m), is offshore of Jones Inlet.

An orthogonal curvilinear model grid was built for simulations when morphological changes of the barrier island are expected. The model grid has variable resolution throughout the domain. The cross-shore resolution varies from values of 50-65 ft (15-20 m) at the barrier island and the intertidal zone, to around 1,150 ft (350 m) at the offshore boundary. The typical model's longshore resolution is around 650-1,000 ft (200-300 m) in areas outside of those described in Table 2-2. Within the extent of the vulnerable areas, the longshore resolution is in the order of 82 ft (25 m). At Moriches and Shinnecock inlets the grid size is in the order of 100 ft (30 m) and it is in the order of 250 ft (75 m) at Fire Island Inlet. Figure 2-23 shows the extent of the grid and a detail of the grid at three locations (Old Inlet, Moriches Inlet and Shinnecock Inlet).

Low Resolution Grid

An additional reduced resolution grid was developed and used for cases were no inundation occurs according to SBEACH simulations. The grid has the same resolution at the inlets as the one previously described but it lacks high resolution at the vulnerable areas. This grid was used in the comparison of ADCIRC and Delft3D results. Results from these comparisons are presented in Chapter 5.2.

Sensitivity to Grid Size

In order to test the sensitivity of the model prediction of peak water levels in the bays to grid resolution, two model grids with varying degrees of resolution in the vicinity of Old Inlet were developed. The rest of the model grid is based on the previously defined low resolution grid only with high resolution at the inlets. The cross-shore resolution is in the order of 50-65 ft (15-20 m) for both model grids which is the same grid size used in the low resolution grid. The grid size in the longshore direction over the potential breach area is 5 and 25 m (16 and 82 ft) for the two cases considered. The largest storm available from the historical set of storms, the September 1938 Hurricane, was simulated using both grids. Differences obtained for this storm are the largest differences that are expected from any storm of the historical set. Table 2-7 present differences in peak water level observed during the simulation using the two different grid resolutions. The locations were the differences have been computed are presented in Figure 2-7 through Figure 2-9.

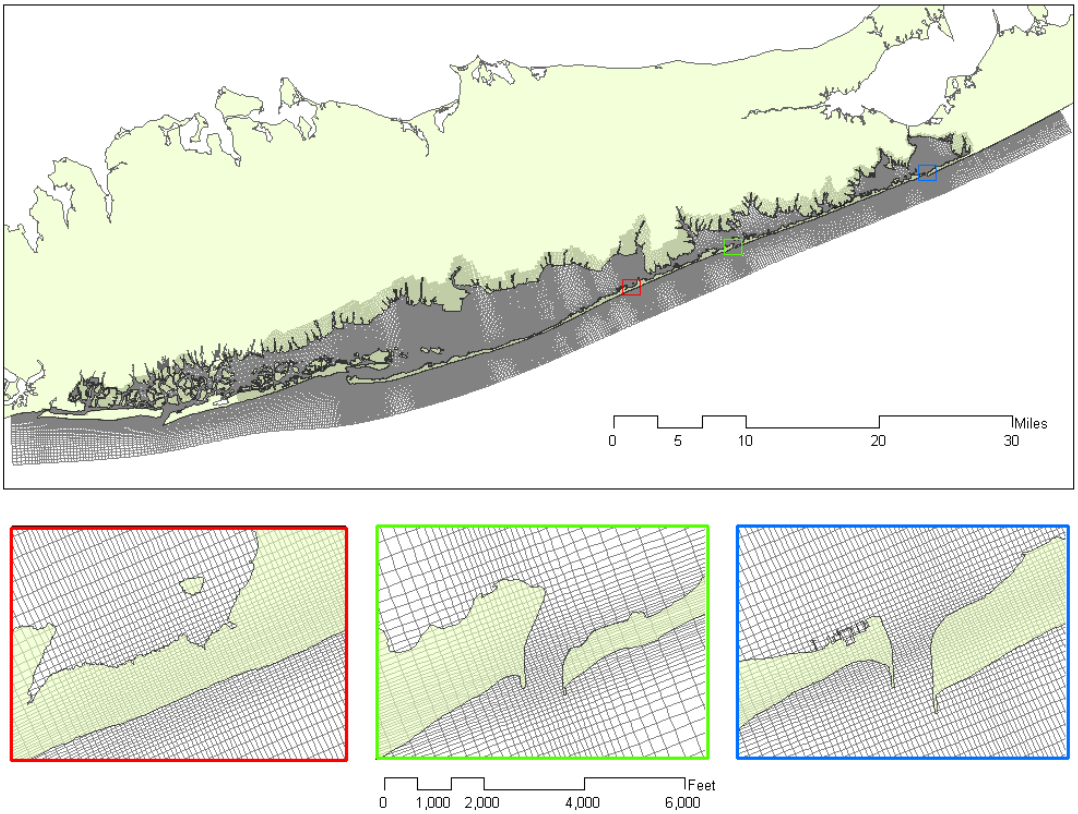

Figure 2-23: Hydrodynamic and sediment transport model grid.

Table 2-7: Sensitivity to grid size resolution. Differences in peak water level between 25 and 5 m resolution grids (inches).

	St.8	St.25	St.10	St.24	St.21	St.22	St.20	St.26
Difference	1.40	1.26	0.73	1.34	1.35	1.27	1.69	0.64

Results indicate that the 25 m grid generates a peak surge in the bay higher than the one produced by the 5 m grid. The largest difference observed is in the order 1.69" in Station 20. This sensitivity tests indicates that in our study the contribution of a breach to peak water levels in the bays is copmparably simulated with a 25 m grid size and that no significant improvement would be achieved using smaller grid size.

Wave Model Grids

Offshore wave conditions calculated from WISWAVE (see Chapter 2.6) are transformed to the nearshore in the morphological model using the HISWA model. HISWA also provides the values of the radiation stresses that are used in the hydrodynamic and sediment transport models to compute the longshore current, wave generated setup and bed shear stress enhancement. HISWA simulates the waves in a rectangular grid oriented to the mean wave direction.

A regional wave grid (See Figure 2-24) extending from Rockaway Inlet to Montauk Point was used. The grid is oriented approximately parallel to the ocean shoreline and has a grid size of 164 ft (50 m) in the cross-shore direction and 820 ft (250 m) in the longshore direction. Wave input conditions (significant wave height, peak wave period and mean wave direction) obtained from WISWAVE simulations are prescribed at 12 points along the offshore boundary of the regional model.

In order to have a good description of the nearshore processes and the wave propagation through the inlets two sets of nested grids with higher resolution were also developed. First, two local grids with a resolution of 82 ft (25m) and 32 ft (10 m) in the longshore and cross-shore directions respectively were developed along nearshore areas fronting Shinnecock, Moriches and Great South bays. Figure 2-24 shows the extents of these local grids. Results from the regional grid are used as boundary conditions for the local grids. Finally, three additional grids were defined at Shinnecock, Moriches and Fire Island inlets with a resolution of 64 ft (20 m) and 32 ft (10 m) in the longshore and cross-shore directions. The additional grids at the three inlets were necessary to optimize wave model performance related to the orientation of the inlets relative to wave propagation direction. These grids are forced by results from the local grids. Figure 2-24 shows the location of the inlet grids.

Wave model parameters were calibrated as part of a separate FIMP study task (Moffatt and Nichol, 2005) using a slightly different grid configuration. The same model parameters were used for this study.

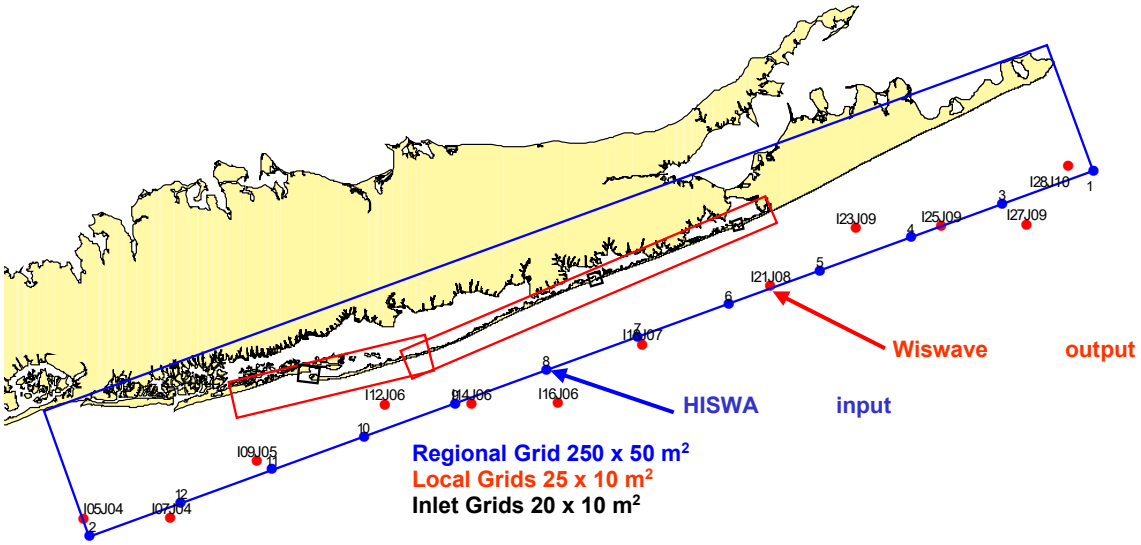

Figure 2-24: Model wave grids.

2.9.2 Description of Model Inputs

Hydrodynamic (tide+surge) data, offshore wave data, and spatial wind speed and pressure fields for each storm in the historic dataset were provided by NAN as input to the Delft3D model. All data was transformed to the Delft3D format using a set of computer programs specifically developed for this effort.

Water Levels from ADCIRC

Water levels at the offshore boundaries were obtained from ADCIRC runs as provided by NAN (see Chapter 2.7). The water level was prescribed at two lateral and seven offshore boundaries in Delft3D, which automatically interpolates the water levels at the intermediate grid points. A computer program was developed to read ADCIRC output files for each storm and generate water level boundary conditions in Delft3D format.

Wind from Oceanweather

Wind speed and pressure were interpolated from the Oceanweather wind fields (see Chapter 2.5) into the Delft3D model grids. The model drag coefficient was defined following a similar formulation to the one applied in ADCIRC. For wind speeds between 0 and 42.5 mph (19 m/s) the drag coefficient is interpolated between 0.00085 and 0.00190. A value of the drag coefficient equal to 0.00190 is applied for wind speeds higher than 42.5 mph (19 m/s). This is consistent to the wind drag treatment for ADCIRC simulations.

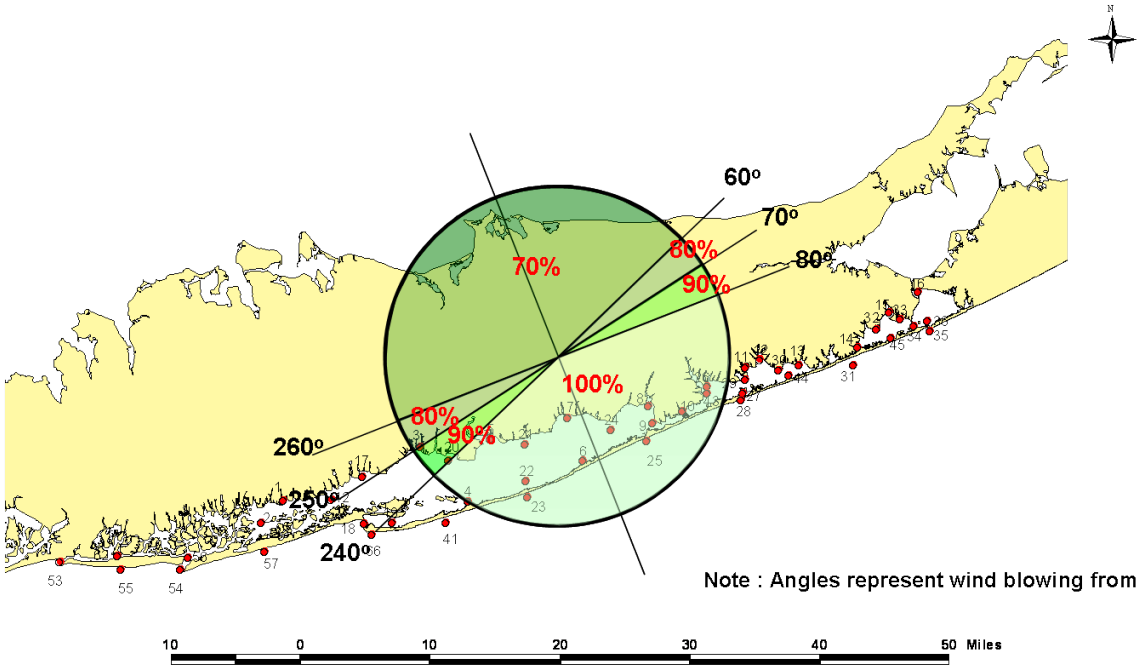

Figure 2-25: Wind speed correction as a function of wind direction.

Since the Oceanweather wind field products do not account for overland effects, they tend to overestimate wind speed for offshore-directed winds, as confirmed by comparisons between the Oceanweather wind fields and measurements made at Shinnecock Inlet and at Islip (Figure 2-26). These findings support comments made by CHL during their review of the Oceanweather wind products (Resio, April 2003). As such, a 30% reduction in all offshore-directed winds was applied to the Oceanweather wind fields for the validation period as well as for every storm of the historical set. The 30% reduction is reasonable approximation of overland effects, as discussed in Resio (April 2003) and demonstrated in Figure 2-26. This correction includes a smooth transition of the wind speed reduction, as shown in Figure 2-25. The reduced wind field better matches the measured wind speed at both Shinnecock Inlet and Islip for the validation period. In addition and for the same period, using this wind speed reduction in the Delft3D model dramatically improves hydrograph shape comparison between measured and simulated results in Great South Bay. In particular, predictions of localized bay wind setup and setdown are improved, as shown in Chapter 7.

Waves from WISWAVE

Values of significant wave height, peak period and mean wave direction were provided for each storm at 12 points offshore from WISWAVE simulations. These points are approximately located along the offshore boundary of the Delft3D regional wave grid. This grid covers the area from the East Rockaway Inlet to Montauk Point. The resolution of this grid is 250 m in the longshore by 50 m in the cross-shore.

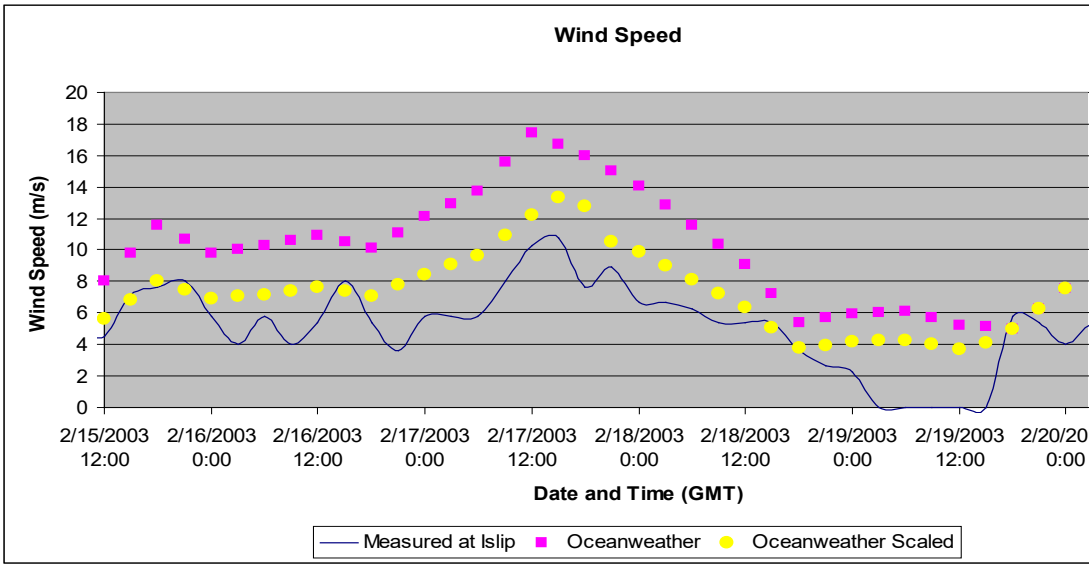

Figure 2-26. Measured wind speed, Oceanweather wind speed, and scaled Oceanweather wind speed in February 2003.

Dune Lowering from SBEACH

Preliminary study findings and recommendations from the Technical Review Panel (TRP) led to the selection of a method for the calculation of the initial dune lowering based on SBEACH. "Initial" refers to the lowering due to wave runup prior to dune inundation as the total water level (tide, plus surge, plus wave setup) exceeds the dune crest elevation. When inundation occurs the "standard" flow and sediment transport model in Delft3D takes over and simulates any additional dune lowering in the same way as it computes sediment transport for any submerged portion of the model. Two main variables obtained from SBEACH can be used in the Delft3D simulations: the overtopping discharge and the dune lowering prior to inundation.

Overtopping Discharge

The term "overtopping" refers specifically to the intermittent volume of water that overtops the dune due to wave runup, while the total water level (tide + storm surge + wave setup) remains below the dune crest elevation. An analysis presented in a memorandum to USACE dated October 2, 2003 suggests that overtopping volumes are insignificant and result in only 0.03% to 1% of typical storm surge values in the bays. Based on this assessment it was considered that overtopping discharge (prior to inundation) be neglected in future FIMP Storm Surge Modeling efforts.

Estimates of Dune Lowering prior to Inundation using SBEACH

A total of 252 barrier island cross-sections (profiles) were extracted from the processed Fall 2000 LIDAR dataset at each of the areas identified as vulnerable to overwash/breaching. The number of profiles analyzed at each vulnerable area is presented in Table 2-2.

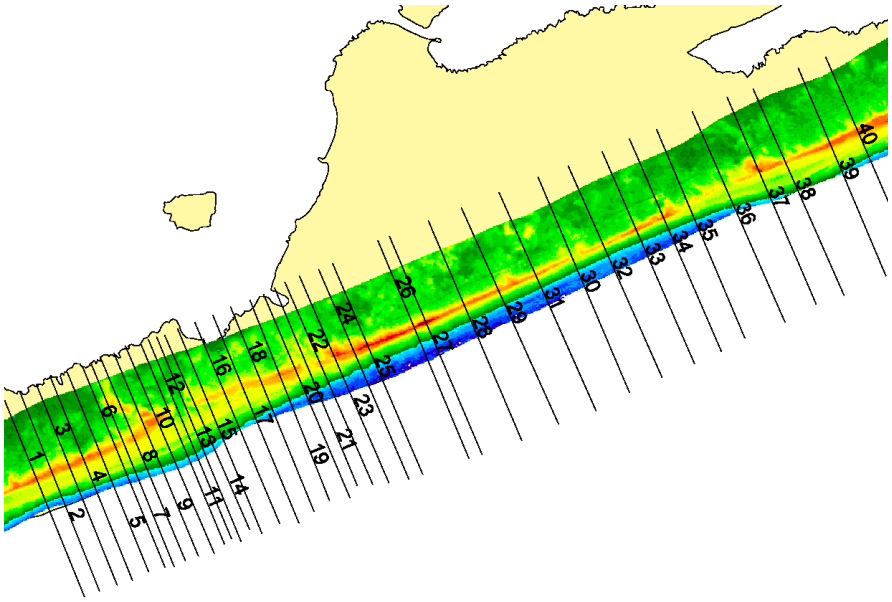

Figure 2-27: LIDAR data and location of extracted profiles at Old Inlet.

The profiles were selected to capture as well as possible the spatial variability of barrier island characteristics (e.g., dune height and width) within each vulnerable area. Figure 2-27 shows an example of the LIDAR 2000 data and representative profiles for the Old Inlet area.

As a first approach, subaerial raw LIDAR profiles were used by CHL to create a representative synthetic set of profiles (including sub-aqueous portion) for each vulnerable area. CHL then ran SBEACH for each set of profiles and each storm in the historical dataset and summarized the results in tables that were used to interpolate dune lowering values along the barrier island. The tables include dune lowering prior to inundation as a function of location, initial dune height, and storm.

An improved methodology was developed to improve the calculation of the dune lowering associated with each storm by better taking into account the variability of the dune along the barrier island. One of the main goals of this new approach was to ensure that the most vulnerable breaching and overwash areas are included adequately in the surge modeling. Revised SBEACH dune lowering results were obtained by analyzing profile response for the 252 profiles extracted from the Fall LIDAR 2000 data. The new SBEACH results capture the variability of the dune with respect to several profile characteristics such as dune height, dune volume, berm width, backbarrier elevations, etc. These results were subsequently incorporated into Delft3D. Two reports entitled "Proposal for Delft3D Profile Lowering by Reach Based on SBEACH Results from all LIDAR Profiles" and "Comparison of SBEACH Results due to Profile Shape (LIDAR vs. Representative)", submitted to the TRP in March 2004, summarize the new SBEACH dune lowering results and method for incorporating the results into Delft3D. Most relevant details of the lowering algorithm are as follows:

1. Each Delft3D grid line in the direction perpendicular to the shore is treated as an individual profile. Every point along the profile above the minimum dune height simulated in SBEACH is lowered by the amount defined in the SBEACH output tables.

2. The total lowered volume is computed as the sum of the individual volumes lowered at every grid point along the profile.

3. The total lowered volume is redistributed landward of the dune crest. A check is performed so that the addition of this volume will not create points higher than the estimated dune crest after lowering. This volume redistribution approach maintains the total profile volume.

2.9.3 SWAN – Bay Wave Setup

As at ocean stations, localized wave setup at bay stations is an important physical process for determining risk of economic damages. As such, a discussion of the methods used to

estimate bay wave setup is included here. Bay wave setup simulations for Baseline Conditions will, however, be presented in a separate report.

The impact of localized wave generation and its impact to bay water levels was determined using SWAN. The third-generation SWAN wave module of Delft3D was used to simulate the evolution of wind-generated waves for each storm event using the wind fields provided by NAN. The results of the SWAN simulations (namely, the significant wave height and period) were then used in conjunction with procedures outlined in the Shore Protection Manual (SPM, 1984) and Coastal Engineering Manual (CEM, 2003) to calculate wave setup at each back bay location given in Table 2-5 and Figure 2-7 through Figure 2-10.

The SWAN wave model, developed at Delft University of Technology in Netherlands, was used to compute wind generated wave in the bays independently of the Delft3D-FLOW simulations used to compute backbay storm surge elevations. Although significantly more computationally intensive, SWAN was used instead of HISWA because the grid in SWAN does not have to be oriented along the mean wave propagation direction as it does in HISWA. Therefore multiple grids covering all wind-generated wave directions are not required. In addition SWAN can perform computations on the same curvilinear grid used by Delft3D-FLOW and previously developed for storm surge simulations.

SWAN is based on the discrete spectral action balance equation and is fully spectral (in all directions and frequencies). The latter implies that short-crested random wave fields propagating simultaneously from widely different directions can be accommodated (e.g. a wind sea with superimposed swell). SWAN computes the evolution of random, short-crested waves in coastal regions with deep, intermediate and shallow water and ambient currents. The SWAN model accounts for refraction effects due to current and depth and represents the processes of wave generation by wind, dissipation due to whitecapping, bottom friction and depth-induced wave breaking and non-linear wave-wave interactions explicitly with state-of-the-art formulations. Wave blocking by currents is also explicitly represented in the model. To avoid excessive computing time and to achieve a robust model in practical applications, fully implicit propagation schemes have been applied. The SWAN model has successfully been validated and verified in several laboratory and complex field cases (Ris et al., 1999).

For this study, the SWAN model operates on the same grid employed for Delft3D hydrodynamic and sediment transport modeling (Figure 2-23). The wind and pressure fields presented in Chapter 2.5 were applied to SWAN using the same wind speed reduction procedures outlined in Chapter 2.9.2. Wave fields were simulated with SWAN for three discrete wind conditions for each of the historical storms and additional storms listed in Table 2-3 and Table 2-4. The three wind conditions represent the wind field at the time of peak water level at Station 9, Old Inlet, the wind field approximately 3 hours before this peak water level, and the wind field approximately 3 hours after this peak water level.

Bay Wave Setup Calculation

Wave setup is the super-elevation of mean water level caused by wave action (CEM, 2003). Wave setup estimates were computed for the selected back bay stations using significant wave heights obtained from the SWAN simulations. The significant wave height represents the condition most suitable for design purposes because the higher values present in the wave spectrum occur too infrequently to contribute significantly to wave setup (SPM, 1984). According to the Shore Protection Manual (CEM, 2003) wave setup at the still-water shoreline is given by:

Equation 2-1

$$\overline{\eta}_s = \overline{\eta}_b + \frac{1}{1+\frac{8}{3\gamma_b^2}} h_b$$

where the first term in Equation 2-1 is setdown at the breaking point and the second term is setup across the surf zone, and

h_b = depth at breaking

γ_b = breaker depth index (ratio of breaker height to breaker depth)

Longuet-Higgins and Stewart (1963) obtained the expression for setdown (the first term in Equation (1)) for regular waves from the integration of the cross-shore balance of momentum assuming linear wave theory and normally incident waves (CEM, 2003).

In order to calculate the setup, the breaking wave depth must first be computed. Breaking wave depth is given by:

Equation 2-2

$$h_b = \frac{H_b}{b - a\left(\frac{H_b}{gT^2}\right)}$$

where the parameters a and b are empirically determined functions of beach slope, given by:

Equation 2-3

$$a = 43.8\left(1 - \exp\left(-19m\right)\right) \text{ and } b = \frac{1.56}{1+\exp\left(-19.5m\right)}$$

where m is the beach slope and was measured using available bathymetric data at each backbay station location. Since the breaking wave height must be estimated a priori, a semi-empirical relationship for the breaking wave height from linear wave theory was used from Komar and Gaughan (1973) (CEM, 2003).

Equation 2-4

$$H_b = 0.56 H_0 \left(\frac{H_0^{'}}{L_0} \right)^{-1/5}$$

where

H_0 = deepwater wave height

$H_0^{'}$ = equivalent unrefracted deepwater wave height

L_0 = deepwater wave length

The equivalent unrefracted deepwater wave height is given by:

Equation 2-5

$$H_0^{'} = \frac{H_s}{K_s}$$

where

H_s = significant wave height (SWAN output)

K_s = shoaling coefficient

Although the methodology discussed in this section applies for regular waves, the setup for irregular waves can be calculated from the decay of the root mean square wave height parameter, H_{rms}. The mean ratio of setup to deepwater root mean square wave height for all 35 backbay locations and 57 storm events is approximately 20%, which is in agreement with the results of the irregular wave setup calculations using the Dally, Dean, and Dalrymple (1985) wave decay model presented in the Coastal Engineering Manual (CEM, 2003).

The methodology outlined in Chapter 2 is comprehensive. It captures all important physical processes that govern storm water levels within the project area. Further, the methodology outlined above takes advantage of all proven state-of-the-art technology.

3. Wind and Barometric Pressure Comparison

In conjunction with ocean storm surge calibration of the ADCIRC model, it was necessary to verify that the model inputs, wind and barometric pressure fields, accurately represent the historical storm conditions. The wind and pressure fields developed for this study were verified for spatial and temporal consistency prior to their use in the wave and hydrodynamic models. The pressure and wind fields provided were verified by graphical representations and comparisons to available data.

3.1 Barometric Pressure

By selecting the closest node to the NOAA station in question, comparisons could be made between provisional NOAA data and the provided barometric pressures. That comparison is shown in Table 3-1 and Table 3-2. Unfortunately, only two NOAA stations contain barometric pressure data within the study area for any of the tropical storms within the study's scope. The difference between the two sets of data is expressed in feet of water because length is the unit required by the ADCIRC model.

It should be reiterated that the NOAA data used in this report has "not been subjected to the National Ocean Service's quality control or quality assurance procedures and do not meet the criteria and standards of official National Ocean Service data. They are released for limited public use as preliminary data to be used only with appropriate caution."

3.2 Wind Fields

In addition to the digital files containing the storm event wind fields also provided were Bitmaps of the wind field for each storm event. The Bitmaps were visually compared to the wind fields for the time frame and position as close as possible. In addition, the storm tracks were verified against the historical movement of the storm. Technical Paper Number 48, "Characteristics of the Hurricane Storm Surge", published by the U.S. Department of Commerce was also utilized for verification of the overall impression of the storms from 1938 to 1961. All wind field comparisons resulted in adequate representations when compared to the available data.

Table 3-1: Barometric pressure comparison of September 1999 tropical storm.

Station: **8531680 (-74.010, 40.466)**				
Day	**Time (GMT)**	**NOAA (millibars)**	**Simulated (millibars)**	**Difference** (feet of water)
09/14/1999	00:00	1020.8	1010.8	0.335
09/15/1999	00:00	1018.5	1010.8	0.256
09/16/1999	00:00	1016.5	1010.4	0.203
09/16/1999	18:00	995.9	1004.2	0.279
09/17/1999	00:00	983.1	988.6	0.184 [peak]
09/17/1999	06:00	998.3	998.7	0.013
09/17/1999	12:00	1007.9	998.7	0.308
Station: **8516945 (-73.765, 40.810)**				
Day	**Time (GMT)**	**NOAA (millibars)**	**Simulated (millibars)**	**Difference (feet of water)**
09/14/1999	00:00	1021.0	1010.9	0.338
09/15/1999	00:00	1018.6	1010.9	0.256
09/16/1999	00:00	1016.7	1010.6	0.203
09/16/1999	18:00	997.8	1005.4	0.253
09/17/1999	00:00	982.9	987.2	0.144 [peak]
09/17/1999	06:00	996.2	996.4	0.007
09/17/1999	12:00	1006.5	996.4	0.338

Table 3-2: Barometric pressure comparison of September 1985 tropical storm.

Day	**Time (GMT)**	**NWS*** **(millibars)**	**M2D (millibars)**	**Difference (feet of water)**
09/27/1985	16:00	961[1]	960.6	0.013
09/27/1985	18:00	964[2]	964.1	0.003

*Taken from the Archive of Past Hurricane Seasons from the National Hurricane Center's Tropical Prediction Center, a service of the National Weather Service (http://www.nhc.noaa.gov/pastall.shtml).

[1] (-73.3, 40.6)

[2] (-72.8, 41.9)

4. Offshore Wave Field Validation

4.1 Offshore Wave Model Validation

Primary validation of the hindcast wave data was performed using data from NOAA buoy 44025 for significant storm events. Comparisons of wave height, peak wave period and peak wave direction for five extratropical (winter) storms and four tropical events are presented in Table 4-1. The five extratropical events (in bold) occurred in January 1992, December 1992, March 1993, February 1998 and February 2003. The tropical events occurred in August 1991, October 1991, October 1996, and September 1999.

The agreement between the hindcast results and the measurements is generally good, especially for the extratropical events. The average difference between the hindcast and the measurements is –2.3 feet (-0.7m) in zero-moment wave height, 0.2 seconds in wave period and -18 degrees in peak wave direction. Most deviations are most often a result of sub-scale processes (squall lines, for example) that can be seen in the March 1993 storm, where the wave direction suddenly changes for a short time period along with a jump in the measured wave height. Tropical storm wind fields were developed using a cyclone wind model that does not account for the sub-scale structure of the storms and subtle nuances of short-term changes in storm track, storm asymmetry, etc. These, in turn, may cause the wave directionality and wave height to deviate from the measurements.

Table 4-1: Comparison of hindcast peak storm wave parameters to measured data at NOAA buoy 44025.

Event (yyyy/mm/dd)	Hindcast			Measured (Buoy 44025)		
	H_{mo} (ft)	T_p (sec)	D_p (deg)	H_{mo} (ft)	T_p (sec)	D_p (deg)
19910817	19.7	11	90	19.0	16	64
19911027	14.1	14	90	16.4	11	76
19920101	**19.0**	**11**	**67**	**20.7**	**11**	**99**
19921208	**27.9**	**14**	**90**	**30.5**	**13**	**83**
19930309	**20.0**	**11**	**90**	**23.9**	**14**	**155**
19961007	15.1	9	45	15.7	8	86
19980202	**15.4**	**14**	**90**	**18.4**	**11**	**96**
19990915	14.8	9	90	22.0	12	155
20030212	**17.4**	**14**	**90**	**20.0**	**10**	**94**

5. Tidal Calibration

The following sections describe ADCIRC and Delft3D calibration for astronomical tide. To match measured tidal water levels, bottom friction was adjusted in ADCIRC and Delft3D. In both cases, final bottom friction values were within reasonable ranges. In ADCIRC, the ocean bottom friction coefficient was set to 0.0035 following calibration. In Delft3D, Manning's n was set to 0.025 following calibration.

5.1 Ocean

The ADCIRC model was calibrated for ocean tide by simulating a 30-day record and comparing model output with measurements at LISHORE (Long Island SHORE) station P1, just offshore of Shinnecock Inlet, and four NOAA stations: Sandy Hook, NJ; The Battery, NY; Montauk Fort Pond, NY; and Newport, RI (see Figure 2-7 through Figure 2-10).

During the 30-day simulation, tidal constituents at the five measurement station locations were computed by ADCIRC. The M2 constituent dominates the tide signal in the FIMP area, and Table 2-6 indicates that its amplitude is four times larger than the next largest constituent's amplitude. As such, the ADCIRC M2 constituents were compared with measured M2 constituents. The ADCIRC results compare very well to measured M2 constituents. At all five stations, M2 amplitude error is less than 1.6 in (4 cm), and, with the exception of The Battery, M2 phase error is within 5 minutes (2 degrees). At The Battery, phase error is 30 minutes (12 degrees). Table 5-1 presents M2 constituent comparisons.

Sixty-day predicted time series constructed from the 7 constituents computed by ADCIRC were compared with predicted time series constructed from the same 7 constituents measured by NOAA and LISHORE at the five measurement locations (Figure 5-1 through Figure 5-5). Table 5-1 presents correlation coefficient and RMS error between the measured and modeled 60-day time series. Percent RMS error is computed as the ratio between RMS error and the NOAA-measured tide range (MHHW – MLLW). Correlation coefficients at all four NOAA locations are 0.97 or better. Further, percent RMS errors are less than 7% at all four locations.

Table 5-1: Comparison of M2 tidal constituents and of predicted time series.

Region	Data Source	Station ID	Model	M2 Amplitude (in)			M2 Phase (degrees)			Predicted Time Series	
				Measured	Modeled	Delta	Measured	Modeled	Delta	RMS Error (in)	Correlation Coefficient
Nearshore	NOAA	Montauk, NY (8510560)	ADCIRC	11.8	11.8	0.0	46.8	46.7	-0.1	0.8	1.00
Nearshore	NOAA	Newport, RI (8452660)	ADCIRC	20.5	19.3	-1.2	2.2	0.4	-1.8	1.2	1.00
Nearshore	NOAA	Sandy Hook, NJ (8531680)	ADCIRC	27.6	26.8	-0.8	7.5	6.3	-1.2	1.2	1.00
Nearshore	NOAA	The Battery, NY (8518750)	ADCIRC	26.4	28.0	1.6	19.4	7.7	-11.7	4.3	0.98
Nearshore	LISHORE	Shinnecock Inlet, Ocean (P1)	ADCIRC /DELFT	18.9	18.5 /18.4	-0.4 /-0.5	346.4	345.3 /345.1	-1.1 /-1.3	0.8 /1.5	1.00 /0.99
Great South Bay	LISHORE	Fire Island Inlet (P8)	DELFT	11.4	9.5	-1.9	4.8	3.9	-0.9	2.8	
Great South Bay	LISHORE	Smith Point Bridge (P7)	DELFT	6.3	6.1	-0.2	74.8	75.2	0.4	0.8	
Great South Bay	NAN03	Bayshore	DELFT	5.3	4.6	-0.7	101.0	80.7	-20.3	1.5	0.94
Great South Bay	NAN03	Patchogue	DELFT	6.3	5.6	-0.7	103.0	102.1	-0.9	0.6	0.99
Great South Bay	NAN03	Watch Hill	DELFT	6.1	5.6	-0.5	102.3	100.6	-1.7	0.6	1.00
Great South Bay	USGS	Lindenhurst	DELFT	7.0	5.9	-1.1	86.3	75.1	-11.2		
Moriches Bay	LISHORE	Moriches CGS (P6)	DELFT	12.1	12.6	0.5	25.2	28.9	3.7	1.1	1.00
Moriches Bay	NAN03	Mastic Beach	DELFT	8.4	11.3	2.9	41.3	32.8	-8.5	2.4	0.99
Moriches Bay	NAN03	Westhampton Dunes	DELFT	11.6	12.9	1.3	38.9	34.1	-4.8	1.4	0.99
Moriches Bay	NAN03	Remsenberg	DELFT	11.7	12.9	1.2	39.9	34.4	-5.5	1.5	0.99
Shinnecock Bay	LISHORE	Shinnecock Inlet, Bay (P2)	DELFT	16.4	16.7	0.3	357.0	359.4	2.4	1.3	1.00
Shinnecock Bay	LISHORE	Cormorant Point (P3)	DELFT	15.4	16.3	0.9	8.5	9.7	1.2	1.4	1.00
Shinnecock Bay	LISHORE	Quogue Canal (P4)	DELFT	12.9	15.4	2.5	48.4	30.2	-18.2	0.4	0.99

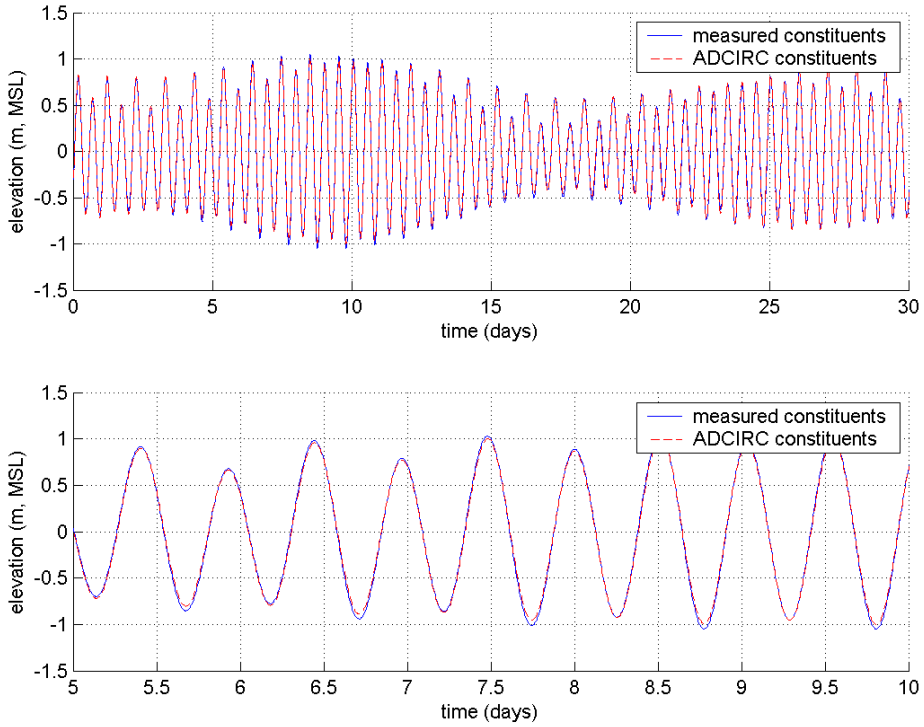

Figure 5-1: Predicted time series starting 0:00 1 March 2001: Sandy Hook, NJ.

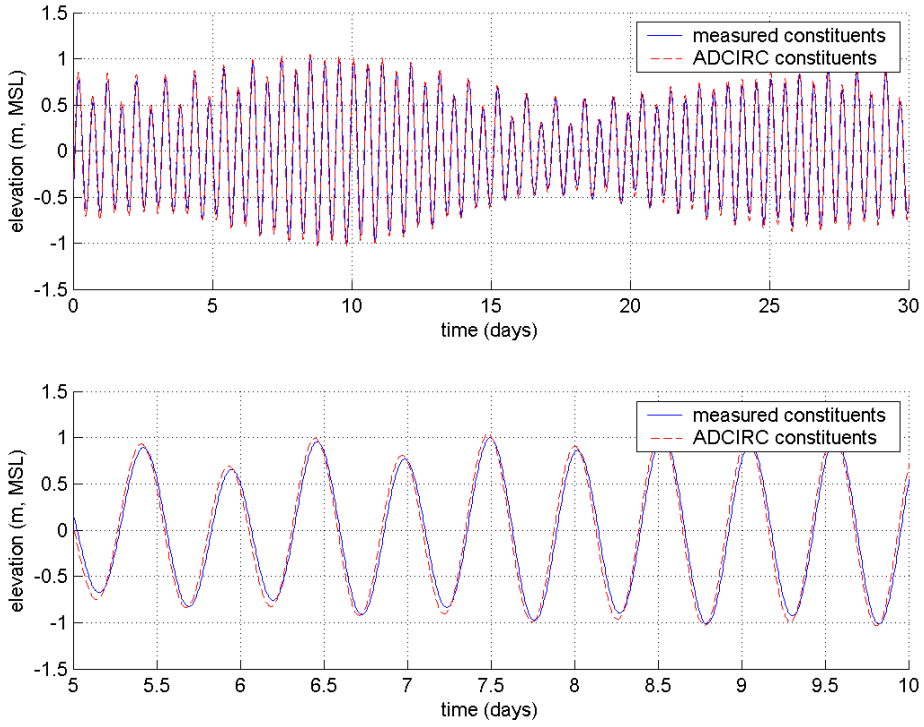

Figure 5-2: Predicted time series starting 0:00 1 March 2001: The Battery, NY.

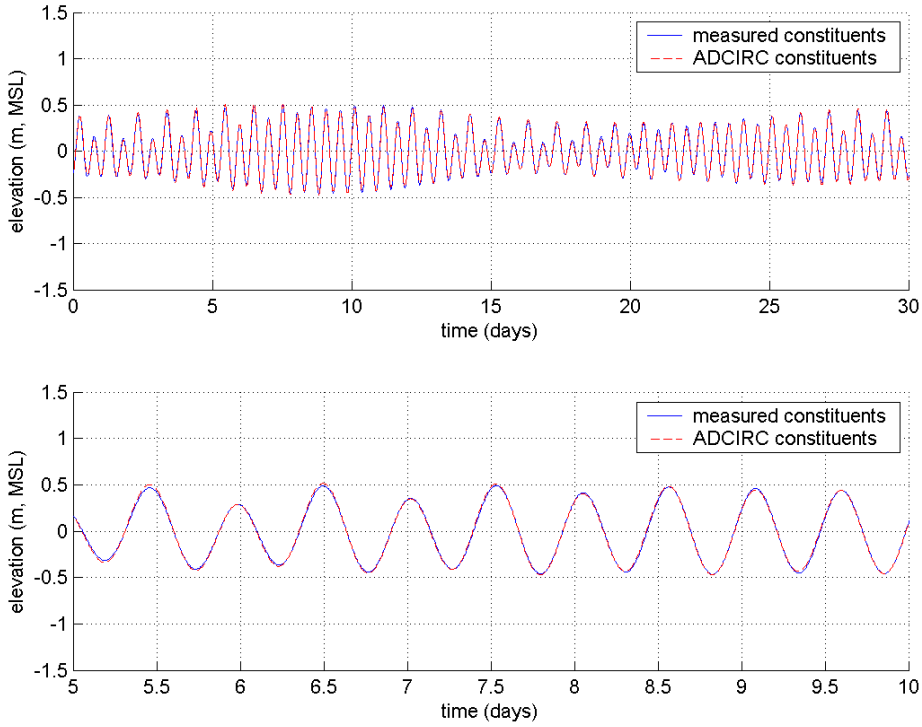

Figure 5-3: Predicted time series starting 0:00 1 March 2001: Montauk, Fort Pond, NY.

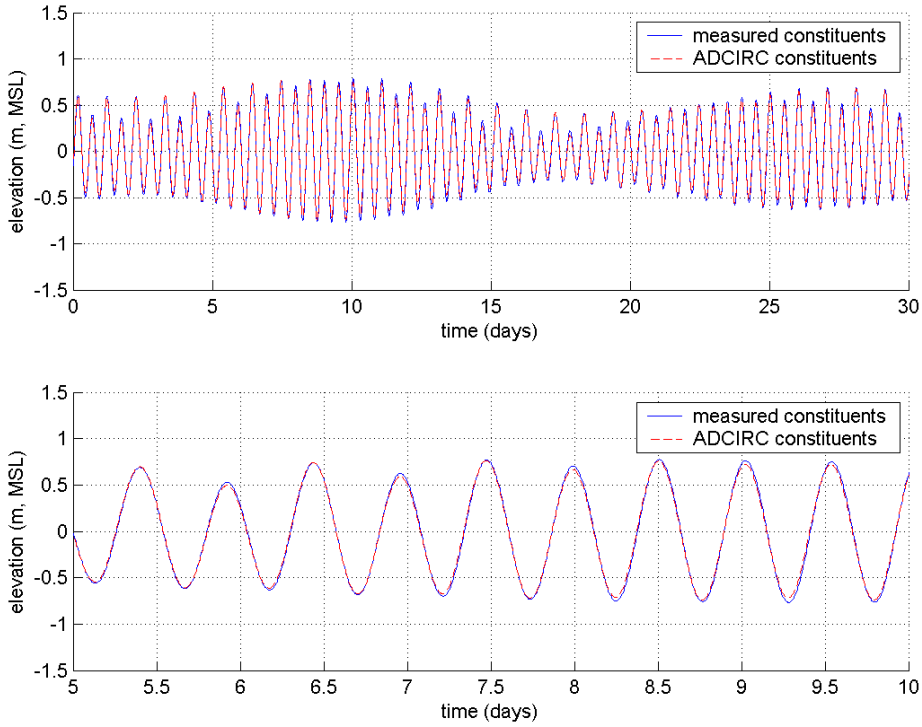

Figure 5-4: Predicted time series starting 0:00 1 March 2001: Newport, RI.

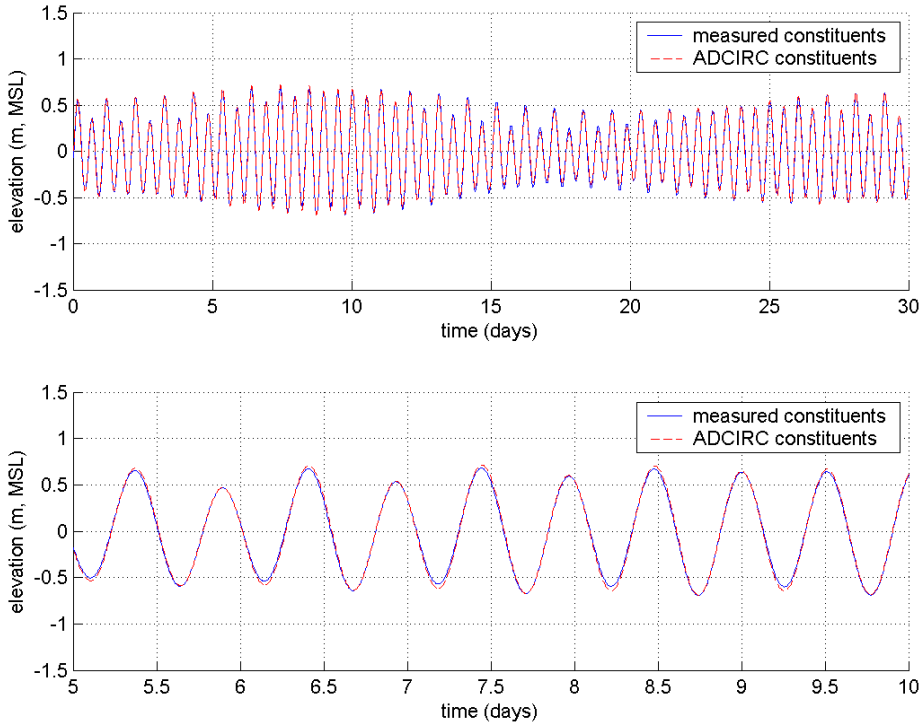

Figure 5-5: Predicted time series starting 0:00 1 March 2001: Shinnecock Inlet (ocean).

5.2 Bay

5.2.1 Water Level

As with the ocean tidal calibration, the Delft3D model was calibrated for bay tide by simulating a 30-day record and comparing model output with measurements at 13 measurement locations. Measurements were available at 6 locations within Great South Bay, 4 locations within Moriches Bay, and 3 locations within Shinnecock Bay (see Figure 2-7 through Figure 2-10). Length of observed water levels at those stations varied from as little as one month to more than one year. Longer-term measurements were collected in the late 1990s to present as part of the LISHORE program at 6 locations and by USGS at one location. During a 3-month field-monitoring program sponsored by the FIMP study in Spring 2003, measurements at 6 additional locations were collected.

Tidal constituents computed from the measured data were compared with constituents computed from Delft3D model output. Within Great South Bay, Delft3D M2 amplitudes are within 0.8 in (2.0 cm)[6]. M2 phase is within 15 minutes (6 degrees) at Patchogue and Watch Hill and within 45 minutes (21 degrees) at Bayshore. The phase error at Bayshore is most likely due to the complex geometry of the embayment near Bayshore. In Moriches Bay, the model overpredicts M2 amplitude by as much as 2.9 in (7.4 cm) at all

[6] The Lindenhurst model output station and the USGS measurement station are not collocated. Therefore, this station was excluded for the presentation of overall statistics. However, these results are presented in Table 7.1.

measurement locations while modeled phase is within 20 minutes (9 degrees). Errors in M2 amplitude in Moriches Bay are most likely attributed to the age and reliability of available bathymetry for the bay. In Shinnecock Bay, M2 amplitudes and phases are within 1.0 in (2.5 cm) and 6 minutes (3 degrees), respectively, at the inlet and at Cormorant Point. However, M2 amplitude and phase error are 2.5 in (6.4 cm) and 45 minutes (18 degrees), respectively, at Quogue Canal. The complex geometry and lack of recent bathymetry data in Quogue Canal is most likely the cause of these differences.

As with ocean tide comparison, predicted time series generated with tidal constituents computed with Delft3D time series were compared with those generated measured constituents. Figure 5-6 and Figure 5-7 show representative bay time series. All RMS errors for interior bay stations are less than 2.5 in (6.4 cm). Correlation coefficients are 0.98 or better for all stations but Bayshore, in Great South Bay. At Bayshore, the correlation coefficient is 0.94.

These figures also demonstrate the consistency between ADCIRC and Delft3D simulations for tide simulation. In both figures, differences between the two simulated time series are negligible.

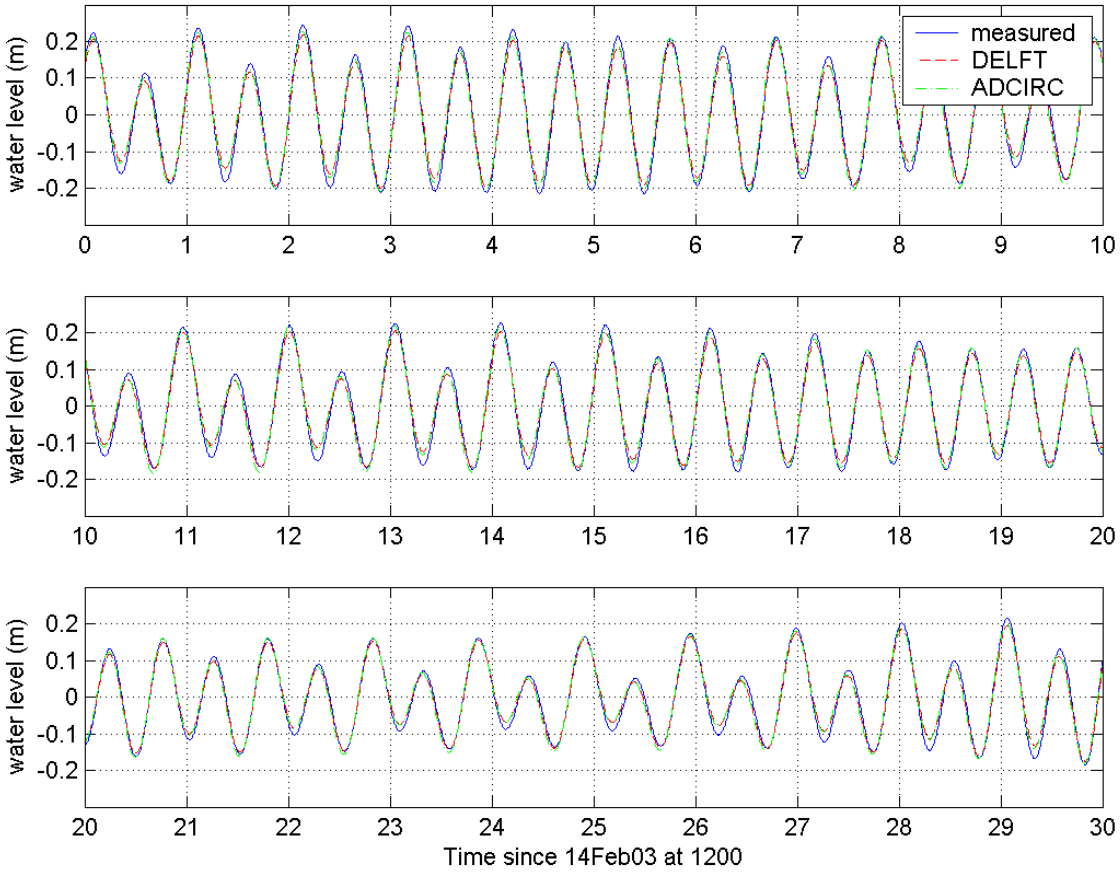

Figure 5-6: Predicted time series: Patchogue, Great South Bay.

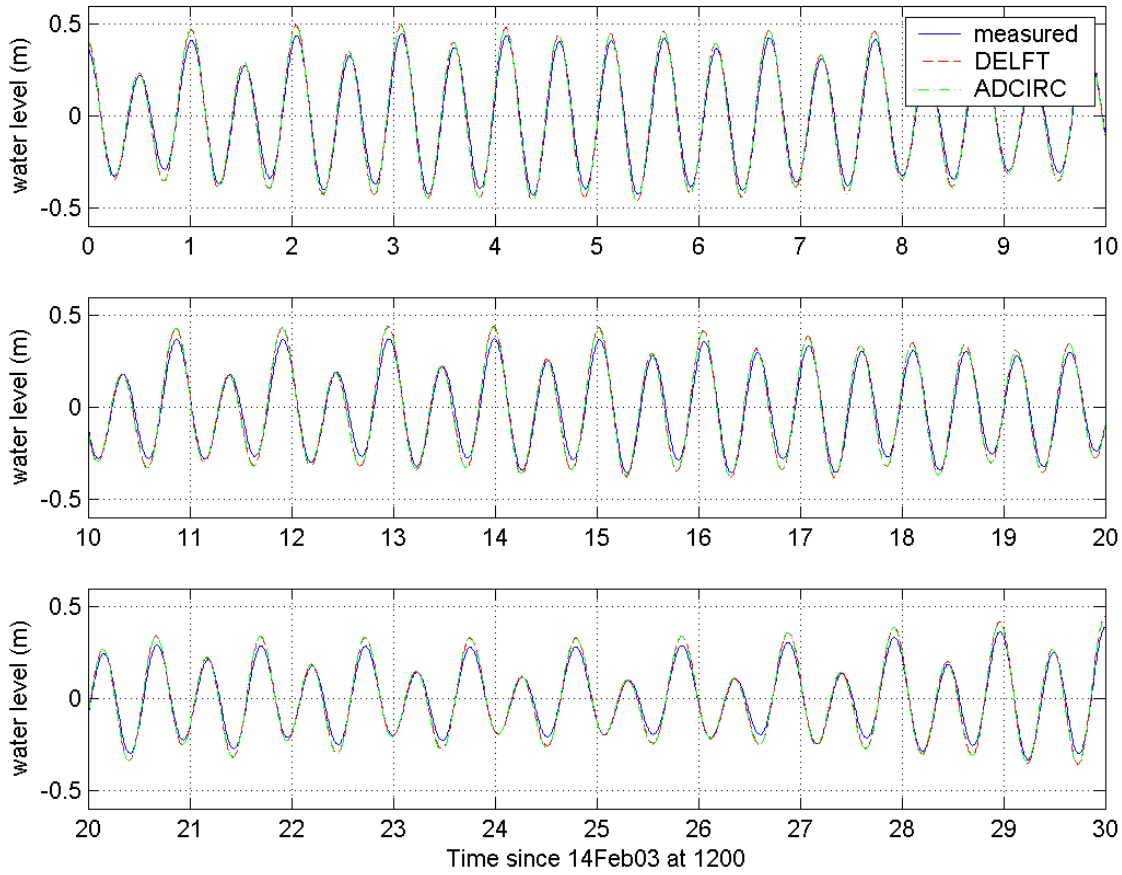

Figure 5-7: Predicted time series: Westhampton Dunes, Moriches Bay.

5.2.2 Inlet Discharge

During the Spring 2003 field-monitoring program, ADCP measurements were collected at Fire Island and Moriches Inlets. These measurements, along with ADCP measurements collected at Shinnecock Inlet in 1998, were compared to inlet discharges and tidal prisms simulated by Delft3D.

Tidal prism is a measure of the extent of tidal flushing of the bay and can be defined as the amount of water that flows into the bay from low tide to high tide. The current effort has used multiple techniques to determine the tidal prisms of the inlets within the Fire Island to Montauk Point (FIMP) Reformulation Study domain. These techniques include both physical measurements, with a boat mounted Acoustic Doppler Current Profiler (ADCP), and Delft3D computer simulations. The ADCP measurements were taken by Offshore and Coastal Technologies, Inc. (OCTI) at Moriches and Fire Island Inlets in 2003 on April 15 and 16 respectively.

ADCP Cruise

Since ADCP data is broken into multiple bins over the water column being surveyed, the data was integrated over the water column depth and the transect length. Specifically, measured current in each bin was multiplied by the bin area and the results summed vertically over the water column. Additionally, the bottom-most and topmost bins were assigned interpolated values due to limits of equipment to collect data in these bins. Then the water columns were summed horizontally for each unique transect. The result of the horizontal summation provides a discharge (volume per time) for each transect during the data collection period. Even though the entire transect was not surveyed instantaneously, the discharge is assumed to have occurred at one unique moment in time. Discharge data over the measurement period, i.e., approximately 12 hours, was used to determine the tidal prism for each inlet. Figure 5-8 through Figure 5-9 show the approximate locations of the transects collected during the boat cruises. ADCP data was not collected at Shinnecock Inlet during the 2003 field-monitoring program, but one transect was included in the Delft3D modeling. The location of the Shinnecock Inlet transect is illustrated in Figure 5-10 below.

Comparison of Methods

When plotting the discharge, flood and ebb conditions were assigned positive and negative values respectively. Figure 5-11 through Figure 5-13 provide the discharge time series for Fire Island, Moriches, and Shinnecock Inlets, respectively. The Keulegan and Hall (K&H) method was used as a crosscheck for the tidal prisms determined from the ADCP and Delft3D discharge time series. The K&H tidal prism was calculated with an average of the peak discharges, as measured by the ADCP, for the three transects at each inlet. The K&H method is a relatively simple equation based on the tidal period, the peak inlet discharge, and a coefficient, which was taken to be 1.0 for this analysis.

Equation 5.1 below provides the form of the Keulegan and Hall method used in this investigation.

$$\Omega = P = \frac{T}{\pi C_k} D_m \qquad \text{[Keulegan and Hall (1950)]} \qquad \text{[Eq. 5.1]}$$

where: C_k = coefficient ($0.81 < C_k < 1$)
D_m = peak inlet discharge (volume per time)

Figure 5-11 and Figure 5-12 illustrate how closely the Delft3D and ADCP time series of flows agree in both shape and magnitude. The minor differences can be partially explained by the inherent difficulties in taking boat mounted ADCP measurements. This includes the inability to collect the entire transect (from bank to bank) due to the draft and turning radius of the boat. Even with on-board GPS, it is difficult to duplicate the straight-line transect in a boat due to wind and currents. These same factors make it difficult to sample the identical transect on the subsequent passes. Considering the sampling error of the instrument and the difficulties in the data gathering and the differences between modeled and observed flows are very minor.

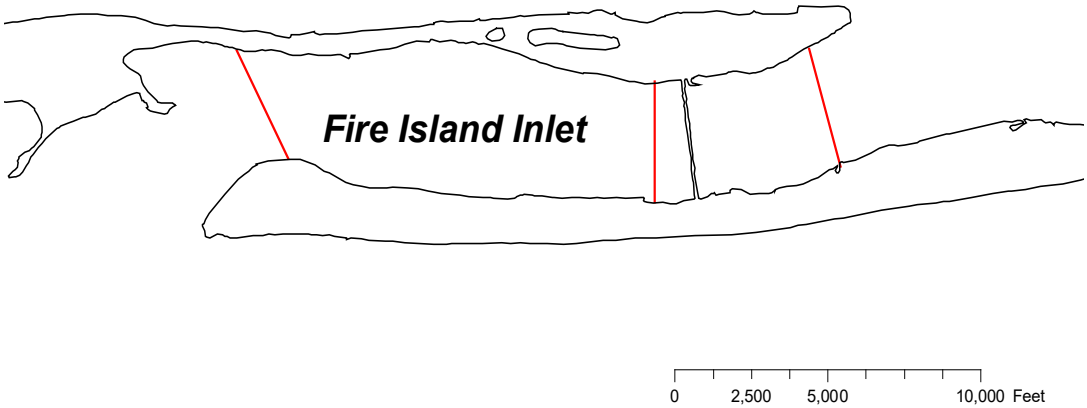

Figure 5-8: Approximate ADCP transects at Fire Island Inlet, NY.

Figure 5-9: Approximate ADCP transects at Moriches Inlet, NY.

Figure 5-10: Approximate transect for Delft3D results at Shinnecock Inlet, NY.

Tidal prisms for the 2003 ADCP and Delft3D data were determined using a numerical integration of the discharge time series over the flood cycle captured during the ADCP cruises. Since the intervals between discharge (m^3/s) observations for the ADCP transects was approximately one hour and only 10 minutes for Delft3D, there is significantly more data available over which to numerically integrate the Delft3D results. However, in order to compare the prisms, appropriate Delft3D data was selected as close to the same interval as possible to the ADCP data. The results, in Table 5-2 below, show slightly larger tidal prisms for Delft3D modeling results than for the measured ADCP results for both methods at Fire Island and Moriches Inlets. Percent differences were calculated in order to better quantify the variation between modeled (Delft3D) and measured (ADCP) data. The percent differences are presented in Table 5-2. No ADCP data was collected at Shinnecock Inlet during the Spring 2003 monitoring. The ADCP values reported in Table 5-2 for Shinnecock Inlet were collected in July 1998 and reported in Technical Report CHL-98-32. The numerical integration prism value for the Shinnecock ADCP data is believed to have been determined in a similar fashion to the numerical integration method in this document. The Keulegan and Hall prism value for the Shinnecock ADCP data was determined using peak discharge from a discharge time series plot in the Technical Report. These values are included here primarily for crosschecking purposes.

Percent differences for Fire Island Inlet demonstrate excellent agreement between the ADCP measurements and Delft3D modeling. The differences at Moriches Inlet are less encouraging, but may be partially explained by the fact that transect 7, presented in Figure 5-9, was the only available ADCP transect to pass through the inlet channel. Transect 7 is located at the extreme landward edge of the inlet channel and variability in the vessel's ability to stay within the channel may have allowed portions of the flow to go unmeasured. Other transects through the inlet channel encountered problems with GPS equipment, water depths due to tide that restricted boat access, and excess turbulence that made them unreliable sources of data.

5.2.3 Calibration Outside of FIMP

ADCIRC model results were used to develop stage-frequency curves for bay areas west of the FIMP study area (i.e. Jamaica Bay, South Oyster Bay, Raritan Bay). However, comparison between measured tides and ADCIRC simulations in these areas was beyond the scope of this study. Therefore, it is recommended that comparisons between measured tidal data and the ADCIRC results in these areas be performed prior to using the ADCIRC results presented herein.

The tidal calibration presented in Chapter 5 demonstrates the effectiveness of ADCIRC and DELFT3D to reliably and accurately predict astronomic tidal water levels within the project area. Further, it demonstrates that bathymetry and inlet and bay geometry are defined properly in the model grids used for this study.

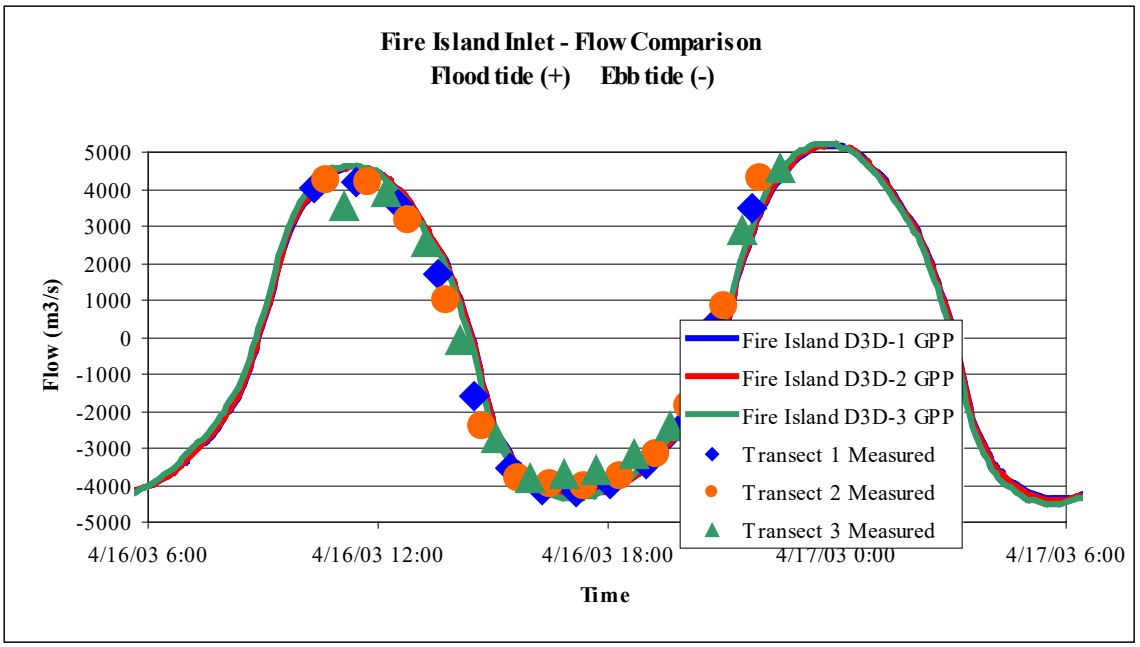

Figure 5-11: Delft3D & ADCP time series of inlet discharge (m^3/s) for Fire Island Inlet.

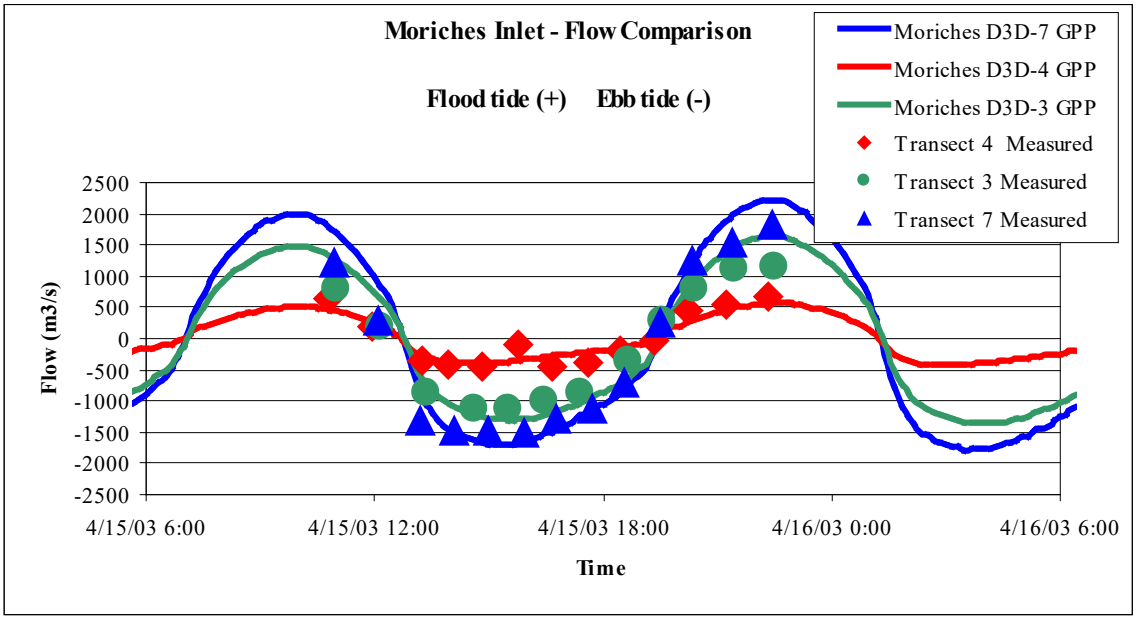

Figure 5-12: Delft3D & ADCP time series of discharge (m^3/s) for Moriches Inlet.

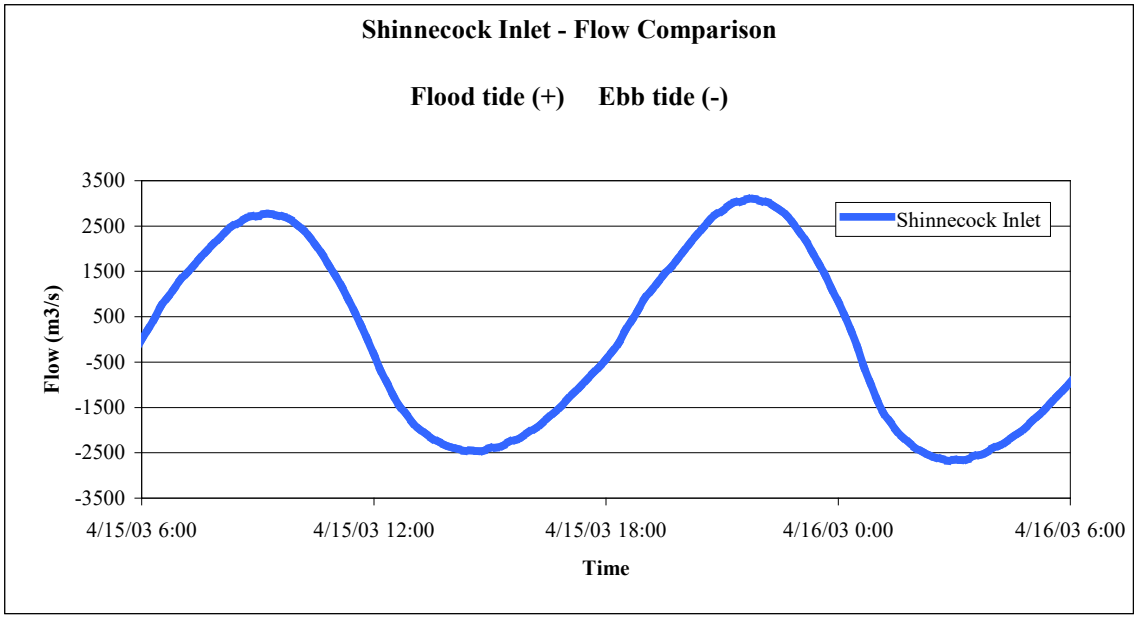

Figure 5-13: Delft3D time series of discharge (m^3/s) for Shinnecock Inlet.

Table 5-2: Summary of tidal prism results for multiple methods for all three FIMP inlets.

	Fire Island Inlet	Moriches Inlet	Shinnecock Inlet
ADCP (integrated)	4.93 x 10^7 m^3	1.74 x 10^7 m^3	3.29 x 10^7 m^3 *
Delft3D (integrated)	5.27 x 10^7 m^3	2.22 x 10^7 m^3	4.24 x 10^7 m^3
Percent Difference	7 %	28 %	29 %
ADCP (K&H)	6.19 x 10^7 m^3	2.58 x 10^7 m^3	3.73 x 10^7 m^3 *
Delft3D (K&H)	6.58 x 10^7 m^3	3.16 x 10^7 m^3	4.40 x 10^7 m^3
Percent Difference	6 %	22 %	18 %

* CHL-98-32 refers to *Shinnecock Inlet, New York, Site Investigation, Report 4, Evaluation of Flood and Ebb Shoal Sediment Source Alternatives for the West of Shinnecock Interim Project, New York* by Adele Militello and Nicholas C. Kraus, March 2001.

6. Ocean Storm Surge Calibration

In the open ocean and nearshore, storm surge from storm winds and barometric pressure were modeled using ADCIRC. As input, ADCIRC requires wind stress and barometric pressure for each node within the ADCIRC grid (Figure 2-12). The barometric pressure fields provided by the PBL model, for tropical events, and NCEP, for extratropical events, were readily interpolated onto the ADCIRC grid. Wind fields, however, required conversion to wind stress during interpolation.

The default wind stress calculation used with ADCIRC employs the wind drag coefficient formulation of Garratt (1977). The Garratt (1977) relationship is based on drag coefficient measurements for wind speeds below 40 knots (20 m/s). Based on this data set, Garratt's (1977) formulation provides a straight-line relationship between wind speed and drag coefficient such that higher wind speeds result in correspondingly higher drag coefficients. However, recent field measurements by Powell (2003) show that drag coefficient gradually decreases with wind speed for hurricane-force winds, or winds over 40 knots (20 m/s). Therefore for the FIMP study, the drag coefficient formulation was based upon Garratt (1977) for wind speeds less than 40 knots (20 m/s) and a straight-line fit to data collected by Powell (2003) for wind speeds greater than 40 knots (20 m/s).

To assess ADCIRC's calibration for storm surge due to wind and barometric pressure, 12 historical tropical and extratropical events were modeled. These 12 storms were selected to represent a range of storm conditions, and priority was given to those storms whose input wind and pressure fields were best defined. Following simulation with ADCIRC, model results were compared with NOAA measured hydrographs at four nearshore locations: Sandy Hook, NJ; The Battery, NY; Montauk Fort Pond, NY; and Newport, RI. In general, the ADCIRC simulated hydrograph shape closely follows measured data. Figure 6-1 and Figure 6-2 show representative hydrograph comparisons.

Figure 6-3 shows comparisons between measured peak water level and ADCIRC simulated peak water level for all four NOAA stations. Mean errors for tropical events vary from +3.5 in (+9 cm) at Montauk Fort Pond to -7.5 in (-19 cm) at The Battery. Mean errors for extratropical events are better than -2.8 in (-7 cm) at three of the four stations. RMS errors for both tropical and extratropical events are (11.0 in) 28 cm or better at all four stations.

The ocean storm surge comparisons presented in this chapter demonstrate the high quality of this surge modeling effort. RMS errors presented herein are within 28 cm and exceed the industry standard, on the order of 30-40cm. This rigorous calibration verified that ADCIRC reliably and accurately simulates storm surge over a regional domain that spans from New Jersey to Rhode Island. Further, this calibration demonstrates ADCIRC's effectiveness in simululated water levels for a wide range of storm intensities and durations.

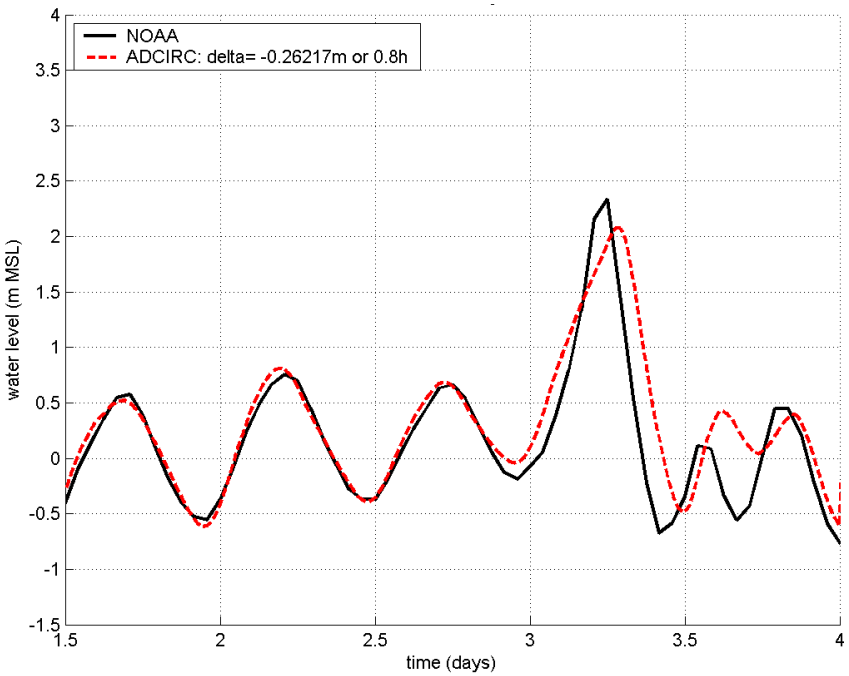

Figure 6-1: Hydrograph comparison for Hurricane Donna (1960): Sandy Hook, NJ.

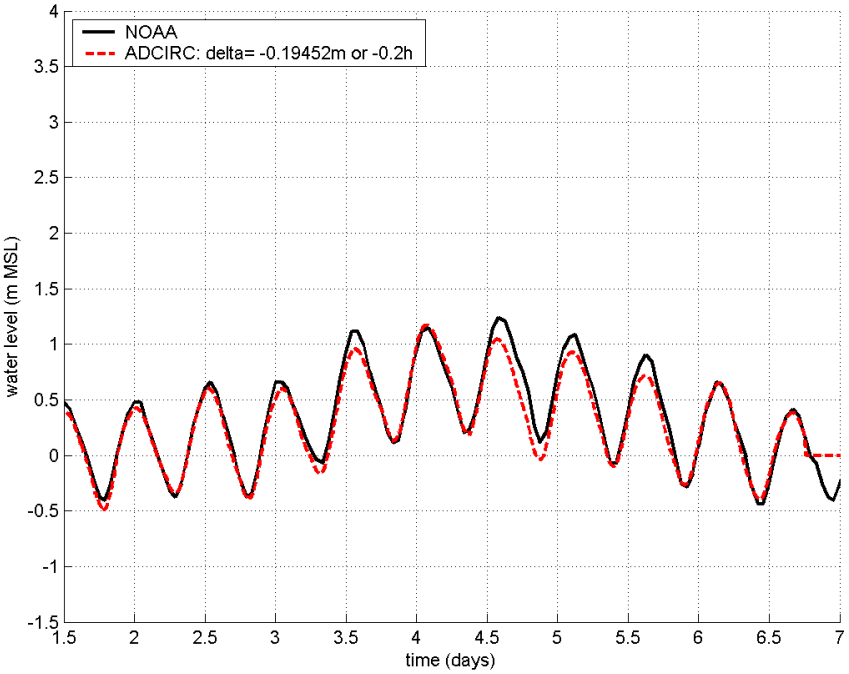

Figure 6-2: Hydrograph comparison for March 1962 Nor'easter: Montauk, NY.

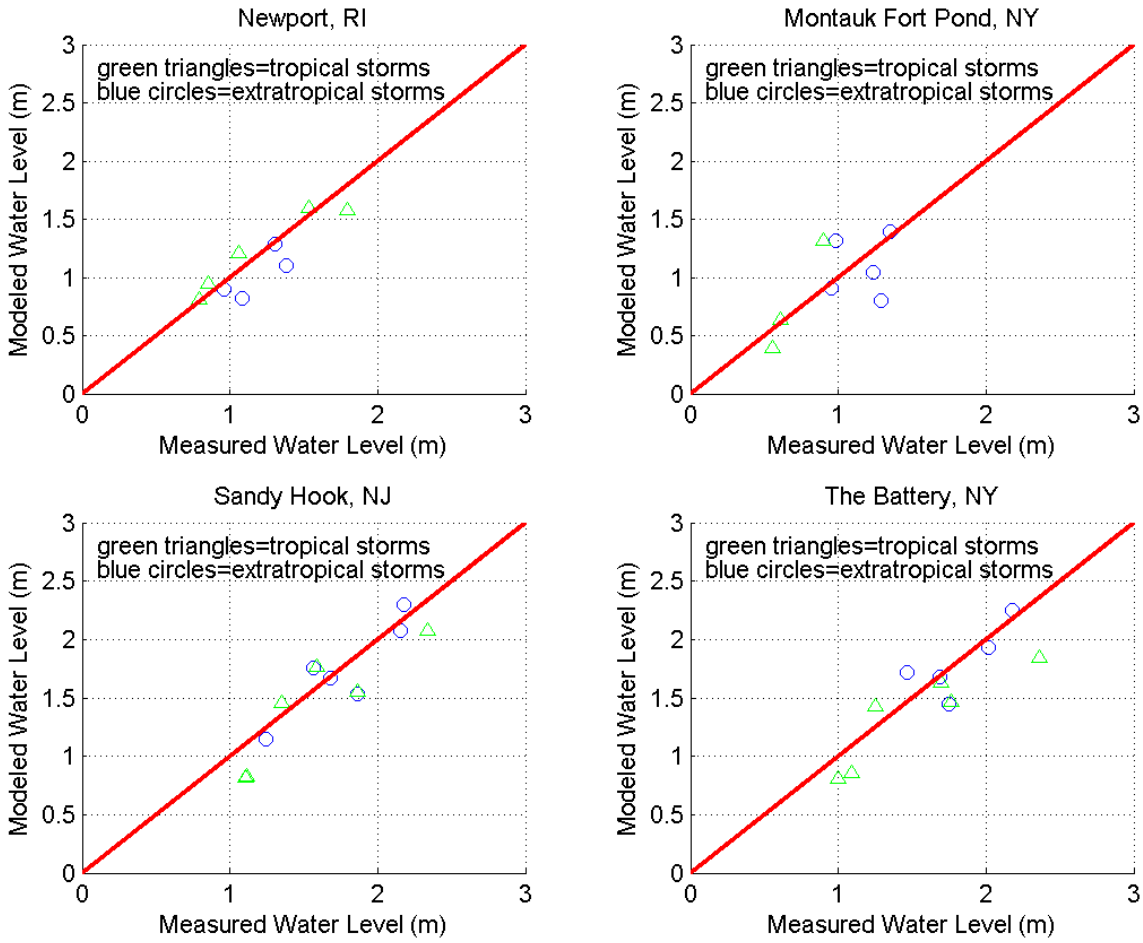

Figure 6-3: ADCIRC simulated versus NOAA measured water levels.

7. Bay Storm Surge Comparison

7.1 February 2003 Nor'Easter

A field investigation conducted in February 2003, afforded the opportunity to assess the performance of the modeling approach for simulating storm water levels. Offshore and Coastal Technologies, Inc. installed water level gages at six locations in Great South and Moriches Bays (Figure 7-1). In addition, water level measurements were also available for NOAA stations at Sandy Hook, New Jersey; The Battery, New York; Montauk Fort Pond, New York; and Newport, Rhode Island. Finally, NDBC Buoy 44025, offshore of Long Island, provided measurements of wave characteristics, wind speed, and barometric pressure.

The blizzard in mid-February 2003, impacting the entire northeastern USA, occurred during the field deployment and resulted in minor coastal flooding and significant snowfall. This extratropical event was characterized by peak offshore wind speeds near 20 m/s resulting in elevated ocean water levels that were as much as 0.5 m above astronomical predictions for 1.5 days. Offshore wave heights over 4 m were sustained for 1 day with peak wave height around 6 m.

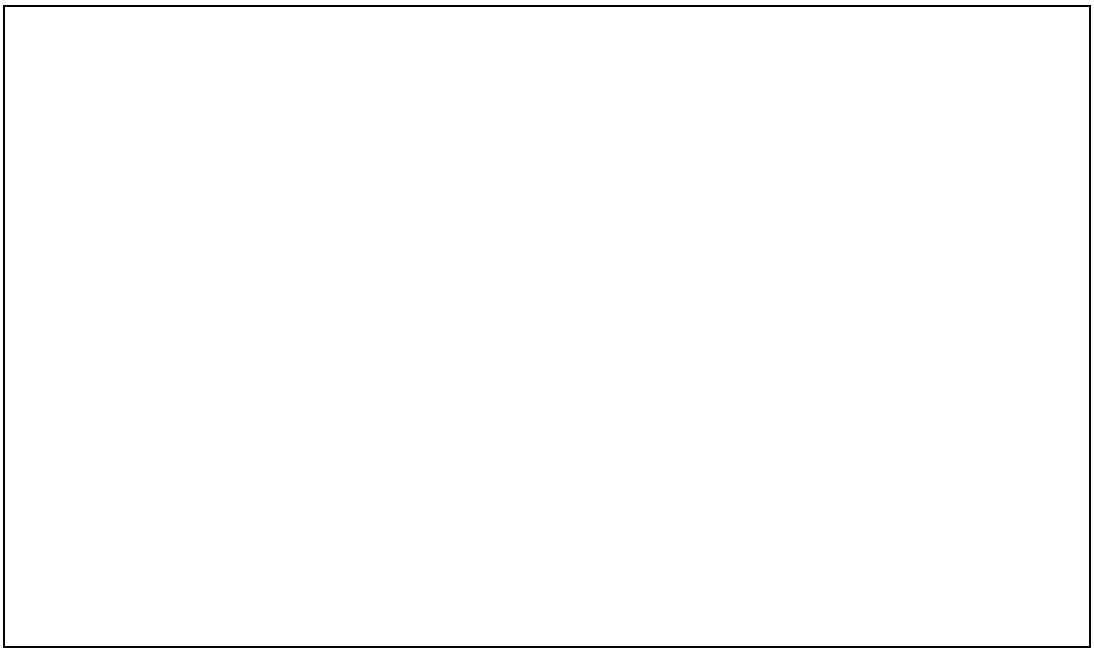

Figure 7-1: Location of bay water level gages.

7.2 Simulation Comparison to Measurements

Following the meteorological hindcasting and storm surge modeling methodology outlined in Chapter 2.5, water levels were simulated for the blizzard of 2003. Computed wind speed, barometric pressure, wave characteristics, and water levels were compared with measurements at a number of locations.

7.2.1 Meteorology

Wind fields developed using IKOA and barometric pressure from NCEP for the 2003 storm were compared with offshore measurements at NDBC Buoy 44025 (Figure 7-2 and Figure 7-3). Wind speed time series shape and magnitude matches well with measured time series, showing that the IKOA performs well for this storm. Peak wind speed comparisons with the offshore buoy are very good, with peak speed differing by less than 1 m/s. NCEP barometric pressure compares very well with measured pressure at the offshore buoy with the peak NCEP pressure only 0.03 m, water, below the measured peak.

7.2.2 Wave Characteristics

Spectral wave height, period and direction computed with WISWAVE were compared with measurements at NDBC Buoy 44025 (Figure 7-4, Figure 7-5, and Figure 7-6). Time series for all three wave parameters compare well with measurements. Differences in peak significant wave height and peak period are 0.8 m and 2.5 s, respectively.

7.2.3 Offshore Water Levels

ADCIRC simulated storm water levels were compared with NOAA measurements at the four NOAA measurement locations near the study area. Time series comparisons at Sandy Hook and Montauk Fort Pond are given in Figure 7-7 and Figure 7-8, respectively. ADCIRC performs well for simulating water levels for this storm. Differences between measured and simulated peak water levels are 9 cm (9%) or better at all four locations. Further, hydrograph shape is very similar to measured hydrograph shape at all four locations.

7.2.4 Bay Water Levels

The DELFT3D-FLOW simulation of the 2003 blizzard included ocean surge, local wind and pressure fields, and ocean waves. The simulation water levels were compared with the measured water levels at the six bay locations. Figure 7-9 shows the simulated and measured results at Watch Hill in Great South Bay. Simulated hydrograph shapes at all locations compare well with measured hydrograph shape, showing that DEFLT3D-FLOW performs well for this storm. This storm is characterized by two peak water levels. Simulated peak water levels for the first and second peaks at the three measurement stations in Moriches Bay are within 3 cm and 10 cm, respectively, of the measured peak water levels. The model also performs well at Watch Hill and Bayshore,

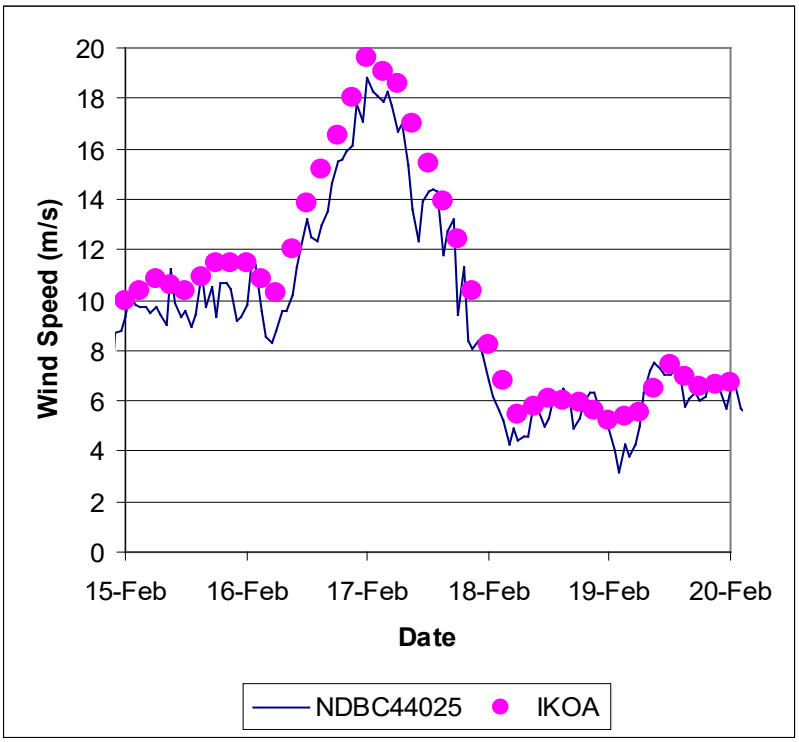

Figure 7-2: Wind speed comparison at offshore NDBC buoy 44025

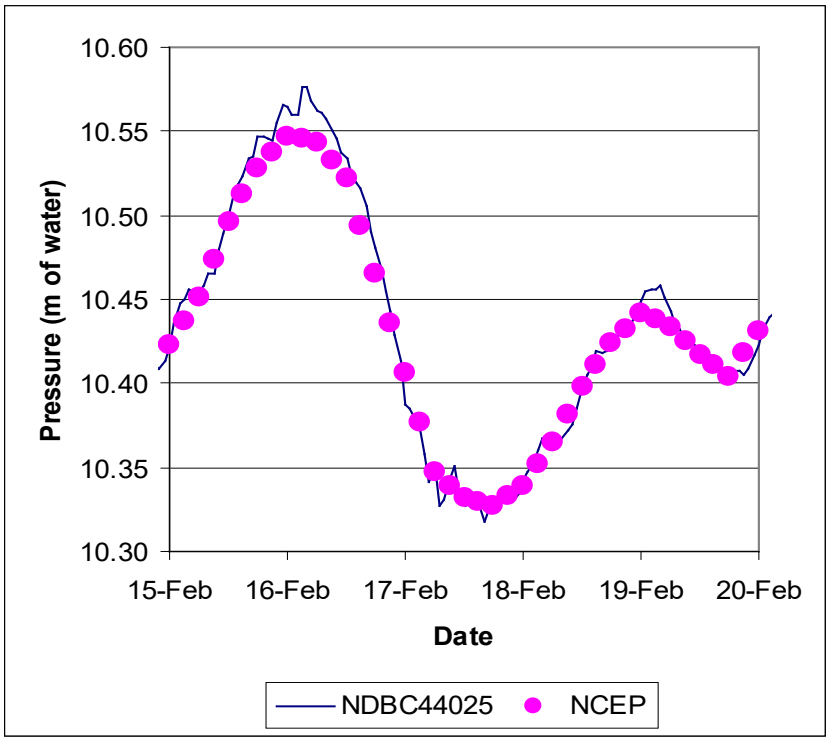

Figure 7-3. Barometric pressure comparison at offshore NDBC buoy 44025.

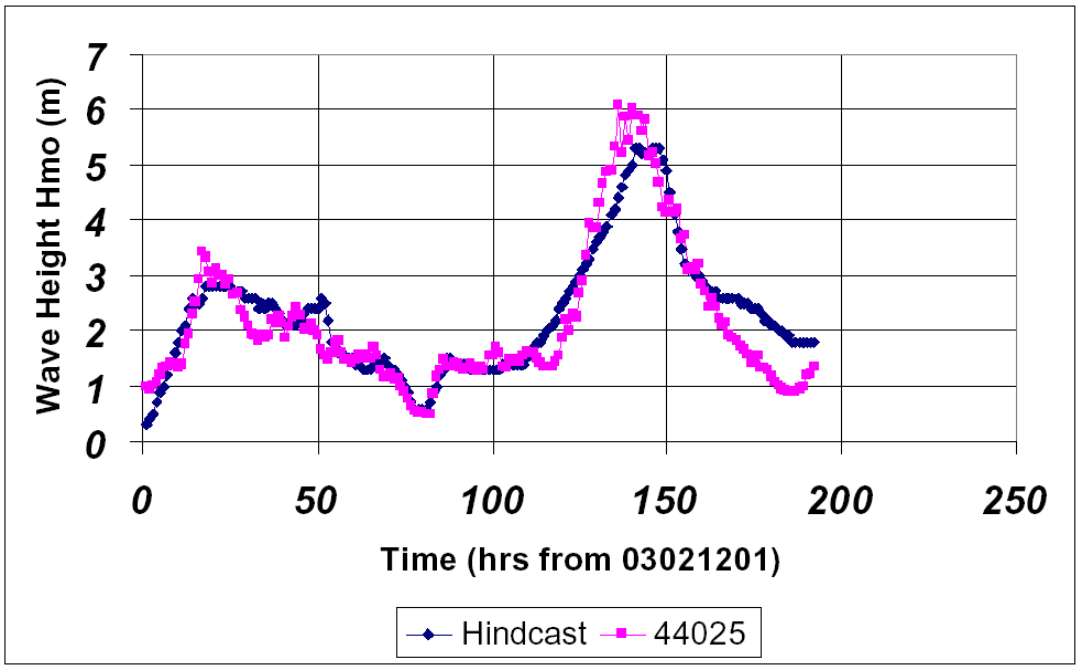

Figure 7-4. Significant wave height comparison at offshore NDBC buoy 44025.

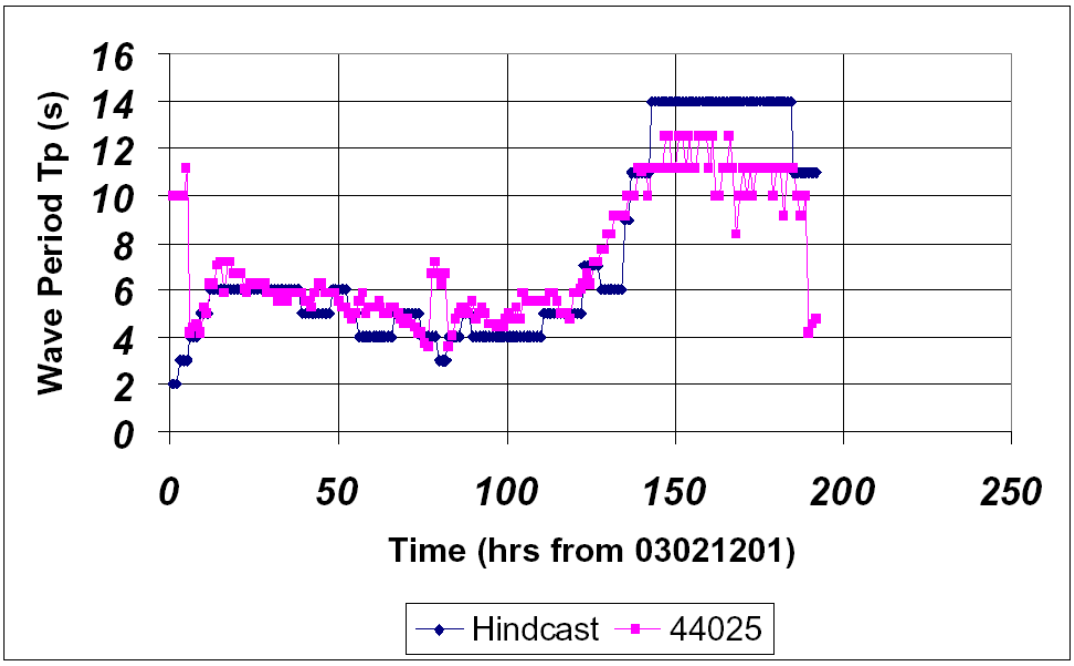

Figure 7-5. Peak wave period comparison at offshore NDBC buoy 44025.

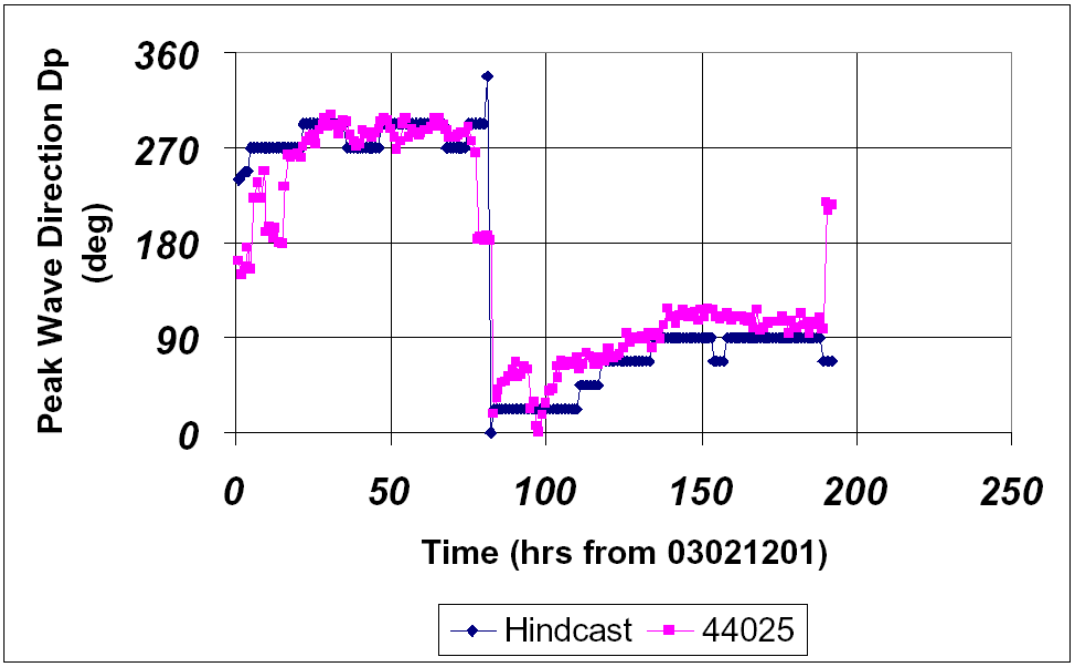

Figure 7-6. Wave direction comparison at offshore NDBC buoy 44025.

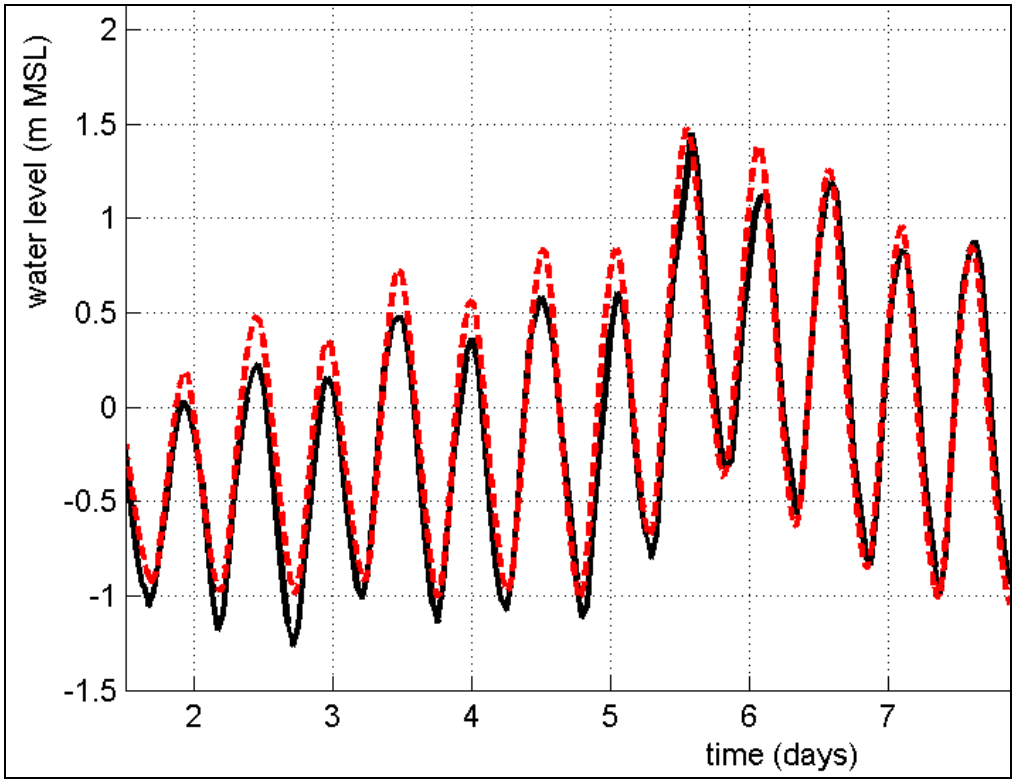

Figure 7-7. Measured (solid) and simulated (dashed) water level at Sandy Hook, New Jersey starting at 0000 GMT on 12 February 2003.

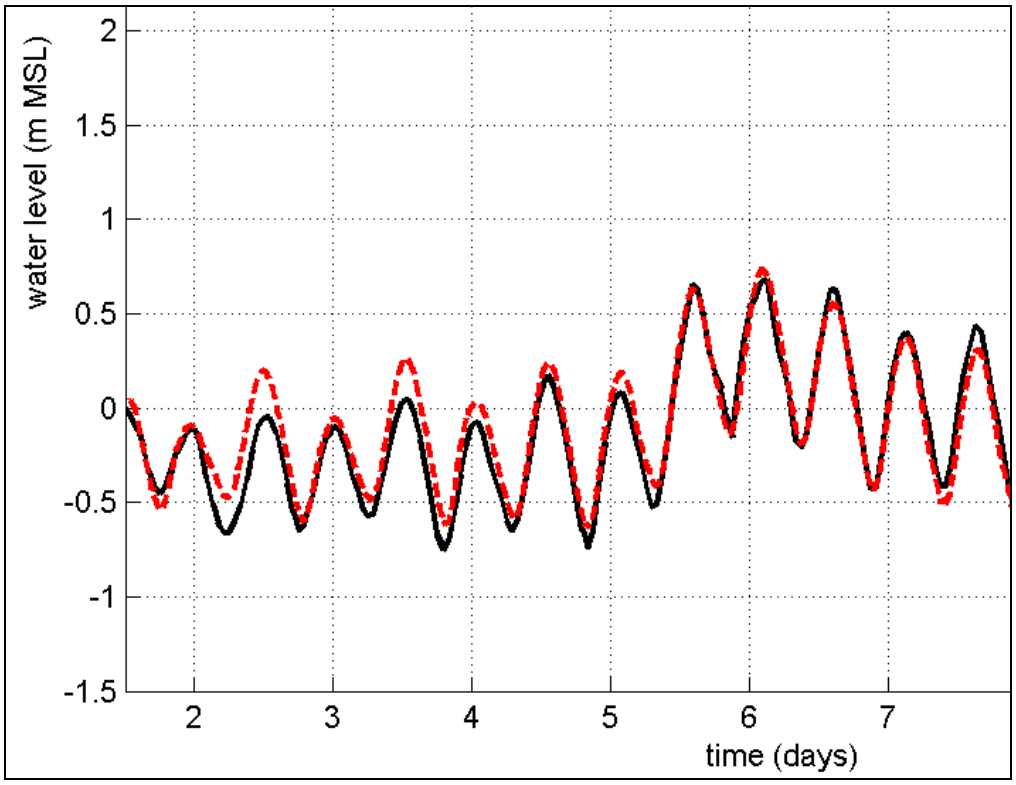

Figure 7-8. Measured (solid) and simulated (dashed) water level at Montauk Fort Pond, New York starting at 0000 GMT on 12 February 2003.

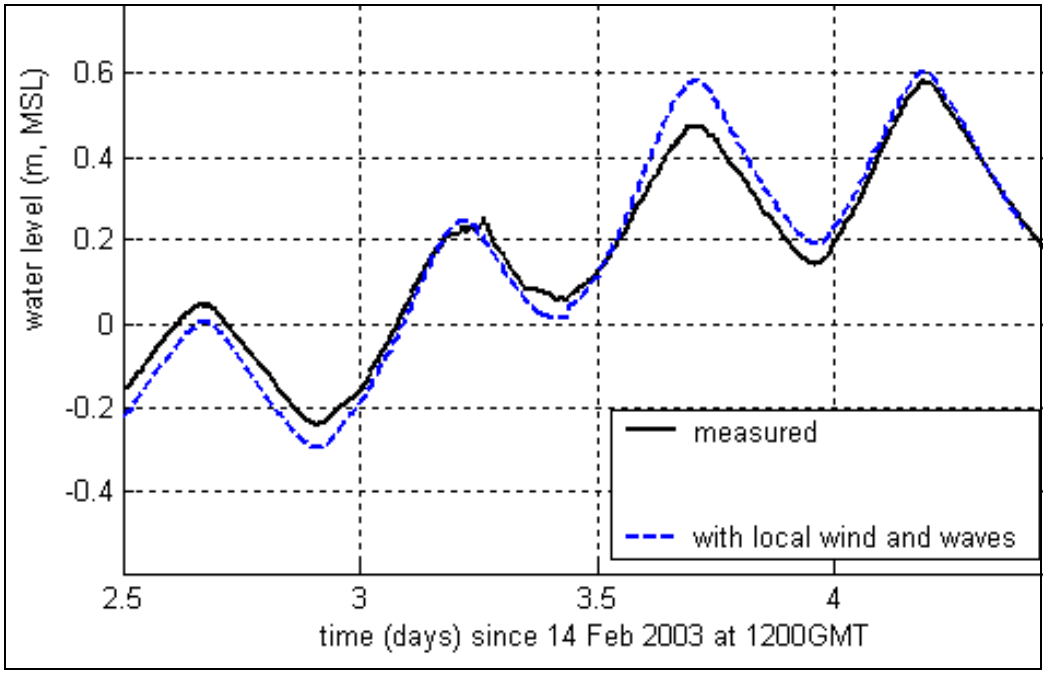

Figure 7-9. Measured (solid) and simulated (dashed) water level at Watch Hill, Great South Bay, during blizzard of 2003.

in Great South Bay, with simulated peak water levels for the first and second peaks within 10 cm and 2 cm, respectively, of measured peak water levels. Peak water level comparisons at Patchogue are within 2 cm.

Comparisons between measured data and simulation results for meteorological forcing, wave characteristics, and ocean and bay water levels show that the modeling strategy performs well for the blizzard of 2003.

7.3 Bay Water Level Contributions from Various Physical Processes

To understand the water level contributions of individual physical processes, a series of DELFT3D-FLOW simulations were performed for the blizzard of 2003:

1. Only offshore boundary forcing with ocean hydrographs from ADCIRC.
2. Simulation 1 plus local wind and barometric pressure forcing throughout the DELFT3D-FLOW model domain.
3. Simulation 2 plus ocean wave forcing from HISWA.

These three simulations allow separation of the effects on bay water levels from: astronomical tide; propagation of ocean surge through tidal inlets; propagation of flow generated by ocean wave setup through tidal inlets; and localized wind setup and setdown.

Figure 7-10 and Figure 7-11 compare the water level time series for three test simulations to measured bay water levels, and Figure 7-12 and Figure 7-13 summarize water level contributions from each process. For the blizzard of 2003, the combined effect of tidal amplitude and tidally generated superelevation makes up about 40% (25cm) of the total peak water level in Great South Bay and 50% (40 cm) of the peak water level in Moriches Bay. Water level contributions from ocean surge alone are about 35 cm in Great South Bay and 30 cm in Moriches Bay.

The addition of local wind has only a small effect on Moriches Bay water levels: DELFT3D-FLOW predicts a small setdown, on the order of 5 cm, at Westhampton Dunes and Remsenburg, on the eastern side of the bay, while the contribution from local wind at Mastic Beach, on the western side of the bay, is negligible. In contrast, the model predicts setdown of 10 cm at Patchogue and Watch Hill, at the eastern end of Great South Bay, and setdown of 6 cm at Bayshore, near the center of Great South Bay.

Wave setup from ocean waves is a significant contributor to water levels in both Great South and Moriches Bays. At all three measurement locations in Great South Bay, water level contribution from wave setup is around 9 cm. At all three measurement locations in Moriches Bay, water level contributions are around 14 cm. For the same offshore wave height, water level contribution from ocean wave setup is 50% larger in Moriches Bay than in Great South Bay. This indicates that inlet and bay geometry, and its effects on hydrodynamics, are important for accurate prediction of bay water levels associated with

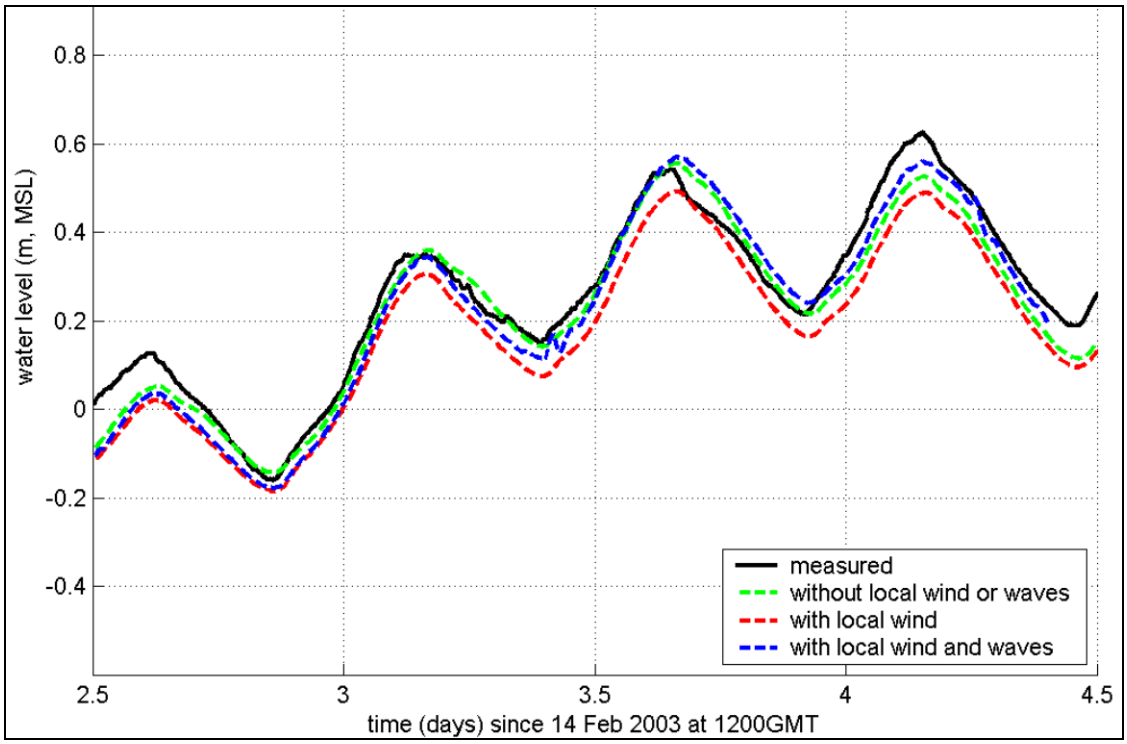

Figure 7-10. Water level contributions from physical processes at Bayshore, Great South Bay.

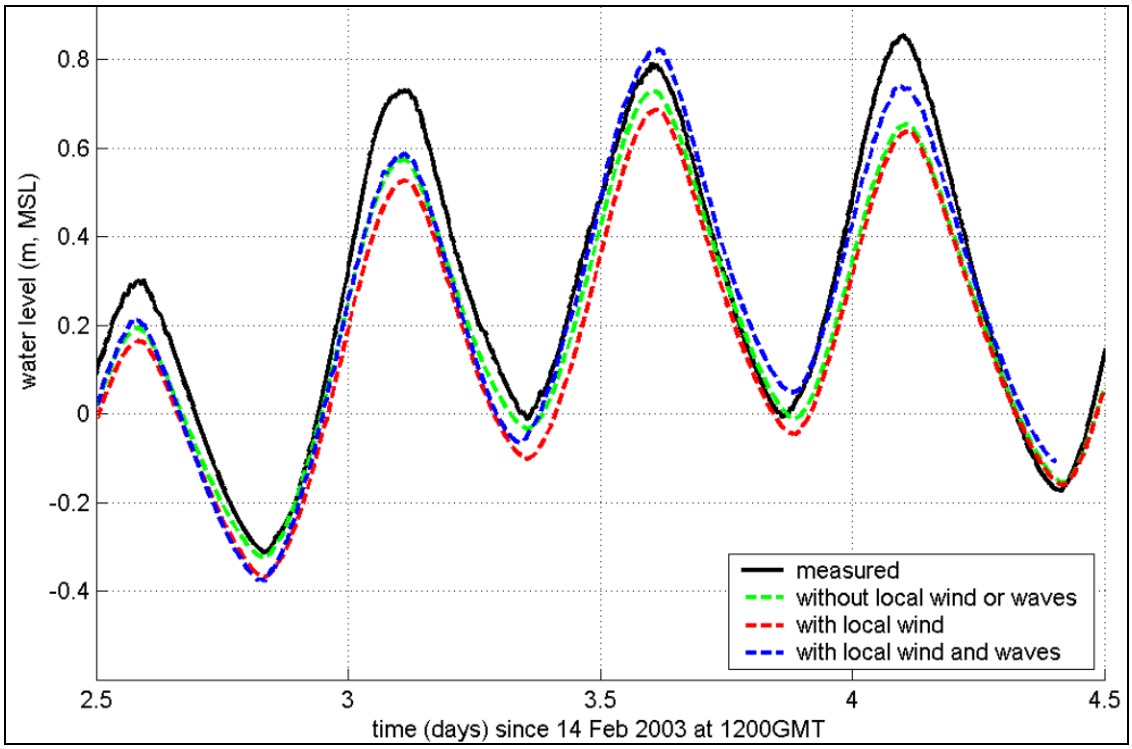

Figure 7-11. Water level contributions from physical processes at Westhampton Dunes, Moriches Bay.

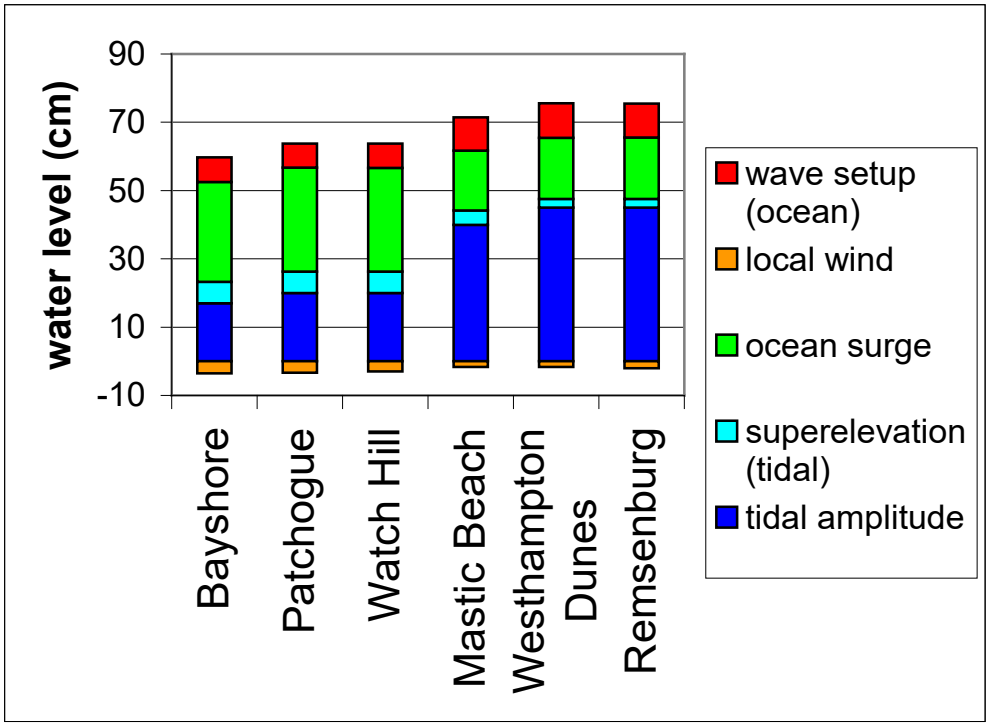

Figure 7-12. Water level contributions from physical processes for peak occurring 18 February 2003 at 0300 GMT.

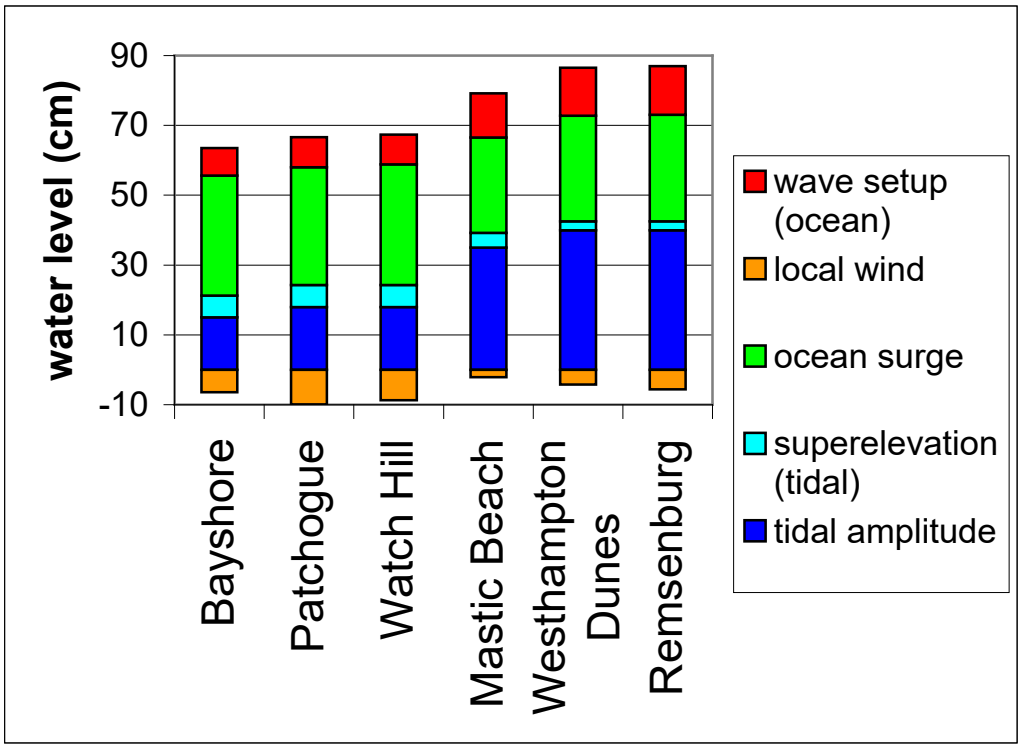

Figure 7-13: Water level contributions from physical processes for peak occurring 18 February 2003 at 1500 GMT.

ocean wave setup. For the blizzard of 2003, flow through the inlets created by ocean wave setup accounts for 15% of the total water levels in the bays. The model simulation comparisons with measurements during the blizzard of 2003 prove the modeling strategy adopted for the FIMP study accurately simulate storm water levels.

In particular, the DELFT3D simulation comparisons with February 2003 storm measurements demonstrate the effectiveness of the DELF3D-FLOW and DELFT3D-WAVE models for this study. Specifically, the DELFT3D model suite accurately captures the influences of ocean surge propagation in to the bays, astronomical tide influences, ocean wave setup propagation into the bays, and localized wind setup and setdown. Given that the February 2003 storm is only a minor coastal event, the comparisons between the simulated and measured results is even more impressive.

Finally, model simulations indicate that propagation of ocean wave setup into back bays is a major contributor to total water level within the study area. This demonstrates the importance of dynamically coupling the nearshore wave model with the hydrodynamic model even for storm that do not result in overwash and breaching.

7.4 Comparisons to Other Historical Peak Water Level Measurements

Two types of water elevation measurements exist for selected historical storms. Of these measurements, those from water level gages (WLG) are the most reliable. Furthermore, these WLG measurements more accurately reflect those processes simulated by the modeling suite. Namely, a WLG measures the quasi-steady state water level from astronomical tide, storm surge, ocean wave setup propagation through the inlet and bay, localized wind setup or setdown, and localize wave setup.

High water mark observations are not as appropriate for verifying simulation performance primarily because they include the effects of individual waves (i.e. runup). Additional discussion of HWM and WLG data is provided in the IMPORTANT DEFINITIONS section, at the front of this report.

The most comprehensive set of WLG bay measurements exists for the 1962 Nor'easter. Figure 7-14 shows comparisons between these measurements and the Baseline Condition simulated water levels for this storm. It must be noted, however, that in contrast to the historical event whose pre-storm topography was severely degraded, minimal overwash occurs during simulation of the 1962 storm using Baseline Conditions (representing conditions in 2000). Nonetheless, these comparisons are informative. The mean, standard deviation, and RMS error for these comparisons are 0.2 ft, 0.3 ft, and 0.3 ft, respectively. The figure and the statistics indicate that the model performs well for this storm.

Table 7-1 demonstrates the differences between peak WLG measurements and HWM observations for the 1962 storm. In Great South Bay, the HWM observations are around

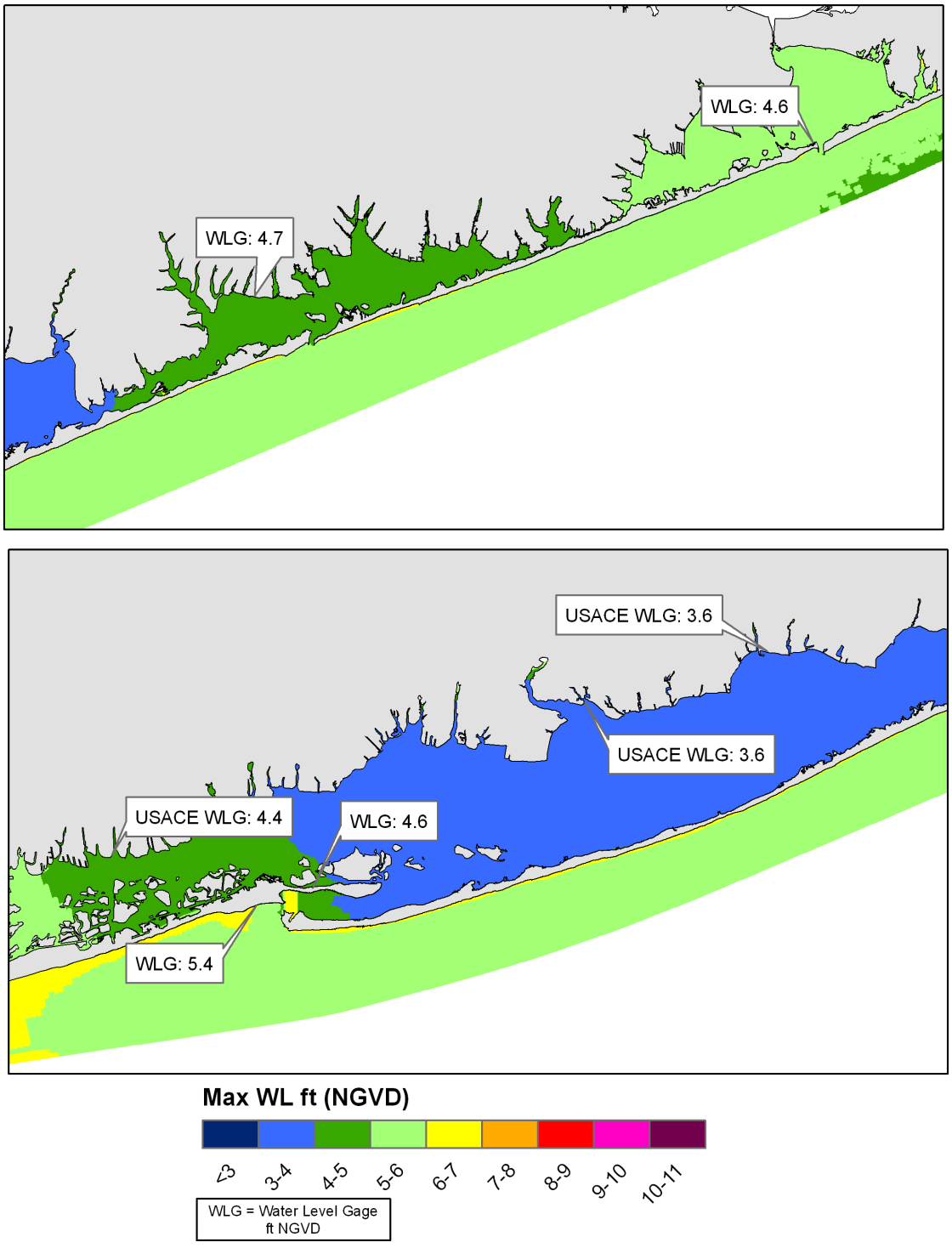

Figure 7-14. Comparison between simulated peak water levels, using Baseline Conditions topography, and peak WLG measurements for the 1962 Nor'easter.

Table 7-1. Peak WLG measurements and HWM observations for 1962 Nor'easter.

Location	Peak WLG (ft)	HWM (ft)	Delft3D (ft)
Station 1 (Great South Bay)	4.4	6.0	4.8
Station 7 (Great South Bay)	3.6	5.0	3.7
Eastern Great South Bay	3.6	5.0	3.5-3.8
Moriches Bay	4.7	5.0	4.3-4.6

1.5 ft higher than the WLG peak measurements. In contrast, the HWM observations and peak WLG measurement are closerin magnitude: 4.7 ft and 5.0 ft, respectively.

Additional bay WLG measurements exist for the September 1938 and August 1954 hurricanes. At the two bay measurements for August 1954, the simulated Baseline Condition peak water level is within 0.9 ft (Great South Bay) and within 0.2 ft (Shinnecock Bay). Given the changes in inlet and bay geometry between 1954 and 2000, these comparisons are quite good.

Comparisons with available bay HWM observations for the 1938 Hurricane and 1992 Nor'easter will be presented in the Realism test discussion in Chapter 8.

This chapter demonstrated that the modeling suite performs well in predicted bay storm water levels, for both small and large storms. In particular, simulations of the February 2003 storm demonstrated that the modeling suite reliably captures the temporal evolution of storm water levels within the three bays.

8. Breaching and Overwash Realism Simulations

Before proceeding with the simulation of the historical and the additional set of storms under Baseline Conditions barrier island topography, the model skill was assessed by comparing model results with available HWM observations and overwash and breaching data for three of the most significant storms of record: the September 1938 Hurricane and the December 1992 Nor'easter. The intent of the comparison was to validate the ability of the model to reproduce observed overwash and breaching impacts within the FIMP project area as well as reported HWM observations during these events. Despite of the lack of reliable pre- and post-storm topographic data, a significant effort was made to represent as well as possible the pre-storm topography for each storm in the model.

8.1 September 1938 Hurricane

The barrier island topography in 1938 was significantly different than under Baseline Conditions. Therefore, it was important to develop a model grid representative of 1938 topography that would result in storm impacts similar to those documented after the storm. Two sources of data were available to develop the model topography. The first one consists of two sets of aerial photography taken almost 3 months before the storm (June 30th, 1938) and a few days after the storm (September 24th, 1938). These photos do not provide barrier island elevation data but they can be used for a qualitative analysis and comparison of pre- and post-storm conditions. The second source consists of an incomplete set of plans depicting approximate pre- and post-storm topographic conditions. In addition, these maps identify locations where overwash and/or breaching were observed. These maps include elevation contours drawn by hand based on pre- and post-storm stereo aerial photography and possibly other sources of information such as USGS quadrangle sheets. An example of the pre- and post-storm maps near Moriches Inlet is presented in Figure 8-1. The maps cover most of the FIMP barrier island from Fire Island Inlet to Tiana Beach, but unfortunately maps including Shinnecock Inlet and areas farther east were lost. Therefore, the area breached by the 1938 storm, which subsequently became Shinnecock Inlet, was assigned a maximum profile elevation of 10 ft NGVD based on the available aerial photography and on the closest elevations obtained from the available maps. Other areas not included in the charts, which in general are not affected by the storm, are based on the Baseline Condition topography (i.e., LIDAR 2000 data). Figure 8-2 and Figure 8-3 show maximum barrier island elevations as defined in the model (typically the dune crest) along the length of the FIMP project area for baseline and 1938 conditions. Note how the elevations were significantly lower in 1938 than in the Baseline Condition in the vicinity of Moriches Inlet, which is the area that suffered the most damage during this storm. Areas in Figure 8-2 and Figure 8-3 where the maximum dune elevation is similar for the pre-1938 and Baseline Conditions, are those where information from the topgraphic maps was not available and therefore baseline topography was used.

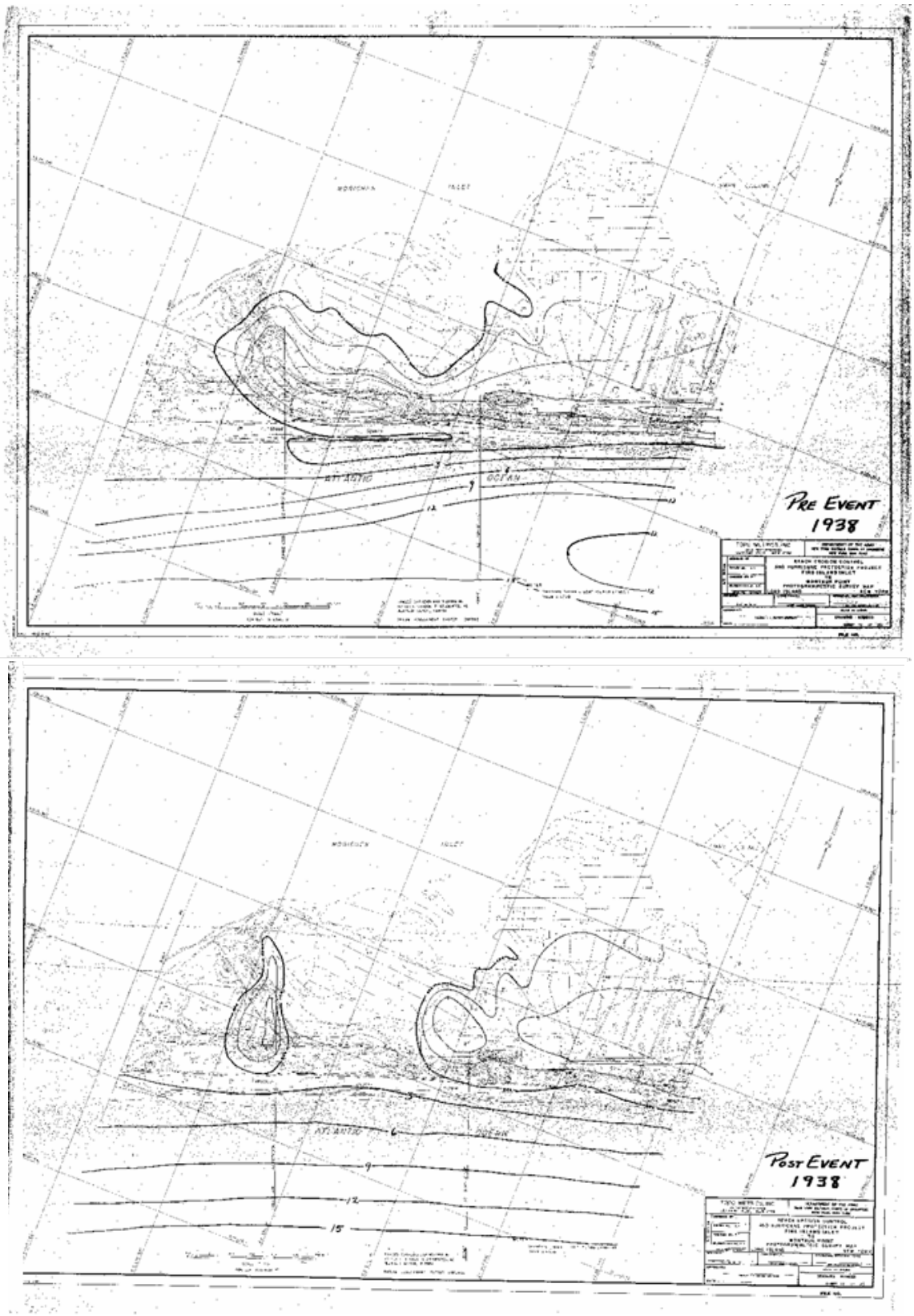

Figure 8-1: Example of pre- and post-1938 Hurricane charts at Moriches Inlet.

Model bathymetry was developed using available NOAA surveys from the 1930's with some modifications based on the maps and the aerial photographs. A dredged channel in the back side of the barrier island about 8 feet deep where Shinnecock Inlet opened was also implemented in the model grid. This channel was a remnant from a previous attempt to artificially open an inlet at the same location. The barrier island in front of the channel, as implemented in the model, had a width of ~350 ft with a dune height of 10 ft and a dune width of 100 ft. East and West of the channel area the barrier island width is around 800-1000 ft. Note that there are some significant discrepancies among the different data sources at some locations. For example the barrier topography near Moriches Inlet and the inlet geometry is similar for the topographic maps and NOAA surveys data while it differs from the pre-storm aerial photo. Data obtained from charts and surveys was used when available since these contain information on elevations.

Initial model topography was modified using the dune lowering relationships (i.e., lowering vs. initial dune elevation) developed by CHL using SBEACH for baseline barrier island conditions. Although barrier island conditions in 1938 differ significantly from the Baseline Conditions, the range of profiles extracted from the Baseline Conditions, to represent each region, covers most of the variability observed in the 1938 topography for the same region. In addition, in areas where the dune height was even lower that those observed under Baseline Conditions, dune lowering prior to inundation was assumed to be zero. This assumption is supported by SBEACH results under Baseline Conditions for the 1938 storm that showed no dune lowering prior to inundation for the lowest profiles (dune height in the order of 8-9 ft (NGVD).

After a two-day spin-up period of the hydrodynamics, the storm was simulated from 21 September 1938 00:00 to 22 September 1938 02:00 forcing the Delft3D model with waves, wind, atmospheric pressure, and water levels at the offshore boundaries. Winds blowing from the land were decreased by 30% in order to account for land effects. This follows recommendations and findings from the February 2003 simulation presented in Section 2.9.2.

The 1938 Hurricane caused widespread overwash and created several breaches across the barrier island (see Figure 8-4). These included four to Shinnecock Bay, three to Quantuck Bay and eastern Moriches Bay, and four to Moriches Bay in the vicinity of the inlet. With the exception of the Shinnecock Inlet opening, these breaches were all closed mechanically shortly after the storm.

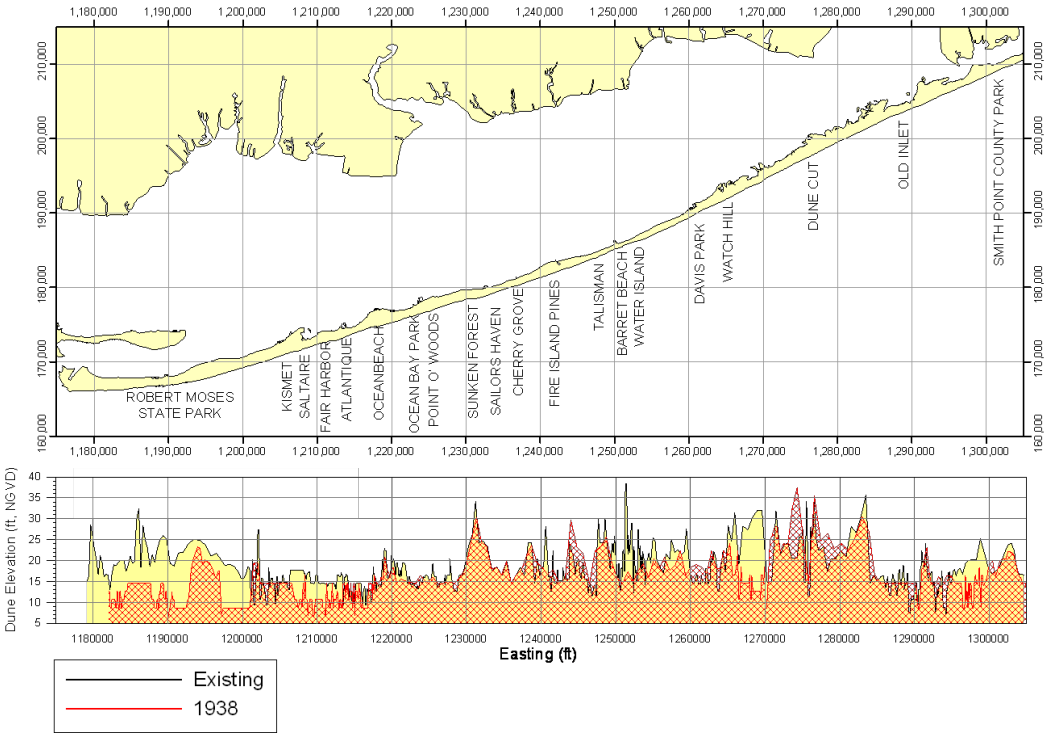

Figure 8-2: Maximum dune elevations for pre-1938 and Baseline (2001) conditions

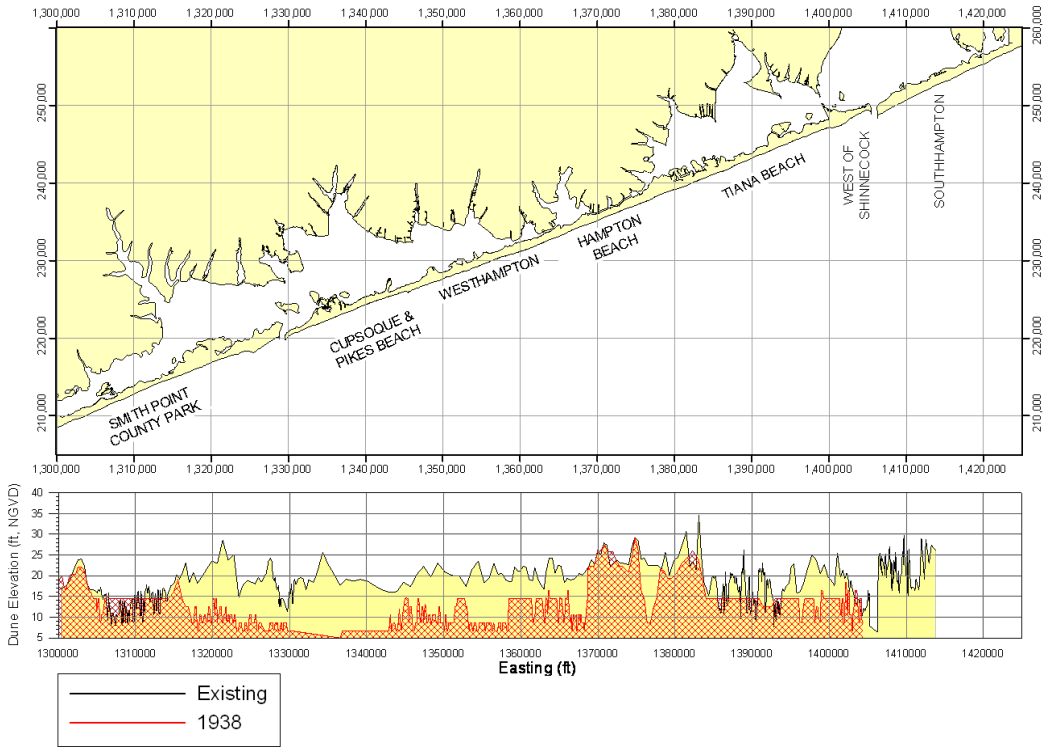

Figure 8-3: Maximum dune elevations for pre-1938 and Baseline (2001) conditions (continued).

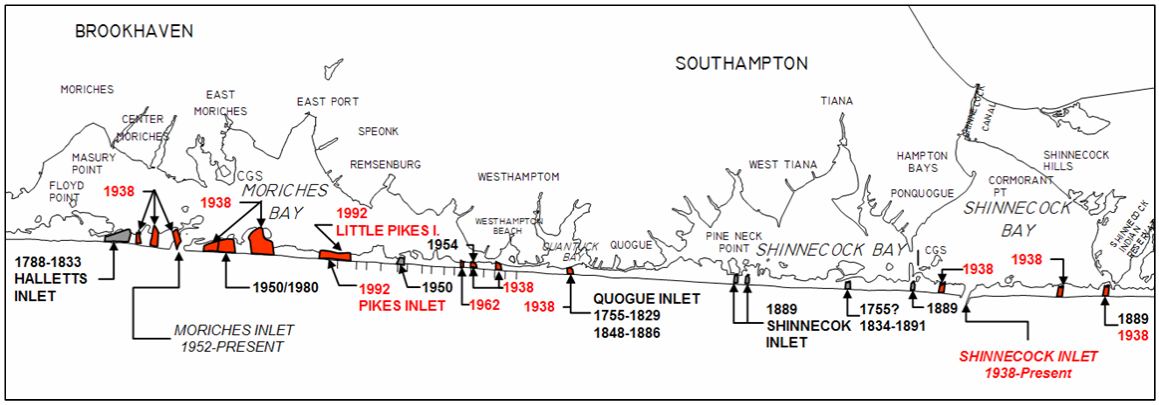

Figure 8-4: Observed overwash and breaching from 1938 Hurricane.

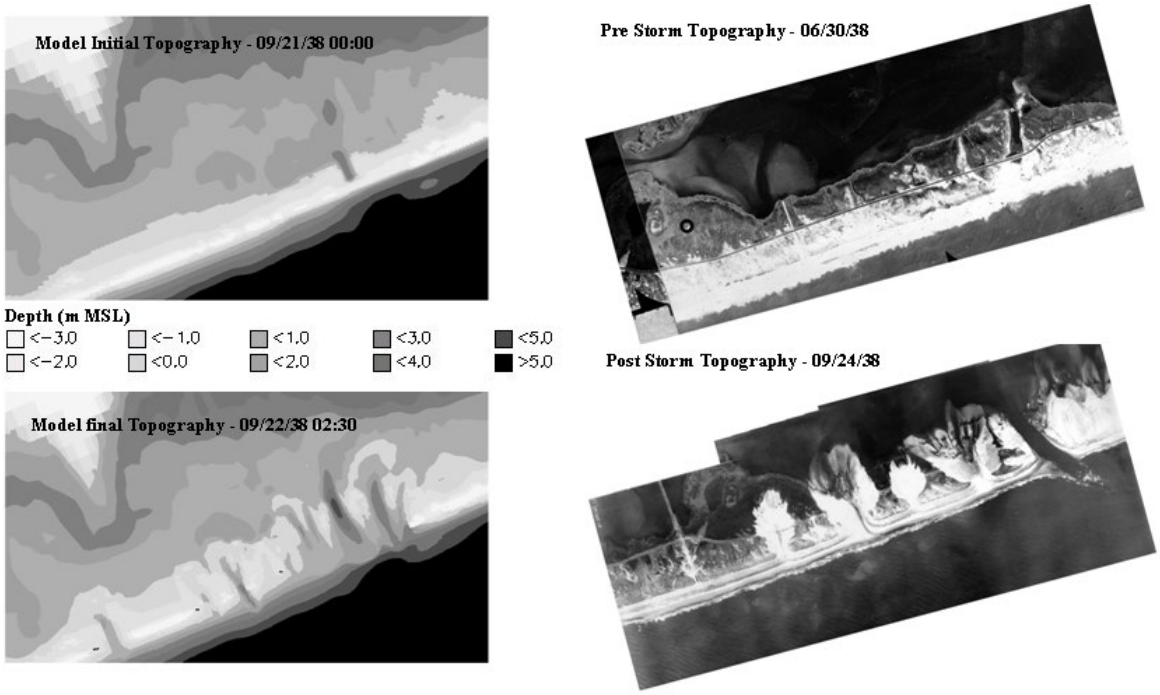

Figure 8-5: Shinnecock Inlet, Realism Test 1938 Storm. Pre and Post-Storm model topography and Aerial Photographs

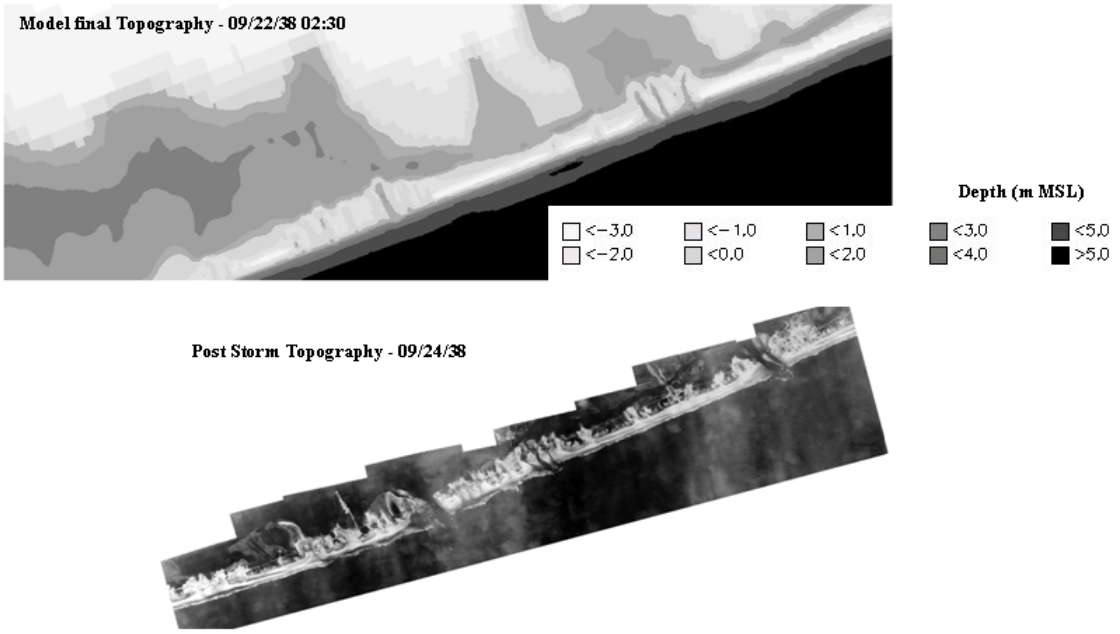

Figure 8-6: East of Moriches Bay, Realism Test 1938 Storm. Pre and Post-Storm model topography and Aerial Photographs

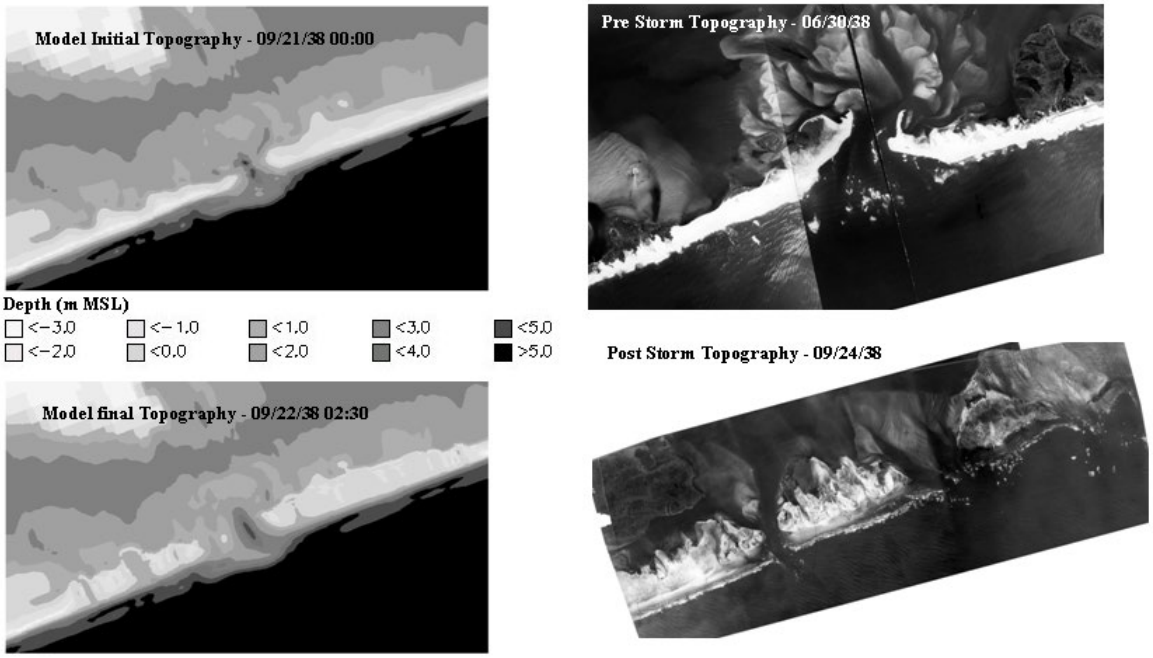

Figure 8-7: Moriches Inlet, Realism Test 1938 Storm. Pre and Post-Storm model topography and Aerial Photographs

The model predicts the opening of a relatively wide and deep full breach[7] at the Shinnecock Inlet location together with significant overwash and two other small breaches in the immediate vicinity. Two additional partial breaches are also observed near Ponquogue bridge. As shown in Figure 8-5, these results are very similar to the observed storm impacts. Note how material is transported bayward in the model. One additional breach and other overwash areas observed east of Shinnecock Inlet were not predicted because the model uses the Baseline Conditions topography and barrier island geometry in that area, which is presumed to be wider and higher than in 1938 since this area has experienced significant accretion after the construction of the east inlet jetty. Three additional breaches and significant overwash were predicted to Quantuck Bay and eastern Moriches Bay, which also roughly correspond with the observed impacts in this area (Figure 8-6), although the breach locations along Westhampton Beach are not exactly the same.

At Moriches Inlet the model also predicts significant overwash and widening of the inlet (Figure 8-7). A large amount of material is deposited bayward of the barrier island during the storm. Breaches are predicted east and west of the original inlet location, which also coincides with observations.

Additional overwash is observed in the vicinity of Democrat Point, east of Fire Island inlet, and at some locations along Fire Island, although no breaches were predicted there and none were observed in the data.

Simulated peak water levels were compared to HWM observations reported by Harris (1963) and they are presented in Figure 8-8. Within eastern Shinnecock Bay, simulated water levels are in the 6 to 7 ft NGVD range which is similar the two reported HWMs (6.5 and 7.2 ft NGVD). This is a remarkably good comparison considering that model simulates the opening of Shinnecock Inlet and at the same time simulates quite accurately the peak water levels at Shinnecock Bay. This indicates that the model also predicts accurately the flow through the breaches and over the barrier island into Shinnecock Bay and to some extent the breach dimensions.

At central and eastern Moriches Bay reported HWMs range from 12 to 15.7 ft NGVD. The largest simulated values are in the order of 11 ft NGVD within eastern Moriches Bay, with a peak water level offshore of Moriches Inlet below 10 ft. Simulated values at western Moriches Bay and Mastic Beach are in the 5-ft to 8-ft NGVD range while reported values are in the 7-ft to 10-ft range. Very good agreement is observed at South Oyster Bay and Central Great South Bay. At these locations reported HWMs are 4.7 and 3.6 ft NGVD respectively while model simulated values are 4.5 and 3.2 ft NGVD. At Eastern Great South Bay simulated values are in the order of 4 ft NGVD witch are roughly 1 ft lower than the HWM.

[7] See the IMPORTANT DEFINITIONS section at the beginning of this report for definitions of full breaching, partial breaching, and overwash for this study.

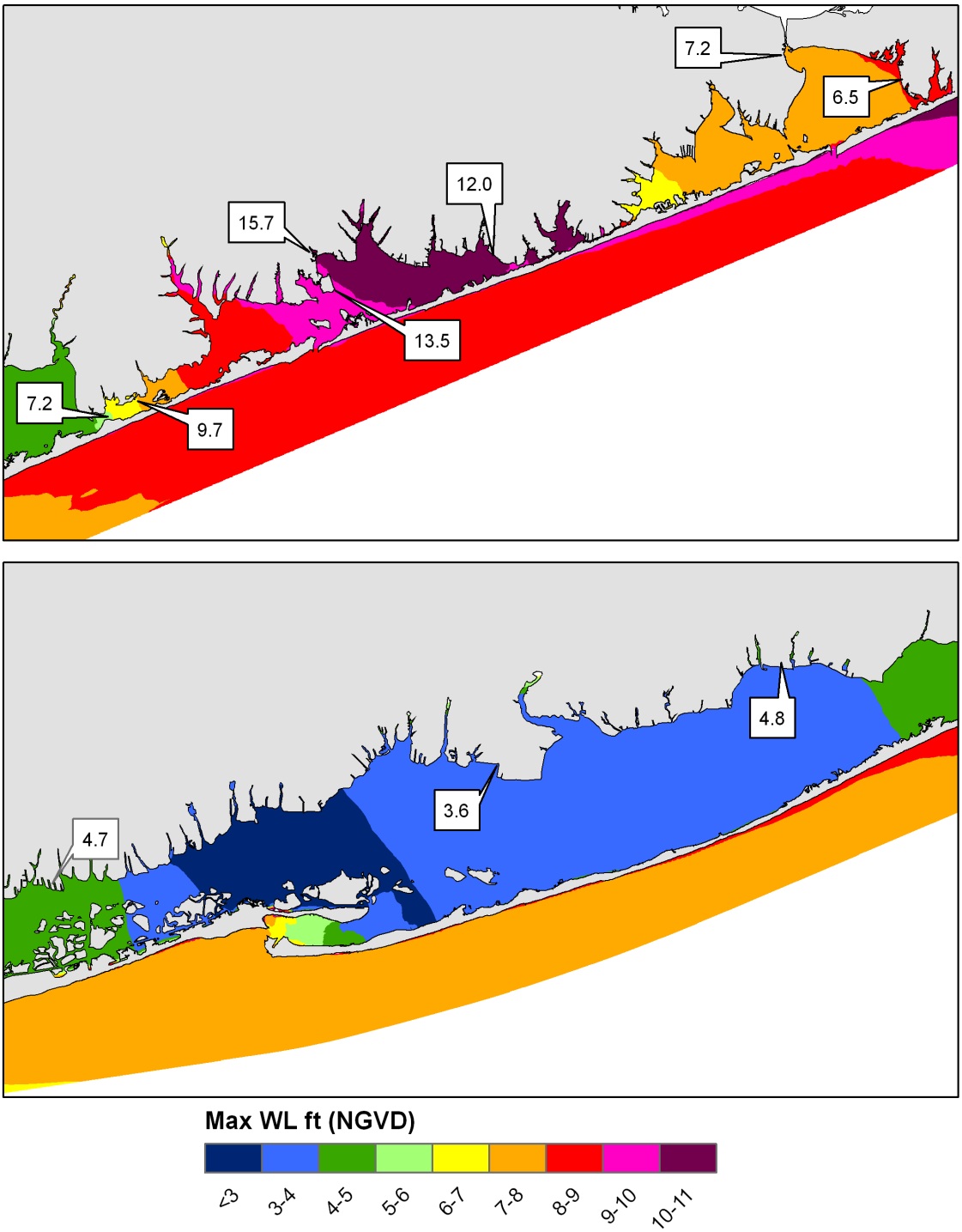

Figure 8-8: Peak water level from the Realism September 1938 test. Boxes present HWM observations from (Harris, 1963) in ft NGVD. Shoreline is representative of 1995 conditions.

Some of these differences between predicted values and reported HWMs, particularly in Moriches Bay, are likely due to the contribution of the waves to the HWM observations. Butler and Prater (1983) considered the wave induced contribution to the flood levels for the September 1938 storm to have a value between 2.5 and 4 ft at different locations throughout the project area. This local wave effect includes the wave setup and 7/10 of the estimated peak wave height at the site.

8.2 December 1992 Nor'easter

The most recent storm that opened a breach in the FIMP area was the December 1992 Nor'easter. This storm created two breaches east of Moriches Inlet in the vicinity of Pikes Beach (Figure 8-9). The westernmost (and initially largest) of the breaches (Pikes Beach breach) was repaired within one month of the storm (2 January 1993). However, the other (Little Pikes Beach breach) remained open to continuous tidal flow for nearly 10 months after the storm, leading to continued growth and loss of numerous structures on the barrier island. Prior to the storm, this area was suffering significant erosion and was particularly vulnerable to storm impacts. The Westhampton Interim project, first constructed in 1997, now provides protection against future storm-induced overwash and breaching. This improved condition is reflected in the Baseline Conditions grid. Therefore, it was necessary to modify this grid to simulate the effects of the 1992 storm. Specifically, a new grid was developed with high resolution at the inlets and at the area between Moriches Inlet and the Westhampton groin field, including the location of the 1992 breaches.

Unfortunately, detailed pre-storm topographic data were not available. Therefore, available 1995 topography was modified using available pre-storm aerial photography and anecdotal information about the minimum barrier elevations prior to the storm. Specifically, Spencer and Terchunian (1997) reported that by 1992 the three mile stretch of beach from the westernmost groin to Moriches Inlet had degraded so badly that the island overwashed during spring tides. In addition, First Coastal (1992) reported that two low areas with elevations around 6.5 ft NGVD had developed over Dune Road in Westhampton after the 1991 Halloween storm (October 1991). Based on this information, barrier elevations in the model were lowered to 6.5 ft NGVD (6.0 ft MSL) at roughly the location where the Pikes Beach breach occurred. Barrier island width at this location prior to the storm was approximately 750-800 ft based on available pre-storm aerial photography dated 29 September 1992. At the area where the Little Pikes Beach breach was observed the maximum barrier island elevation was set to 8 ft NGVD (7.5 ft MSL) and the barrier island width was as narrow as 500 ft, also based on the available pre-storm aerial photography.

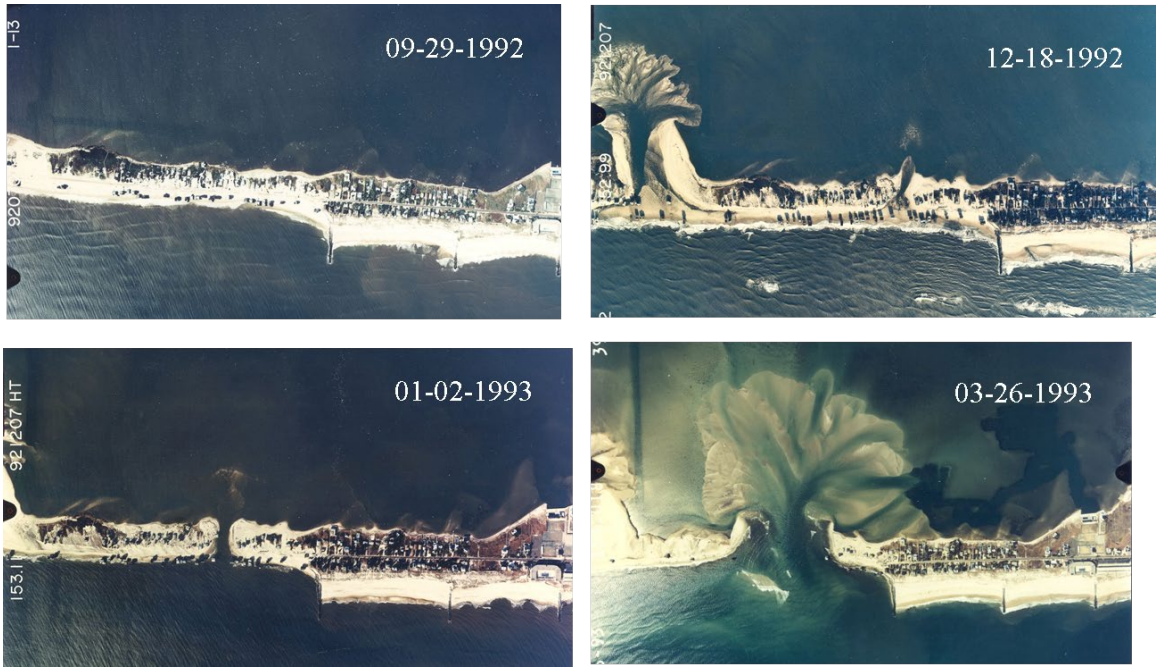

Figure 8-9: Pre- and Post-Storm aerial photographs of Pikes Beach Breach during the December 1992 Storm

Under these conditions the model predicts the opening of the western breach similar to the observed Pikes Beach breach. In addition, the model predicts the opening of a partial breach at the eastern location (Little Pikes Beach breach). Initial and final model topographies are shown on the two left panes of Figure 8-10. In general the simulated bathymetry at 12-13-1992 looks very similar to that observed in the 12-18-1992 photograph. That is, opening of a relatively small breach immediately west of the groin field and a larger one farther west with a large fan of accumulated material on the bay side. The dimensions of the breaches are probably not perfectly matched by the model since the initial topography, as previously mentioned, was based on anecdotal dune height values, aerial photographs, and the available 1995 topography and shoreline. Also note that this visual comparison is done between a photograph taken more than 5 days after the end of the storm (12-18-1992) while the model result corresponded to the end of the simulation on 13 December 1992.

In the days following this storm, normal tide levels exceeded the breached elevations in both locations (the partial breach location and the full breach location) over at least part of the tidal cycle. Specifically, the full breach remained inundated throughout the tide cycle, while the partial breach was inundated only when the normal tide height exceeded the breach's deepest elevation This provided potential for both breaches to continue to deepen. This post-storm deepening process was most likely further accelerated by the presence of spring-tide conditions.

Sheffner and Wise (2000) presented a table of flood marks for the December 1992 storm. These values are presented in Figure 8-11 including the name of the township, the range of recorded surges (and number of observations points in the data set) and the average

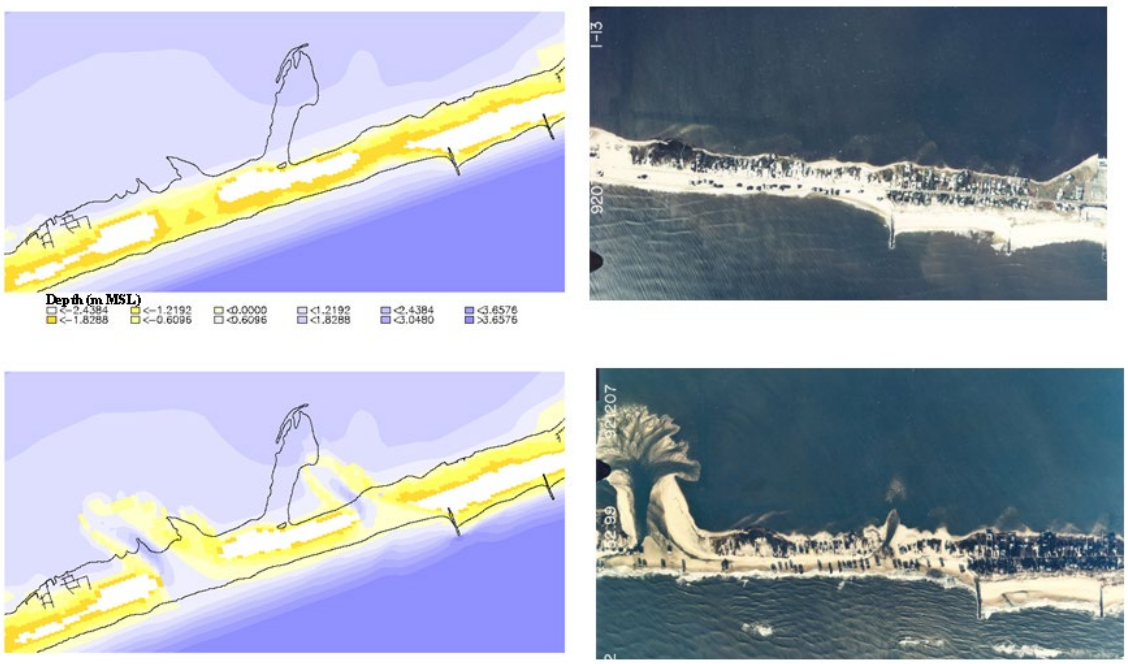

Figure 8-10: December 1992 model results. Top: Pre and Post-Storm Topography for 6.5 ft initial dune height. Bottom: Pre and Post-Storm Topography for 6.5 and 5 ft initial dune height

surge. Figure 8-11 shows that the simulated peak water levels agree within the range of observed values in the vicinity of the township where data were collected. At Moriches Bay, modeled values at Mastic Beach, Remsenburg and Central Moriches match very closely to the reported ones. In other locations at Moriches Bay the average reported HWMs are in the order of 1 ft higher although the simulated values are within the range of reported values. At Great South Bay, simulated values at Bay Shore agree with the average of the reported values. At Patchogue and Lindenhurst the model results are within the reported range although the average reported HWMs are underestimated by approximately 1 ft.

Overall, peak water levels obtained from the simulation of the December 1992 storm agree very well with the reported HWM considering the uncertainty in the observations and the large range of reported values. It is also noted that although the model includes the effect of winds in the hydrodynamics and also the effect of waves offshore, some local wave effects in the bays are not represented in the model and should account for some of the observed differences.

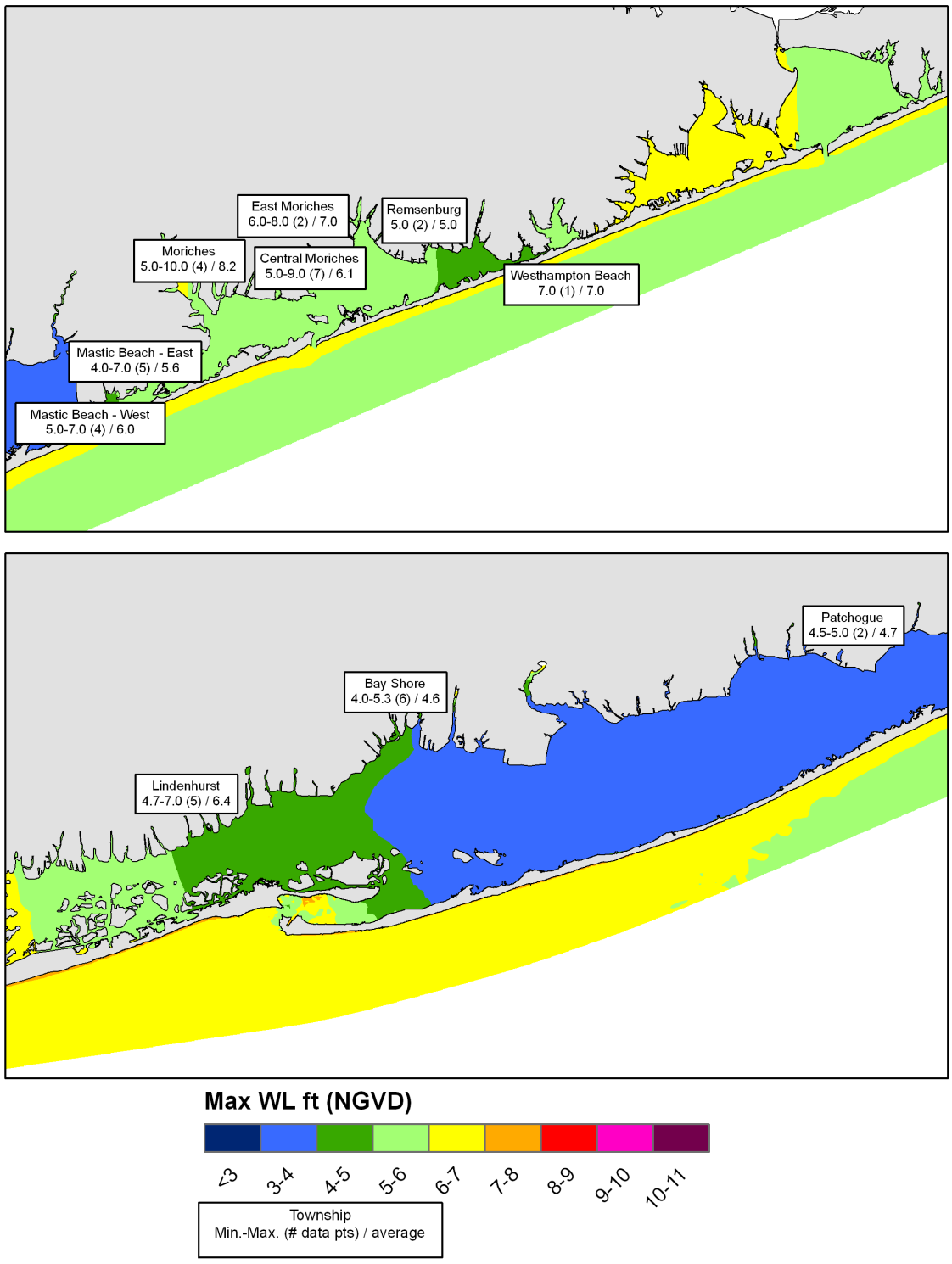

Figure 8-11: Peak water level from the Realism test of December 1992. Boxes present HWM from Sheffner and Wise (2000) in ft NGVD (range (number of observations): average). Shoreline is representative of 1995 conditions.

8.3 Summary

Overall the model simulations for these historic storms provide very realistic results and compare remarkably well with the available data, particularly when considering the uncertainty in the input hydrodynamic conditions (see Chapters 5 through 7) and, more importantly, the pre-storm topography. The simulation results are particularly accurate in the case of the 1938 storm, for which seemingly better topographic data in the vicinity of some of the damaged areas were available. Nonetheless, given the uncertainty with regards to the pre-storm topography and the possible errors in the input hydrodynamic, wind and wave conditions, the results of the 1992 Nor'easter simulation are also judged to be very accurate. Overall, the agreement between simulated and observed morphological impacts and also between peak water levels for the two storms and the reported HWMs can be considered excellent considering the uncertainty associated to this type of data.

9. Simulation Results

This section presents the results from the simulation of 36 historical storms and 21 additional storms under Baseline Conditions barrier island topography. The following is a discussion of the response of the bays to storm events, peak simulated water levels, water level contributions during storms, and morphological changes in the barrier island.

9.1 Response of the Bays to Storm Events

Tide and surge enter Great South Bay from the west through Jones Inlet and South Oyster Bay, from the east through Narrow Bay, and from the south through Fire Island Inlet. In addition, during extreme storm conditions ocean surge may inundate the barrier island and propagate into the bay. During normal conditions the main tidal flow contributor to Great South Bay is Fire Island Inlet. The influence of the tidal inflow through Jones Inlet is limited to the eastern part of South Oyster Bay. Therefore, during tidal flood conditions flow across the Robert Moses Causeway is generally towards the west. Flow through Fire Island Inlet reaches central and eastern Great South Bay although the main contributor to the eastern Great South Bay is the flow through Narrow Bay coming from Moriches Bay. During normal tidal conditions the flow through Narrow Bay changes direction from west to east during flood and ebb tide, respectively, due to the phase lag between the tides at Moriches and Fire Island Inlets. During storm events, the water elevation is higher in Moriches Bay than in eastern Great South Bay. This gradient generally creates a predominant flow westward through Narrow Bay at all tidal stages. Another important force influencing the water level distribution in the bays is the effect of wind during storms, which typically causes the formation of a water level gradient in the bays from west to east. This effect is particularly important in Great South Bay because it is the largest of the three bays in the FIMP study area. It is observed, especially during tropical storms, that water elevation increases in the western portion of the bay while it decreases in the eastern portion. Immediately after the storm and once the effect of the winds decrease, the water accumulated in western Great South Bay starts to move east. Therefore, during tropical storms the peak water level in eastern Great South Bay is observed 2 to 3 hours later than offshore. On the other hand, during extratropical events (e.g. March 1962 or December 1992) the peak water level at eastern Great South Bay is observed at high tide but one or two tides after the one that presented the peak water level offshore. This is a consequence of the dominance of flood over ebb flow through the inlet for the duration of the storm.

Water flows into Moriches and Shinnecock Bays through the existing inlets. During extreme storm conditions, additional water may enter the bays over the barrier island due to barrier overwash and inundation. Moriches and Shinnecock Bays are linked through Quantuck and Quogue canals. Tidal waters flow through Quantuck canal from eastern Moriches Bay and through Quogue Canal from Western Shinnecock Bay and converge at Quantuck Bay. This convergence of flow produces a water level gradient along Quantuck and Quogue canal with the peak elevation at Quantuck Bay.

Tidal and surge propagation into the bays depends strongly on the hydraulic efficiency of the existing inlets and bay hydrographic conditions. Ocean tides are reduced by 25% at Shinnecock Bay, from a range of 3.46 ft offshore to 2.62 ft at Quogue Canal. On the other hand, in Moriches Bay the tidal range is reduced by more than 60 percent from offshore of the inlet to Smith Point Bridge. In Great South Bay, the observed tidal range at WES-TG6 station near Nicoll Point is only 0.83 ft, representing a more than 75% reduction of the offshore tide. At the Fire Island Coast Guard Station near the Robert Moses Causeway the observed tidal range is 2.05 ft where the offshore tide has been reduced already by approximately 40%. This indicates a large reduction of the tidal range as the tide propagates into Great South Bay.

9.2 Peak Water Levels in the Bays

The distribution of flow through the bays observed during normal tidal conditions changes during storm conditions. For example, Moriches Bay fills more rapidly with storm surge flows than Great South Bay because of its smaller size and more efficient inlet, disrupting the normal tidal flood and ebb flow and producing a continued flow westward from west Moriches Bay through Narrow Bay into eastern Great South Bay.

Maps of simulated peak water levels for nine historical storms and three additional variations of the historical storms at high tide under Baseline Condition barrier island topography are presented in Figure 10-1 to Figure 10-4. These maps help to illustrate the following discussion. Shinnecock Inlet is the most efficient of the three inlets. During storm conditions (for both tropical and extratropical storms) the peak water levels simulated at Shinnecock Bay are generally on the same order or higher (due to offshore wave setup and local wind effects in the bay) than those observed offshore. This is not the case in Moriches Bay and especially in Great South Bay, where the peak water levels during storm conditions are significantly smaller than the peak water levels offshore. During storm conditions a significant exchange of water is observed between Moriches and Shinnecock Bays, particularly influencing Quantuck Bay. At the onset of the storm water enters through both inlets. A larger percentage of water that has accumulated in Quantuck Bay leaves through Shinnecock Inlet because the inlet is more efficient and also because the ebb tide occurs earlier at Shinnecock than at Moriches.

The efficiency of Shinnecock Inlet and, to a lesser degree, Moriches Inlet has a significant effect on the propagation of the offshore surge into the bays. As a consequence, the peak simulated water levels in Moriches Bay and especially at Shinnecock Bay are obtained for the largest tropical storms (See Figure 10-1 to Figure 10-4). The opposite applies for Great South Bay due to the low efficiency of Fire Island Inlet. The average peak water level produced by the extratropical storms of the historical set is around 0.5 ft higher than that obtained from the tropical storms in South Oyster Bay and Great South Bay. The storm surge associated with a tropical storm that lasts for only a few hours is significantly dampened at Fire Island Inlet while the surge generated by extratropical storms that last for several tidal cycles continues to increase the total discharge through the inlet during the storm, resulting in higher peak water levels in Great South Bay for extratropical than for tropical events.

Peak water levels at Great South Bay obtained from the numerical simulations of historical storms are on the order of 4.8 ft (NGVD) at the eastern and western ends of the bay, and decrease towards the center of the Bay to a value of 3.8 ft (NGVD). Peak simulated water levels in Great South Bay from the set of historical tropical storms are on the order of 0.5 ft lower than those obtained from the extratropical storms. At Moriches Bay peak water levels are observed at the western part of the bay with values on the order of 6.7 ft (NGVD), while at eastern Moriches Bay the peak simulated water levels are in the order of 5.5 ft (NGVD). At central and eastern Moriches Bay the peak water levels associated with a tropical storm are on the order of 1.2 ft higher than those from the largest extratropical storm. In western Moriches Bay, peak water level values obtained from both types of storms are practically the same because extratropical peak water levels are higher than tropical peak water levels in Great South Bay and in the vicinity of Smith Point Bridge. This is also because overwash occurs at Smith Point County Park during the simulation of the largest tropical storm (September 1938).

At Shinnecock Bay the peak simulated water levels from the historical set of storms are 8.9 ft (NGVD) to the east and around 7.6 ft (NGVD) at the west. This peak water level, produced by a tropical storm (September 1938), yields to peak water levels higher than those associated with extratropical storms on the order of 3 ft and 1 ft at the eastern and western parts of the bay respectively. Since the peak values are associated with the 1938 storm, this difference from west to east is due to the wind setup generated inside the bay during this particular storm.

For all the simulated storms, the peak water levels in the bays occurred during the September 1938 storm at high spring tide (See Figure 10-4). With differences in peak water levels offshore on the order of 0.75 to 1.25 ft higher than those associated with the historical storm simulation, peak water levels in the bays vary from bay to bay. It must be noted here that the contribution of overwash/inundation from this additional storm is higher than the contribution from the historical storm. At Shinnecock Bay, peak water levels for the additional storm at high tide are just over 1 ft higher than for the historical storm. At Moriches Bay, these differences are on the order of 1 ft. In Great South Bay, the differences vary along the bay. At western Great South Bay differences are in the order of 1 ft while at the east are from 0.5 to 0.75 ft. Finally at central Great South Bay differences are very small, less than 0.1 ft. Despite the fact that the September 1985 additional storm at high tide has the largest peak water levels offshore at the western part of the project, peak water levels in the bays are smaller than for the September 1938 additional storm at high tide.

In the case of extratropical storms, the peak simulated water levels are not produced by the same storm throughout the study area. Within the historical set, the peak water levels in central Great South Bay are associated with the March 1962 storm while peak water levels to the east correspond to the November 1953 storm. In addition, the December 1992 storm produces the peak water levels at Moriches and Shinnecock Bay. Figure 10-3 presents the simulated peak water levels for these three historical storms, and Figure 10-2 presents the simulated peak water level for the November 1950 extratropical storm.

Regarding the additional extratropical storms, the November 1953 storm produced the peak water levels in Great South Bay while the additional (high spring tide) November 1950 storm is associated with the peak water levels in Moriches and Shinnecock Bays. The lower pane of Figure 10-4 presents the simulated peak water levels for this additional November 1950 extratropical storm.

9.3 Water Level Contribution During Storm Conditions

The peak water levels presented in the previous section include the contribution of water from barrier island overwash, though for all the storms of the historical set only the September 1938 storm results in a significant contribution of water to the bays from overwash and inundation of the barrier island. The contribution from overwash events associated with the extratropical storms of the historical set is very small compared to the discharge through the inlets. Therefore, its contribution to the simulated peak water levels in the bays is minimal.

In order to quantitatively illustrate the overwash events during the 1938 storm, as it historically occurred, a discussion using model simulated values of peak discharges follows.

The September 1938 storm, the largest storm in the historical set, produces peak overwash discharge at Smith Point County Park on the order of 53,000 ft^3/s. This represents 33% of the peak storm flow through Moriches Inlet at the same time, and 70 % of the peak flow during normal tidal conditions. At Shinnecock Bay, overwash at Tiana Beach is on the order of 60,000 ft^3/s during the peak of the storm which represents about 17% of the flow through Shinnecock Inlet during the peak of the 1938 storm and over 67% of the flow during normal tidal conditions. On the other hand, overwash over the low area west of Shinnecock Inlet also results in a significant contribution. Here, a peak flow of 25,500 ft^3/s represents 28% of the normal tidal conditions flow through the inlet and 7% of the peak flow during the storm. In Great South Bay, water entering Fire Island Inlet (peak flow during the 1938 Hurricane was 349,000 ft^3/s) flows mostly eastward, because there is also a large flow entering the bay from the west through Jones Inlet and South Oyster Bay. Contribution due to the overwash at Old Inlet during the 1938 storm has a peak flow of 40,000 ft^3/s.

Other tropical storms, such as September 1944, August 1954 or September 1960, also produce significant, albeit smaller, overwash discharges. Peak storm flows over the barrier island for these storms at Old Inlet, Tiana Beach, and Smith Point County Park are below 1,000 ft^3/s, and barrier island inundation lasts for only a few hours. Therefore, the contribution of these inflows to the peak water levels in the bays is expected to be insignificant.

The largest water contributions from overwash/inundation are simulated for the additional tropical storms of September 1938 and September 1985 at high spring tide. Overwash contribution from the additional September 1938 storm at high spring tide is on the order of 2 to 3 times larger than the contribution from the historical September

1938 storm at Old Inlet, Smith Point County Park, Tiana Beach, and West of Shinnecock. Additional contribution at Western and Central Fire Island are small. The largest water contribution due to overwash/inundation in Western Fire Island is associated with the September 1985 additional storm at high spring tide, with peak storm flows on the order of 5,000 to 7,000 ft^3/s. For this storm, peak storm flows at Tiana Beach and West of Shinnecock are very small. At Smith Point County Park, the peak flow is 90,000 ft^3/s which is 30% smaller than the one associated with the September 1938 additional storm (high spring tide). At Old Inlet, the September 1985 additional storm at high spring tide produces the largest peak flow of all the simulated storms with a value of 130,000 ft^3/s.

The water contribution to peak water levels in the bays due to overwash/inundation from all the extratropical storms of the historical set is very small. Peak storm flows are below 1,500 ft^3/s for November 1950 and December 1992 and well below that value for the next two largest storms, November 1953 and March 1962. Out of all the simulated extratropical storms, the only storm that presents a significant flow over the barrier island due to overwash/inundation is the November 1950 additional storm (high spring tide). This storm presents peak storm flows of 22,000 ft^3/s and 14,000 ft^3/s at Old Inlet and Smith Point County Park, respectively.

9.4 Morphological Impacts

Morphological changes to the barrier island during storms are produced by overwash or by complete inundation of the dune (see IMPORTANT DEFINITIONS section). SBEACH results suggest that for many of the small storms that show no morphological response (Figure 9-5 and Figure 9-6), wave runup and overtopping result in the transport of sand landward from the beach berm and face of the dune leading to a very small accumulation of sand at the crest of the dune; therefore; creating a post-storm dune that is narrower but slightly higher than the pre-storm one. Some of the storms within the historical set that produce this type of morphological response are August 1976, March 1984; and December 1994 among others.

In other cases, overwash processes lead to erosion of the dune crest and transport of the sand behind the dune. Consequently, this type of overwash process leads to a lower dune crest and an accumulation of sand behind the dune. This process is present in a total of 15 storms (6 tropicals and 9 extratropicals) from the 36 storms of the historical set and a set of 18 additional storms (12 tropicals and 6 extratropicals). Figure 9-5 and Figure 9-6 present for each storm of the historical and the additional sets, the type of morphological response observed in the barrier island based on the definitions presented in the IMPORTANT DEFINITIONS section.

For the September 1938 historical storm, overwash is predicted for dunes with elevations of up to 17 to 20 ft (NGVD). In general, these are narrow dunes fronted by narrow berms. In some cases, dunes with wide berms and/or wide dunes and with a dune height elevation within the aforementioned range or in some cases even lower do not overwash

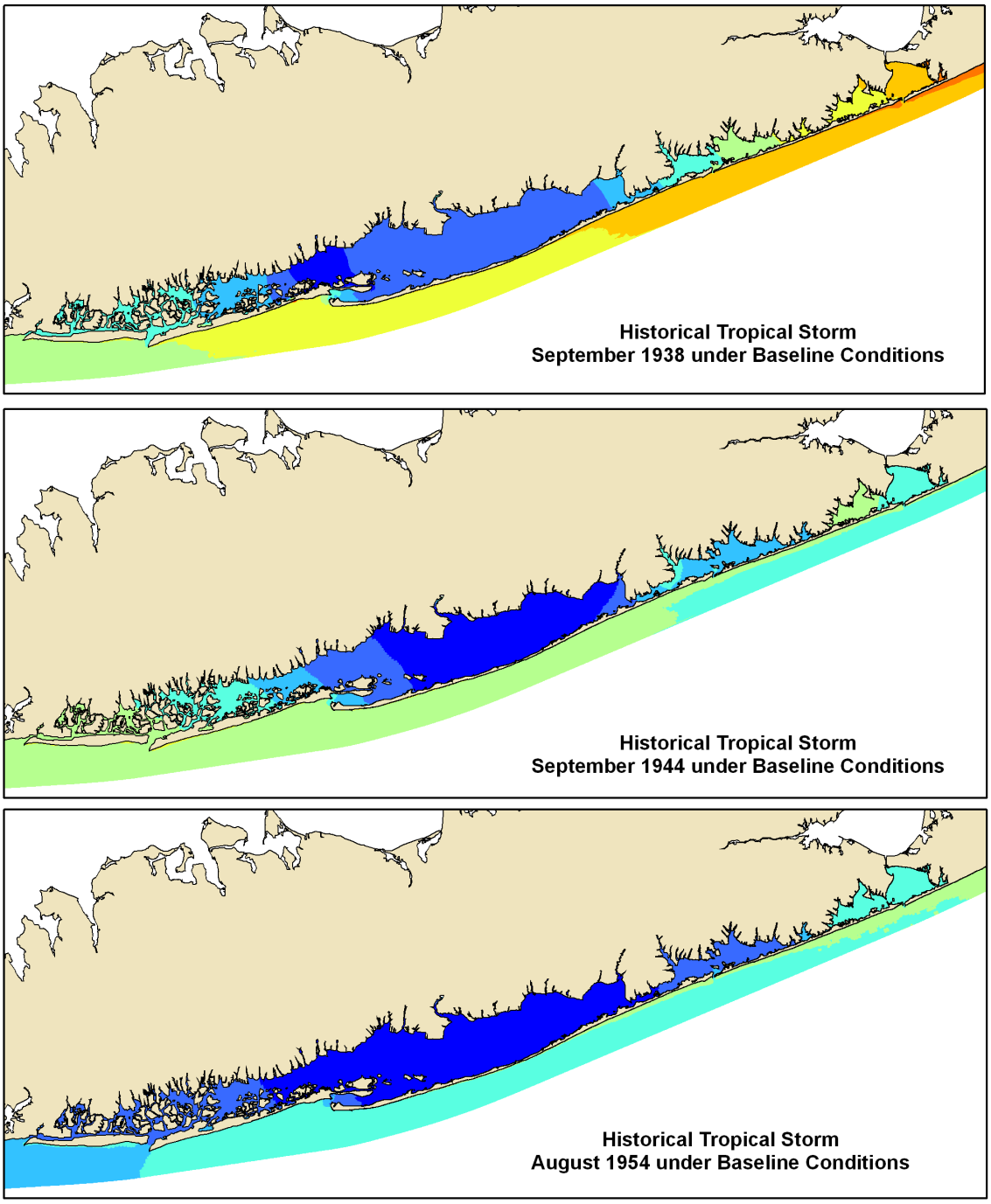

Figure 9-1: Peak water level in ft (NGVD) for the September 1938, September 1944, and August 1954 historical storms.

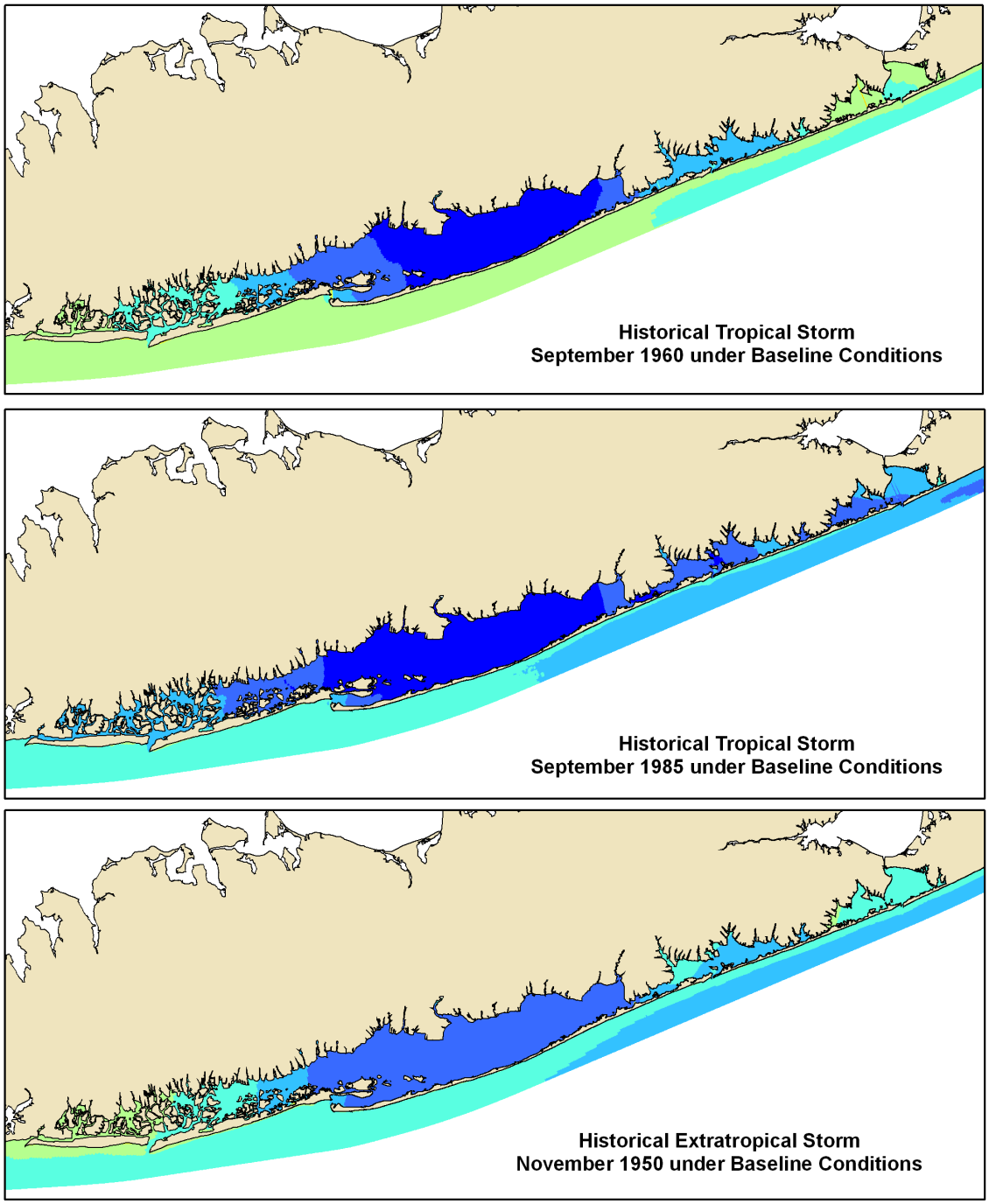

Figure 9-2: Peak water level in ft (NGVD) for the September 1960, September 1985, and November 1950 historical storms.

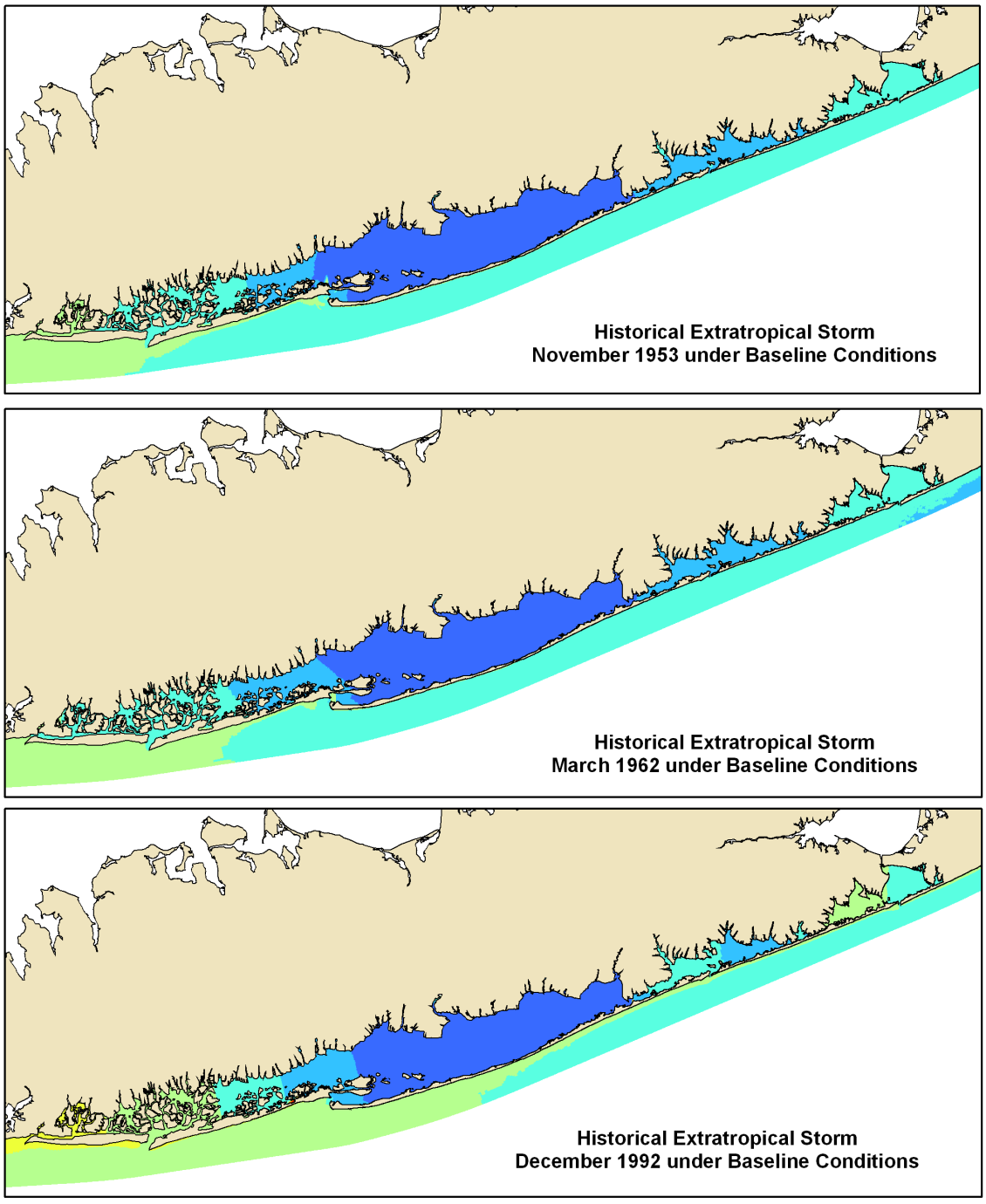

Figure 9-3: Peak water level in ft (NGVD) for the November 1953, March 1962, and December 1992 historical storms.

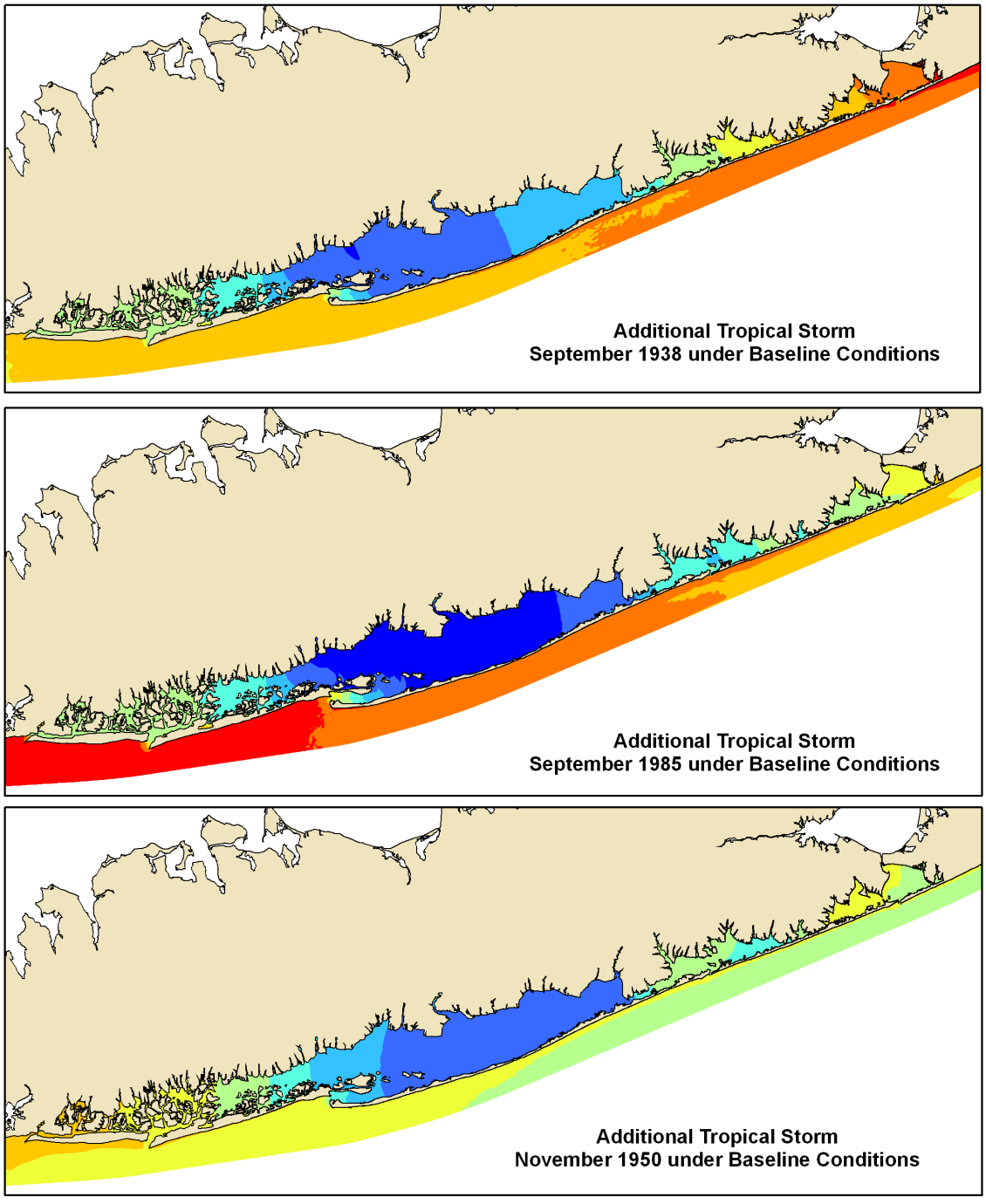

Figure 9-4: Peak water level in ft (NGVD) for the September 1938, September 1985, and November 1950 additional storms at high spring tide.

for the September 1938 storm. Therefore, dune height cannot be considered as the only factor leading to overwash. Overwash occurs at a maximum dune height that varies by storm and location. For example at Smith Point County Park, storms such as September 1944, September 1960, November 1950, and December 1992 overwash occurs with dune heights as high as 14 ft NGVD. On the other hand, the September 1985 and the 9 March 1993 storms only produce overwash for dunes lower than 11 ft NGVD.

In addition to the sediment transport due to runup, some storms present continued flow over the barrier island after the water level offshore reaches the dune crest (i.e., inundation). This effect was simulated for 3 tropical (September 1938, September 1944, and September 1960) and 4 extratropical (November 1950, November 1953, March 1962, and December 1992) storms of the historical set. Most of the storms included in the additional set present some degree of barrier island inundation with the exception of those cases associated with low tide conditions. The maximum dune heights at which inundation is observed for the September 1938 historical storm vary with location, but the values are on the order of 13-15 ft (NGVD). These areas normally contain narrow dunes where significant dune lowering prior to inundation occurs. Inundation for the rest of the storms of the historical set occurs mainly at Old Inlet, within the Wilderness Area. Inundation occurs at low profiles (about 9 ft NGVD) or at relatively narrow profiles with dune heights between 12 and 15 ft NGVD where the dune was lowered about 4 to 6 ft prior to inundation by wave runup (in SBEACH).

Inundation of the dunes can lead to the formation of a full breach or a partial breach. Figure 9-5 and Figure 9-6 present the locations and storms for which either a full breach or a partial breach occur. From the historical set of storms, only the September 1938 storm produced a breach at the Wilderness Area, specifically at Old Inlet. As observed in Figure 9-8 the storm opens a breach at Old Inlet at a location where the initial dune height was just below 9 ft NGVD. East of this location, and in areas with similar or even lower initial dune heights, the storm only creates a partial breach with a large washover fan. This morphological response is a consequence of a wider barrier island and the presence of shallow marshes at the bay side of the barrier island in the eastern location. The September 1938 storm also created partial breaches at Smith Point County Park, Tiana Beach, and West of Shinnecock. About ten large washover fans were created by channelized overflow at these locations. Figure 9-7 to Figure 9-11 present the pre- and post-storm model topography in these areas together with the morphological changes produced during the simulation. As these figures demonstrate, depth and width of these overwash channels vary from location to location.

Figure 9-12 presents cross sections through 4 locations within the vulnerable areas where the largest dune erosion values were modeled. In general, these profiles correspond to the lowest profiles in the vulnerable area, and they inundated before any dune lowering prior to inundation occurred. Here, inundation occurs prior to any pre-inundation dune lowering. Consequently, all morphological changes at these locations are simulated by Delft3D. It should be noted that in other profiles with higher dunes the pre-inundation contribution , simulated with SBEACH, to morphological changes is more important, and in some cases, the dune is only lowered due to runup if inundation does not occur. From

the profiles presented in Figure 9-12, only the West of Shinnecock profile includes some dune lowering prior to inundation.

The simulation of the September 1938 storm during high spring tide produces larger morphological changes in the barrier island than those changes produced by the historical storm. The September 1938 storm at high tide produces additional full breaches at Smith Point County Park and West of Shinnecock and a partial breach at Tiana Beach. At Old Inlet the storm develops a wide and deep full breach and a smaller breach at the eastern area where only a partial breach developed for the historical storm. In addition, significant overwash is observed at Robins Rest within the Western Fire Island reach. Morphological results from the September 1938 at high spring tide are presented in Figure 9-13 to Figure 9-18.

The second largest storm of the historical set is the September 1985 hurricane Gloria. This historical event happened during low tide and its simulation under Baseline Condition topography results in a limited number of overwash events, due to runup only. The additional simulation of the Hurricane Gloria at high spring tide under Baseline Conditions topography opens a wide and deep full breach at Old Inlet and a second one east of this location. In addition it also opens several partial breaches at Smith Point County Park. This storm creates the most pronounced morphological changes at the Western Fire Island reach though none of these overwash events developed into a full or partial breach. Figure 9-19 to Figure 9-23 present the pre- and post-storm model topography for Hurricane Gloria at high spring tide under Baseline Conditions topography together with the morphological changes produced in the barrier island during the simulation. Finally, Figure 9-24 presents cross sections through 4 locations at the vulnerable areas where the largest dune erosion values were simulated.

9.5 Summary

A total of 36 historical and 21 additional storms were simulated under Baseline Conditions of the barrier island. Within the historical set, the peak water elevations at Great South Bay are produced by extratropical storms while tropical storms generate the peak water levels at Moriches and Shinnecock Bay. Out of the 57 simulated storms, the additional September 1938 storm at high spring tide produces the highest peak water levels in all the bays. Only a small number of storms (the historical September 1938, the additional September 1938 at high spring tide, the additional September 1944 at high spring tide, the additional September 1985 at high spring tide, and its variations, and the additional November 1950 extratropical storm at high spring tide) have a significant contribution to the water levels in the bays due to overwash/inundation of the barrier island. In addition, only these storms produced full breaches or partial breaches at the barrier island. Modeling results indicate that the Wilderness Area ,and particularly Old Inlet, is the most vulnerable location of the barrier island being followed closely by Smith Point County Park. These areas represent the lowest dunes of the study area under baseline conditions.

	Storm Date	WFI	CFI	WA	SPCP	TIANA	WOSI
Tropicals	38/9/18						
	44/9/12						
	51/10/2						
	54/8/27						
	54/9/8						
	54/10/13						
	60/9/9						
	61/9/17						
	71/8/25						
	72/6/19						
	76/8/7						
	85/9/24						
	91/8/16						
	99/9/14						

	OVERWASH
	PARTIAL BREACHING
	FULL BREACHING

	Storm Date	WFI	CFI	WA	SPCP	TIANA	WOSI
Extra-tropicals	50/11/22						
	53/11/4						
	55/10/11						
	56/9/25						
	62/3/3						
	77/11/5						
	78/1/17						
	78/2/4						
	79/1/22						
	80/10/22						
	84/3/26						
	85/2/9						
	91/10/27						
	92/1/1						
	92/12/8						
	93/3/2						
	93/3/9						
	94/2/28						
	94/12/21						
	96/1/5						
	96/10/6						
	98/2/2						

Figure 9-5: Morphological response of the barrier island for the Historical Set of storms by vulnerable area (WFI: Western Fire Island; CFI: Central Fire Island; WA: Wilderness Area; SPCP: Smith Point County Park; TIANA: Tiana Beach and WOSI: West Of Shinnecock Inlet)

	Storm Date	WFI	CFI	WA	SPCP	TIANA	WOSI
Tropicals	38/9/18 A 1.0						
	38/9/18 A 0.5						
	44/9/12 A 1.0						
	44/9/12 A 0.9						
	44/9/12 A 0.3						
	54/8/27 A 1.0						
	60/9/9 A 1.0						
	60/9/9 A 0.3						
	85/9/24 A 1.0						
	85/9/24 A 0.9r						
	85/9/24 A 0.9f						
	85/9/24 A 0.5						
	85/9/24 A 0.37						
	85/9/24 A 0.2						
Extra-Tropicals	50/11/22 A 1.0						
	52/11/3 A 1.0						
	62/3/3 A 1.0						
	80/10/22 A 1.0						
	92/12/8 A 1.0						
	93/3/9 A 1.0						

	OVERWASH
	PARTIAL BREACHING
	FULL BREACHING

Figure 9-6: Morphological response of the barrier island for the Additional Set of storms by vulnerable area (WFI: Western Fire Island; CFI: Central Fire Island; WA: Wilderness Area; SPCP: Smith Point County Park; TIANA: Tiana Beach and WOSI: West Of Shinnecock Inlet)

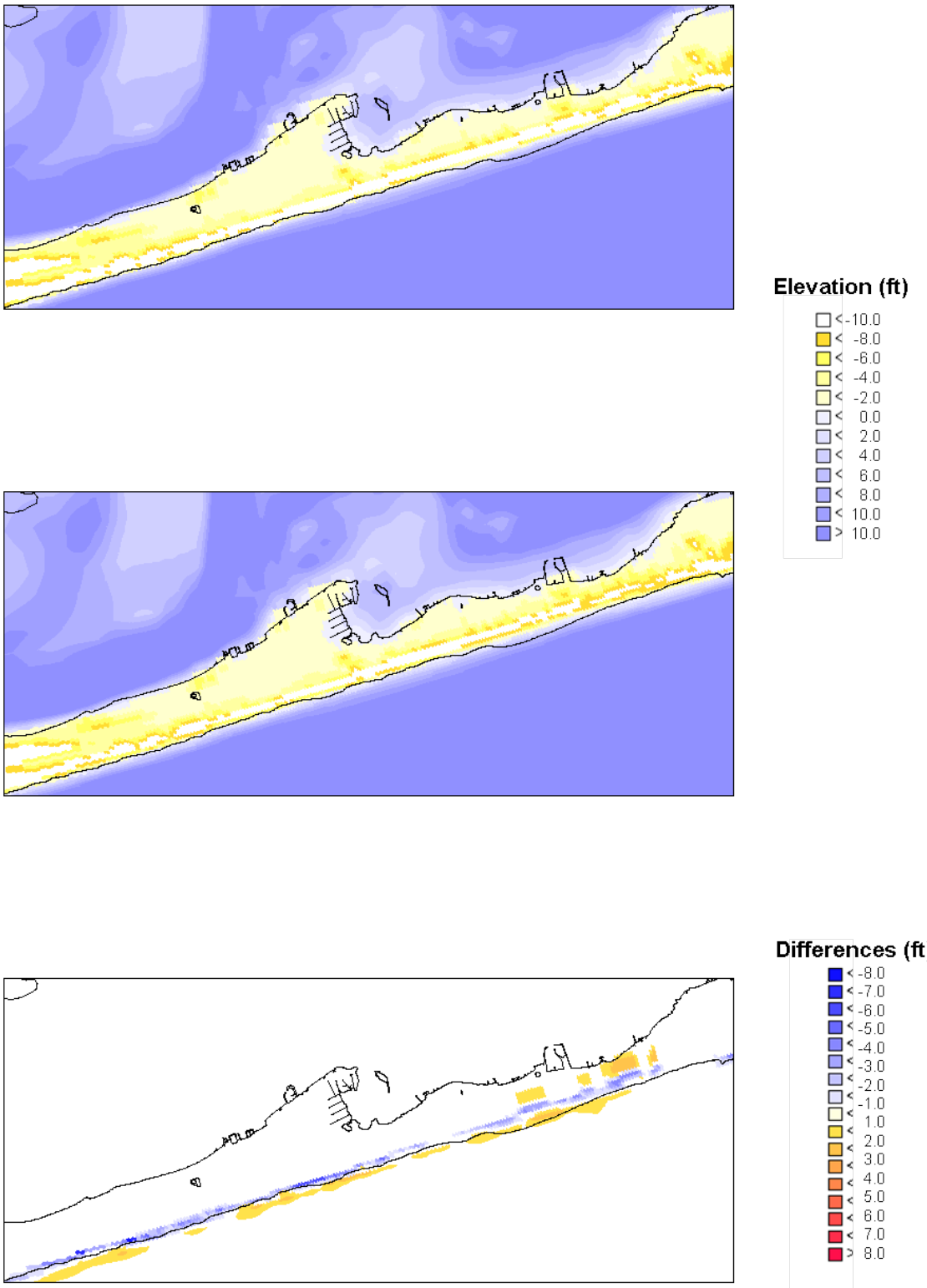

Figure 9-7: Historical Storm September 1938 under Baseline Conditions Topography. WESTERN F.I. COMMUNITIES. Model topography: (Top) Pre-Storm (ft MSL) and (Middle) Post-Storm(ft MSL) . (Bottom) Storm induced morphological changes in ft. (Blue – Erosion, Red – Deposition).

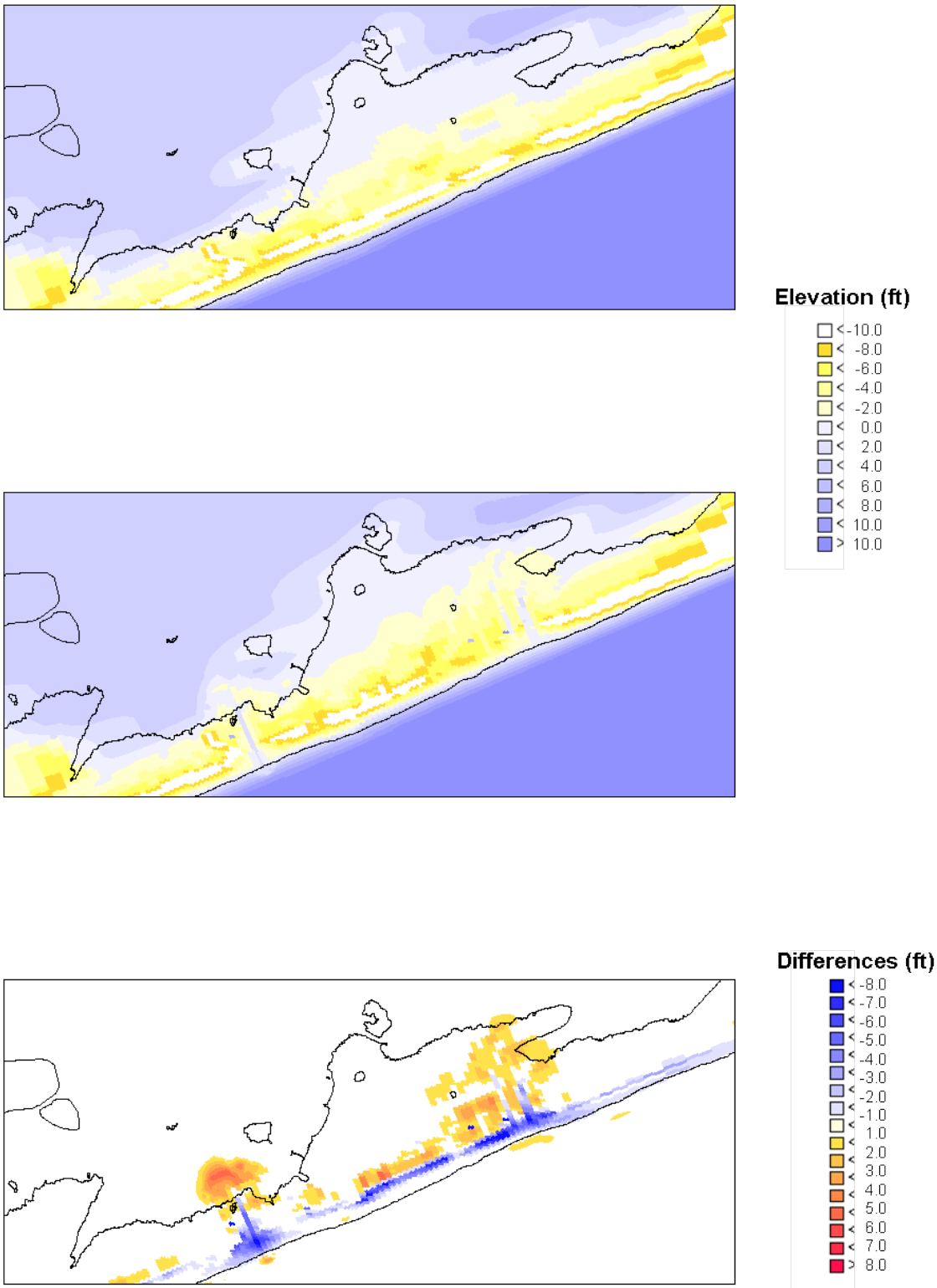

Figure 9-8: Historical Storm September 1938 under Baseline Conditions Topography. OLD INLET. Model topography: (Top) Pre-Storm (ft MSL) and (Middle) Post-Storm(ft MSL) . (Bottom) Storm induced morphological changes in ft. (Blue – Erosion, Red – Deposition).

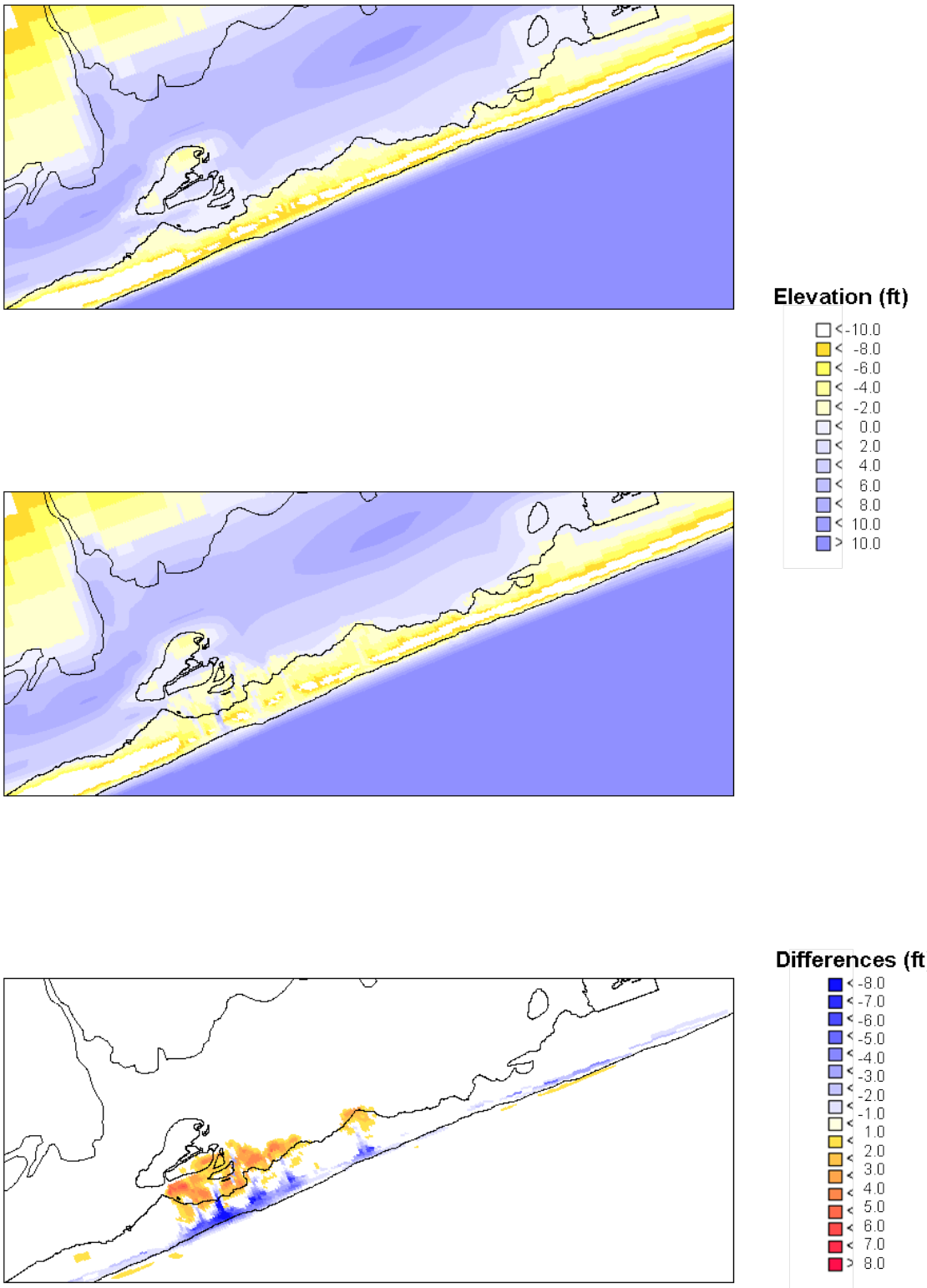

Figure 9-9: Historical Storm September 1938 under Baseline Conditions Topography. SMITH POINT C. P. Model topography: (Top) Pre-Storm (ft MSL) and (Middle) Post-Storm(ft MSL) . (Bottom) Storm induced morphological changes in ft. (Blue – Erosion, Red – Deposition).

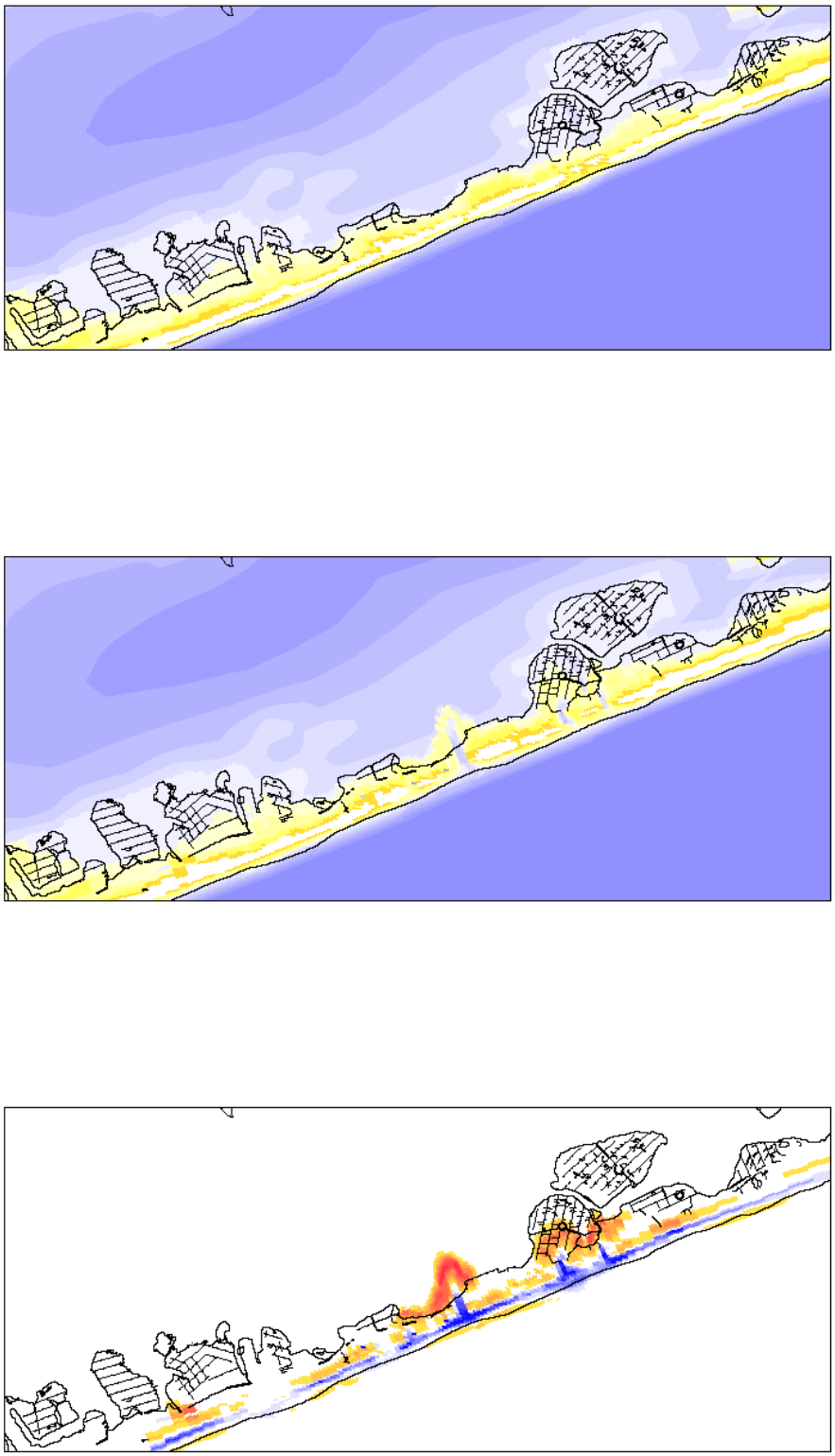

Figure 9-10: Historical Storm September 1938 under Baseline Conditions Topography. TIANA BEACH. Model topography: (Top) Pre-Storm (ft MSL) and (Middle) Post-Storm(ft MSL) . (Bottom) Storm induced morphological changes in ft. (Blue – Erosion, Red – Deposition).

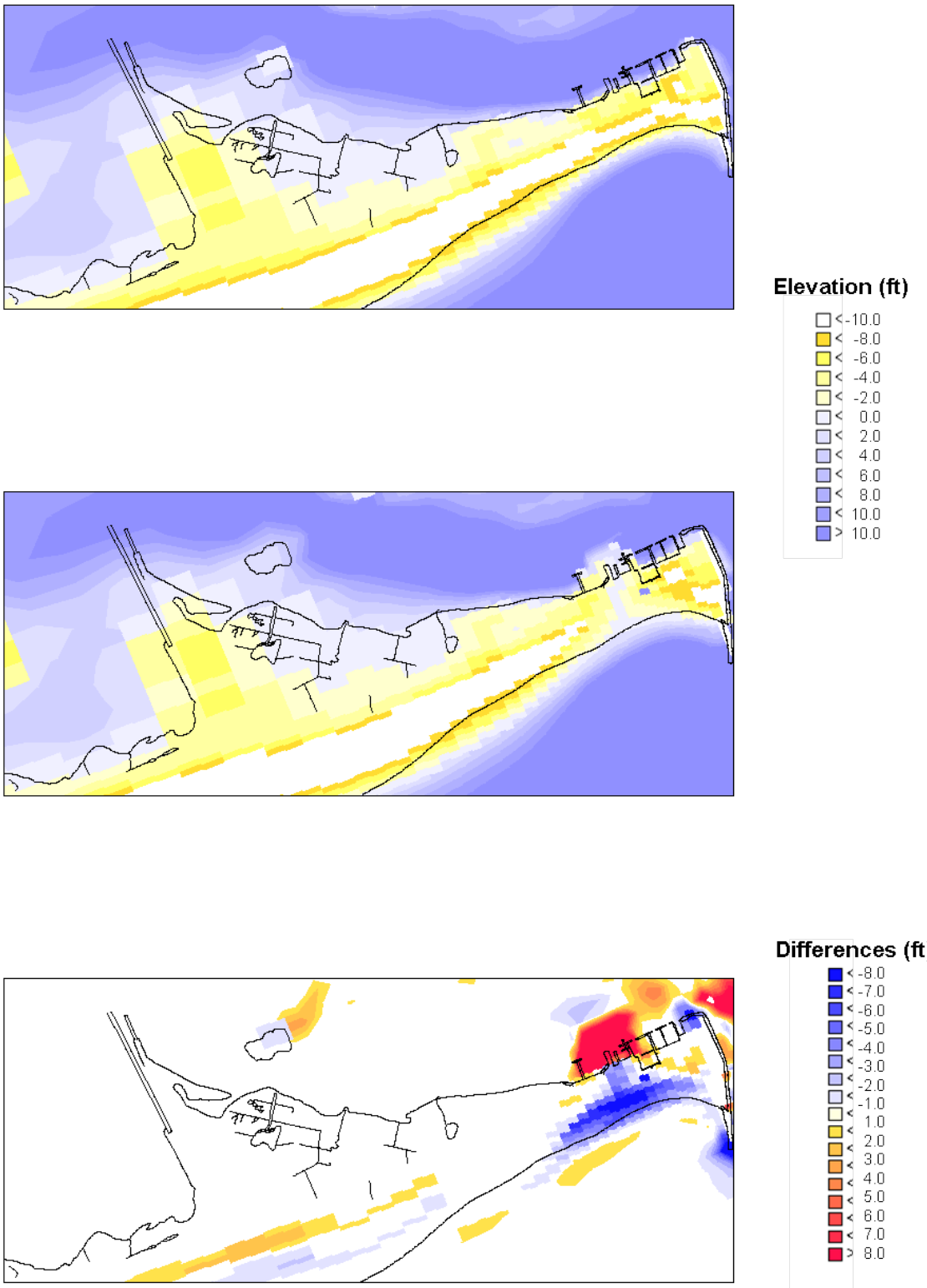

Figure 9-11: Historical Storm September 1938 under Baseline Conditions Topography. WEST OF SHINNECOCK. Model topography: (Top) Pre-Storm (ft MSL) and (Middle) Post-Storm(ft MSL) . (Bottom) Storm induced morphological changes in ft. (Blue – Erosion, Red – Deposition).

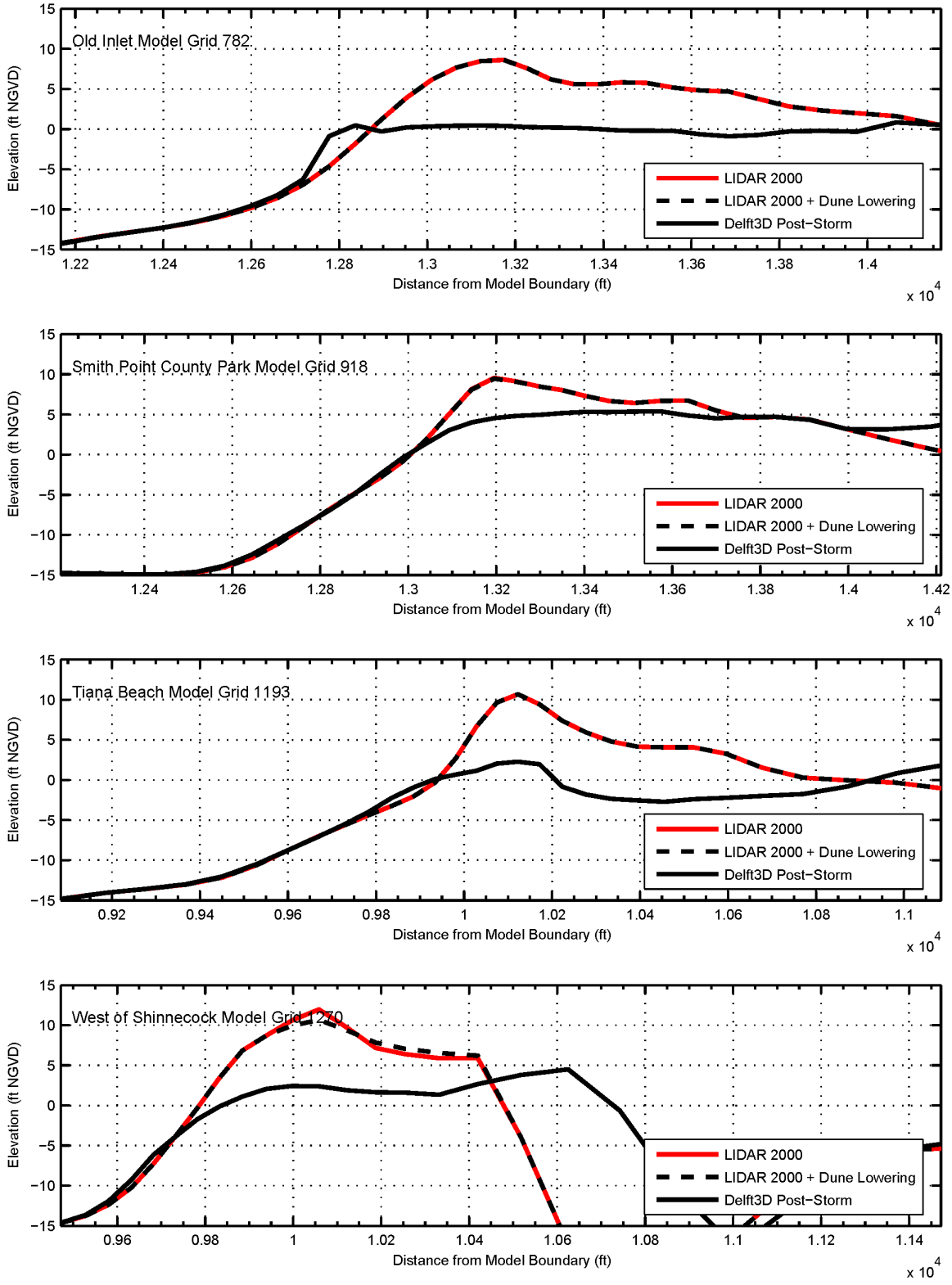

Figure 9-12: Historical Storm September 1938 under Baseline Conditions Topography. Morphological changes along Cross-sections (note: Dune lowering refers to lowering prior to inundation of the dune)

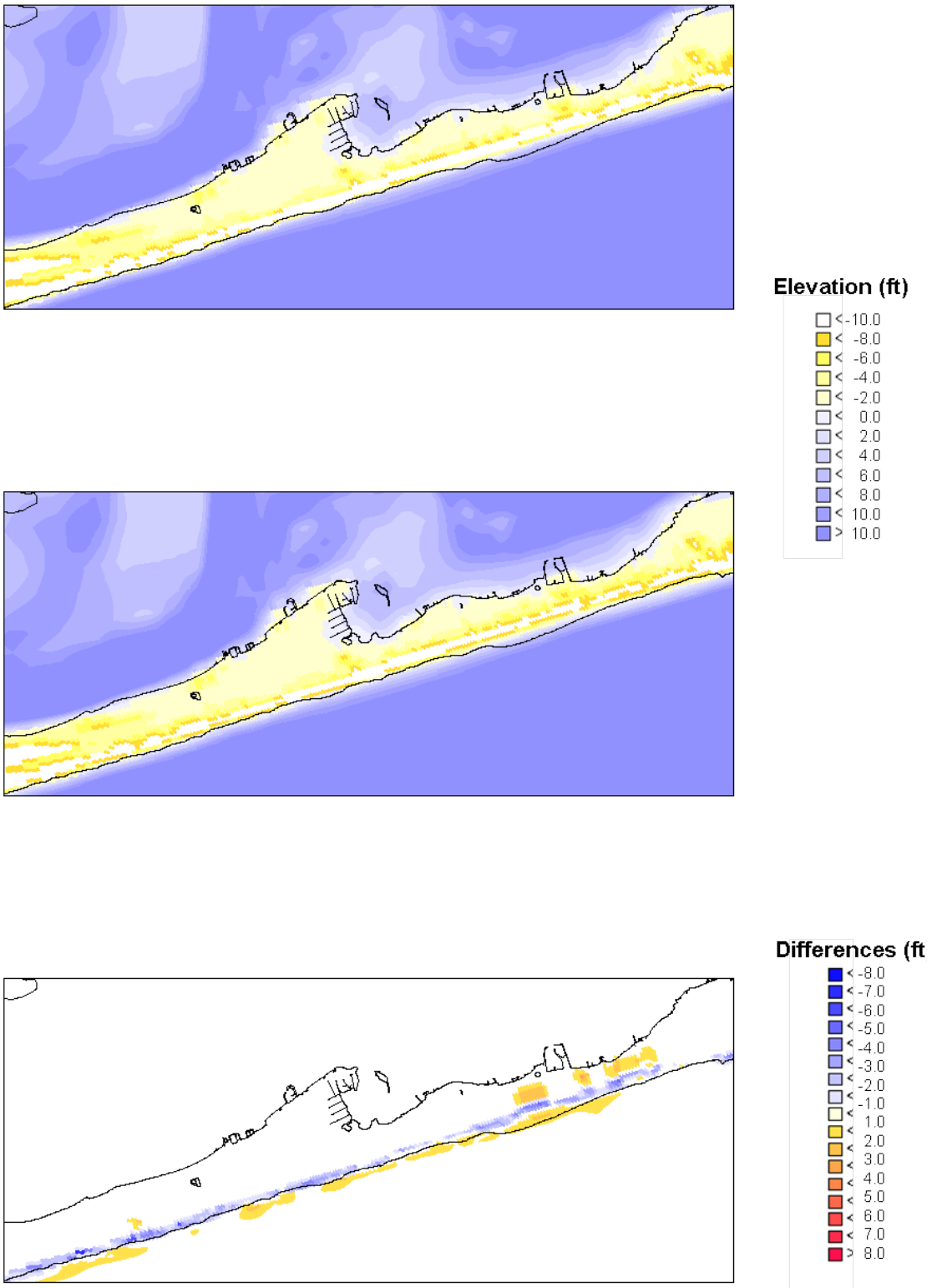

Figure 9-13: Additional Storm September 1938 under Baseline Conditions Topography. WESTERN F.I. COMMUNITIES. Model topography: (Top) Pre-Storm (ft MSL) and (Middle) Post-Storm(ft MSL) . (Bottom) Storm induced morphological changes in ft. (Blue – Erosion, Red – Deposition).

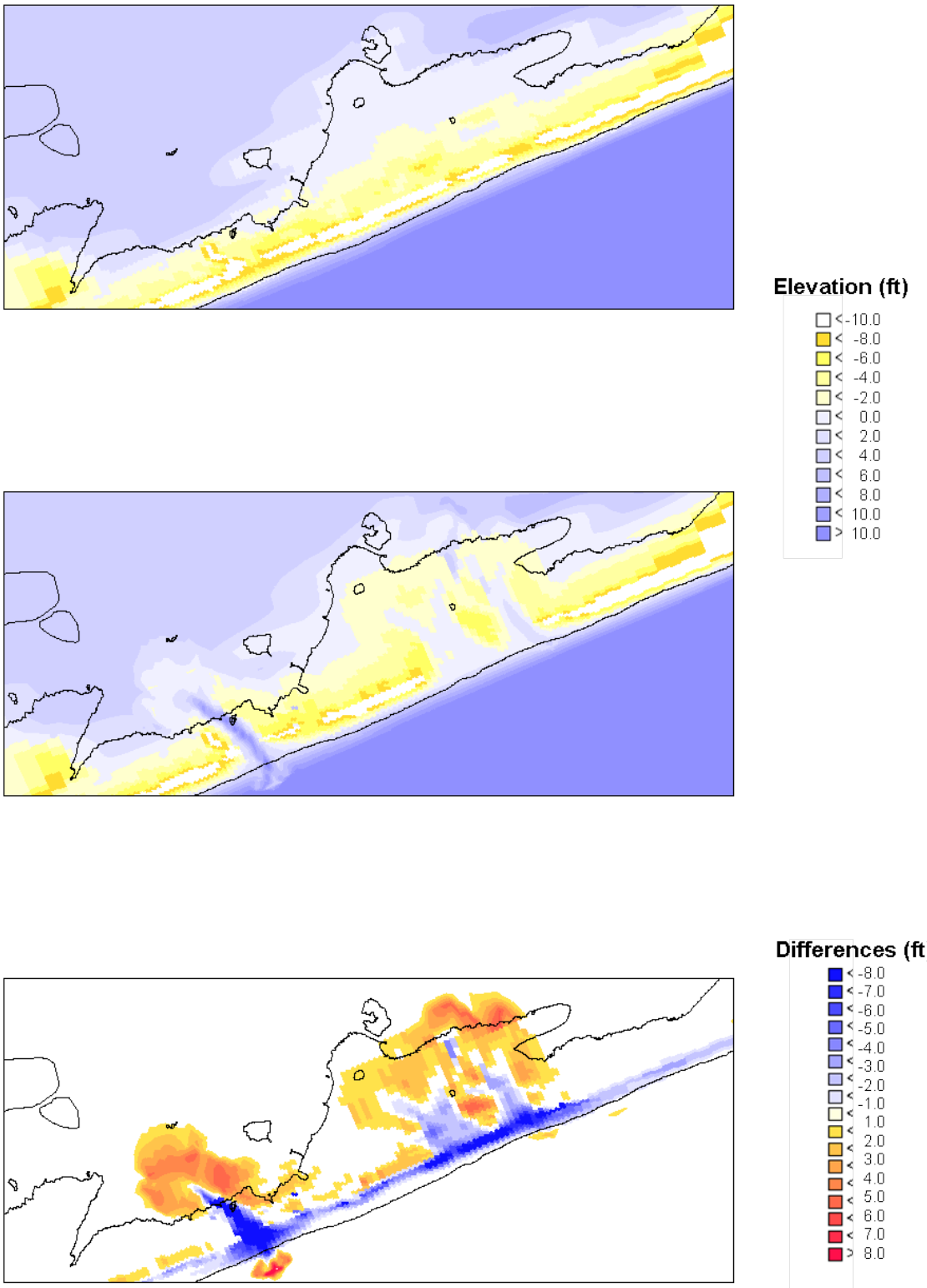

Figure 9-14: Additional Storm September 1938 under Baseline Conditions Topography. OLD INLET. Model topography: (Top) Pre-Storm (ft MSL) and (Middle) Post-Storm(ft MSL) . (Bottom) Storm induced morphological changes in ft. (Blue – Erosion, Red – Deposition).

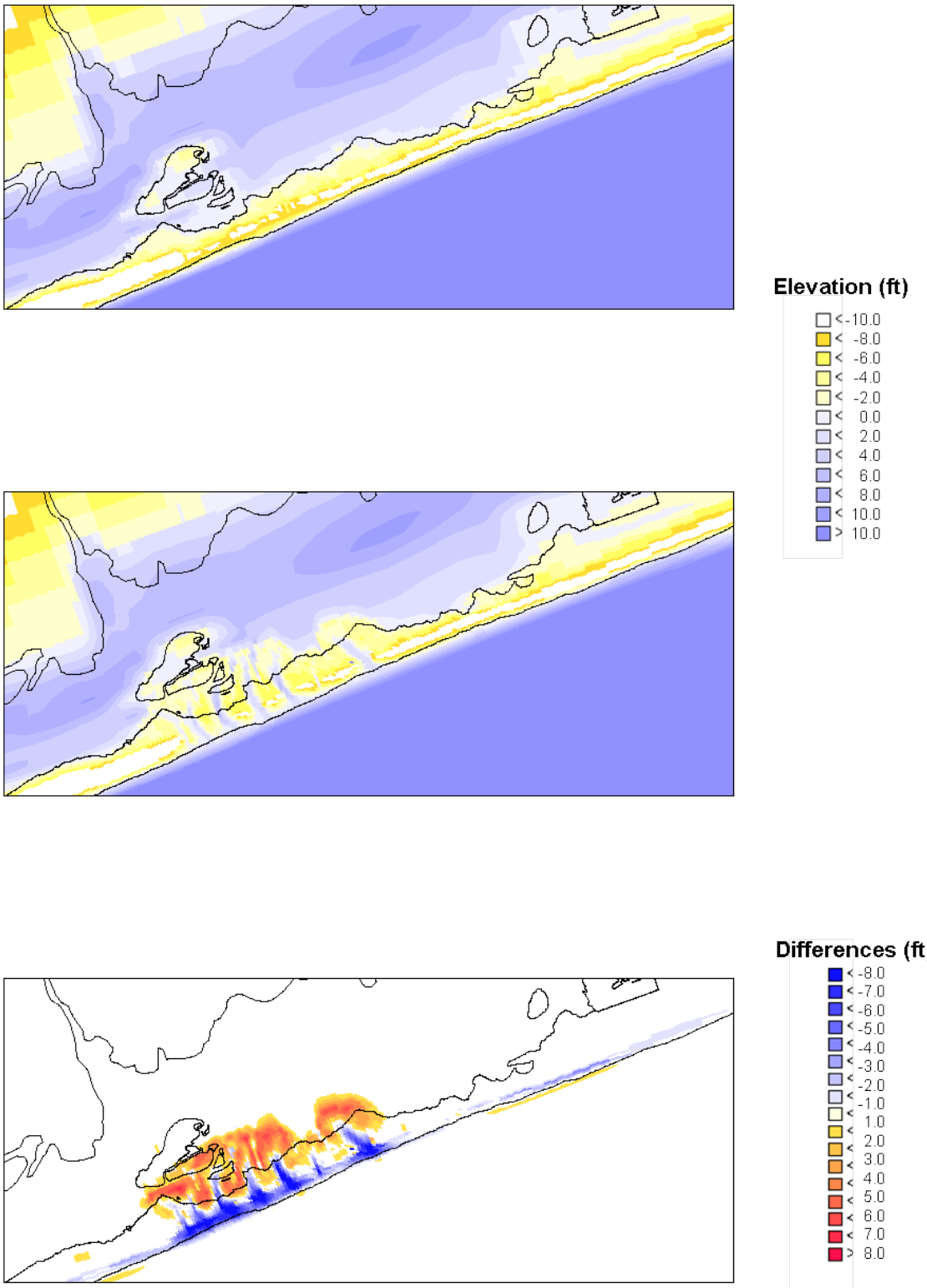

Figure 9-15: Additional Storm September 1938 under Baseline Conditions Topography. SMITH POINT County Park Model topography: (Top) Pre-Storm (ft MSL) and (Middle) Post-Storm(ft MSL) . (Bottom) Storm induced morphological changes in ft. (Blue – Erosion, Red – Deposition).

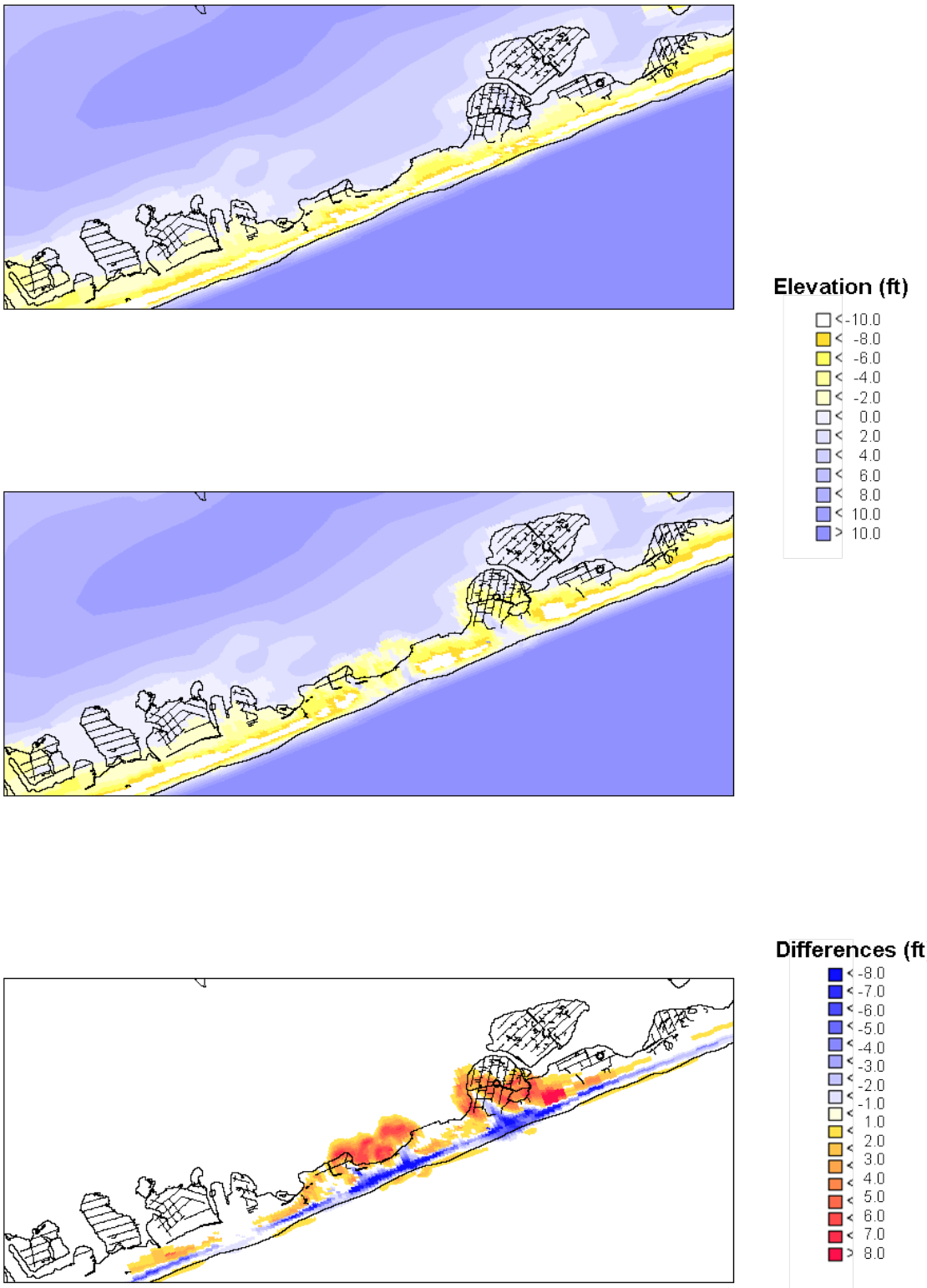

Figure 9-16: Additional Storm September 1938 under Baseline Conditions Topography. TIANA BEACH. Model topography: (Top) Pre-Storm (ft MSL) and (Middle) Post-Storm(ft MSL) . (Bottom) Storm induced morphological changes in ft. (Blue – Erosion, Red – Deposition).

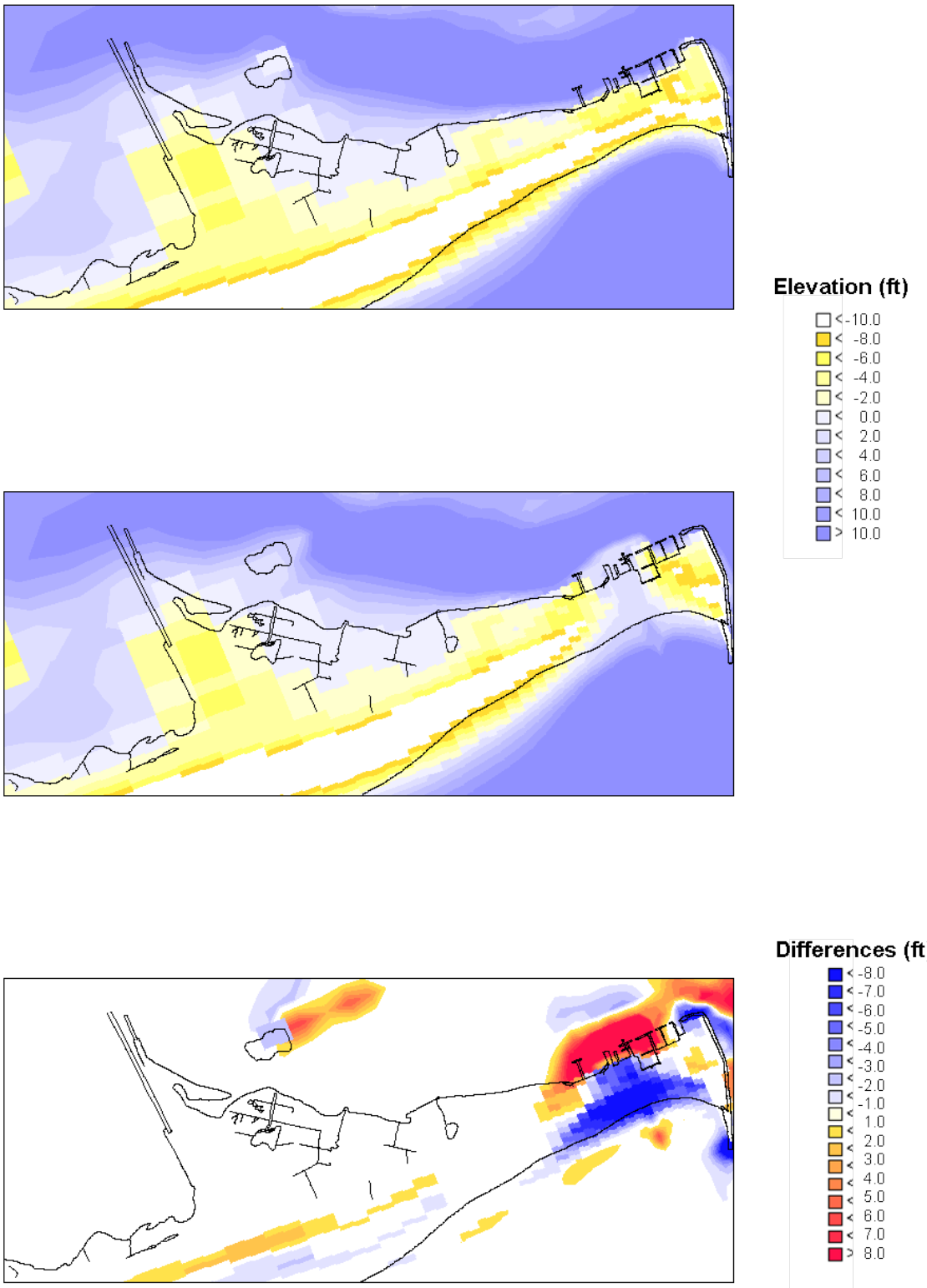

Figure9-17: Additional Storm September 1938 under Baseline Conditions Topography. WEST OF SHINNECOCK. Model topography: (Top) Pre-Storm (ft MSL) and (Middle) Post-Storm(ft MSL) . (Bottom) Storm induced morphological changes in ft. (Blue – Erosion, Red – Deposition).

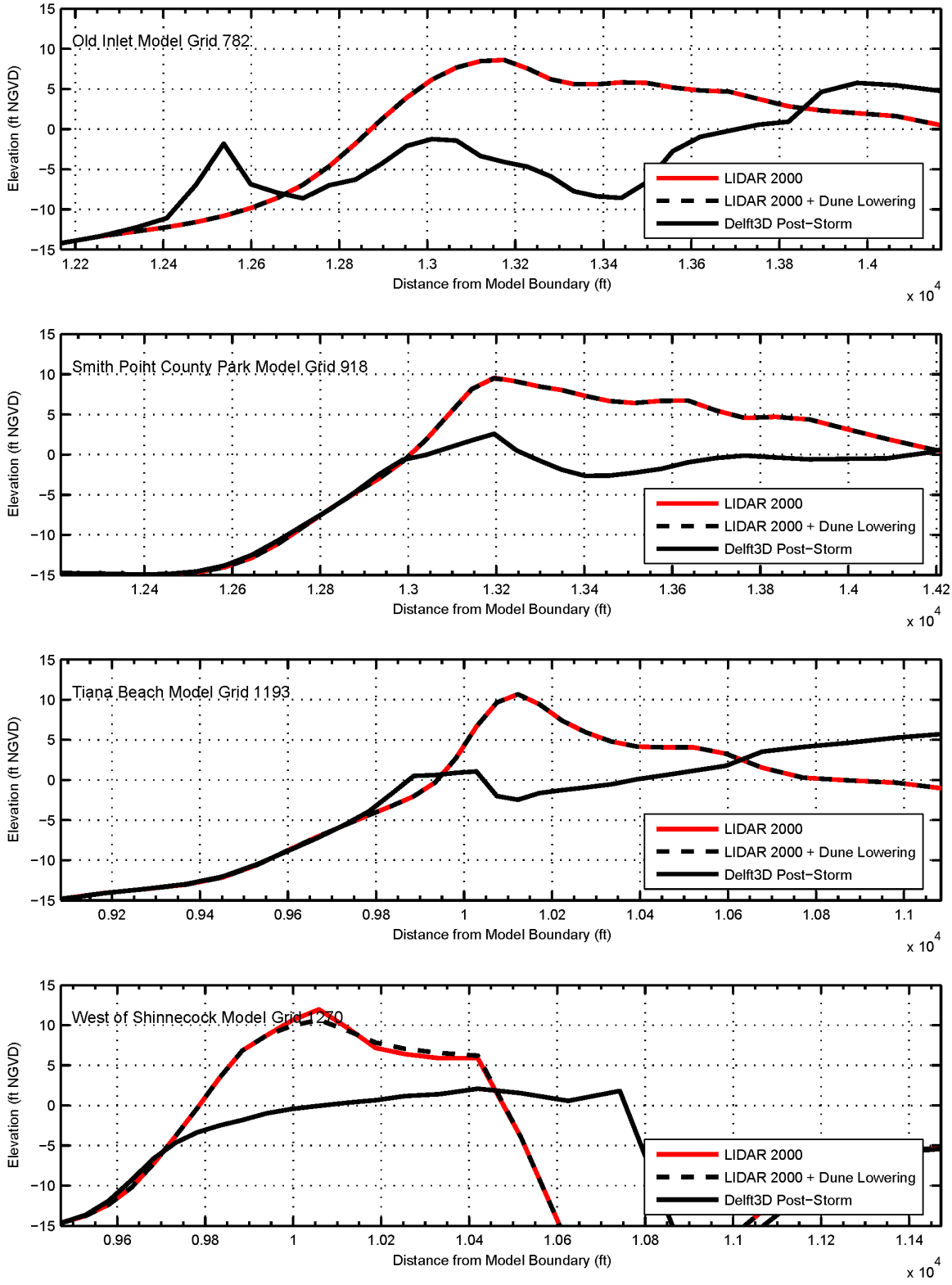

Figure 9-18: Additional Storm September 1938. Morphological changes along Cross-sections (note: Dune lowering refers to lowering prior to inundation of the dune)

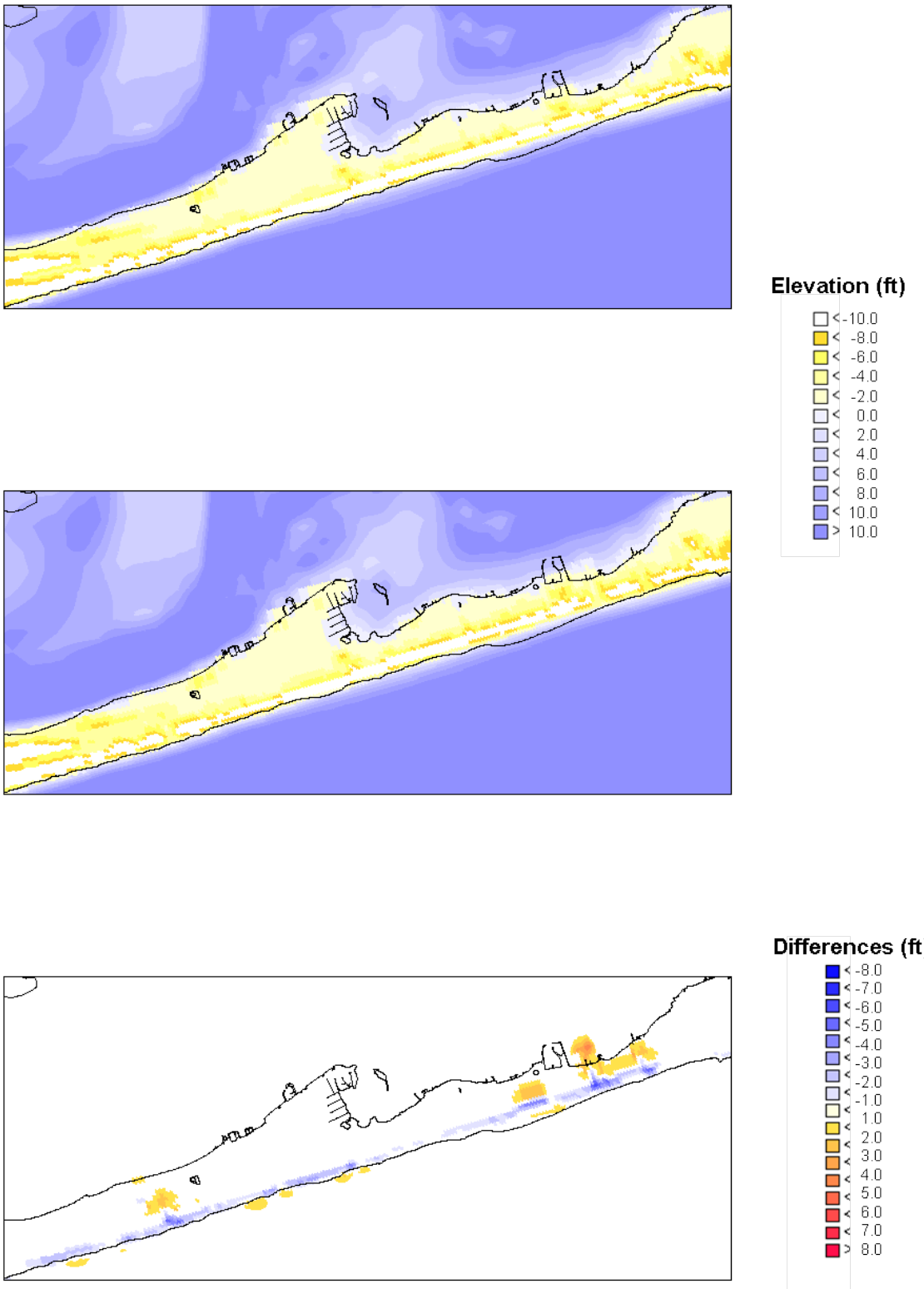

Figure 9-19: Additional Storm September 1985 under Baseline Conditions Topography. WESTERN F.I. COMMUNITIES. Model topography: (Top) Pre-Storm (ft MSL) and (Middle) Post-Storm(ft MSL) . (Bottom) Storm induced morphological changes in ft. (Blue – Erosion, Red – Deposition).

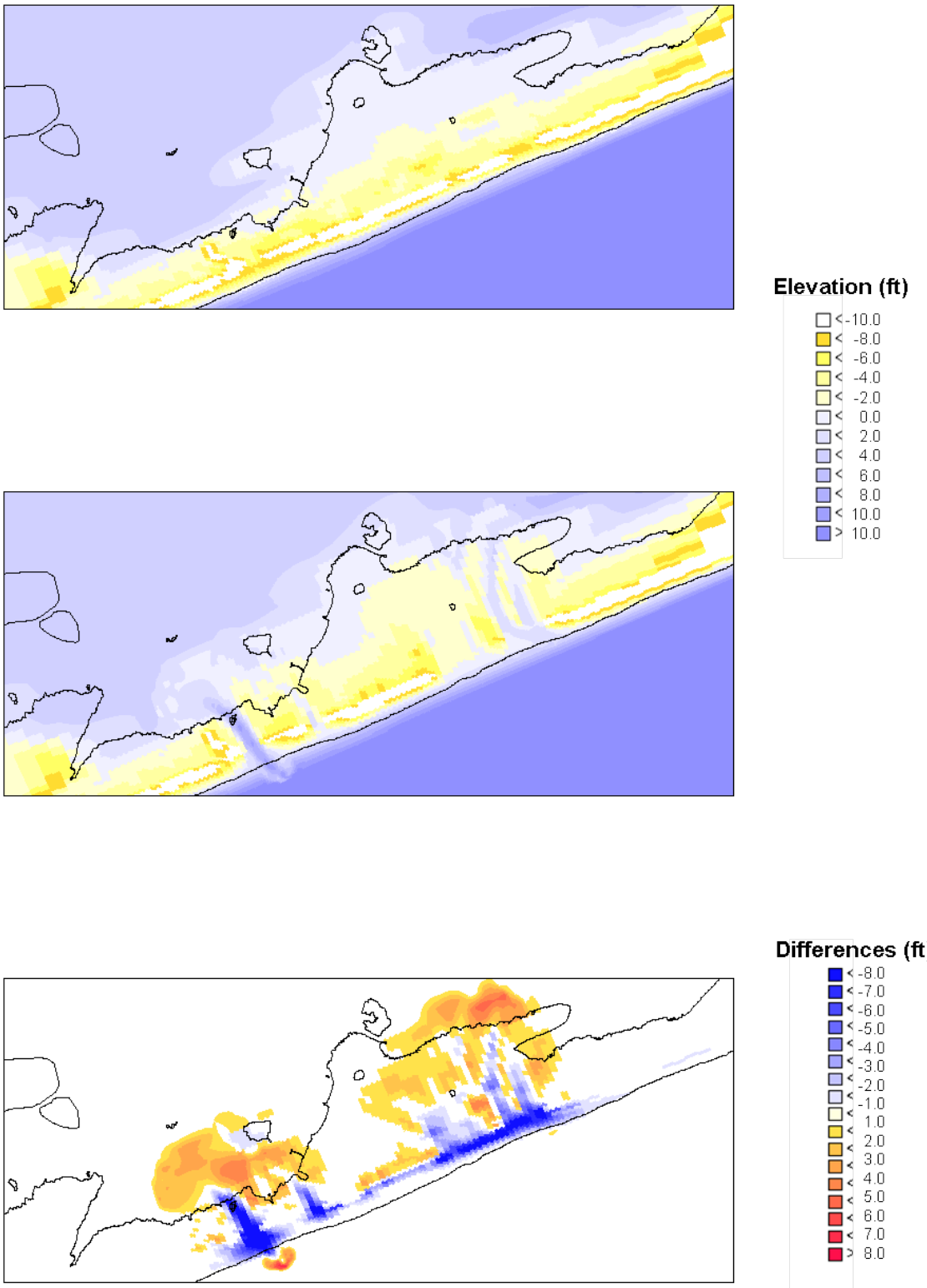

Figure 9-20: Additional Storm September 1985 under Baseline Conditions Topography. OLD INLET. Model topography: (Top) Pre-Storm (ft MSL) and (Middle) Post-Storm(ft MSL) . (Bottom) Storm induced morphological changes in ft. (Blue – Erosion, Red – Deposition).

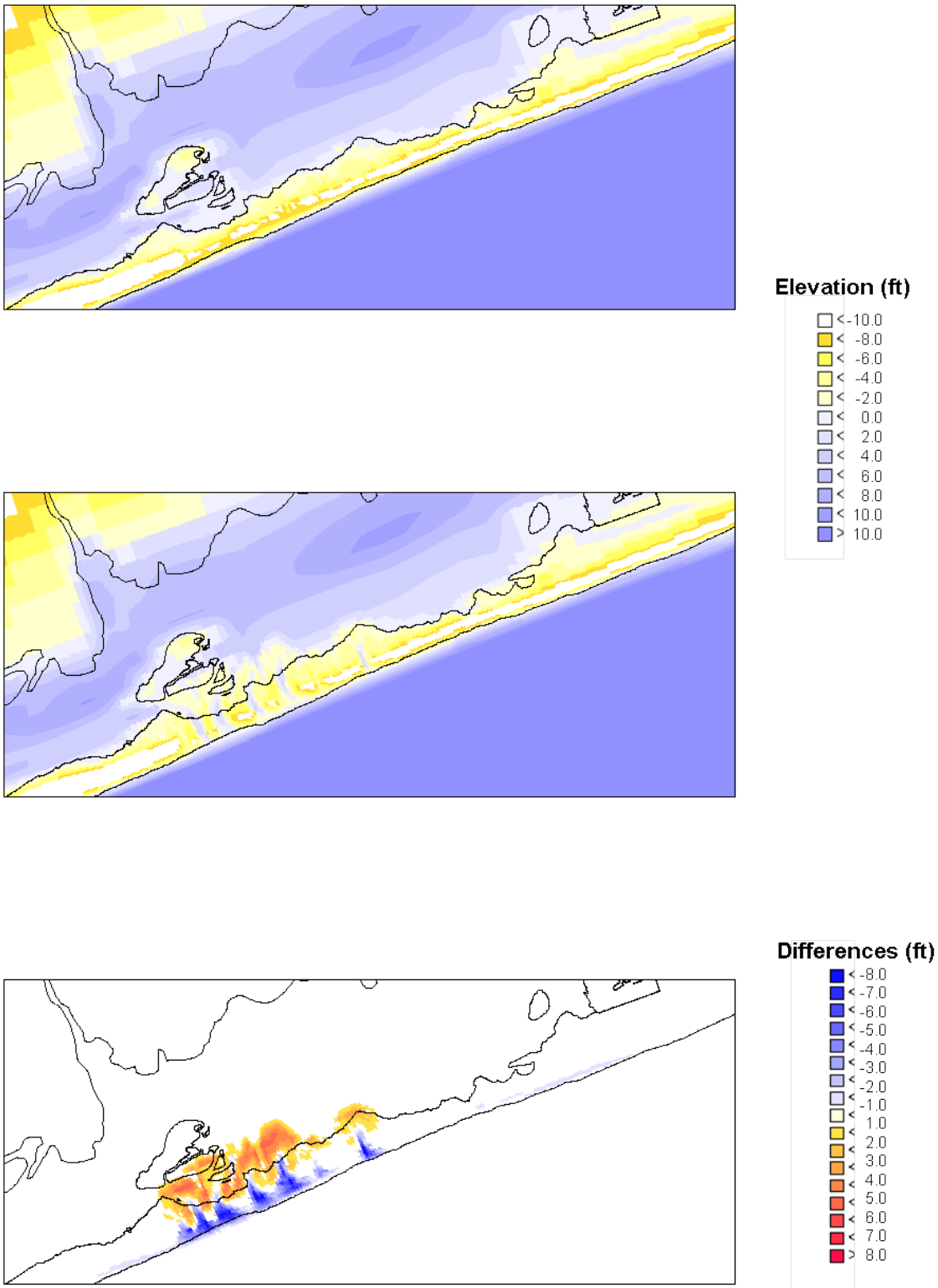

Figure 9-21: Additional Storm September 1985 under Baseline Conditions Topography. SMITH POINT COUNTY PARK Model topography: (Top) Pre-Storm (ft MSL) and (Middle) Post-Storm(ft MSL) . (Bottom) Storm induced morphological changes in ft. (Blue – Erosion, Red – Deposition).

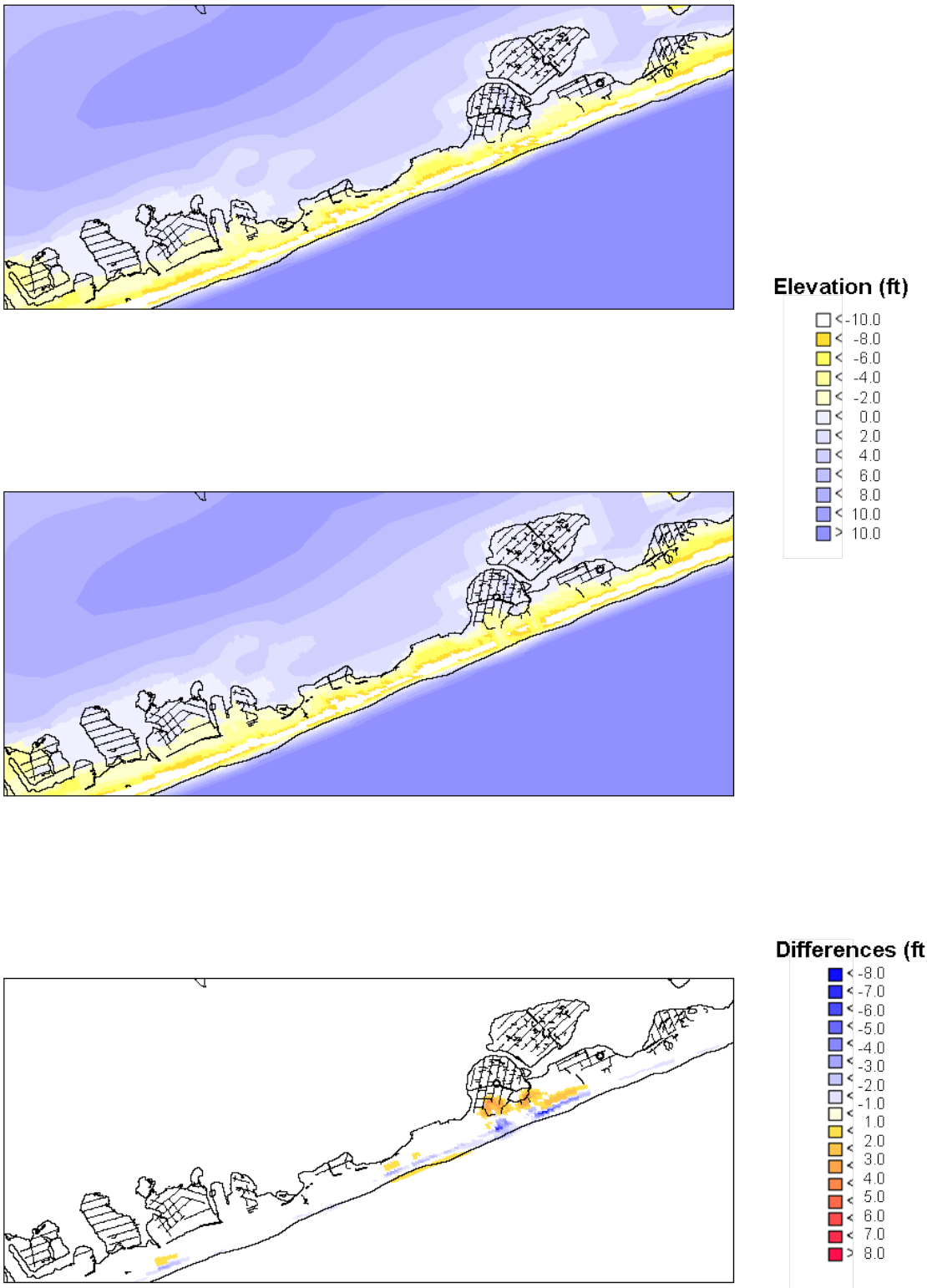

Figure 9-22: Additional Storm September 1985 under Baseline Conditions Topography. TIANA BEACH. Model topography: (Top) Pre-Storm (ft MSL) and (Middle) Post-Storm(ft MSL) . (Bottom) Storm induced morphological changes in ft. (Blue – Erosion, Red – Deposition).

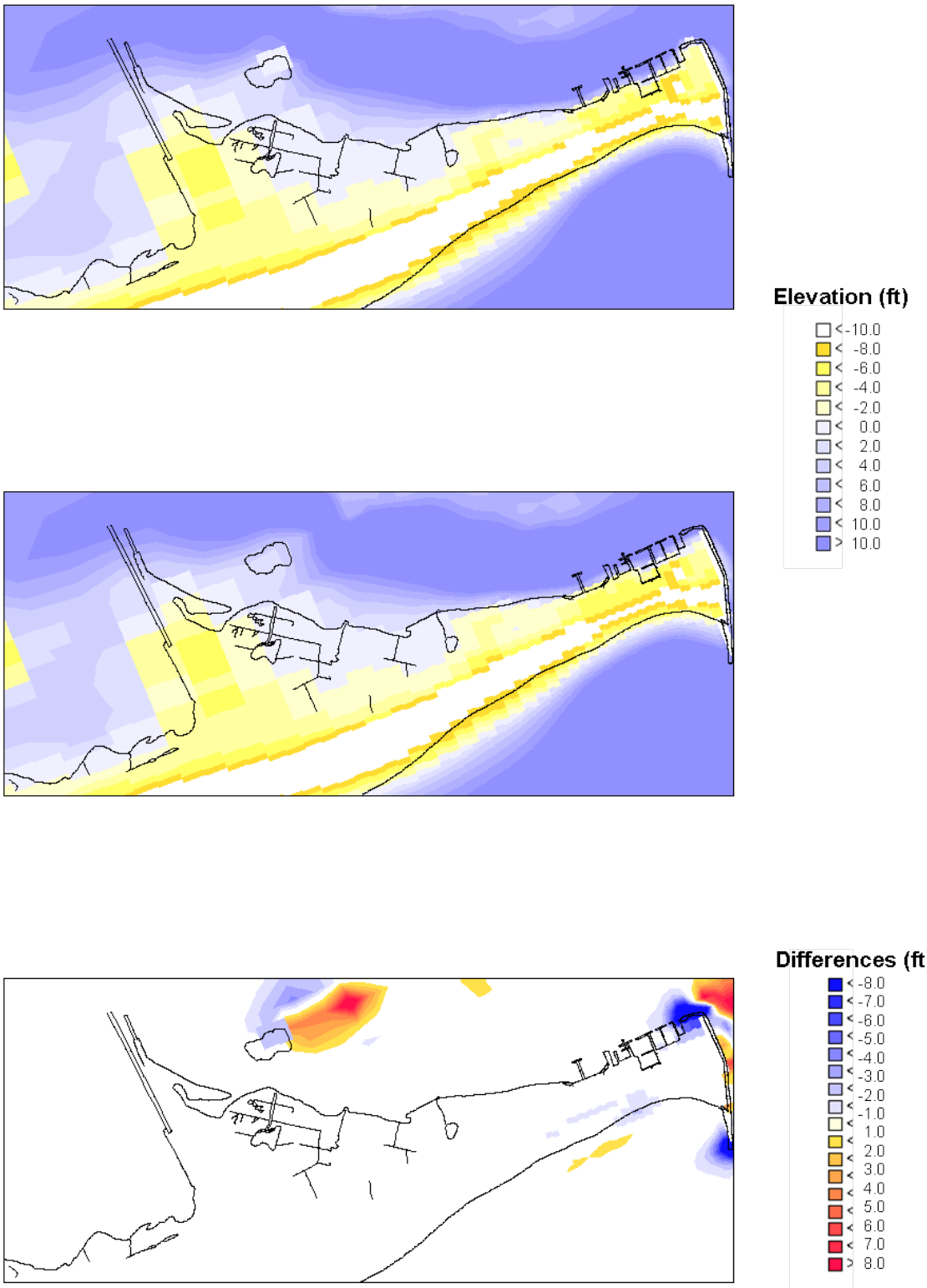

Figure 9-23: Additional Storm September 1985 under Baseline Conditions Topography. WEST OF SHINNECOCK. Model topography: (Top) Pre-Storm (ft MSL) and (Middle) Post-Storm(ft MSL) . (Bottom) Storm induced morphological changes in ft. (Blue – Erosion, Red – Deposition).

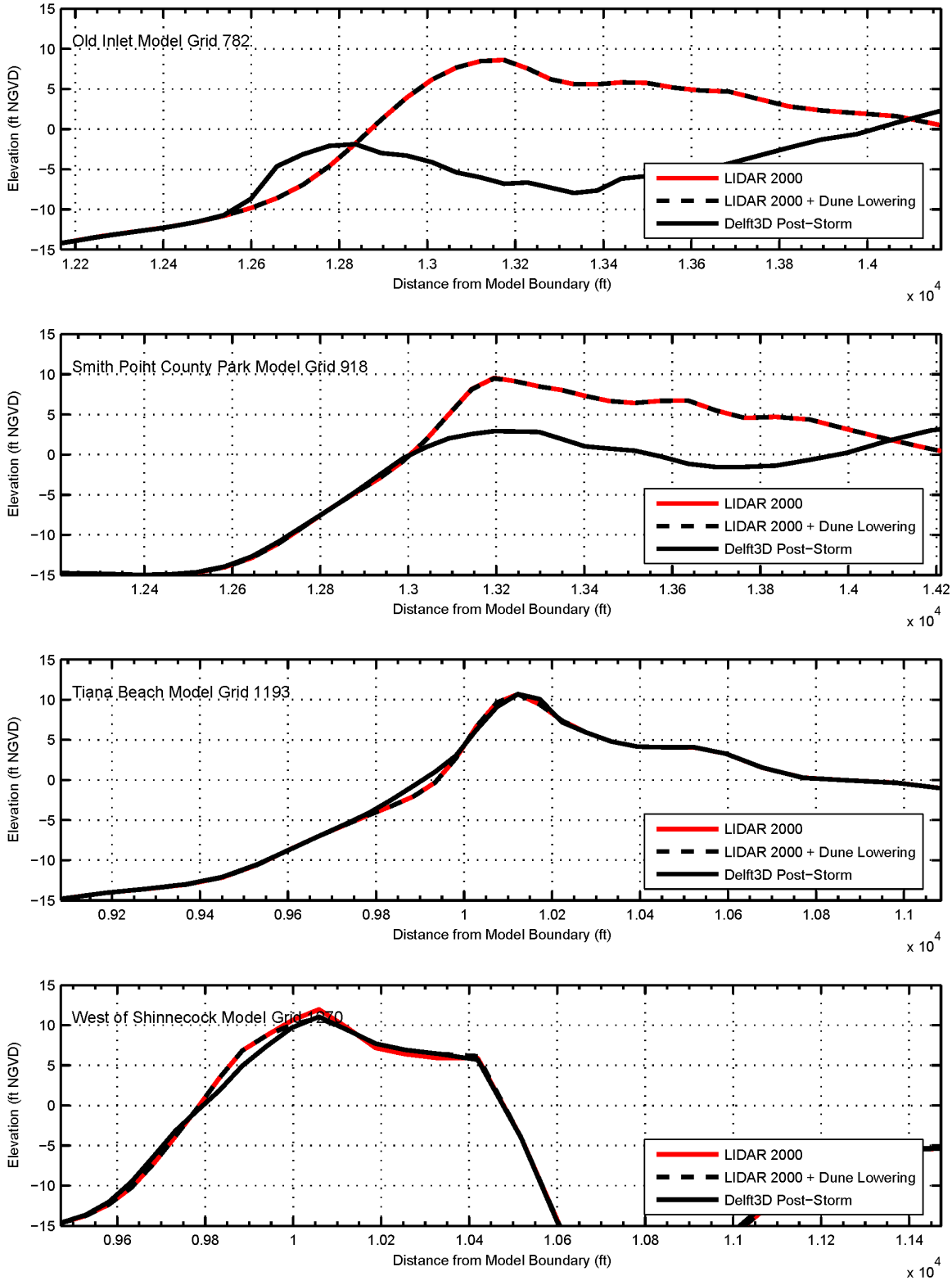

Figure 9-24: Additional Storm September 1985 under Baseline Conditions Topography. Morphological changes along Cross-sections (note: Dune lowering refers to lowering prior to inundation of the dune)

10. Stage Frequency Methodology

10.1 Important Probability Concepts

To develop stage-frequency relationships, probability methods must be applied based on peak water level records (historical or simulated). The **probability, P(X=x),** is the probability that an event, X, will occur and be equal to some prescribed value, x. **Probability of exceedance, P(X≥x),** is the probability that an event, X, will occur, in some prescribed time interval, and exceed x. Probability of exceedance, P(X≥x), is equal to the sum of all probabilities, $P(X=x_i)$, where $x_i \geq x$. For example, if a peak water level of 1 m has a probability of exceedance of 0.9, there is a 90% chance that peak water level will exceed 1 m. Conversely, the **probability of nonexceedance, P(X≤x)**, is equal to 1-P(X≥x) and is the probability that no event, X, will occur and exceed some prescribed value, x. For this study, probability of exceedance is analogous to **frequency**. Typically, engineers present stage-frequency relationships in terms of return period. **Return period, T_r,** is the reciprocal of the probability of exceedance ($T_r(x)=1/P(X\geq x)$).

To associate probability with a given event, it is necessary to assume the population of events follows some defined probability distribution. A **cumulative distribution function (CDF), F(x),** is a function that describes the probability of nonexceedance, such that F(x)= P(X≤x). The **probability density function (PDF), f(x),** is defined as the derivative of the cumulative distribution function, f(x)=d/dx(F(x)). The most well-known PDF is the normal (Gaussian) distribution function, or bell curve.

Two approaches were adopted for this investigation: 1) peak-over-threshold analyses to determine the frequency of moderate and large water level events and 2) annual maximum analyses to estimate the frequency of small water level events. Further, the population of storms was divided into two distinctly different sets: extratropical and tropical.

10.1.1 Peak-Over-Threshold Analyses

Peak-over-threshold methods involve analyses of peak water level records to extract a subset of N peak values exceeding some prescribed cutoff criteria, such as a maximum expected annual tide or similar. This subset is then ranked, with rank n, in order of magnitude and assigned a probability, P. For peak-over-threshold analyses, the probability of water level event occurring during a particular interval along with the probability of that event exceeding a certain value must be determined. The **Empirical Simulation Technique (EST)** was used to determine CDF, F(x), values that correspond to probability of an event causing a water level at or below a specified water level, given that an event occurs. The EST is detailed in Chapter 10.2. For this study, the number of storms in a **time interval, t,** is modeled with the Poisson distribution (Borgman, 2003). The **Poisson distribution** is:

Equation 10-1

$$F(M = m) = \frac{e^{-\lambda t}(\lambda t)m}{m!}$$

where:

λ is the **average rate of occurrence**
(ex. 14 storms in 72 years gives λ=(14/72)=0.194)
P(M = m) is the probability of M=m occurrences in the interval t.

Then, the return period for a particular event (water level) is:

Equation 10-2

$$T_r(x) = \frac{1}{\lambda(1 - F(x))}$$

For peak-over-threshold analyses, 22 extratropical events in 49 years and 14 tropical events in 72 years were used (Chapter 2.2 and Table 2-3). This corresponds to $\lambda_{tropical}$=0.194 and $\lambda_{extratropical}$=0.449.

10.1.2 Annual Maximum Analyses

Annual maximum methods involve extracting the peak water level occurring in each year of the record, N values (N equals number of years). These annual values are then ranked, with rank n, in order of magnitude and assigned a probability, P. For annual maximum analyses, the Weibull plotting position formula was used to determine CDF, F(x), values:

Equation 10-3

$$F(x) = \frac{n}{N+1}$$

Return period is then computed as:

Equation 10-4

$$T_r(x) = \frac{1}{1 - F(x)}$$

Details on how annual maximum analyses were conducted for this study are in Chapter 10.3.

10.1.3 Combined Storm Populations

Two distinct storm populations were considered for this study: extratropical events, characterized by extratropical weather patterns and durations on the order of days, and

tropical events, characterized by cyclonic weather patterns and durations on the order of hours. Assuming that the extratropical and tropical storm populations are mutually exclusive, the probability of a given water level occurring for both (combined)events is the sum of the probabilities for extratropical and tropical events (Ang and Tang, 1975). Thus, the combined return period, including both extratropical and tropical events, is defined as:

Equation 10-5

$$T_{combined}(x) = \frac{1}{\left(\frac{1}{T_{tropical}(x)} + \frac{1}{T_{extratropical}(x)}\right)}$$

10.2 Empirical Simulation Technique (EST)

Parametric[8] and nonparametric methods may be used to determine probability distributions. Parametric methods assume that the storm population follows some prescribed probability distribution, for example a normal (Gaussian) distribution. In contrast, nonparametric methods do not presume a distribution; instead the distribution is computed from the available data. When selecting a method for use with a particular data set, it is important to realize that nonparametric methods are more appropriate when the population distribution is unknown, while parametric methods are more appropriate if the distribution is known beforehand. As such, nonparametric methods are more appropriate for the storm water levels in the FIMP study.

Empirical Simulation Techniques (EST) are a group of nonparametric methods for proceeding directly from hydrometeorological storm data to simulations of future storm activity and coastal impact, without introducing parametric assumptions concerning the probability law formulas and related parameters of the data.

Two procedures, one univariate (1-D) and the other multivariate, were used in the FIMP studies. The 1-D EST methodology, using water level as the dimension, and the reasoning behind its selection for creating the stage-frequency curves for this study are discussed in more detail below.

The multivariate EST will be used in conjunction with SBEACH for modeling of beach profile response and estimation of storm-induced coastal changes, primarily for economic life-cycle analysis. Since the multivariate EST uses multiple dimensions including water level, storm duration, and wave height, it is an appropriate choice for evaluating erosion responses since there is more than one order-one process influencing profile erosion response. This SBEACH modeling and subsequent frequency analysis is a separate effort;

[8] Here, the parametric and nonparametric are terms describing statistical methods and are not related to references to parameters (such as wind speed, water level, etc.).

therefore, it is not addressed in this report. See TR-CHL-99 (Scheffner et al., 1999) for a complete description of the multivariate EST.

10.2.1 Univariate (1-D) EST Methodology

The 1-D EST method used herein employs the inverse interpolation method of Zelen and Severo (1964). This method uses uniform random numbers to interpolate water levels from an empirical CDF (EDF) constructed from the augmented historical storm population to simulate possible future peak water level CDF's. In comparison with the multivariate EST, the 1-D, inverse-interpolation EST incorporates a much better control of the extremal behavior of the simulated CDF's, specifically for the EDF upper tail (extreme values not defined by the historic record). The upper-tail fit of the historical EDF is carefully examined to ensure that it is reasonably consistent with the curvature of the largest few historical data points. This examination is direct and allows simple intuitive evaluation. In contrast, the simulated extremes for the multivariate, kernal-smoothed EST is much more difficult to verify. The disadvantage of the 1-D EST is that it is restricted to one dimension, water level. For this study, 1-D EST is the better choice for accurate stage estimation for long return periods that reach beyond the length of the historical record. Specifically, it is a more scientifically-conservative approach because it improves the reliability at longer return periods. However, caution should still be used any time stage estimates are extrapolated beyond those reflected in the historical record.

While the 1-D EST is more advantageous for analyzing peak storm water levels, the multivariate and 1-D EST methods do serve as good checks on each other. For a few output locations, comparisons were made between the 1-D EST employed herein and the multivariate EST adopted by USACE CHL. All of these comparisons show that the results vary little from one another, and that any variation is well within the reliability bands.

Using the final representation of Delft3D- and ADCIRC-simulated storm water levels, including both historical storms and additional non-historic storms, the development of the stage-frequency curves with the 1-D EST proceeded in three steps: (1) construction of historical EDF, (2) inverse-interpolation to generate future CDF possibilities, and (3) generation of stage-frequency relationships. The following describes each of these steps.

Historical Empirical Distribution Function (EDF)

For each output location in Table 2-5, peak storm water levels predicted by DELFT3D or ADCIRC were analyzed to develop an EDF. These storm peak water levels were ranked in order of increasing magnitude and assigned a probability based on:

Equation 10-6

$$EDF(x) = \frac{n}{N+1}$$

where:

n is the individual storm rank
N is the total number of peak water levels in the set (tropical or extratropical).

The equation above creates an empirical estimate of the cumulative distribution function for tropical and extratropical events, separately. A sample EDF is given in Figure 10-1. A smoothing spline, least-square, curve-fitting method was use to extend the EDF curve from the plot position of the extreme values out to probability 1.0 (dashed line at the upper right portion of the curve in Figure 10-1) and out to probability 0.0 (dashed line at the bottom left portion of the curve in Figure 10-1). Thus, the EDF was fully estimated for all probabilities on [0.0, 1.0].

The curve-fitting method, or tail-completion method, for extending the EDF to 0 and 1, is based on Borgman (2003, draft). This tail-completion method uses weighted spline methods and decreases the extent by which subjective decisions are required. For this study, the upper tail was designated as unbounded. To encourage realistic behavior in the unbounded upper tail, a magnet point was employed. This magnet point was assigned a very small weight in the spline calculations and was set at a water level equal to the mean plus 5 standard deviations of the storm water levelpopulation and at EDF(x) = 0.9999997. Sensitivity analysis on the selection of the magnet point showed negligible changes in the resulting upper tail fit.

It should be noted that the upper tail-completion method employed for FIMP is consistent with other well-known parametric methods, such as Gumbel. Specifically, select tests on the upper tail fit employed here show that alternate upper tail-completion methods produce extreme values that fall well within the reliability bands of the 1-D EST tail-completion method.

For this study, the lower tail was designated as bounded since the lowest possible extreme water level is limited to an annually occurring peak water level, usually associated with a small storm event. Details on bounding the lower tail are presented in Chapter 10.3, below.

EDT Perturbations by Inverse Interpolation

To develop alternate future "pseudo-historic" EDFs, inverse interpolation was employed. In developing these future EDF representations, it is inherently assumed that all future storm surge events will be statistically similar to past storm surge events. Uniform, independent, random numbers were generated and used on the historic EDF [0.0, 1.0]-axis to inversely interpolate back to the water level axis (Figure 10-2). These selected water levels were used to create new, "accidental" sets of supplemental storm peak water levels that are consistent with the historic EDF and present a random perturbation of what might occur during the same length of time at some future date. One thousand such sets of possible future "pseudo-historical" data sets were produced for each output station. The upper and lower tails of their EDFs were computed in the same manner as for the historical EDFs (see above).

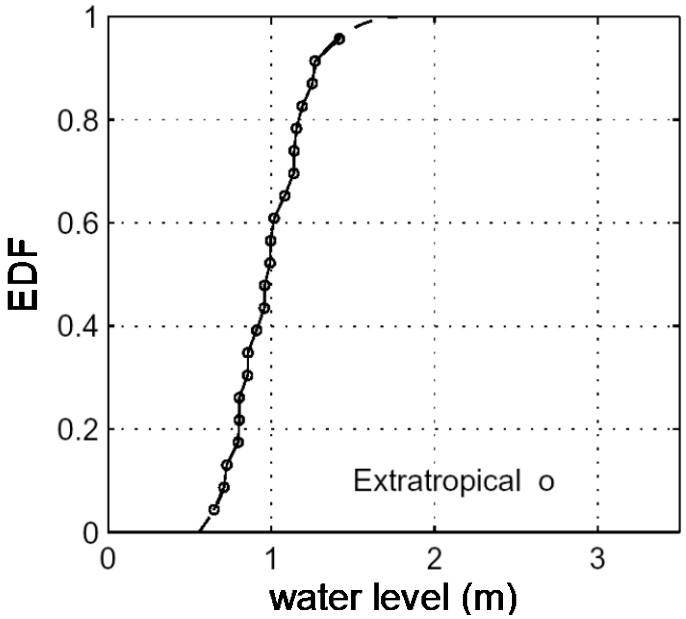

Figure 10-1. Sample EDF for historical extratropical events.

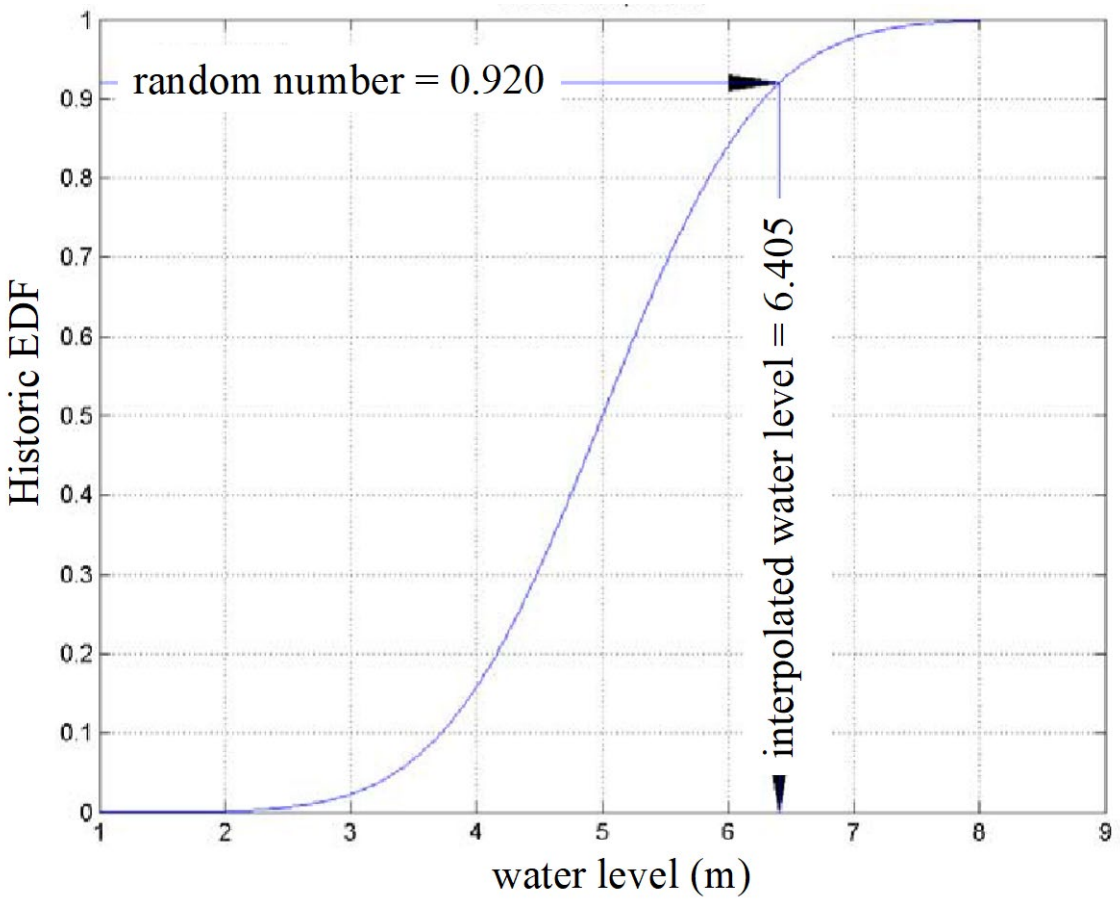

Figure 10-2. Sample inverse interpolation from historic EDF.

Stage-Frequency Curves

The 1000 EDF perturbations were ranked in order of increasing magnitude to estimate the median and the two quartiles (i.e., the 50- percentile, the 25-percentile, and the 75-percentile)[9] of the EDF distribution. Then the EDF median and quartile EDF results were converted to stage-frequency curves following Equation 10-2. The median result was plotted as the stage-frequency curve, while the two quartile results were plotted above and below the median curve as indications of reliability, or spread (Figure 10-3). The mean and standard deviation were also computed and will be used in subsequent economic analyses. The mean and standard deviation calculation method employed for this study assumed a robust lognormal distribution that allows skewness and provides a stable estimate based on the statistical distribution of the EDF perturbations.

This treatment was made to tropical and extratropical storms separately, and then combined using Equation 10-5 to produce combined stage-frequency curves.

10.2.2 Accounting for Other Non-Historical Storm Possibilities

Storm landfall timing relative to astronomical tide conditions is accidental. The peak flooding in the storm could just as well have happened a few hours sooner or later when the background astronomical tides were different. Also slight differences in meteorological conditions could have caused the storm path a few miles left or right of where it actually passed. Thus, one might be justified in saying that these variations on what actually occurred should be given equal likelihood with the actual historical event in any engineering decision arising from the data analysis.

However, there is a limit on how far one should go in incorporating non-historic storms in the analysis process. The selection of additional scenarios involves considerable judgment. Therefore, it may not be defensible to include them in the analysis unless there is a good physical basis for it. For example, landfall timing may be totally random, but storm path and landfall location are at least partially determined by coastline geometry and typical background meteorological conditions.

Non-historical storm events were considered to account for other plausible scenarios. Specifically, these additional storms account for more severe events and achieve a smooth alongshore distribution of stage-frequency relationships. All decisions made regarding the inclusion or exclusion of non-historic storm events were made such that 1) probability of the event could be well defined and 2) reasoning was both physically sound and defensible.

Astronomical Tide Variation

The peak water level that occurs during the passage of a storm depends on the sequencing of the astronomical tide with the storm surge. This is illustrated in Figure 10-4, which shows sample time histories of astronomical tide, storm surge, and the two combined as a

[9] For example, the 25th percentile is defined as the value where 25 percent fall below and 75 percent lie above.

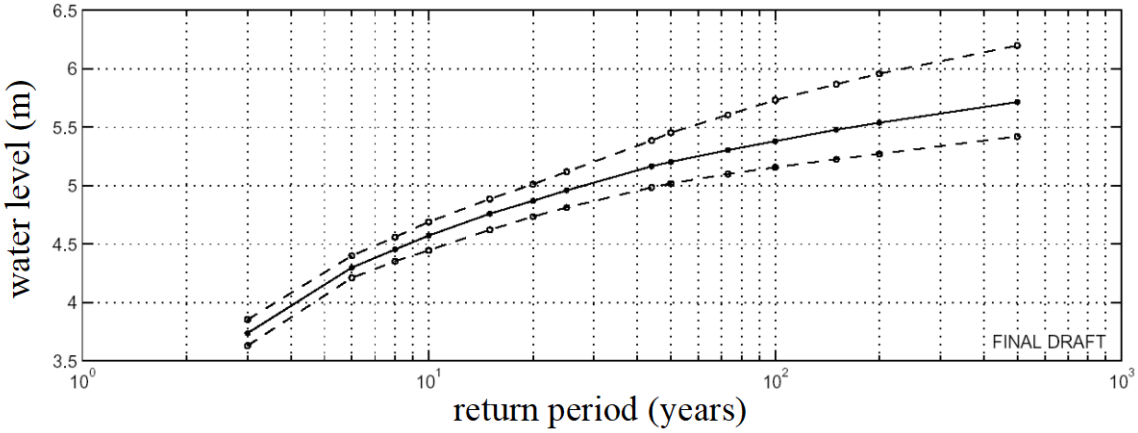

Figure 10-3. Sample stage-frequency curve.
Solid line is median while dashed lines are quartiles.

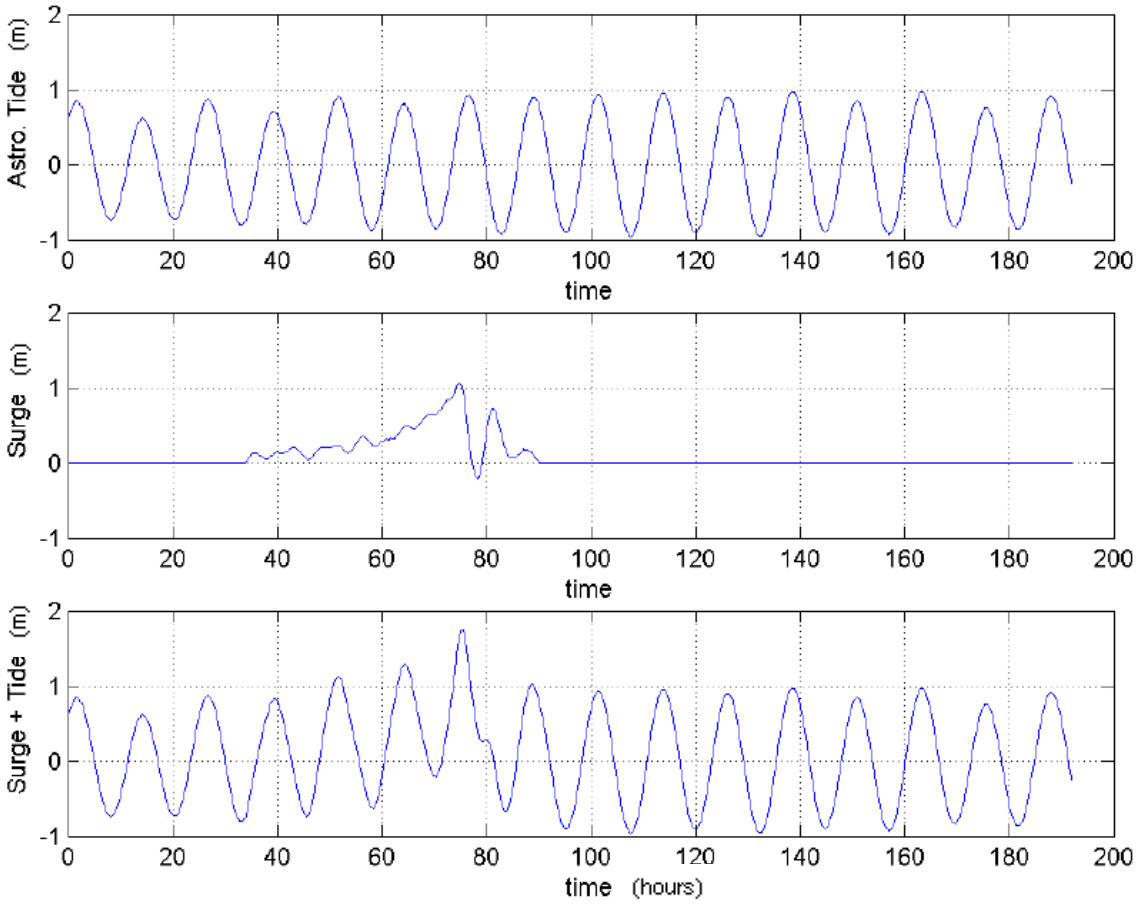

Figure 10-4: Illustrative example of astronomical tide timing and storm surge.

prediction of what happened in the storm. The bottom time history shows that the peak water level was about 1.8 m (5.9 ft) and occurred about 75 hours after the start of the simulation (approximately 40 hours after the arrival of the storm). Knowing that the historical timing of any given storm is accidental, it is reasonable to assume that the storm could occur at any time within some interval. Therefore, the accidental occurrence of the astronomical tide anywhere within the 4-week period, one lunar cycle, surrounding the historical occurrence was considered. For this study, the accidental occurrence of storm surge relative to astronomical tide cycle for any given storm could result in peak water level differences of as much as 1.5 m (5 ft) at ocean stations.

The problem of astronomical tide timing relative to storm occurrence can be studied easily if the hydrodynamic conditions are such that water level is a simple linear sum of surge plus tide. The linear combination case was investigated by moving the surge hydrograph (i.e. the middle plot in Figure 10-4), to new arrival or start times relative to the top plot of tide time history, and computing a new alternate peak water level from the maximum of the shifted surge plus tide. This computation was repeated with the surge hydrograph shift incremented by 0.1 hour within the 4-week period surrounding the historical occurrence. Thus, for each of the 36 historic events listed in Table 2-3, a set of 6720 peak water levels was obtained for the range of arrival times. This 0.1-hour time stepping was performed separately for each of the 80 output locations.

The bottom graphs in Figure 10-5 and Figure 10-6 graphically display the 6720 peak water levels computed at Old Inlet (Station 9) for the 1938 Hurricane and Hurricane Gloria (1985), respectively. As the figures indicate, peak water level distribution over the 4-week period is continuous. If the storm arrives a little more out of phase with high tide, the peak water level will be much less. On the other hand, if the storm arrived so as to reinforce high tide a little more, the peak water level could have been still higher than what historically happened. Computing the probability density, and associated cumulative probability, summarizes the peak water level variation with storm-start time. The resulting CDFs (tide-CDF) for the peak water levels plotted in the bottom graphs in Figure 10-5 and Figure 10-6 are plotted at the top of each figure. These tide-CDFs represent the variability in peak water level resulting from the random occurrence of the storm with astronomical tide. As the figures show, peak water levels when the surge peak is coincident with extreme, or spring, high and low tide conditions have a small occurrence probability. This result is intuitive as astronomic water levels associated with high and low spring tide occur only a handful of times during each lunar cycle. Also, as expected the median peak water level condition occurs when the surge peak is approximately coincident with a mid-range, rising or falling, tide. The median peak water level is about 1.93 m (6.33 ft) and 1.97 m (6.46 ft) for the 1938 and 1985 hurricanes, respectively. The square and vertical line on the top plots in both figures shows the peak water level from the historical occurrence of the event.

Figure 10-5 shows that the historical 1938 Hurricane made landfall along Long Island nearly at high tide. Consequently, the peak water levels are somewhat larger than what such a storm would produce on average. The opposite is true for the historical occurrence of Hurricane Gloria in 1985. Here, the storm made landfall around low tide

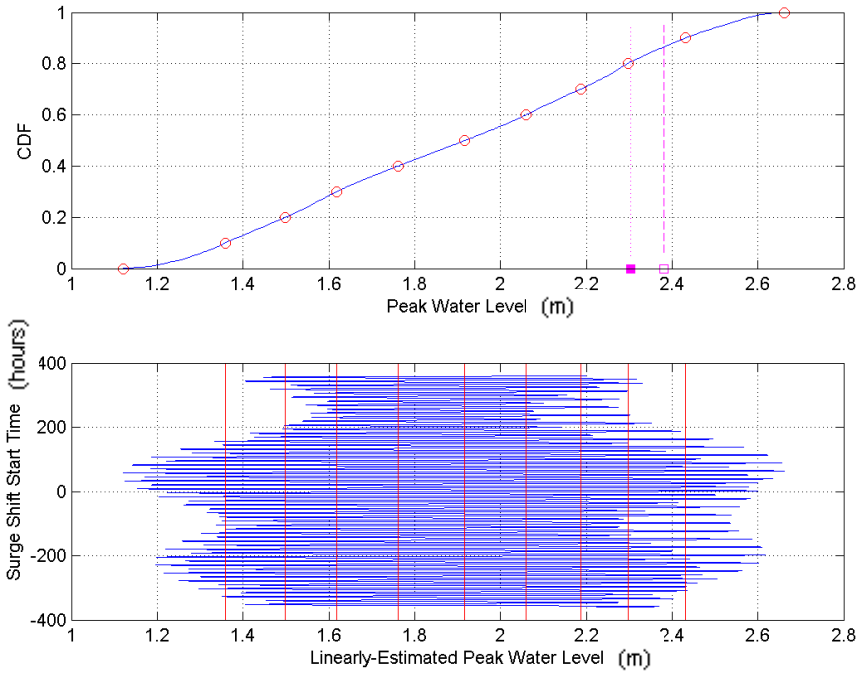

Figure 10-5: Peak water level variation with astronomical tide (bottom) and tide-CDF (top) at Old Inlet (Station 9) for the 1938 Hurricane. The square marks the historical storm.

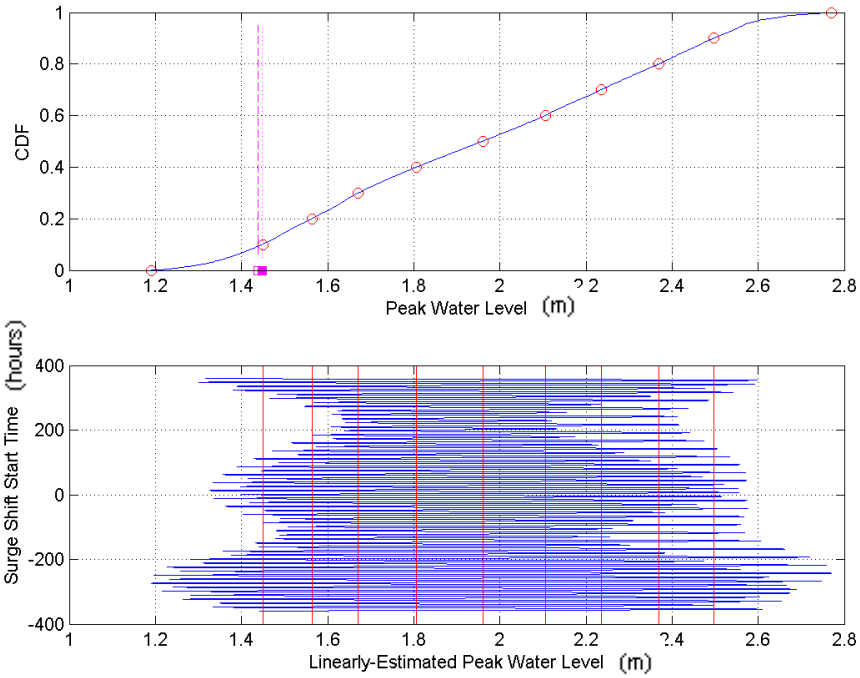

Figure 10-6: Peak water level variation with astronomical tide (bottom) and tide-CDF (top) at Old Inlet (Station 9) for Hurricane Gloria (1985). The square marks the historical storm.

such that peak water levels were much smaller than what the storm would produce on average. The timing of these historical storms occurred with timing to place its peak water level at about the 80th and 10th percentiles for the 1938 and 1985 hurricanes, respectively.

The tide-CDFs in Figure 10-5 and Figure 10-6 provide a natural means for accounting for storm water level extremes and distribution as they relate to the accidental occurrence of tide with surge. Folding this information into the EST analysis discussed in Chapter 10.2.1 results in a smoothing of the 1-D EDF curves. The lump of probability assigned to each historic water level can be apportioned out with the tide-CDF. This is achieved by replacing the historic peak water level with the median tide-CDF peak water level (corresponding to tide-CDF=0.5) at its appropriate location on the EDF curve, and assigning the probabilities over the interval of peak water levels based on the tide-CDF. Figure 10-7 and Figure 10-8 illustrate this process. Within the EST program, this is accomplished by using the Tide CDF as akernel for smoothing the raw 1-D EDF (Borgman, 2003).

A significant advantage of incorporating the tidal CDFs is that upper tail of the 1-D EDF is more adequately estimated with a procedure that grows naturally out of the tidal sequence information. The validity of the return periods estimated with the upper tail is strengthened by the improvement of the upper tail determination. This will not necessarily reduce the magnitude of uncertainty bands, but does make neighboring, hydrodynamically similar sites more consistent with one another. As will be discussed further in Chapter 12, accounting for astronomical tide variation for the FIMP study produced stage-frequency results that slowly vary alongshore and are consistent within the bays.

To implement the above approach, total water level hydrographs during the historical passage of the storm were simulated with ADCIRC and Delft3D. Storm-surge-only hydrographs were then extracted from the total water level hydrographs for use in generating tide CDFs.

Unfortunately, the linear superposition assumption employed in developing the tide CDFs is not always applicable for all storms or for all stations within FIMP. In particular, bay stations (those modeled with Delft3D) are influenced by nonlinear effects including overwash, breaching, and flow constriction at the inlets. As such, additional simulations with Delft3D were required to provide better tide-CDF estimates for some storms. The procedure for selecting and simulating additional storms for this purpose is discussed in Chapter 10.5.

Hypothetical Storms

The storm surge at specific location depends on the "strength" of the storm, which is mostly determined by its size (i.e., typically characterized by the radius of maximum winds), forward velocity, and pressure deficit, the physical characteristics of the area (i.e.,

coastline geometry and bathymetry), and the storm track (i.e., how close is the location of

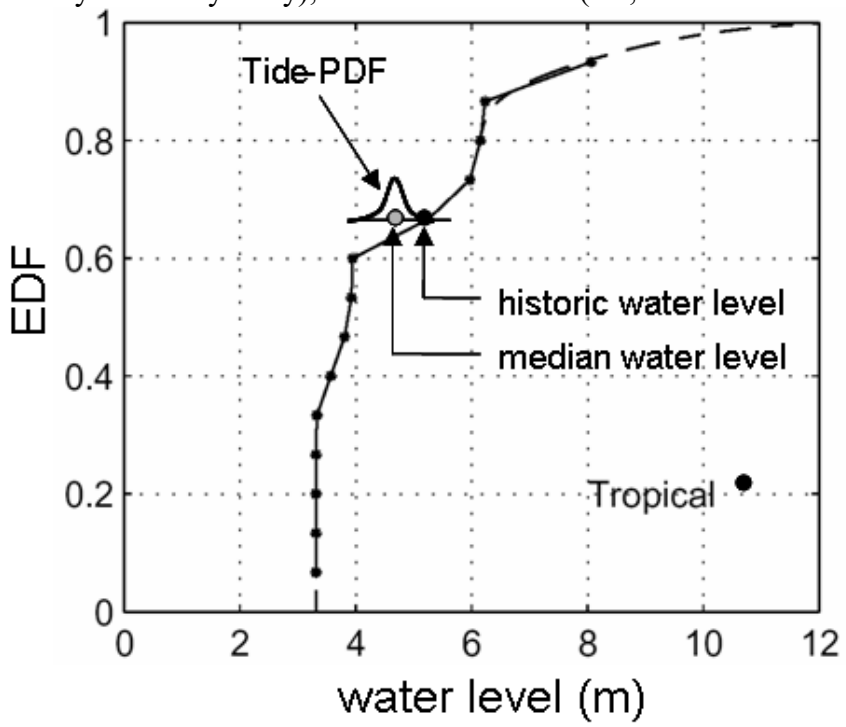

Figure 10-7. Illustration of tide-CDF kernal application on historic storm EDF. The EDF shown is the EDF computed from the simulated peak water levels for historical tide conditions.

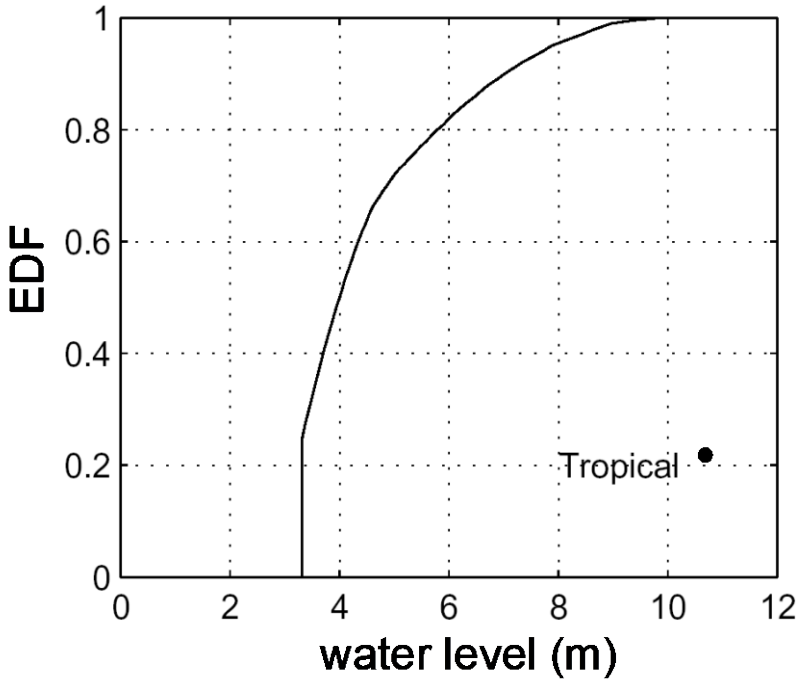

Figure 10-8. Illustration of an adjusted EDF following tide-CDF kernal application.

interest to the storm path). Therefore, previous storm surge studies in this area, including FIMP studies using WIFM (Butler and Prater, 1983) and using ADCIRC (Scheffner and Wise, 2001), considered the possibility of additional hypothetical storms based on perturbations of the historic events. In the WIFM study, synthetic or hypothetical storms were developed as a required step in the Joint Probability Method (JMP) used to develop stage-frequency results. In the Scheffner and Wise study, these storms were used to "supplement the training set [of historic storms] so that all stations within the study [area] experience a maximum intensity event" (Scheffner and Wise, 2001). A similar approach was considered for the present study and ultimately rejected for the following reasons:

1) Stage-frequency relationships for the present study have been developed using the Empirical Simulation Technique (EST). A detailed description of the methodology and results are presented in the above sections and Chapter 12, respectively. The principal advantage of this method is that it does not rely on assumptions concerning parametric descriptions of the water level statistics or the statistics of underlying storm characteristics (e.g., storm track). Therefore, it does not require development of hypothetical or synthetic storms representative of probability distributions for various storm parameters like the JPM method does.

2) Storm landfall timing may be totally random, but other storm parameters such as pressure deficit, radius to maximum winds, storm path and landfall location are at least partially determined by the local coastline geometry and typical background meteorological conditions. Hurricane track and landfall location are arguably more accidental and easier to assign hypothetical values to than other storm parameters. However, the historic data available for the project area (see Figure 10-9) suggest that most storms follow a southwest to northeast track parallel to the New Jersey coast striking Long Island east of Jones Inlet and few follow a track from south-southeast (i.e., from sea) to north-northwest. Furthermore, only one significant hurricane, in 1893, made landfall west of Jones Inlet.

However, the possibility of major hurricanes impacting any location along the project length should be considered. To that end, Scheffner and Wise supplemented the historic set of storms with two synthetic 1938 storms making landfall 40 mi (64 km) to the west of the historic landfall location in eastern Great South Bay. The authors argued that the 1938 hurricane, which is the storm of record for FIMP, produced larger surge values at the east end of the project area than at the west end. Therefore, they introduce this track variation so all stations along the project area experience this "maximum intensity event". While there is no strong physical justification for shifting the track by that specific or that large a distance, it is recognized that such large variations in storm track could produce significant changes in storm surge.

To determine how stage-frequency relationship would be impacted by track variation for this study, a set of sensitivity tests were conducted. A 9.3-mi (15-km) track shift distance was selected as a reasonable random variation distance based on the radius to maximum winds for this storm (Edge, personal communications). This distance was considered to be representative of a small track perturbation, rather than a completely new track, as

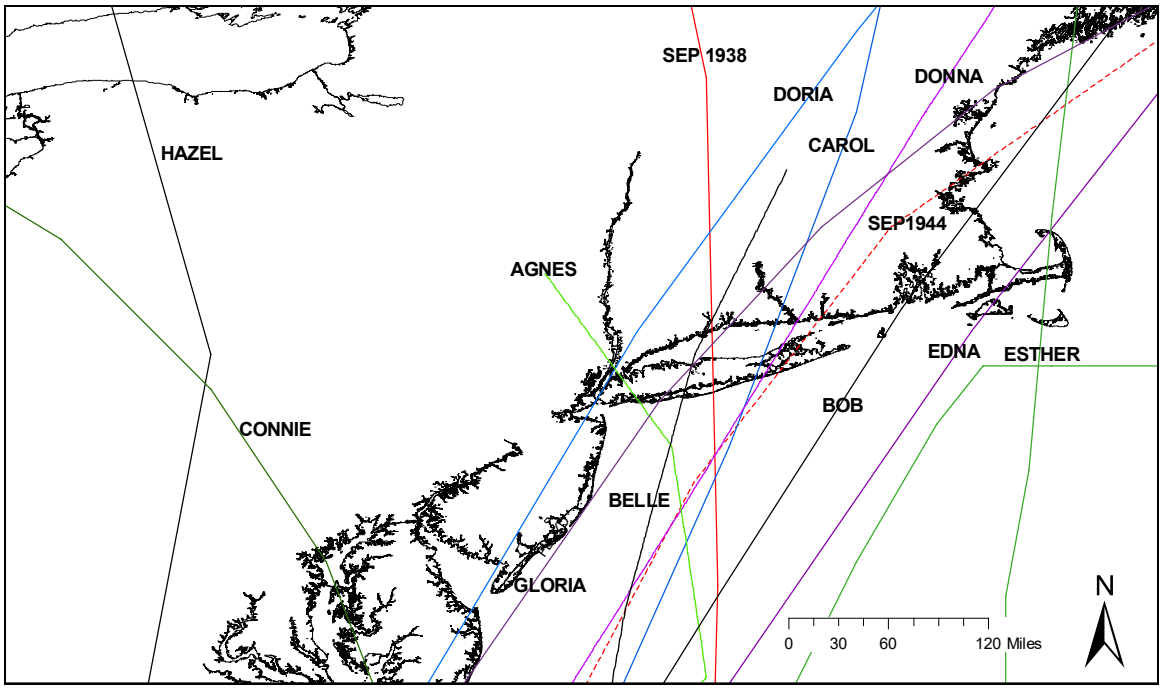

Figure 10-9: Historical hurricane tracks between 1850-2003 (NHC online database).

considered in the Scheffner and Wise study. Consideration of track variations larger than one radius to maximum winds was considered impractical for this study for the reasons above.

The sensitivity tests, conducted with ADCIRC by shifting the historic wind and pressure fields for the 1938 hurricane, a major hurricane, 9.3 mi (15 km) to the east and 9.3 mi (15 km) to the west, demonstrated that water level differences with respect to the historic event were well within 0.3 m (1 ft) at ocean stations and around 0.15 m (0.5 ft) or less at stations in the three bays (Figure 10-10 to Figure 10-13). These peak surge differences are small compared to differences associated with the accidental astronomical tide timing. Furthermore, water level differences for the westerly-shifted storm generally showed a positive bias while the easterly-shifted storm generally showed a negative bias of equal magnitude. This indicates, that if both shifts are equally weighted in the statistical analyses to determine stage-frequency, their effects will nearly cancel each other. Because the predicted differences in surge as a function of storm track are small with respect to those differences in surge as a function of astronomical tide, it is assumed for this study that any contributions to the range (maximum and minimum) about the mean stage value by track variation are negligible.

3) More importantly, a similar effect (i.e., all alongshore stations experiencing a maximum intensity event) may be accomplished with the tide phase shifting approach described above. Specifically, Hurricane Gloria in 1985 produced storm surge (no tide)

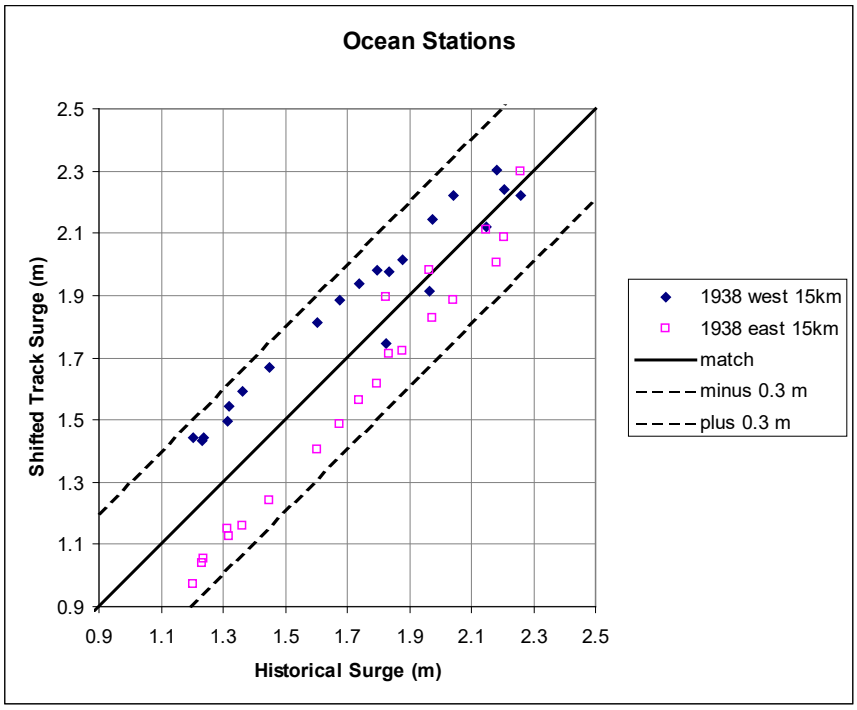

Figure 10-10. Difference in ocean peak water levels from simulations of the 1938 hurricane with wind and pressure fields shifted 15 km to the east and west and peak water levels from the historical simulation.

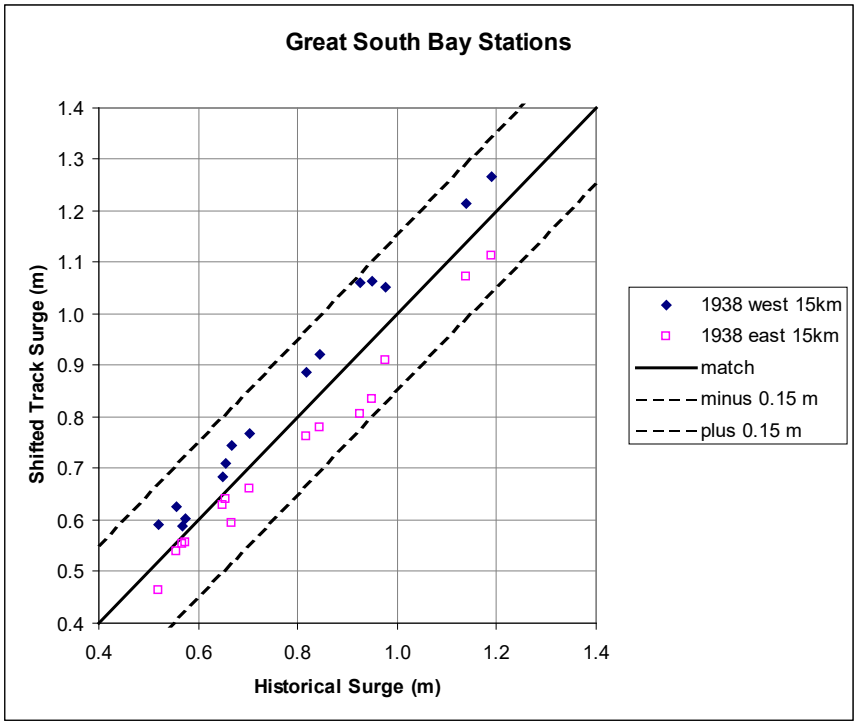

Figure 10-11. Difference in Great South Bay peak water levels from simulations of the 1938 hurricane with wind and pressure fields shifted 15 km to the east and west and peak water levels from the historical simulation.

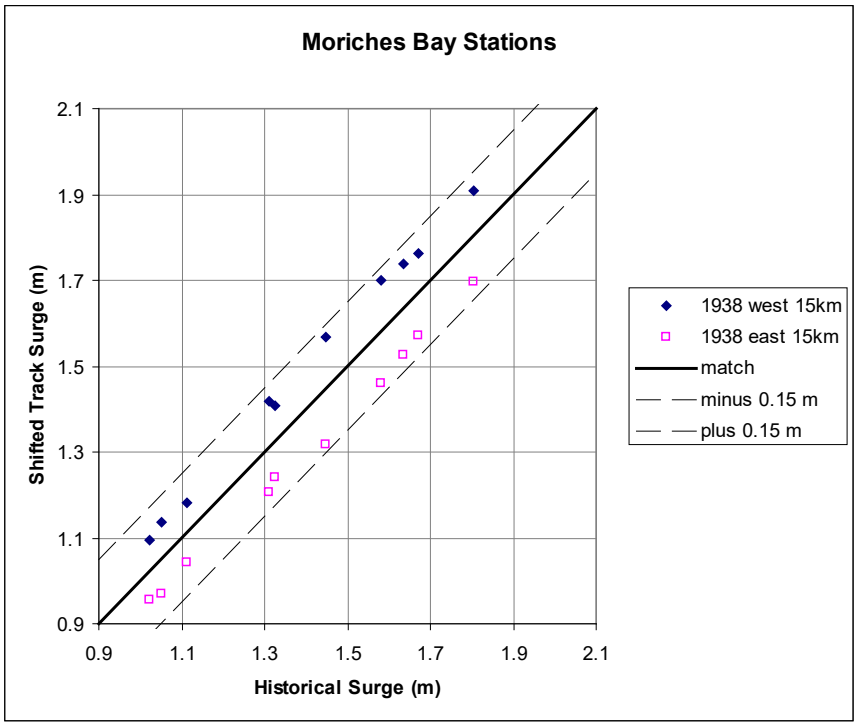

Figure 10-12. Difference in Moriches Bay peak water levels from simulations of the 1938 hurricane with wind and pressure fields shifted 15 km to the east and west and peak water levels from the historical simulation.

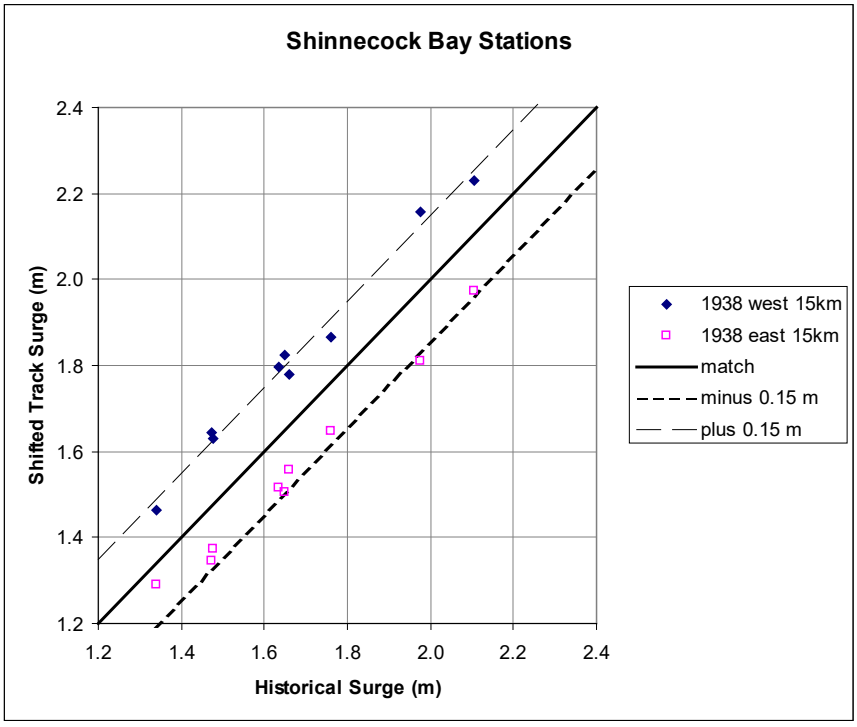

Figure 10-13. Difference in Shinnecock Bay peak water levels from simulations of the 1938 hurricane with wind and pressure fields shifted 15 km to the east and west and peak water levels from the historical simulation.

values along the western portion of Long Island that are similar to those generated by the 1938 Hurricane along the eastern portion of Long Island (Figure 10-14). In addition, the storm tracked farther west (through Jones Island and close to the western hypothetical track of the 1938 Hurricane used by Scheffner and Wise in their study). However, as explained above, the timing of this storm and the tide resulted in total water levels significantly lower, by about 1.5 m (5 ft), than those that would have occurred had the storm hit close to high tide. By considering additional storm-surge combinations during Hurricane Gloria, maximum water levels along the western end of the project are very close to those measured during the 1938 Hurricane along the eastern end of the project. In fact, Figure 10-15 shows that peak water levels along the project shoreline after considering all storm-tide combinations are very similar (the maximum difference is less than 1 ft (0.3 m)).

In conclusion, the peak water level conditions for FIMP are evenly distributed alongshore by incorporating the tide CDF's introduced above (see Chapter 12). Therefore, for the FIMP study hypothetical storm tracks were not used to further smooth alongshore water level variability.

10.3 Employing Annual Maximum Analyses

EDFs developed only from the peak-over-threshold storm set, i.e. large events, presented in Chapter 2.2 underestimate water levels for events associated with return periods less than 10 years, as determined by comparison with NOAA gage data at the 3 NOAAlocations. Because it is impractical to simulate all storms with surges exceeding the
annual event surge, an adjustment to the EDF lower tails was required to better reflect water levels associated with small events within the project region.

Because long-term measured peak water level records do not exist for the 80 output stations of interest, several assumptions were made, based on available measurements, to account for the effects of small storms. To use as much information as is known from measurements regarding lower return period water levels, long-term measurement records were analyzed. These analyses allowed development of lower-tail criteria that force low return period water levels at the 80 FIMP output stations to more reasonably match trends in measured low return period water levels. The following paragraphs outline the procedure adopted for this study.

First, data from 3 NOAA stations (Sandy Hook, The Battery, and Montauk Fort Pond[10]) were analyzed to extract annual peak water levels for the extratropical storm population. Peak monthly water levels were extracted from each NOAA time series for the long-term gage record. Gage record lengths varied between 55 years, at Montauk Fort Pond, and 72 years at The Battery. Then the annual peak extratropical water level for a given year was selected as the peak of the monthly water levels, excluding any peak water levels associated with a tropical event. Finally, for each measurement station, CDFs were

[10] Data from Newport, RI were not analyzed here because ADCIRC simulations at this location were only available for the 6 calibration extratropical storms.

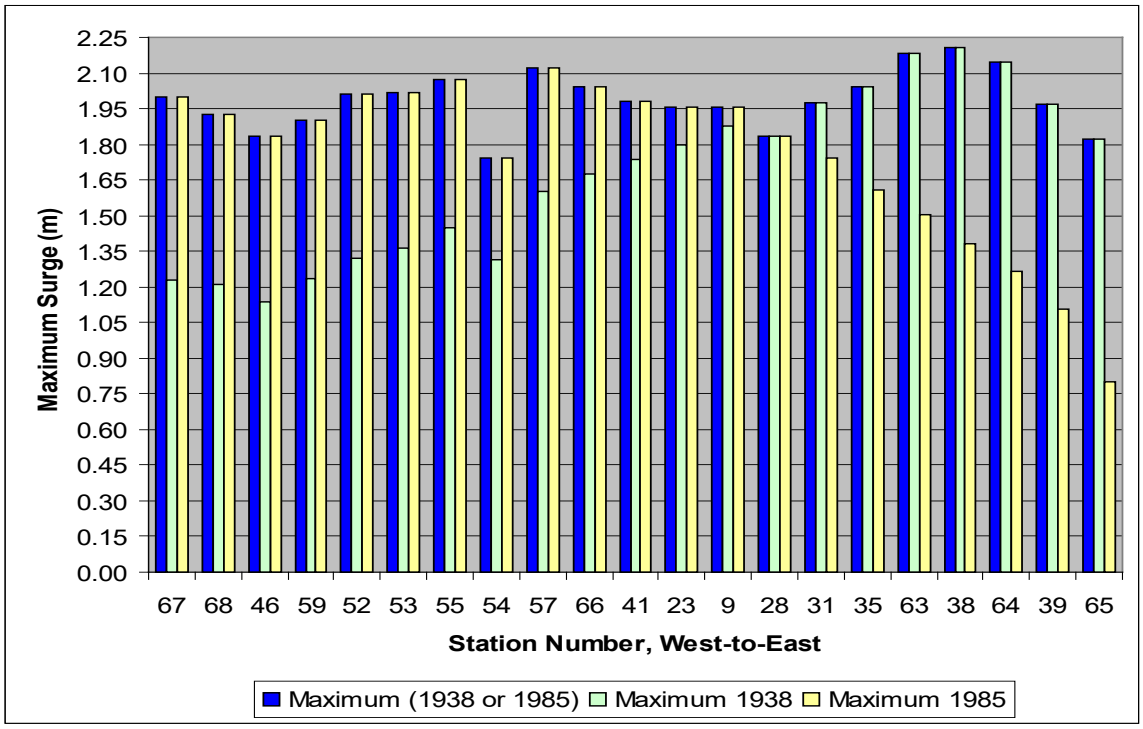

Figure 10-14: ADCIRC-simulated surge-only results for the 1938 Hurricane and Hurricane Gloria (1985). See Figure 2-7 through Figure 2-10 for station locations.

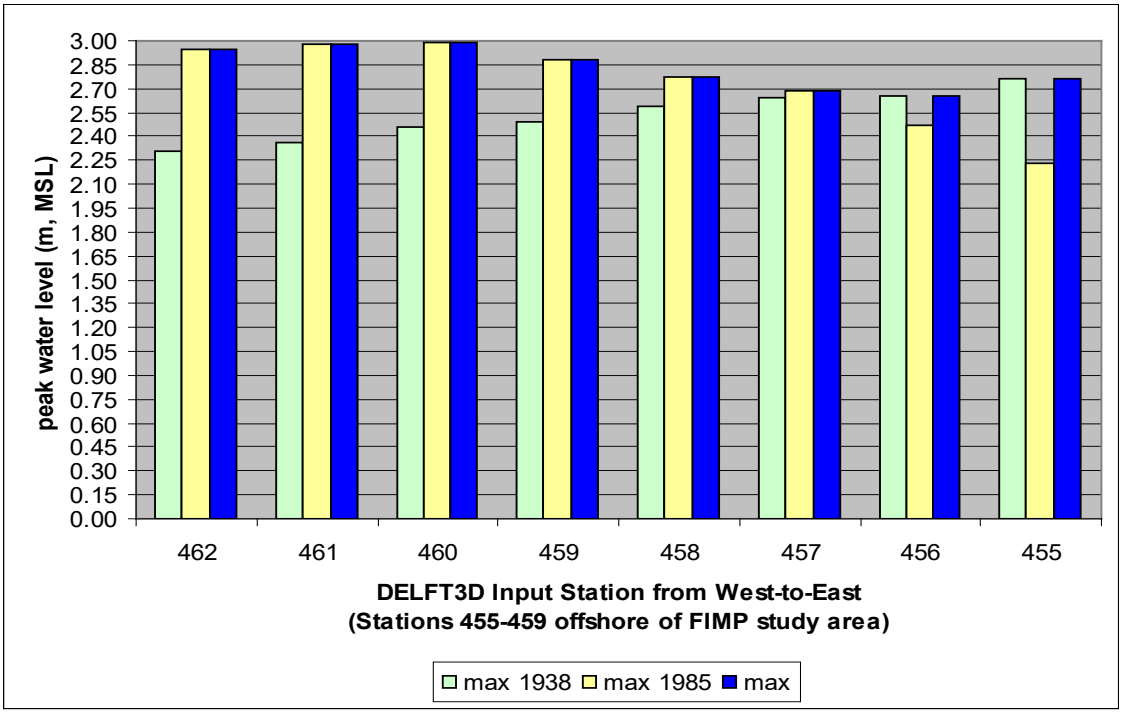

Figure 10-15: ADCIRC-simulated total water level for maximum-tide simulations of the 1938 Hurricane and Hurricane Gloria (1985).

generated for the extratropical annual maximum records following the methods outlined in Chapter 10.1.

10.3.1 Applying Annual Maximum Analyses to Bound CDF: An Adjustment for Small Events

To determine the appropriate adjustment to the peak-over-threshold EDF developed from the training set of storms, the extratropical measured annual peak distributions for the 3 NOAA locations were analyzed to determine their lower tail EDF properties. Based on this analysis, a simplified truncation method was used in this study to adjust extratropical EDFs at all stations. Based on the extratropical storm training set and the NOAA annual data at Sandy Hook and Montauk Fort Pond, a small extratropical event was selected to represent the minimum expected annual peak water level. This minimum peak water level was used to truncate the peak-over-threshold EDF. Finally, the approach was incorporated at all FIMP output stations. The final resulting adjusted EST EDFs represent both the larger events simulated with the hydrodynamic modeling suite and smaller events observed within the project region.

The approach adopted here for adjusting the EST EDF for small events satisfactorily captures the effects of small events, as determined from measured data, while allowing variation with station location and hydrodynamic properties (see Chapter 11).

10.4 Special Treatment of the October 1991 Storm Event

It is especially difficult to describe the physical properties of the October 1991 nor'easter in the project area because it is such a unique storm. This storm is the only one in the FIMP training set that was formed by the merging of two storm systems, making the meteorological patterns highly complex. Furthermore, water level and waves impacting the Long Island area were generated in the Atlantic far from Long Island. As such, it is difficult to simulate storm surge, wave characteristics, and morphological changes well for this storm. Consequently, the ADCIRC simulations using the available wind fields within the ADCIRC modeling domain predict virtually no storm surge for this storm while NOAA measurements indicate that storm surge for this event is significant. In fact, the October 1991 event is the extratropical storm of record at Montauk Fort Pond, at the eastern end of the project area. The difference in ADCIRC-simulated and measured storm surge at Sandy Hook and Montauk Fort Pond for the October 1991 are 0.7 m (2.3 ft) and 0.8 m (2.6 ft), respectively.

Because this storm is historically significant within the project region, it was necessary to approximate its impacts without the direct use of the October 1991 numerical model simulations. For this study, the impacts of the October 1991 storm will be estimated by a weighted average of the November 1953 and February 1978 extratropical events. These two events were selected because their measured water level and measured wave height hydrographs (namely shape variation with time) were the most similar to those observed during the October 1991 storm event. The replacement water level hydrographs developed at Sandy Hook and Montauk, Fort Pond to replace the October 1991 numerical

simulations are presented in Figure 10-16 and Figure 10-17. The replacement hydrographs reasonably match, within a few cm, the NOAA measured hydrographs at Sandy Hook and Montauk, Fort Pond for the 12-hour period around the peak of the storm. While the replacement hydrographs do underpredict water level away from the peak (more than or less than 6 hours from the peak), they provide a far better estimate than that predicted by ADCIRC for the October 1991 storm.

The November 1953 and February 1978 storm weights computed to create the replacement hydrographs for the Sandy Hook and Montauk, Fort Pond locations were linearly interpolated using longitude to determine the appropriate weights for all FIMP output locations.

While the resulting replacement storm characteristics are not a true match to those characteristics observed in October 1991, they are a vast improvement over those simulated with the modeling suite. As such, the stage-frequency relationships will better reflect the true extratropical storm population.

10.5 Supplemental Surge Modeling Simulations

10.5.1 Astronomical Tide Variation

As discussed in Chapter 10.2, the stage-frequency relationships will account for astronomical tide variability by linearly superimposing storm surge and astronomical tide time series and stepping through a full lunar cycle, 28 days. However, for intense storms, linear superposition of surge and tide will not adequately account for the nonlinear impacts to FIMP bay stations such as breaching, overwash, and flow constriction at the inlets. Ideally, every storm's tide-CDF curve would be established by ten or more peak water levels, each representing an additional simulation beyond the historical event. However, the number of model runs, 120 to 360, required for this approach would be so time consuming and expensive that it is not cost effective, nor justified by the limited potential for accuracy gains. As such, 12 of the most severe events, combined with select tide conditions, were chosen for SBEACH and Delft3D modeling to better define the tide-CDF curves.

The first priority in selecting these additional events was to capture nonlinear impacts from overwash and breaching. Initial additional storms were selected based on ocean peak water level, which governs overwash and breaching. For each severe event, the most extreme tide and surge combination (CDF=1.0), as evaluated at Old Inlet (station 9), was simulated (see Figure 10-5 and Figure 10-6). Old Inlet was chosen for this purpose because it is an ocean station that is centrally located alongshore, relative to the three bays. These simulations are summarized in the column headed Group 1 in Table 10-1.

Following simulation in Delft3D, the simulated peak water levels were compared with those computed by linear superposition. If the resulting simulated peaks did not deviate significantly from the linear superposition predictions, additional tide and surge

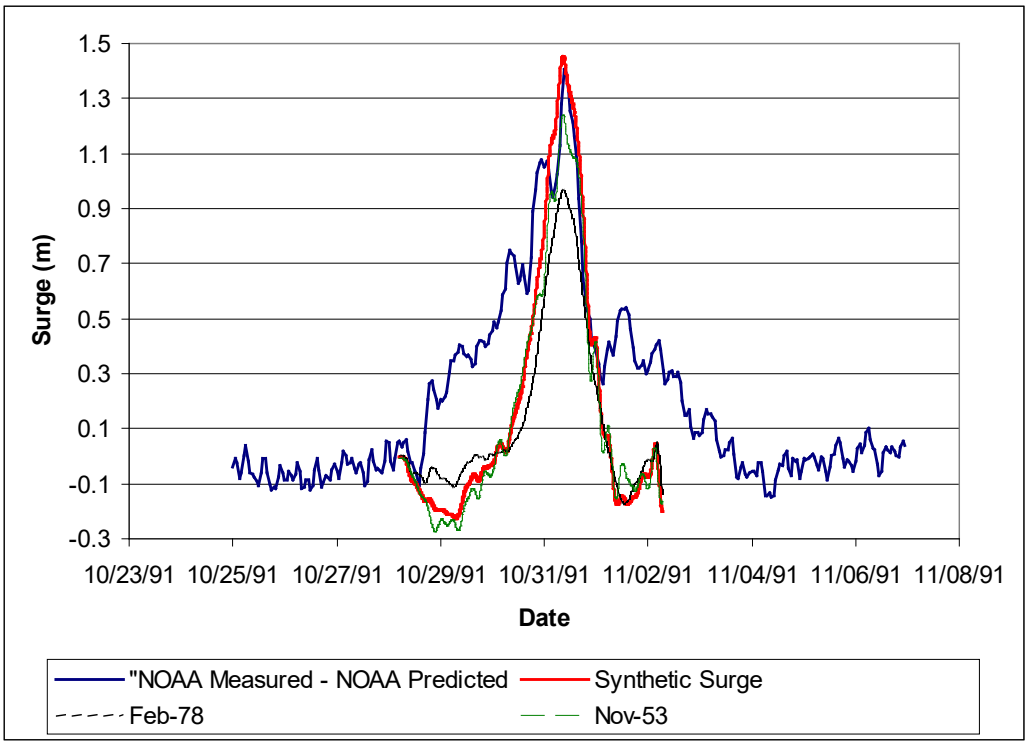

Figure 10-16. Synthetic surge hydrograph at Sandy Hook, NJ for the October 1991 extratropical event.

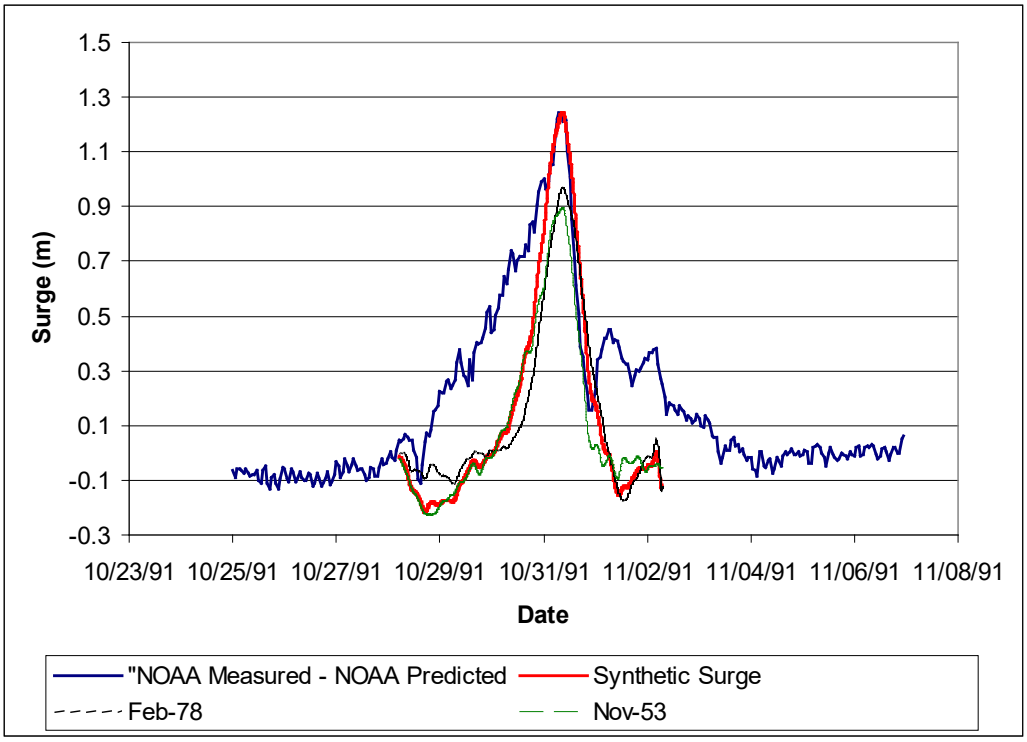

Figure 10-17. Synthetic surge hydrograph at Montauk Fort Pond, NY for the October 1991 extratropical event.

Table 10-1: Additional surge modeling simulations for defining tide-CDF curves.

Storm Date	Tide-CDF Value (0 to 1)					
	Group 1	Group 2		Group 3		
Sep-38	1.00	0.50				
Sep-44	1.00	0.90	0.30			
Aug-54	1.00					
Sep-60	1.00	0.30				
Aug-76	1.00					
Sep-85	1.00	0.50	0.90 (rising)	0.90 (falling)	0.20	0.37
Nov-50	1.00					
Nov-53	1.00					
Mar-62	1.00					
Oct-80	1.00					
Dec-92	1.00					
9-Mar-93	1.00					

combinations were neither identified nor modeled, and the tide-CDF curves were adjusted according to the rules presented below.

For several tropical events, this variation was measurable, more than 0.5 ft (15 cm), at a number of bay stations. For these cases, alternate tide combinations were simulated until differences between the simulated results and those predicted by linear superposition converged, or enough simulations were made to reasonably redefine the tide-CDF curves. Selection of these additional storms was determined not only by breaching and overwash potential, but also by anticipation of flow constriction at the inlets. Table 10-1 summarizes these additional storm simulations. In all, 21 additional simulations with SBEACH and Delft3D were performed.

Once the additional simulations were completed, the tide-CDF curves were adjusted using the set of rules below. Every tide-CDF, for each storm and each output location, was treated individually for this adjustment. The procedures below make every effort to weight the tide-CDFs towards the more accurate peak water level predictions provided by the model simulations while continuing to use the predicted information from linear superposition, based on 6720 (0.1-hour increments for 28 days) peak water levels, to augment the simulation set.

Historical peak water level plus one additional peak water level Points with vertical (tide-CDF value) separation greater than or equal to 0.45: The superposition tide-CDF rotated and shifted horizontally (in peak water level) to make the tide-CDF pass through the two simulated peak water levels.

Points with vertical (tide-CDF value) separation less than 0.45: The superposition tide-CDF shifted horizontally (in peak water level) to the 2-D midpoint of the two new water level simulations (no rotation). The reason this was adopted was that peak water levels too close together gave exaggerated accidental slope impositions that could not be

justified from physical considerations. The midpoint horizontal shift was much more stable, and gave reasonable fits.

Historical peak water level plus two or more additional peak water levels: A full smoothing spline, weighted least square fit was made through the simulated peak water levels to determine the tide-CDF. It was determined that three or more water levels were sufficient to justify using least square methods.

Figure 10-18 and Figure 10-19 present the adjustments made to the tide-CDF curves, by applying the results from the additional simulations, for Hurricane Gloria (1985) and the November 1950 Nor'easter. The tide-CDF adjustment for Hurricane Gloria is the most dramatic of the 12 storms selected for additional modeling. Because Hurricane Gloria was such an intense and fast-moving storm, flow constrictions at the inlets cannot allow the bays to fully respond to the ocean surge. As such, the assumption that a surge-only simulation of water level can be directly added to astronomical tide does not adequately describe surge propagation into the bays. For other fast-moving hurricanes, this effect is less measurable and the linear-superposition assumption, with minor adjustments for the most extreme tide and surge combination, sufficiently describes the tide-CDF curves.

For the extratropical storms, in some cases, the simulated most extreme tide and surge combination resulted in peak bay water levels in excess of the peak water level predicted by linear superposition. This is most likely a result of significant overwash. As a result, many of the extratropical tide-CDF curves were shifted to account for this non-linear process. Figure 10-19 for the November 1950 storm illustrates this shift.

10.6 Sea Level Rise

Because baseline conditions topography is represented by the September 2000 lidar survey, the stage-frequency relationships presented in this report are adjusted for sea level rise to the year 2000 by adding 0.3 ft (0.09 m) to all water levels. The 0.3-ft (0.09-m)sea level conversion was computed as the average of the sea level rise rates reported by NOAA at Sandy Hook, The Battery, and Montauk Fort Pond between 1969 (midpoint of tidal epoch) and 2000.

Sea level rise adjustments were only applied to the stage-frequency relationships as the last step in the EST analysis. Sea level rise effects were not incorporated into any of the numerical modeling simulations.

10.7 Summary

The stage-frequency methodology outlined in this chapter and employed for this study rigorously addressed the accidental occurrence of storms with astronomical tide and ensured that impacts of historically significant as well as small storms are captured.

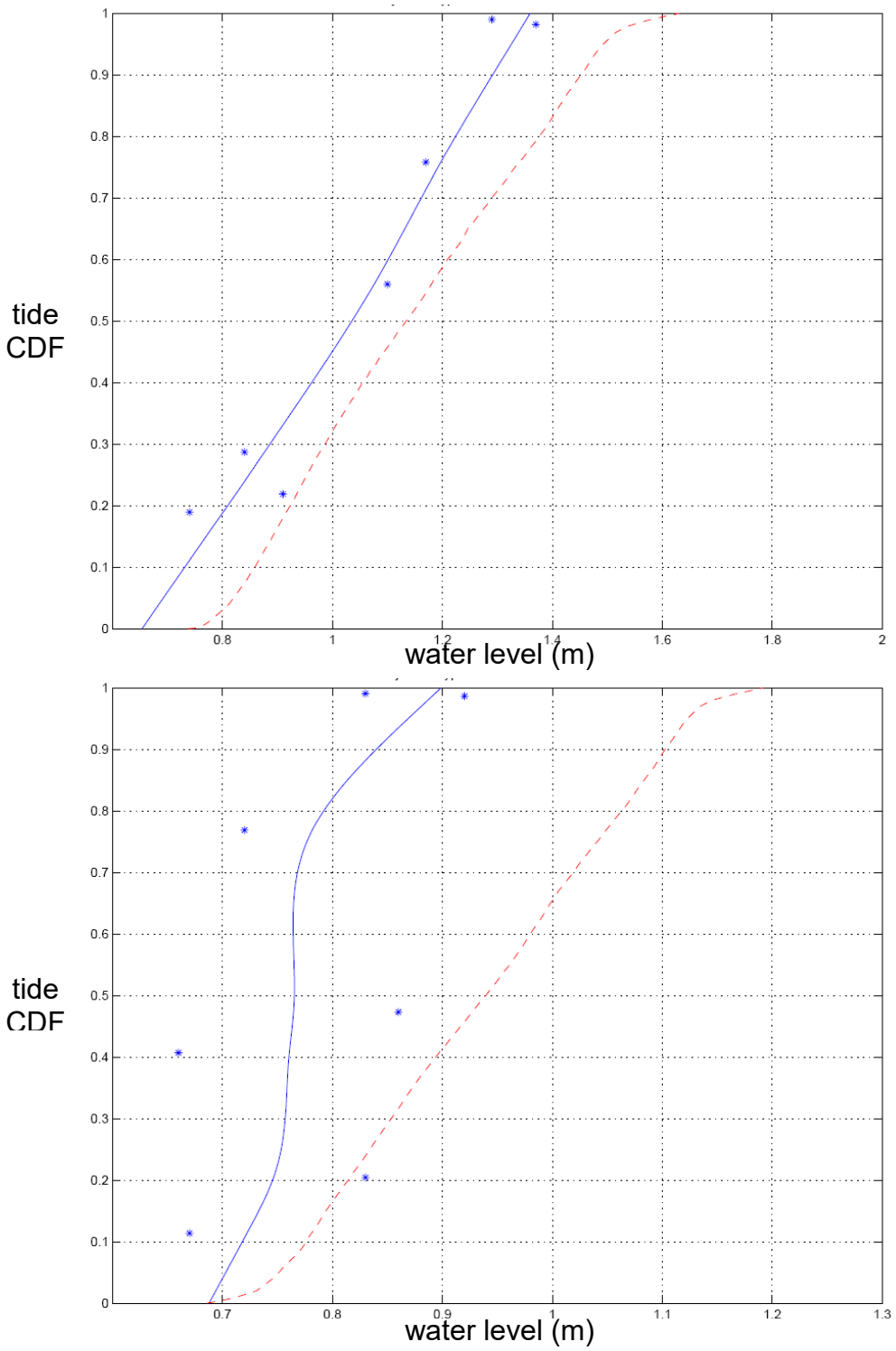

Figure 10-18. Sample tide-CDF adjustments for Hurricane Gloria (1985) at stations 43 in Moriches Bay(top) and 8 near Sandy Point (bottom). Additional simulation peak water levels are represented by blue asterix. Red dashed line is the tide-CDF curve from linear superposition where blue solid line is the adjusted CDF curve based on additional simulations.

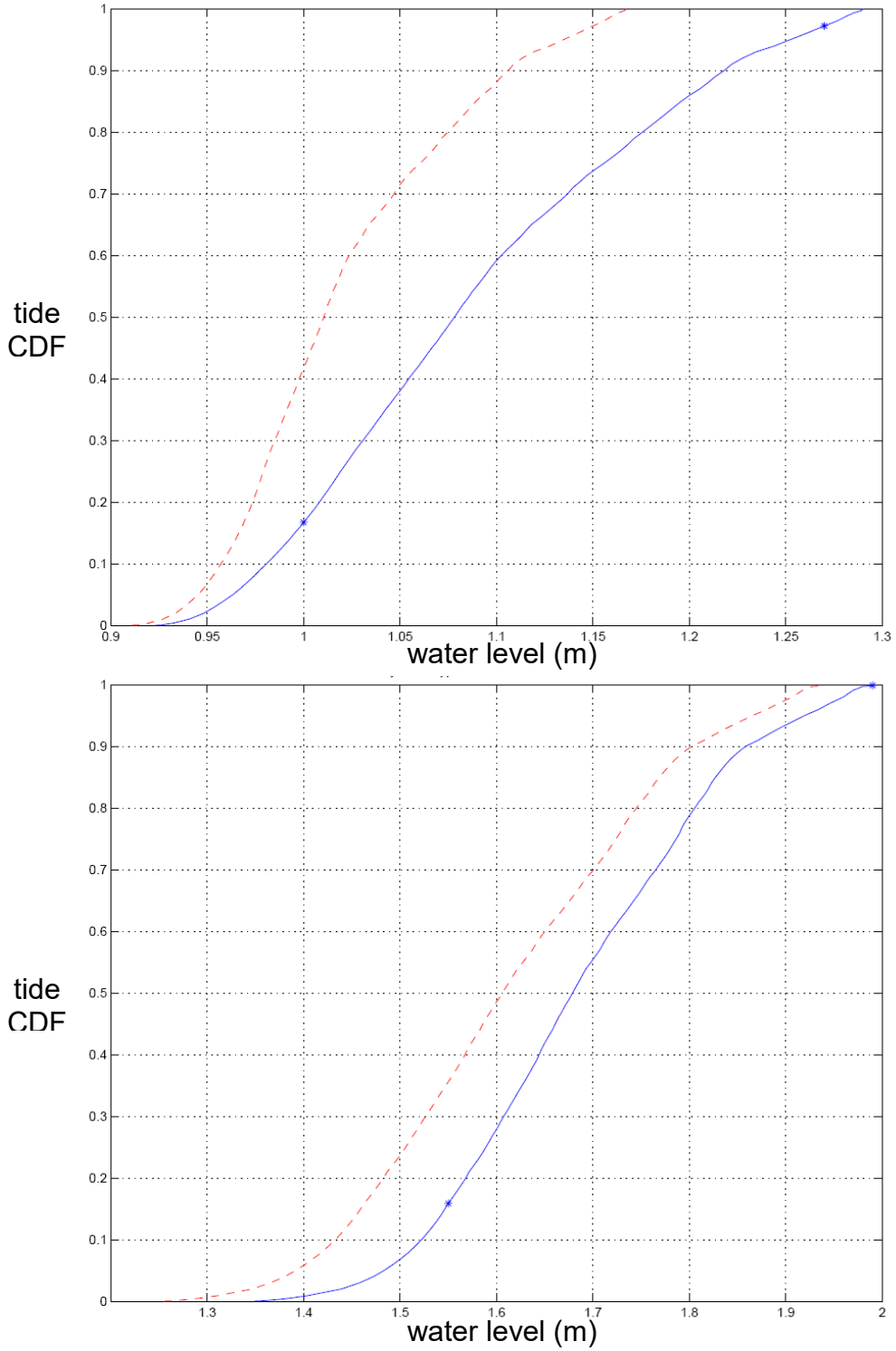

Figure 10-19. Sample tide-CDF adjustments for November 1950 Nor'easter at stations 17 near Sampawams Point (top) and 34 near Shinnecock Bridge(bottom). Additional simulation peak water levels are represented by blue asterix. Red dashed line is the tide-CDF curve from linear superposition where blue solid line is the adjusted CDF curve based on additional simulations.

11. Stage-Frequency Comparison

The stage-frequency relationships developed with the EST for this study compare well to NOAA measured data at Sandy Hook, Montauk Fort Pond, and The Battery. The Sandy Hook and Montauk Fort Pond comparisons for extratropical and tropical events are shown in Figure 11-1 through Figure 11-4. The extratropical EST relationships for return periods of 10 years and lower reasonably match with the NOAA measured annual maximum curves at both locations (Figure 11-1 and Figure 11-2). In this region, the difference between the NOAA curves and the curves developed for this study area about 0.3 ft at Sandy Hook. This is seen as a small low bias in the EST result. At Fort Pond, the EST extratropical result falls about 0.5 ft below the NOAA annual maximum estimate. The computed differences here are most likely attributed to the approximation approach adopted for this study and presented in Chapter 10.3.

The extratropical EST relationships for return periods greater than 10 years match well with both the NOAA measured peak-over-threshold and annual maximum curves. Figure 11-1 and Figure 11-2 show that the differences below the 25-year return period are less than 0.5 ft. This results in a small low bias in the Fort Pond EST result. Differences are larger for return periods above 25 years. The EST results based on ADCIRC-simulated peak water levels are 0.5 ft to 1 ft higher than the results derived directly from NOAA measured peak water levels for return periods above 30 years. These differences are most likely attributed to the influences of astronomical tide smoothing in the EST analysis, ADCIRC simulation RMS error (0.6 ft), and limited storm record length (50 years).

The tropical EST relationships also compare well with the NOAA measured peak-over-threshold curves for all return periods (Figure 11-3 and Figure 11-4; note that a lower tail adjustment was not applied for tropical EST relationships). Here, differences between the EST and NOAA relationships are generally smaller than 0.5 ft. The tropical EST simulations are particularly influenced by the astronomical tide smoothing process employed during EST analyses. As such, the differences between the EST and NOAA relationships are most likely attributed to astronomical tide smoothing; however, ADCIRC simulation error may also contribute to these differences.

In conclusion, the EST stage-frequency relationships developed for this study at Sandy Hook, to the west of the project area, and Montauk Fort Pond, at the eastern end of the project area, accurately represent the stage-frequency relationships derived directly from NOAA measured data at these two locations. These comparisons indicate the numerical modeling and statistical (EST) approaches adopted for this study reliably characterize storm water levels in this region over the period of historic information.

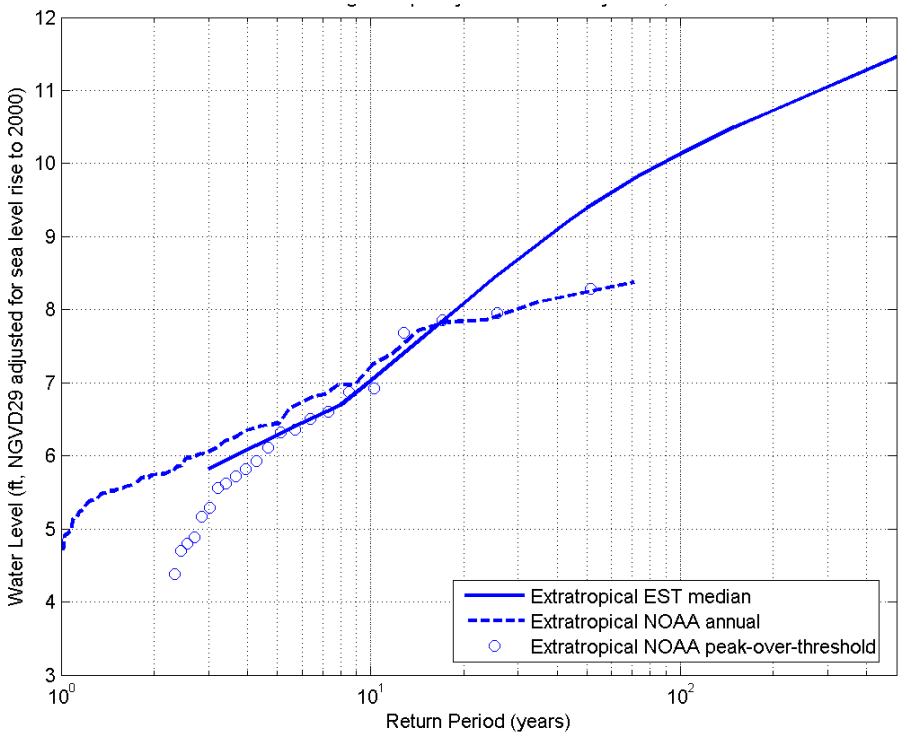

Figure 11-1. Extratropical stage-frequency curves at Sandy Hook, NJ.

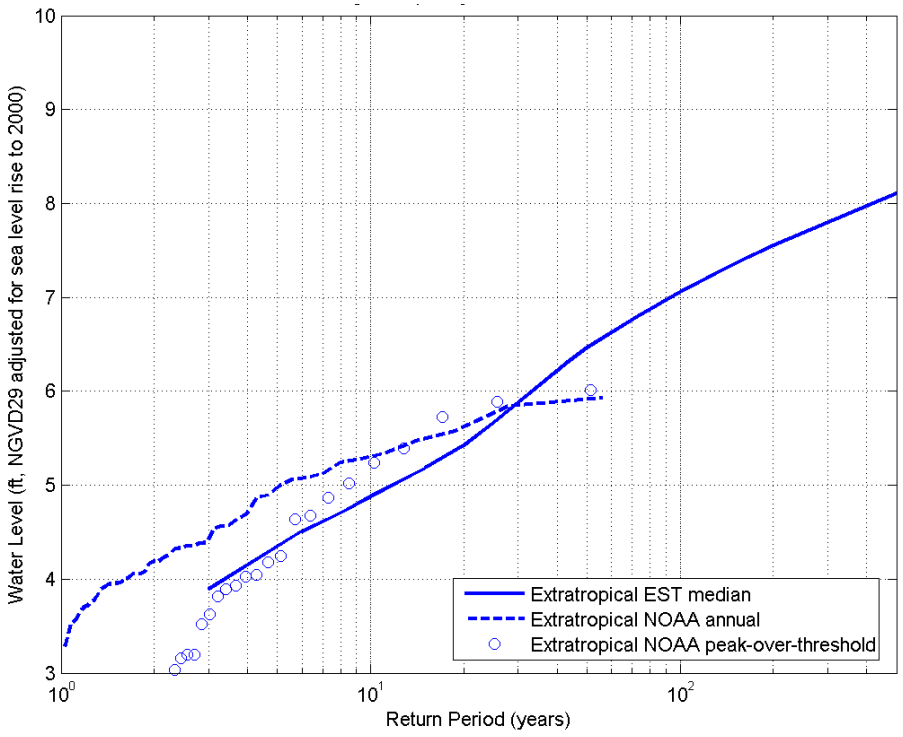

Figure 11-2. Extratropical stage-frequency curves at Montauk Fort Pond, NY.

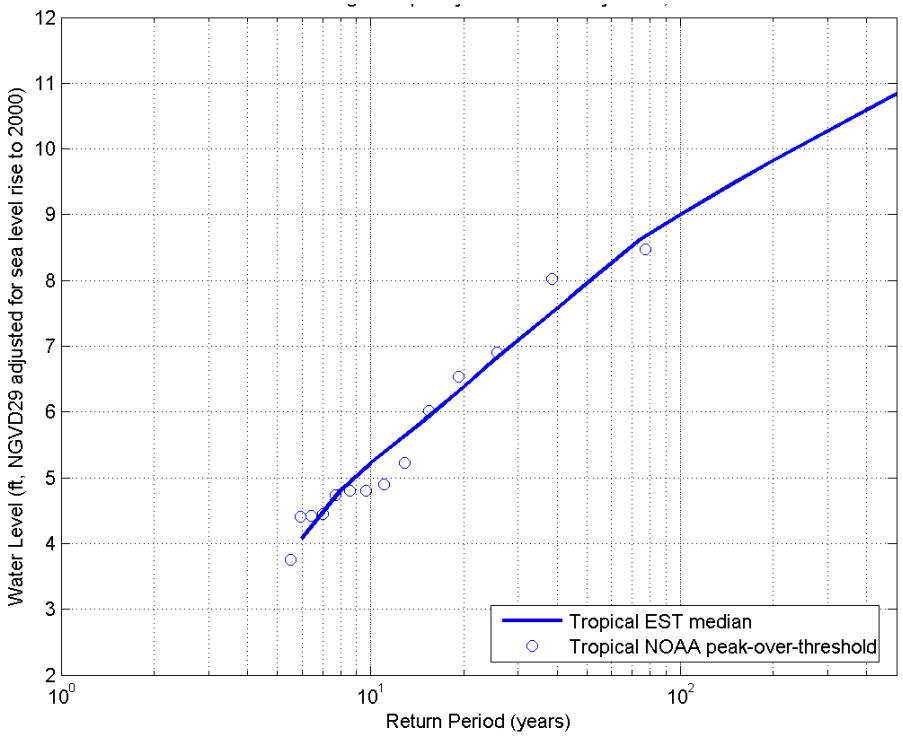

Figure 11-3. Tropical stage-frequency curves at Sandy Hook, NJ.

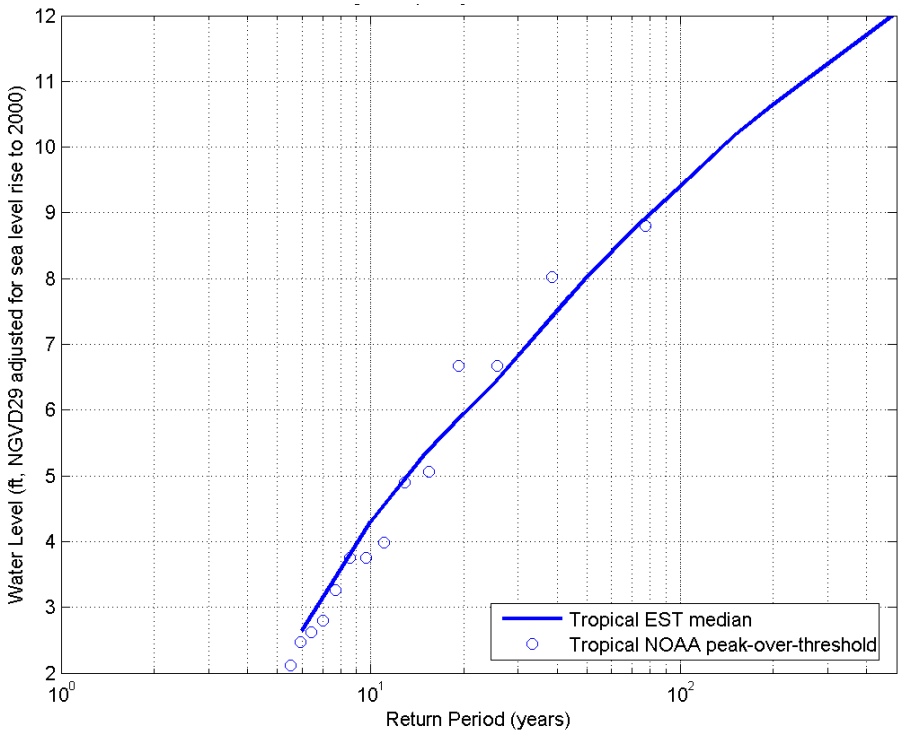

Figure 11-4. Tropical stage-frequency curves at Montauk Fort Pond, NY.

12. Stage-Frequency Relationships

Following the methods discussed in Chapter 10, stage-frequency relationships were developed for all FIMP output locations using the water levels simulated with the numerical modeling suite. The following presents select stage-frequency results from this study for discussion. The full set of stage-frequency curves are presented in the appendix and representative plots at Great South Beach (Station 23) are show in Figure 12-1 through Figure 12-3.

All stage-frequency results presented in this report represent peak-over-threshold analyses. As such, return period represents the theoretical average waiting time between exceedences of its peak water level. It should be noted that return periods derived from peak-over-threshold analyses and annual maximum analyses, while related, are not the same (Borgman, 2004).

All figures in this report represent the peak water levels from the combined effects of ocean storm surge, generated by both wind and barometric pressure fields, and astronomical tide. At bay stations within the FIMP project area, the peak water level also includes contributions from localized wind setup, from propagation of ocean wave setup through the tidal inlets, and from water flowing over the barrier island as a result of overflow and breaching. These peak water levels do not include the effects of local wave setup (these results will be presented in a separate report). All peak water levels presented on stage-frequency curves and discussed in this chapter are in feet, referenced to NGVD, and are adjusted to the year 2000 for sea level rise.

Stage-frequency results for bay stations outside the FIMP project area, particularly in other bays, should be checked carefully against available data prior to their use in engineering studies. Again, it is noted that local wave setup is not included in the results presented in this report, and, therefore, these stage-frequency curves may not be consistent with past curves developed for this region. A rigorous evaluation and validation of these output stations, comparable to that undertaken for the output stations within the FIMP study, was beyond the scope of this study. Furthermore, the stage-frequency results for Jamaica Bay stations do not include water level contributions from ocean wave setup propagation into this bay.

Finally, the stage-frequency curves presented in the appendix are extrapolated to the 500-year return period. As the period of historical record limits the reliability of stage-frequency predictions, stage-frequency results for all stations for return periods greater than 100 to 150 years should be used with caution. In this report, the median result along with the quartile bands are presented. These represent the expected result and the expected spread about the median result. In the FIMP economic analysis, the mean and standard deviation are employed. These two representations are mathematically related through a lognormal distribution that is a function of all fractiles.

12.1 Ocean Stage-Frequency Discussion

Figure 12-4 through Figure 12-9 show the spatial distributions of tropical, extratropical, and combined peak water levels along the open coast and within the three bays for the 6-year, 10-year, 25-year, 50-year, 73-year, and 100-year return periods. These figures demonstrate that the introduction of astronomical tide variation, as discussed in Chapter 10.2.2, results in a smooth variation in ocean peak water level for all storm types at all return periods. Extratropical peak water levels increase from east to west. Because the New York and New Jersey land masses effectively funnel water to the west as winds are typically from the east. This trend is expected for extratropical events. For return periods smaller than 50 years, the tropical peak water levels also decrease from west to east. However, peak tropical water levels for return periods greater than 50 years increase alongshore to the east of Shinnecock Inlet.

Peak 6-year combined ocean water level slowly varies from about 5 ft to 7 ft, increasing from east to west. The 6-year water level is dominated by extratropical events, whose peak water level also varies within the same range. Around the 25-year return period at eastern stations and around the 50-year return period at stations in the western FIMP area, Figure 12-7, extratropical and tropical events nearly equally contribute to the combined ocean peak water level along the project length. Peak combined water level for the 50-year return period varies from about 7.5 ft in the eastern project area to about 9 ft in the western project area. At the 100-year return period, the contributions to the combined stage-frequency estimate for extratropical and tropical events are still nearly equal for stations west of Moriches Inlet. In contrast, combined peak water levels are dominated by tropical events to the east of Moriches Inlet. In this region, tropical peak 100-year water levels are about 2 ft to 3 ft higher than extratropical peak 100-year water levels. Combined peak 100-year water levels vary from 9 ft to 10.5 ft in the project area, where the water level slowly increases easterly and westerly about Moriches Inlet.

12.2 Bay Stage-Frequency Discussion

The figures also demonstrate the consistency of peak water levels within each bay. In Great South Bay, peak water levels at all return periods are spatially consistent. For all return periods, extratropical events are the dominating contributor to the combined stage-frequency estimate at all Great South Bay locations except stations 8 and 25 at the far eastern end of the bay. This is indicative of the hydraulic inefficiency of Fire Island Inlet. Numerical modeling simulations for this study show that Great South Bay is slow to respond to water level changes in the ocean. Consequently, water levels in this bay do not respond as dramatically to faster-moving tropical events as they do to the longer-duration extratropical events. The peak water levels in this bay are generally much lower than those computed for the same return period at ocean stations. Peak water levels in Great South Bay are approximately between 3.5 ft and 4.5 ft, 4 ft and 5 ft, and 4 ft and 6 ft, for the 6-, 50-, and 100-year return periods, respectively. These stage-frequency values do not include the effects of locally-generated wave setup.

Stage-frequency results in Moriches Bay are generally higher than those in Great South Bay as this bay more readily responds to ocean conditions. Peak water levels in Moriches Bay are approximately between 4 ft and 5 ft, 6 ft and 7 ft, and 6.5 ft and 7.5 ft, for the 6-, 50-, and 100-year return periods, respectively. The combined stage-frequency curves are dominated by extratropical events for return periods below 25 years. However, extratropical and tropical events more equally contribute to the combined relationships for return periods of 50 years and larger. This demonstrates that Moriches Bay responds more quickly to fast changes in ocean water level.

Of the three bays within the FIMP area, Shinnecock Bay is characterized by the highest peak water levels. In Shinnecock Bay, peak water levels are approximately between 5 ft and 6 ft, 7 ft and 8 ft, and 7.5 ft and 8.5 ft, for the 6-, 50-, and 100-year return periods, respectively. Furthermore, Shinnecock Bay is more influenced by tropical events for larger return periods. This is a direct consequence of the relative efficiency of Shinnecock Inlet and the stage-frequency trends along the ocean. Near Shinnecock Inlet, and at eastward ocean locations, the ocean combined stage-frequency relationships are dominated by tropical events for return periods larger than 50 years. This trend is carried through to the Shinnecock Bay combined stage-frequency relationships.

12.3 Summary

This report has demonstrated that the stage-frequency results developed in this study represent NOAA gage measurements, display slowly varying alongshore trends in ocean water levels, and display spatial uniformity in bay water levels.

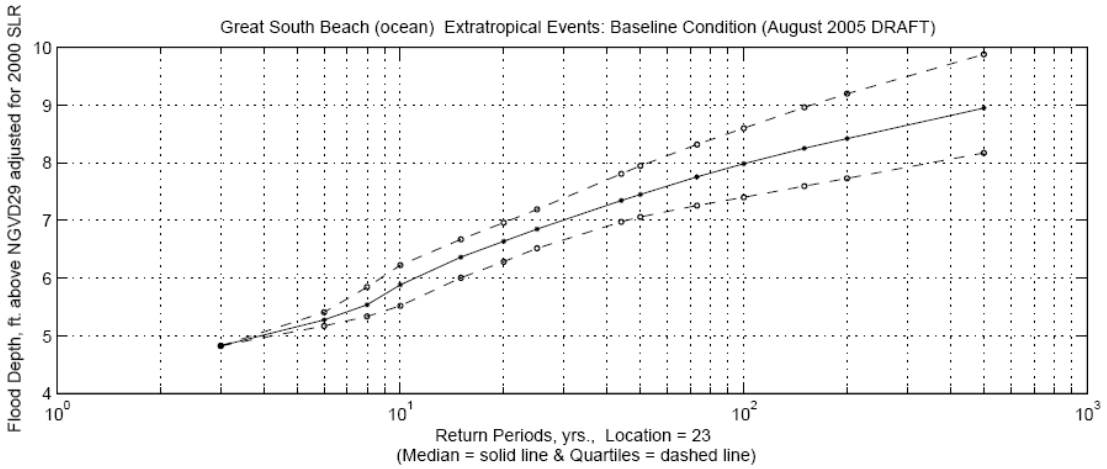

Figure 12-1. Extratropical stage-frequency curve for Station 23, Great South Beach. Peak water level is adjusted to sea level rise in 2000.

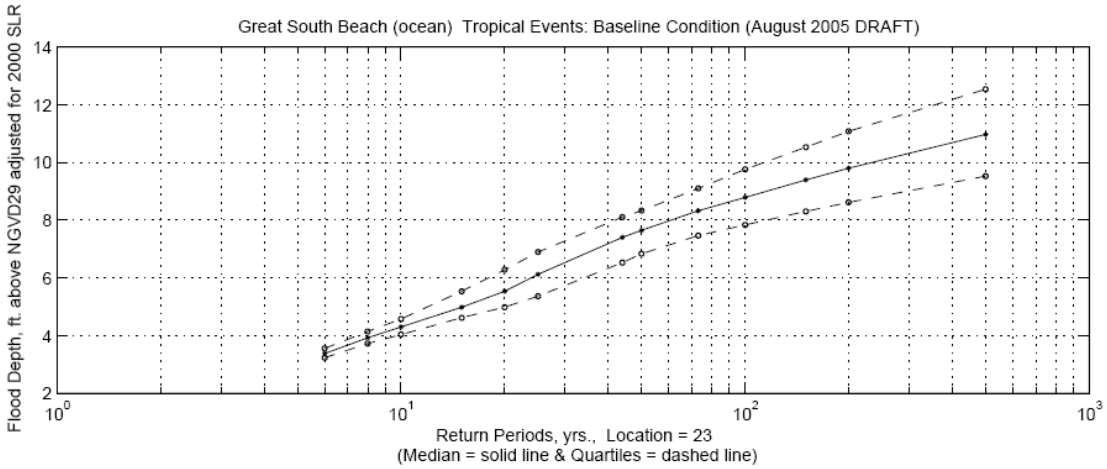

Figure 12-2. Tropical stage-frequency curve for Station 23, Great South Beach. Peak water level is adjusted to sea level rise in 2000.

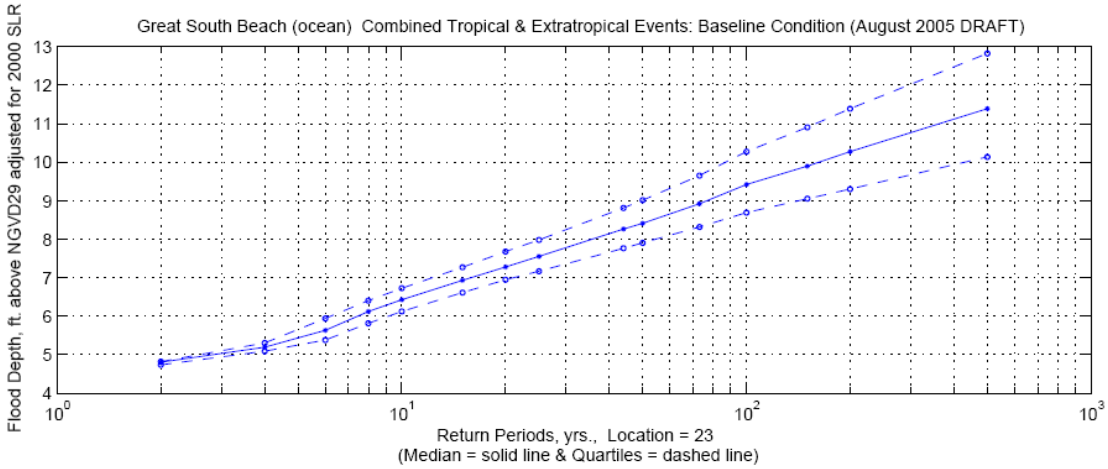

Figure 12-3. Combined stage-frequency curve for Station 23, Great South Beach. Peak water level is adjusted to sea level rise in 2000.

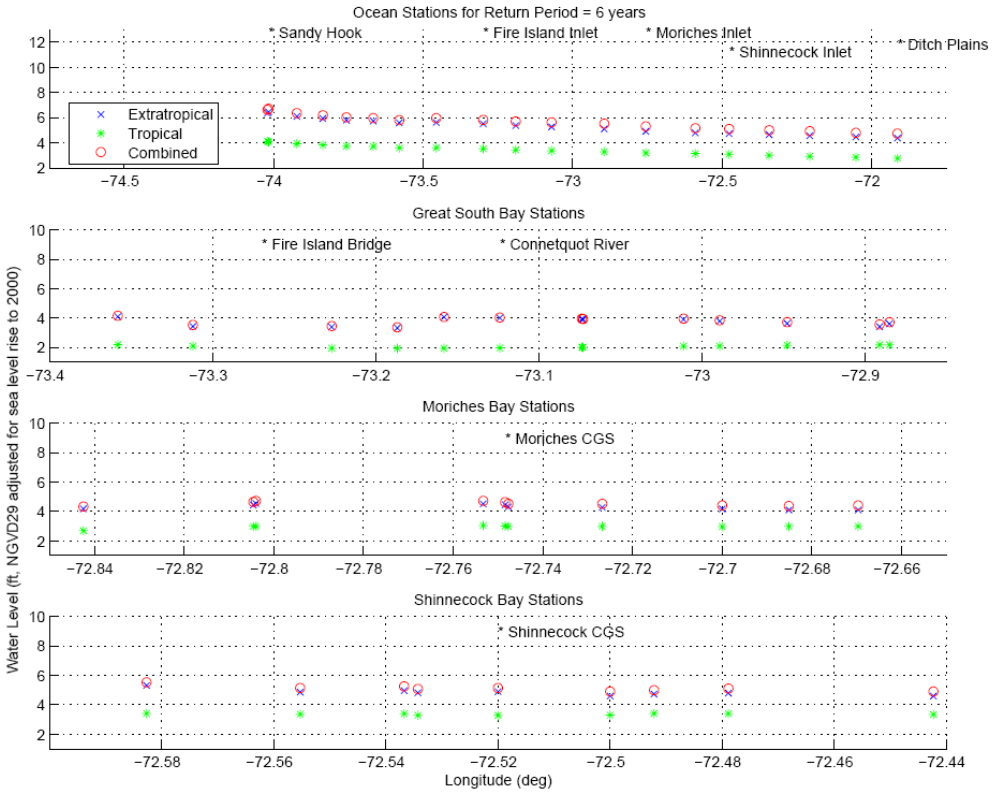

Figure 12-4. Spatial distribution of 6-year return period peak water levels.

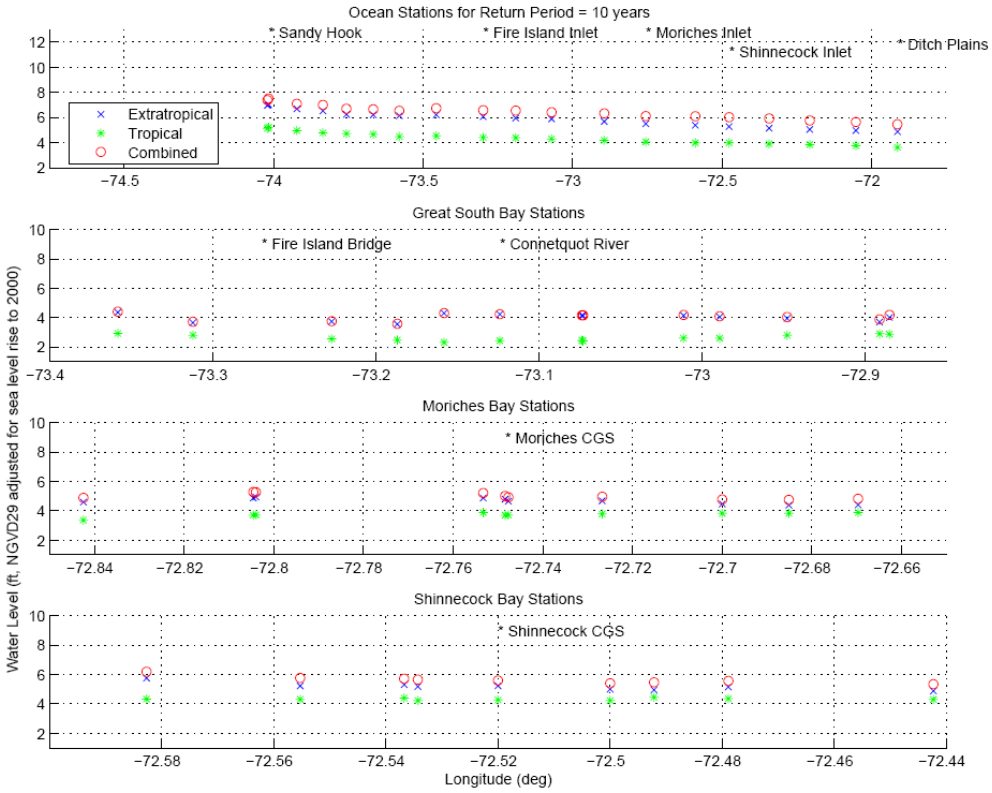

Figure 12-5. Spatial distribution of 10-year return period peak water levels.

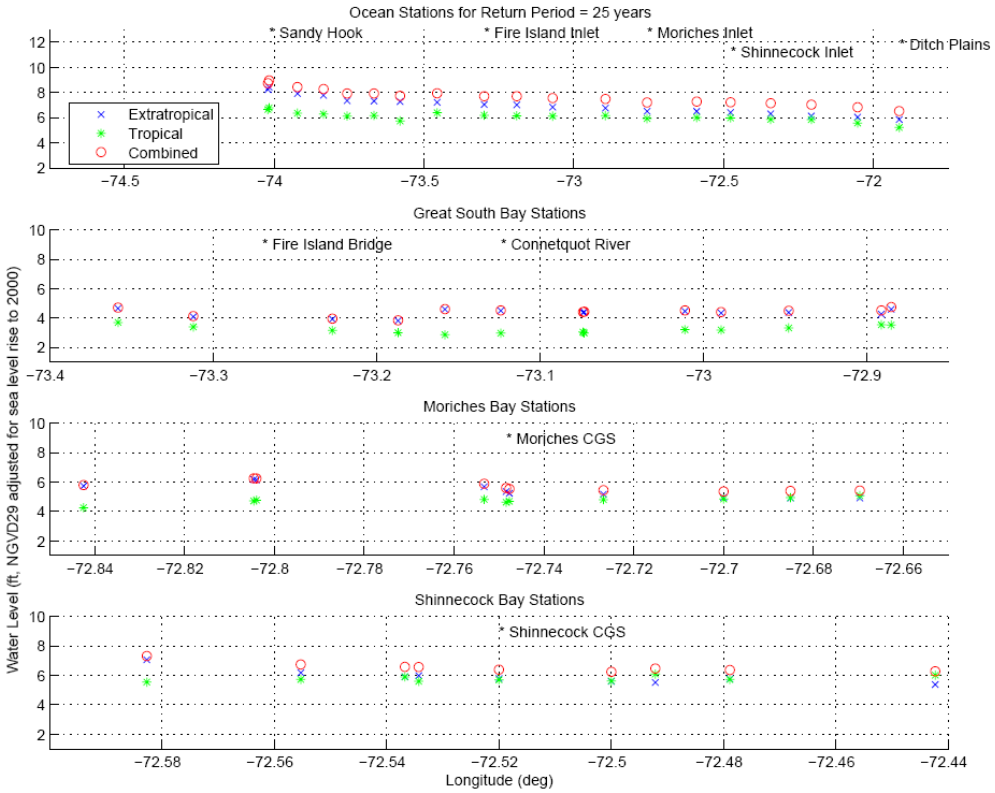

Figure 12-6. Spatial distribution of 25-year return period peak water levels.

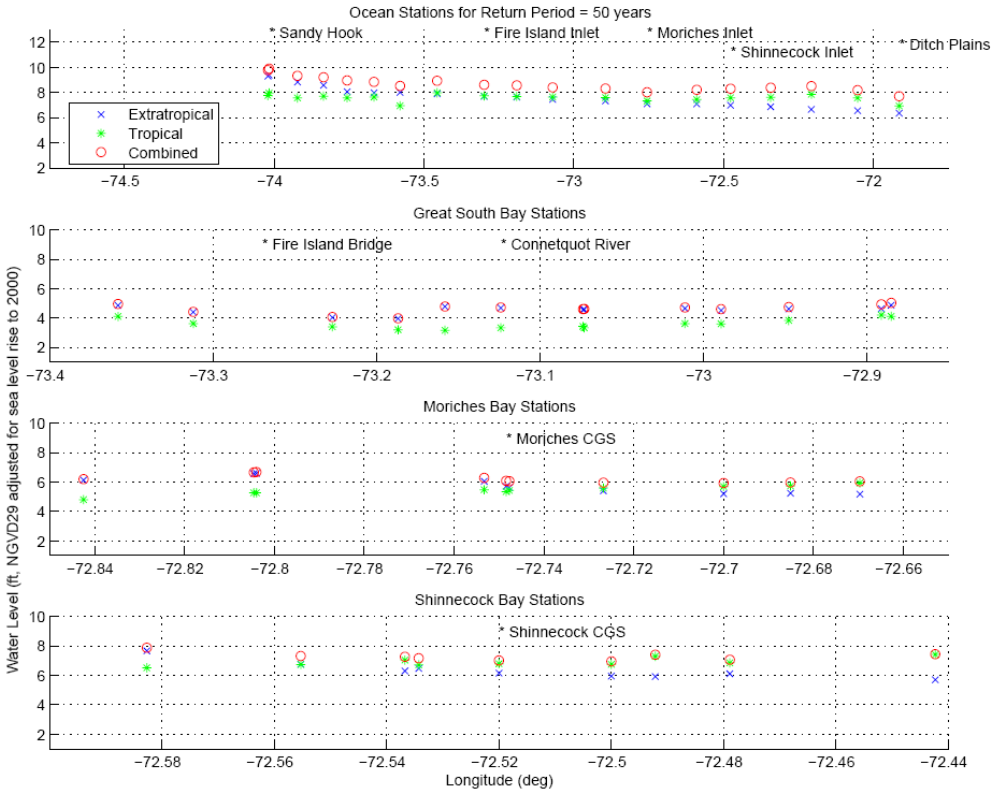

Figure 12-7. Spatial distribution of 50-year return period peak water levels.

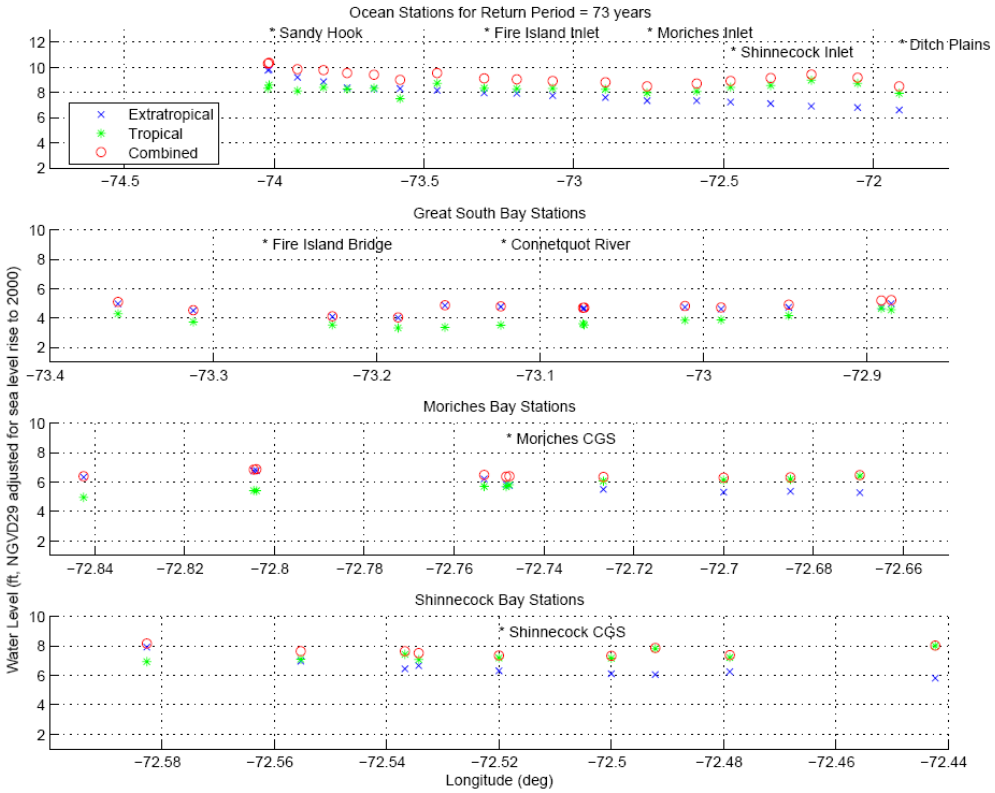

Figure 12-8. Spatial distribution of 73-year return period peak water levels.

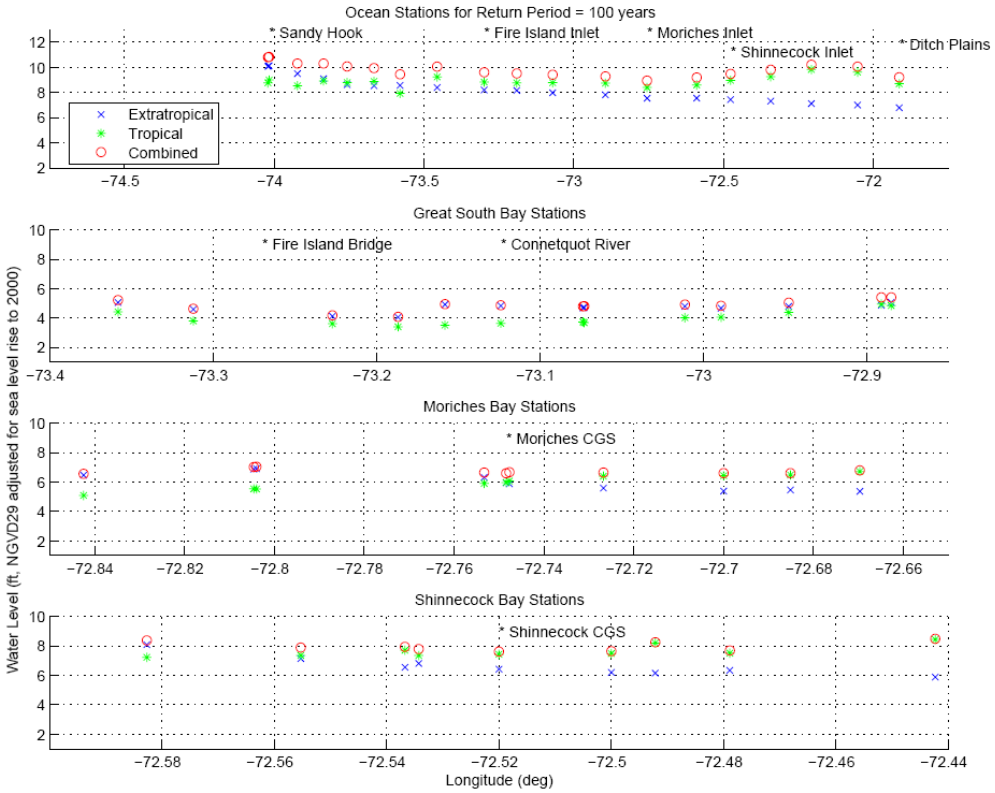

Figure 12-9. Spatial distribution of 100-year return period peak water levels.

13. Past Storm Surge Modeling Studies and Comparisons with Current Work

Since the early 1980's, three main iterations of storm surge modeling were undertaken for the study area: the 1980's study using WIFM (Butler and Prater, 1983); the mid-1990's study using ADCIRC (Scheffner and Wise, 2001); and the current study using a combination of ADCIRC, Delft3D, and SBEACH. Methodology and calibration highlights for the three modeling efforts are summarized in Table 13-1 and Table 13-2. The following section describes known details of the 1980s WIFM study.

13.1 WIFM Study

Unfortunately, only limited documentation is available on the storm surge modeling study employing WIFM (**W**aterways Experiment Station **I**mplicit **F**looding **M**odel). The following is a list of draft documents available:

- Butler, L. E. and M. D. Prater, 1983. "Fire Island to Montauk Point storm surge study," Draft Report, US Army Waterways Experiment Station.
- Prater, M. D., 13 February 1985, "Global stage frequency curves for the Fire Island to Montauk Point storm surge study," Memorandum for Record, US Army Waterways Experiment Station.
- Prater, M. D., 18 February 1985, "Revised results of the nearshore phase of the Fire Island to Montauk Point storm surge study," Memorandum for Record, US Army Waterways Experiment Station.
- Prater, M. D., 19 February 1985, "Revised results of the nonovertopping barrier alternative for the Fire Island to Montauk Point storm surge study," Memorandum for Record, US Army Waterways Experiment Station.
- Prater, M. D., 6 May 1985, "Assorted results, summaries, and responses for the Fire Island to Montauk Point storm surge study," Memorandum for Record, US Army Waterways Experiment Station.

The Butler and Prater (1983) draft report details calibration and setup of WIFM for use in simulating ocean and bay storm water levels for FIMP. WIFM, a finite-difference model that solves the vertically integrated momentum and continuity equations, was the USACE-accepted coastal hydrodynamic model up until the USACE replaced it with the more advanced ADCIRC coastal hydrodynamic model. WIFM has been used to simulate water levels associated with astronomical tides and storm surge. For the 1980's FIMP study, a nested grid approach was adopted using a global grid extending south to Delaware and east past Cape Cod, Connecticut and a nearshore grid spanning from Jones Inlet to Montauk Point.

Barrier island breaching was treated using a simple, deterministic method. This approach accounted for wave effects (setup and runup) following methods outlined in the 1977 Shore Protection Manual (SPM). It should be noted that the 1977 SPM methods have

since been replaced with updated methods based on coastal research advancements over the last few decades (CEM, 2002). Barrier island breaching was activated when the total water level at the shoreline exceeded the dune elevation The total water level was computed as the sum of wave effects using the SPM (1977) methods and WIFM-simulated water level. Under these conditions, the barrier island was lowered at a rate of 10 ft/hr (3.1 m/hr) to a pre-determined post-storm level. The Butler and Prater (1983) report states, however, that "the lowering rate doesn't appear to be critical." Barrier island baseline conditions for WIFM production simulations were based on barrier island conditions in 1979 (sometimes referred to as 1981).

13.1.1 WIFM Model Calibration

WIFM was calibrated for astronomical tide from the M2 constituent only. Adjustments were made to the M2 boundary forcing (based on Swanson, 1976) as well as the friction coefficient to match NOAA water level measurements within the FIMP study area.

Storm surge calibration was performed using historical storm wind speed, wind direction, and atmospheric pressure computed with unknown (not specified in Butler and Prater, 1983) meteorological models for extratropical events and the Standard Project Hurricane (SPH; NOAA TR NWS 23) for tropical events. The following five storms were used for calibration: November 1950, March 1962, September 1938, August 1954 (Carol), and August 1960 (Donna). However, Butler and Prater (1983) stated that, for the 1938 hurricane "numerous [SPH] simulations were made before a track and other storm parameters were accepted" because of unreliability in hurricane forcing parameters for this event.

Storm surge calibration was first performed to match NOAA water level measurements at Sandy Hook, NJ; The Battery, NY; Willets Point, NY; Montauk, NY; New London, CT; and Montauk, NY, as measurements were available. Time series and peak water level comparisons are reasonable for most storms, and it appears that a thorough comparison with available data was performed.

For the calibration events, WIFM-simulated bay peak water levels were compared with flood marks. To produce a reasonable match with observed flood marks, Butler and Prater (1983) state that the WIFM peak water levels were adjusted for wave effects. This was accomplished using highly simplified methods given by the National Academy of Sciences Panel (1977) to include "wave setup and 7/10 of the peak wave height." This additional wave effects amount added to the WIFM result is on the order of 1 to 4 ft (0.3 to 1.2 m). Regarding these wave effects computations, Butler and Prater (1983) state, "we must keep in mind the effect of the considerable uncertainty involved in the basic data being used… on the resulting estimate of wave height, no matter how rigorously computed."

Table 13-1: History of FIMP storm surge modeling for stage-frequency development – methodology.

	WIFM (Butler and Prater, 1983) (1980s) *not published*	**ADCIRC (Scheffner and Wise, 2001) (1995-2001) *not published***	**ADCIRC/SBEACH/ DELFT3D (2002-2004)**
Astronomical Tide	• Boundary forcing condition for M2 tidal constituent only developed during tidal calibration.	• LeProvost database. • 1 constituent (M2 only).	• ADCIRC East Coast 2001 database. • 7 constituents.
Wind and Barometric Pressure	• Parametric mathematical model by Reid et al. (1977) for tropical wind and pressure. • WIS data (1956-1975) for extratropical storms.	• Planetary Boundary Layer (PBL) model for tropical wind and pressure. • FLEET forecast for extratropical wind (NOTE: barometric pressure was not included).	• Improved PBL with refined input hurricane parameter set. • Kinematic reanalysis assimilation (using measured data) for wind and NCEP for pressure.
Offshore Waves	• Not used.	• Not used.	• WISWAVE wave generation model applied using wind fields for each storm.
Ocean Water Levels	• WIFM (USACE model now superceded by ADCIRC).	• ADCIRC.	• ADCIRC, with improved wind stress calculation.
Nearshore Waves	• Calculation based on Shore Protection Manual (USACE, 1977) applied within WIFM.	• Calculation based on Shore Protection Manual (USACE, 1984) applied within ADCIRC.	• DELFT3D-WAVE (HISWA) wave propagation model using WISWAVE results (integrated with hydrodynamic and morphologic models).
Dune Lowering (prior to inundation[11])	• Barrier island lowered 10 ft/hour in WIFM when total water level (surge + tide + wave setup + runup) exceeded dune elevation.	• Not included.	• SBEACH morphological model using ADCIRC water level and WISWAVE wave conditions.
Overwash and Breaching (after inundation)	• Barrier island lowered 10 ft/hour in WIFM when total water level (surge + tide + wave setup + runup) exceeded dune elevation.	• Ackers and White (1973) calculation applied within ADCIRC without sand conservation.	• DELFT3D-MOR sediment transport model based on van Rijn (1993) (integrated with hydrodynamic and wave models).

[11] For this study, inundation is defined as: (surge + tide + wave setup) > dune elevation.

	WIFM (Butler and Prater, 1983) (1980s) *not published*	**ADCIRC (Scheffner and Wise, 2001) (1995-2001) *not published***	**ADCIRC/SBEACH/ DELFT3D (2002-2004)**
Inlet and Bay Water Levels	• WIFM (USACE model now superceded by ADCIRC).	• ADCIRC without advection terms to save computational time.	• ADCIRC and DELFT3D-FLOW with 1) advection terms to adequately model conditions at inlets and into bays and 2) improved wind stress calculation. • Improved resolution at inlets. • Ocean wave setup allowed to propagate through inlets and into bays.
Bay Wave Setup	• Calculation based on Shore Protection Manual (USACE, 1977).	• Calculation based on Shore Protection Manual (USACE, 1984).	• SWAN wave generation model using wind fields for each storm.
Baseline Conditions	• Topometrics survey (1979?) and 1979 beach profiles.	• Based on best available topography and bathymetry in 1995 (barrier island described by 1995 topography from aerial photographs).	• Based on best available topography and bathymetry in 2001 (barrier island described by 2000 lidar topography).
Storm Set	• Tropical: 54 hypothetical events based on the Standard Project Hurricane. • Extratropical: unknown.	• Tropical: 16 historical events plus 4 hypothetical events created by varying storm track and storm radius-to-maximum-wind. Astronomical tide variation was addressed by simulating 4 discrete tide phases for each historical storm (M2 tide only). • Extratropical: 9 historical events (period limited by availability of FLEET forecast information).	• Tropical: 14 historical events between 1935 and 2001 plus 6720 additional variations (by linear superposition) of each historical storm to reliably account for astronomical tide variation. • Extratropical: 22 historical extratropical events between 1950 and 2001 plus 6720 additional variations (by linear superposition) of historical storms to reliably account for astronomical tide variation.
Stage-Frequency	• Joint probability method.	• Multivariate EST (initially developed for Panama City, FL).	• Improved Univariate EST methodology with updated tail fitting algorithm. Method improvements include rigorous approach for including astronomical tide variation.

Table 13-2: History of FIMP storm surge modeling for stage-frequency development measurement, calibration, and comparison.

	WIFM (Butler and Prater, 1983) (1980s) *not published*	**ADCIRC (Scheffner and Wise, 2001) (1995-2001) *not published***	**ADCIRC/SBEACH/ DELFT3D (2002-2004)**
Tidal Calibration	• Calibrated to match M2 tidal constituent at 5 NOAA measurement stations. • Calibrated to match M2 tidal constituent at 8 measurement locations from the 1980s. • Calibrated to match peak ebb and flood currents at 7 measurement locations.	• No ocean calibration; however, FIMP grid based on Atlantic Ocean ADCIRC grid. • Calibrated to match M2 tidal constituent at 8 measurement locations from the 1980s (Butler and Prater (1983)).	• Calibrated for ocean tide at 4 NOAA measurement stations, east and west of project area, to match time series and 7 tidal constituents. • Calibrated for bay tide at 16 measurement stations (LISHORE (1998-present), USGS (1997-present), and USACE (spring 2003)) to match time series and 7 tidal constituents. • Simulated tidal inlet flow compared with ADCP measurements (2003) at Fire Island, Moriches, and Shinnecock inlets.
Ocean Surge Calibration	• Calibrated at NOAA measurement stations for five historical hurricanes and Nor'easters.	• Tuned PBL input parameters for some tropical events to match peak water level at 2 NOAA measurement stations, both west of project area. • No calibration for extratropical events.	• Calibrated at 4 NOAA measurement stations, east and west of project area, using 6 tropical and 6 extratropical events to match time series and peak water level.
Bay Surge Comparisons	• Calibrated peak water level (surge plus tide) with observed watermarks (debris line) reported in TMI (1982)[12] for September 1938 hurricane (compared to TMI water marks for remaining 4 storms).	• Compared peak water level (surge plus tide) with observed watermarks (debris line) reported in TMI (1982) and with Butler and Prater (1983) results.	• Compared time series and peak water level at 6 measurement locations for the February 2003 blizzard.

[12] The uncertainty associated with the high water marks reported in the TMI (1982) report is large.

	WIFM (Butler and Prater, 1983) (1980s) *not published*	ADCIRC (Scheffner and Wise, 2001) (1995-2001) *not published*	ADCIRC/SBEACH/ DELFT3D (2002-2004)
Breaching and Overwash Comparisons	• Dune lowering and breaching algorithm calibrated to qualitatively match breaching and overwash reported for the September 1938 hurricane.	• Breaching and overwash simulations using Baseline Conditions topography qualitatively compared with historical information on breaching (BCP, 1995) to assess overall amount of breaching and overwash.	• Calibrated breaching model to available laboratory and field data. Simulated breaching and overwash for September 1938 Hurricane, March 1962 Nor'easter, and December 1992 Nor'easter using historical condition topography. Results qualitatively compared with post-storm photography at specific overwash and breaching locations.
Stage-Frequency Comparisons	• N/A	• Compared with WIFM (1985) results.	• Compared with relationships developed from the long-term measured peak water level record at the Sandy Hook NOAA measurement station.

13.1.2 WIFM Production Simulations for Stage-Frequency Development

Storm forcing, both wind stress and barometric pressure, for these production WIFM simulations for use in stage-frequency analysis was provided using the SPH criteria (NOAA TR NWS 23) for tropical storms and with WIS wind fields for extratropical storms. Nothing specific is provided in any of the documents that indicate what storms were simulated, and how probabilities were assigned, for extratropical events. The USACE speculates that all relevant extratropical events covered by the WIS database available in 1983, namely storms between 1956-1975, were simulated and that probabilities were assigned using extreme-value statistical methods.

For tropical events, the Joint Probability Method (JPM) was applied to generate final stage-frequency relationships. Use of the JPM requires assigning probability distribution to storm parameters, such as central pressure deficit and forward speed. Therefore, no historical tropical events were considered for stage-frequency development during WIFM study. Instead, a series of hypothetical storms were simulated following standard practices in the 1980s. The hurricane parameters for these storms were based on SPH criteria, and are listed in Table 13-3 and result in 18 different storm parameter combinations. Documents state that 3 sets of 18[13] hypothetical storms using these hurricane parameters were simulated with WIFM, totaling 54 separate storm simulations. From this statement, the USACE believes that 3 different track approaches were considered. However, no documentation is available to state specifics on these tracks, other than they approach from 180° N.

Each of the 54 storm simulations was assigned a probability based on the distributions listed in Table 13-4. For discussion herein, these storm classifications are labeled M1 through S3 where M and S indicates moderate and severe intensity, respectively, based on central pressure deficit, and 1 through 3 indicate forward speed of the storm, where 1 is the worst case being the slowest moving storm. With this classification, S1 is the worst storm scenario in terms of intensity and forward speed. Note that probabilities are distributed between the Moderate category and Severe category separately such that each totals one. None of the documentation states how the Moderate and Severe categories were weighted relative to each other for stage-frequency development. Further, this weighting cannot be deduced from the information given.

Of the 54 storms simulated, 9 storms fall into the S1 category, assigned a 0.0 probability of occurring. Rather than omitting these storms from the final stage-frequency analyses, storm parameters were adjusted so that these high-water level events could be included. The 18 February 1985 MFR states:

> "a total of 9 storms had pressure deficits greater than 2 inches Hg and had forward speeds of 12 knots. Since this combination is given no probability of occurring, the information gained throughout the simulation

[13] The 18 February 1985 MFR states "3 sets of 17", but based on information in other MFRs, the Engineering Division New York District believes this is a typographic error and should read "3 sets of 18 storms."

Table 13-3: WIFM hypothetical storm parameters (based on 19February 1985 MFR).

Hurricane Parameter	SPH	1980s WIFM Study		
Pressure Deficit (in of Hg)	1.88	1.7	2.1	2.3
Forward Speed (knots)	16-52	12	19	27
Radius to Maximum Winds (nmi)	15-39	20	36	
Angle of Approach (degrees)	73-200	180		

Table 13-4: Assigned (from 6 May 1985 MFR) and historical probabilities.

	Forward Speed (knots)	Pressure Deficit (in of Hg)	Assigned Probability (WIFM)	# Historical Events (1930 – 2001)	Probability Computed from Historical Record
M1	12	≤ 2.1[14]	0.10	3	0.23
M2	19	≤ 2.1	0.45	8	0.62
M3	27	≤ 2.1	0.45	2	0.15
S1	12	> 2.1	0.00	0	0.00
S2	19	> 2.1	0.10	0	0.00
S3	27	> 2.1	0.90	1	1.00

Table 13-5: Historical storm classification based on WIFM criteria.

Storm Name	Classification
1938	S3
1944	M2
Carol (Aug 1954)	M1
Edna (Sep 1954)	M2
Hazel (Oct 1954)	M3
Connie (Aug 1955)	M1
Donna (1960)	M3
Esther (1961)	M1
Doria (1971)	M2
Agnes (1972)	M2
Belle (1976)	M2
Gloria (1985)	M2
Bob (1991)	M2
Floyd (1999)	M2

Table 13-6: WIFM design storm parameters (from Butler and Prater, 1983).

Storm	Maximum Wind Speed (knots)	Forward Speed (knots)	Radius to Maximum Winds (nmi)	Pressure Deficit (in of Hg)
1938 Hurricane	70	42	50	2.13
Design Storm	97	42	50	2.78
1979 SPH	83-97	10-53	13-39	1.89

[14] Based on other comments made in the 18 February 1985 MFR, the Engineering Division New York District believes this cutoff limit is 2.1 in Hg, rather than 2 in Hg as stated in the 18 February 1985 MFR.

> of such a storm is of no value when creating a stage frequency curve. To correct this, nine additional storm events were chosen as replacements. Each new storm produces approximately the same water level along the coast as the event it replaces. Therefore, the same number of storm event simulations were involved in the creation of the stage-frequency results…"

In the documentation, there is no mention of the hurricane parameters that characterize these replacement storms. The logical interpretation of the above statement is that the replacement storms account for water levels larger than the assumed hurricane parameter probability distribution allows. This will result in larger return-period water levels.

To assess the reliability of the probability distributions used during the WIFM study, all tropical events between 1930 and 2001 in NHC's HURDAT database that effected Long Island were analyzed to extract the maximum central pressure deficit and minimum forward hurricane speed for this comparison. Based on these values, each historical tropical storm was assigned a category, M1 through S3 (Table 13-5). As the table indicates, only one storm is classified in the Severe category, September 1938, and being a fast-moving storm, it is in the weakest of the three Severe categories. The remainder of these historical events fall into the three Moderate categories. This indicates that the assumed probability distribution used for the WIFM study does not adequately reflect today's historical record. The historical probability distribution is presented in Table 13-4. First, a substantial percentage (documentation indicates 35-50%) of the simulated storms fall into the Severe category in the WIFM study. In contrast, the historical data indicate that less than 10% of the storms impacting Long Island have been classified as Severe. Second, the historical storm distribution within the Moderate category shows more than 60% of the probability going to the middle M2 category with M1 and M3 each having about 20% of the probability. In contrast, the WIFM distribution equally distributes 90% of the probability between the M2 and M3 categories. While it is not known how the moderate and severe categories were weighted relative to each other, it is clear that the probability distribution assumed for each category in the 1980s study does not reflect the current-day historical storm probability distribution.

It should also be noted that Butler and Prater (1983) also present a design storm that was used to evaluate with- and without- "hi-level barriers". Butler and Prater (1983) state that "the design storm was based on a transposed track of the hurricane of 1944 with a wind pattern similar to that of the 1938 storm." Table 13-6 present the hurricane parameters used in WIFM for this design storm. Based on available documentation, it appears that this storm was only used to evaluate design alternatives and was not used to develop stage-frequency relationships. In fact, the 6 May 1985 MFR states that this design storm "produced water levels beyond any meaningful stage-frequency analysis." The selected design storm does, however, demonstrate the relative intensity of hypothetical storms considered for the 1980s investigations.

In conclusion, the WIMF hydrodynamic model appears to be well calibrated for ocean surge; however, the wave calculations and breaching mechanism are simplified. More

importantly, no historical tropical storms were used to develop the stage-frequency relationships based on the current historical record. Instead hypothetical storms, that do not appear to follow the historical distribution, were used. Further, severe high water level events that are unlikely to occur within the project area, were included in stage-frequency development.

A thorough investigation into the WIFM study, method, and results was beyond the scope of this study. A rigorous investigation into the 1980s WIFM study could further clarify the relative accuracy and identify other study components that impact the stage-frequency results.

13.2 Stage-Frequency Comparisons with the WIFM Study

In general, the current study employs more advanced numerical models that include wave effects and morphological response in an integrated manner. This study is also based on improved storm wind and pressure fields, an improved tidal database, an expanded historical storm set, improved stage-frequency methodology, and rigorous calibration and comparison with measured data. Figure 13-1 through Figure 13-15 present comparisons between the newly developed stage-frequency relationships and those from the 1980s WIFM study.

At Sandy Hook, the NOAA measured annual maximum and peaks-over-threshold relationships, as discussed in Chapter 11, are again presented for comparison (Figure 13-1 and Figure 13-2). Both the new relationship and the WIFM relationship for extratropical events follow the measured data within the range of measured data, (return periods less than 50 years). The new extratropical curve lies above the NOAA data between the 20-year and 500-year return periods. This is likely attributed to the incorporation of alternate tide scenarios, as discussed in Chapter 10. The WIFM extratropical curve deviates from the new curve in this region as well. However, the WIFM curve approaches the new curve again beyond the 100-year return period. Difference between the two extratropical curves varies from 0.5 ft to 2.0 ft.

The tropical curves at Sandy Hook show that the WIFM result is on average 2 ft higher than the new result. However, the WIFM curve does not match the measured peak-over-threshold curve derived from the NOAA gage data. For all return periods, the WIFM result shows a higher water level than that observed. In contrast, the curve developed with EST in this study matches the NOAA curve well within the range of return periods represented by the gage data. The differences between the WIFM curve and the NOAA curve are most likely attributed to the statistical approach adopted for the WIFM study, namely the use of the Standard Project Hurricane and an assumed tropical storm probability distribution. It is interesting to note, however, that both the WIFM curve and the new curve, developed using EST, display similar characteristics, particularly in slope, in the upper tail extrapolation.

The WIFM combined curve at Sandy Hook (Figure 13-3), dominated by the tropical relationship, is slightly higher than the new curve, which is dominated by the

extratropical relationship. The differences between the curves are less than 0.5 ft for return periods less than 100 years.

The draft combined stage-frequency relationship for Sandy Hook developed in the mid-1990s for FIMP is also presented in Figure 13-3. The mid-1990s study combined curve displays a more curved shape. The mid-1990s curve is on the order of 0.5 ft higher than the new curve for return periods between 5 and 100 years and is nearly 2 ft lower at the 2-year return period. The lower portion of the mid-1990s curve is similar in shape and magnitude to the NOAA peak-over-threshold extratropical relationship (Figure 13-1) indicating that this relationship does not fully capture the effects of smaller annual events.

The comparison between the WIFM and new extratropicals curves begins to deviate more at locations east of Sandy Hook. The largest deviations are observed at the eastern end of the project area, at Napeaque Beach (Figure 13-13). In all cases the new extratropical result is 0.5 ft to 2 ft higher than the WIFM result for return periods greater than 10 years. These differences are most likely attributed to differences in the training sets used in the two studies (20 years for WIFM and 49 years for this study). In particular, the October 1991 storm occurred after the WIFM study was completed and was, therefore, not included. The October 1991 storm is associated with the highest-recorded extratropical storm water level at the Montauk Fort Pond NOAA gage, at the eastern end of Long Island.

The tropical curve comparison between the WIFM and new results are more similar to the east towards Shinnecock Inlet (Figure 13-11), relative to locations to the west (i.e. Sandy Hook). At Shinnecock Inlet, the two relationships are very similar. However, comparisons at more easterly stations begin to deviate again. This time, the new curve shows higher water levels than the WIFM curve for larger return periods. Again, these differences are most likely attributed to the differences in statistical approaches employed in the WIFM study versus those employed for this study.

The WIFM and new study combined curve comparisons display the trends observed in the extratropical and tropical comparisons. The new combined curves are similar in magnitude to the WIFM combined curves for locations between Sandy Hook (Figure 13-3) and Moriches Inlet (Figure 13-9) for return periods below 100 years. Above the 100-year return period, the WIFM curves are slightly higher than the new curves at these locations. East of Moriches Inlet, the WIFM combine curves begin to deviate more from the new combined curves. At Napeaque Beach (Figure 13-15), the combined WIFM curve is between 0.5 ft and 2 ft lower than the new curve between the 10-year and 100-year return periods.

In conclusion, the differences seen in the stage-frequency curves from the WIFM and this study are not surprising, and are expected, given the differences in training sets and statistical approaches. The new curves represent an improvement to previous curves because a longer-duration historical record was available, improved numerical modeling methods were used, and improved statistical approaches were employed.

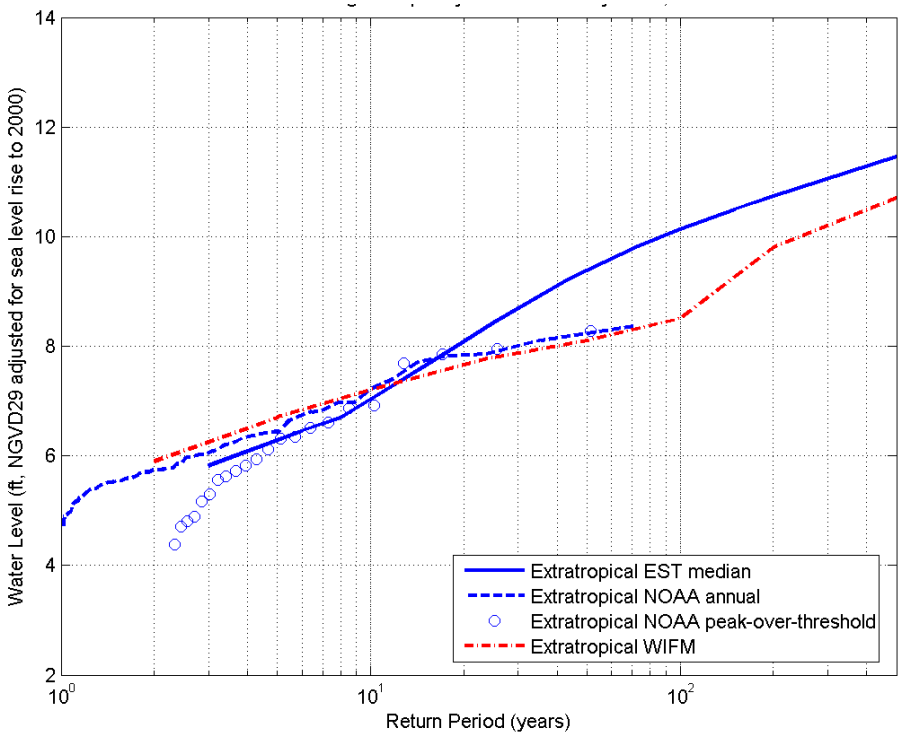

Figure 13-1. Comparison between new, past, and measured extratropical stage-frequency curves at Sandy Hook, NJ (station 67).

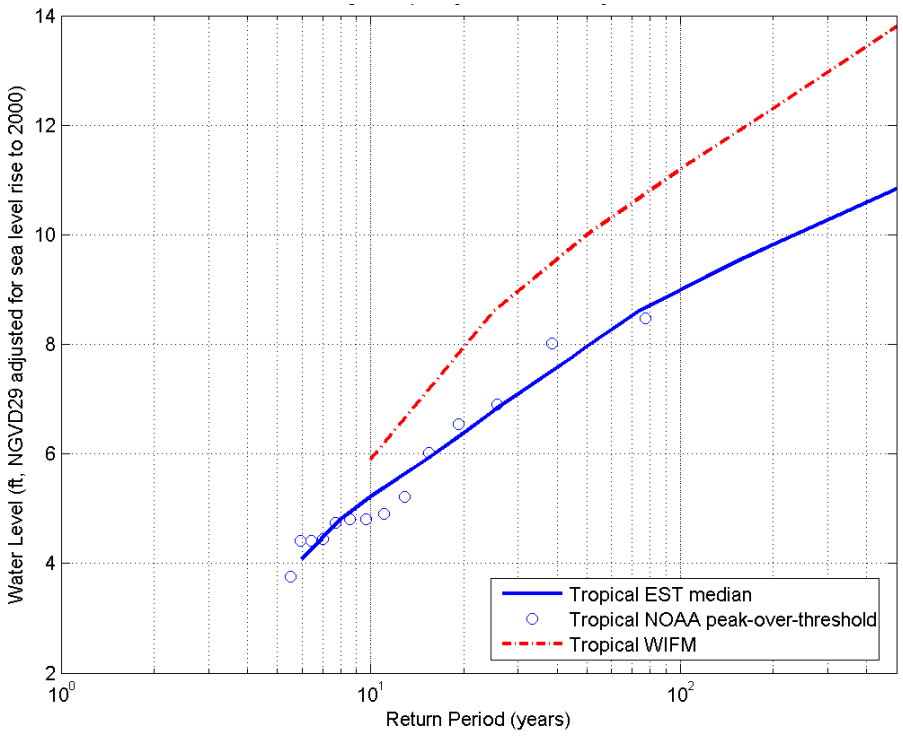

Figure 13-2. Comparison between new, past, and measured tropical stage-frequency curves at Sandy Hook, NJ (station 67).

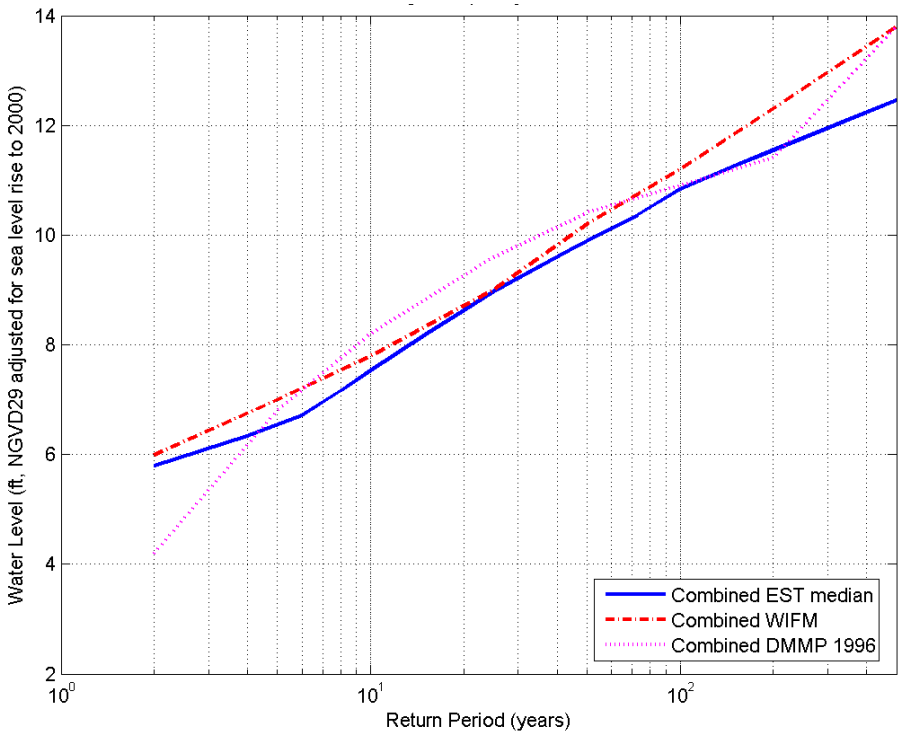

Figure 13-3. Comparison between new and past combined stage-frequency curves at Sandy Hook, NJ (station 67).

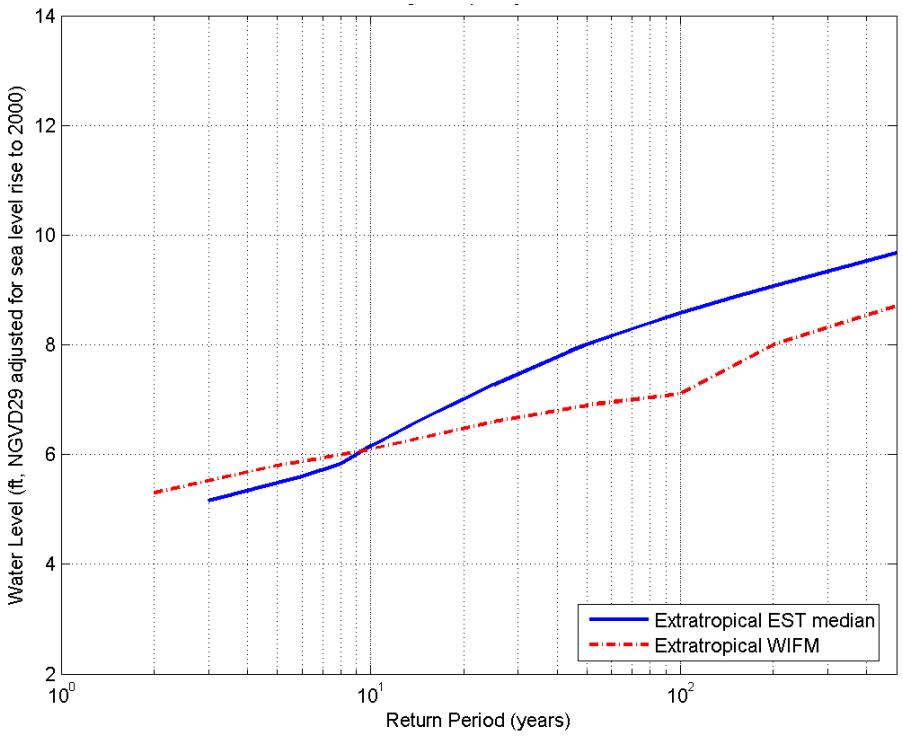

Figure 13-4. Comparison between new and past extratropical stage-frequency curves at Jones Inlet (station 54).

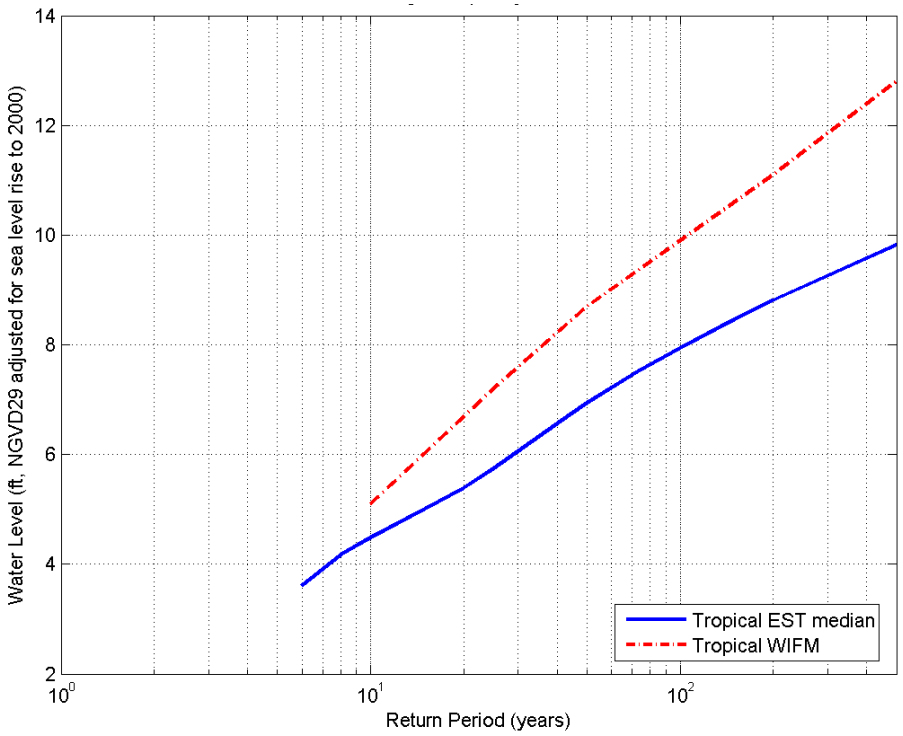

Figure 13-5. Comparison between new and past tropical stage-frequency curves at Jones Inlet (station 54).

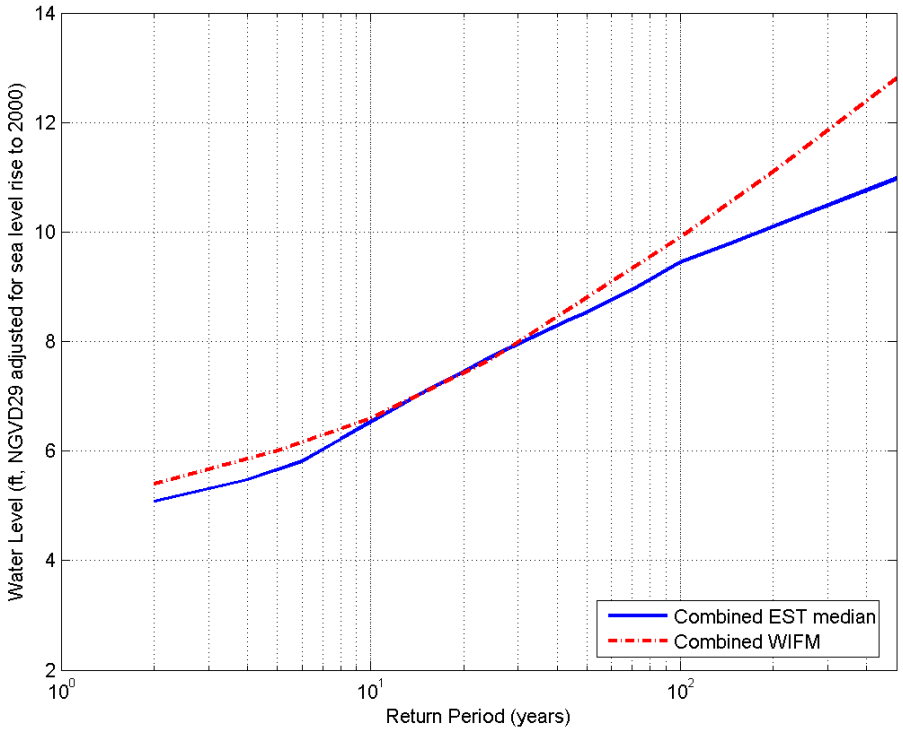

Figure 13-6. Comparison between new and past combined stage-frequency curves at Jones Inlet (station 54).

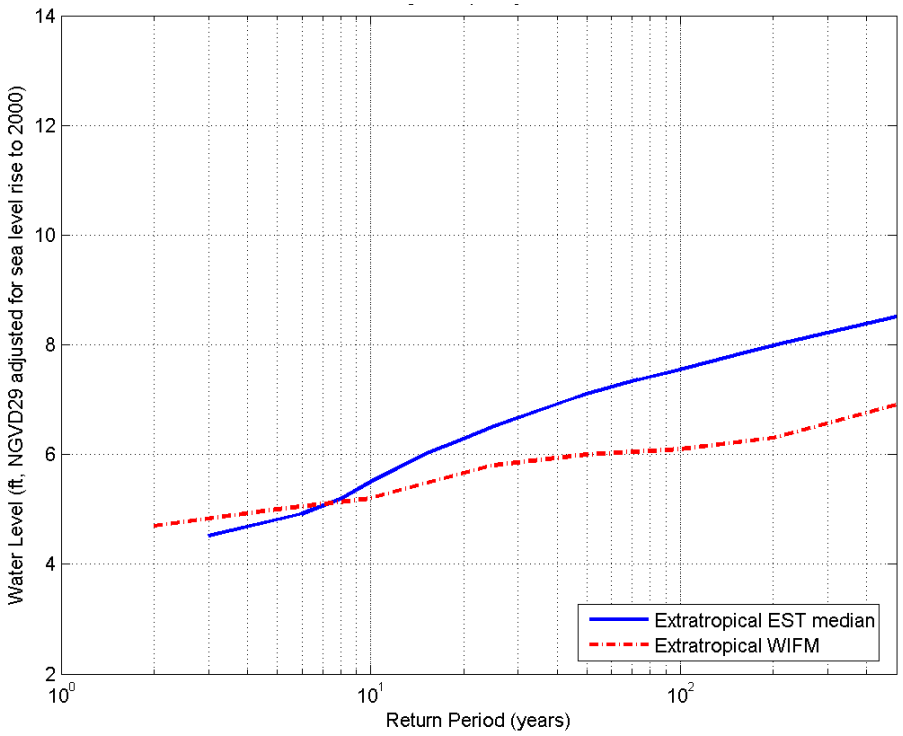

Figure 13-7. Comparison between new and past extratropical stage-frequency curves at Moriches Inlet (station 28).

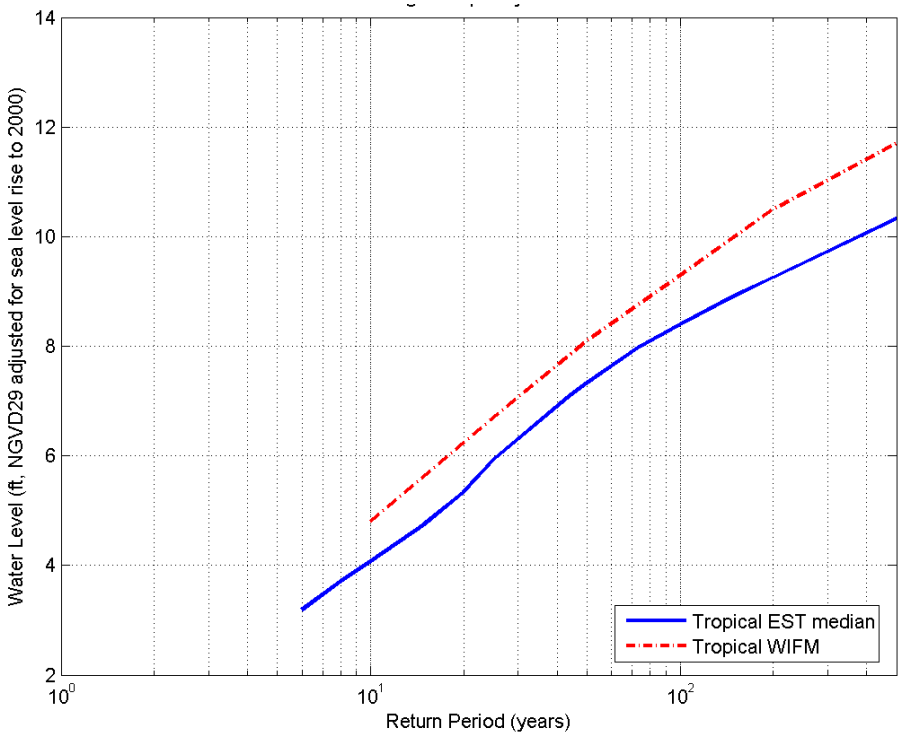

Figure 13-8. Comparison between new and past tropical stage-frequency curves at Moriches Inlet (station 28).

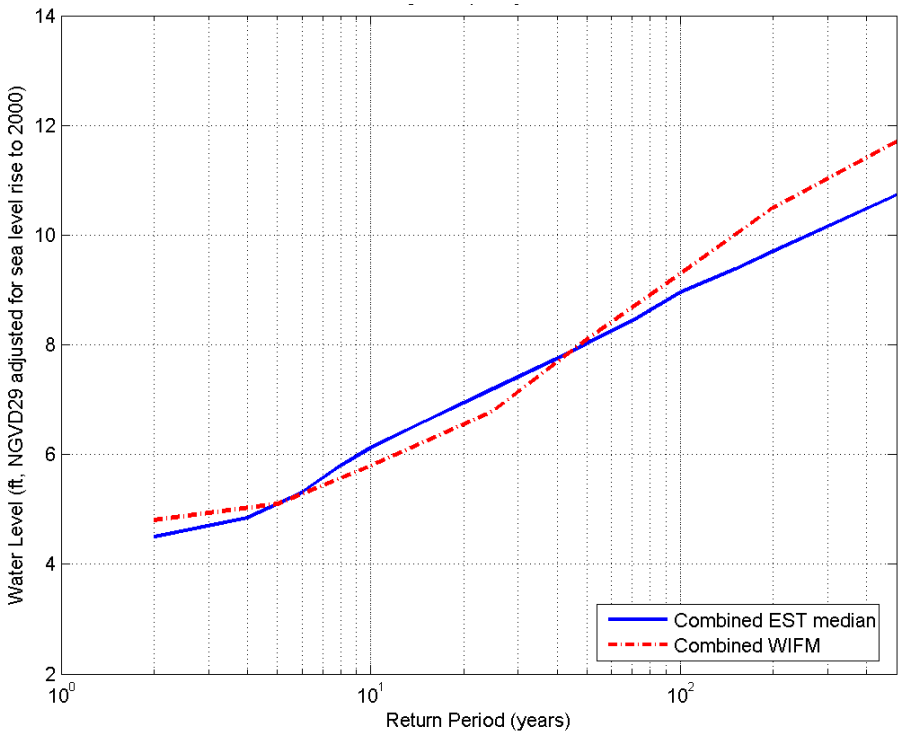

Figure 13-9. Comparison between new and past combined stage-frequency curves at Moriches Inlet (station 28).

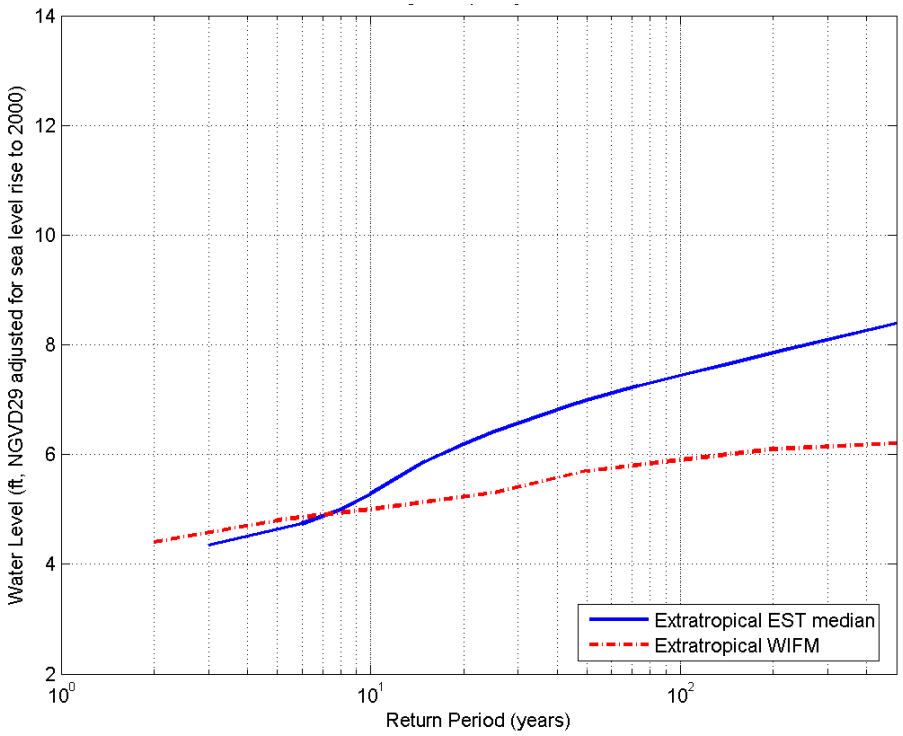

Figure 13-10. Comparison between new and past extratropical stage-frequency curves at Shinnecock Inlet (station 35).

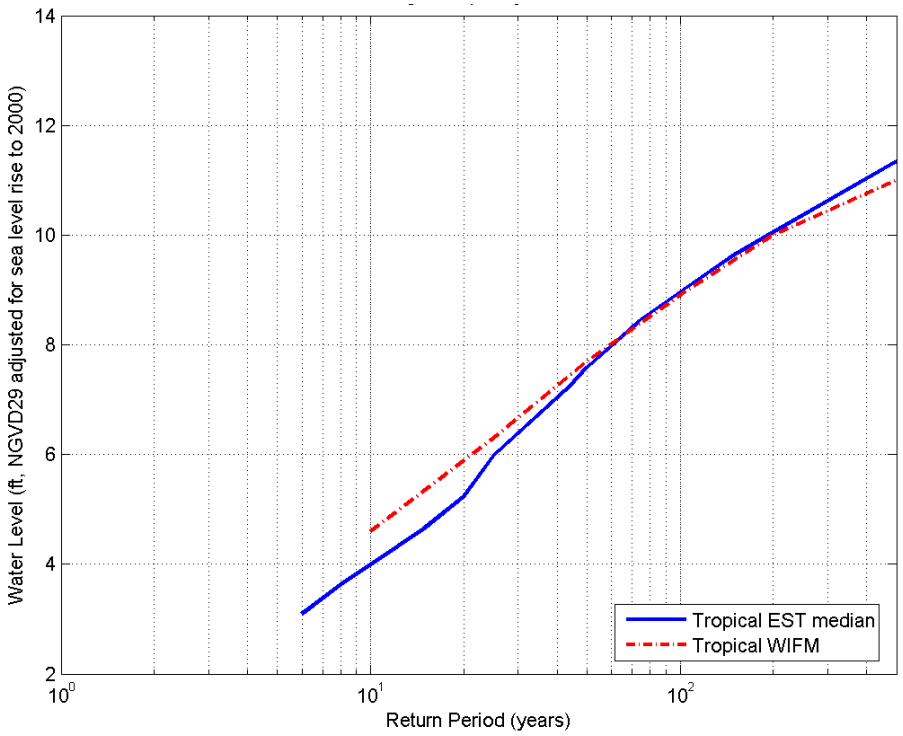

Figure 13-11. Comparison between new and past tropical stage-frequency curves at Shinnecock Inlet (station 35).

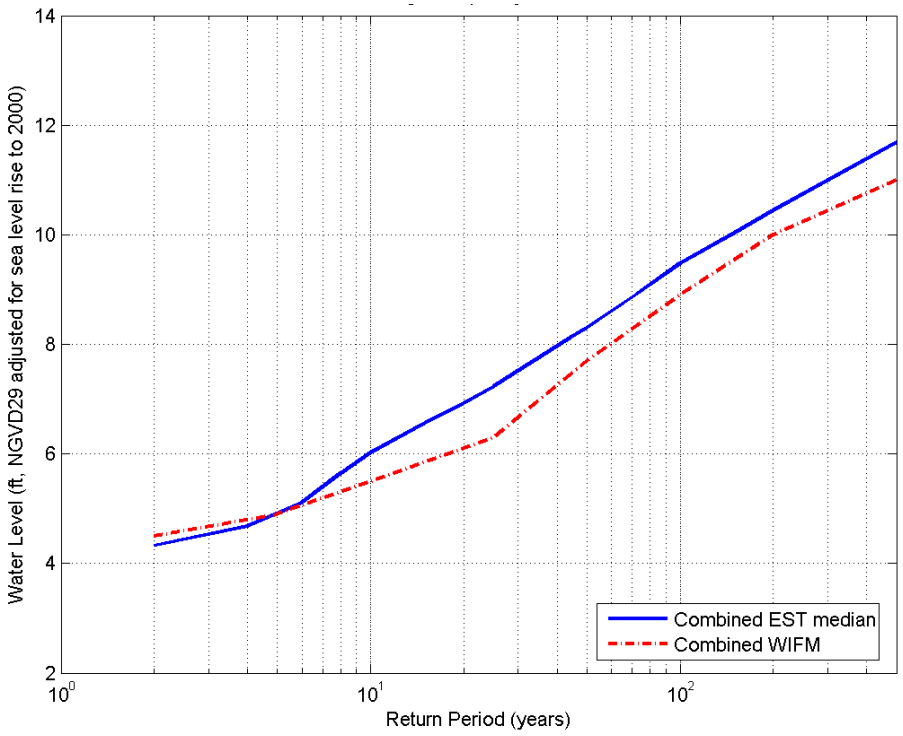

Figure 13-12. Comparison between new and past combined stage-frequency curves at Shinnecock Inlet (station 35).

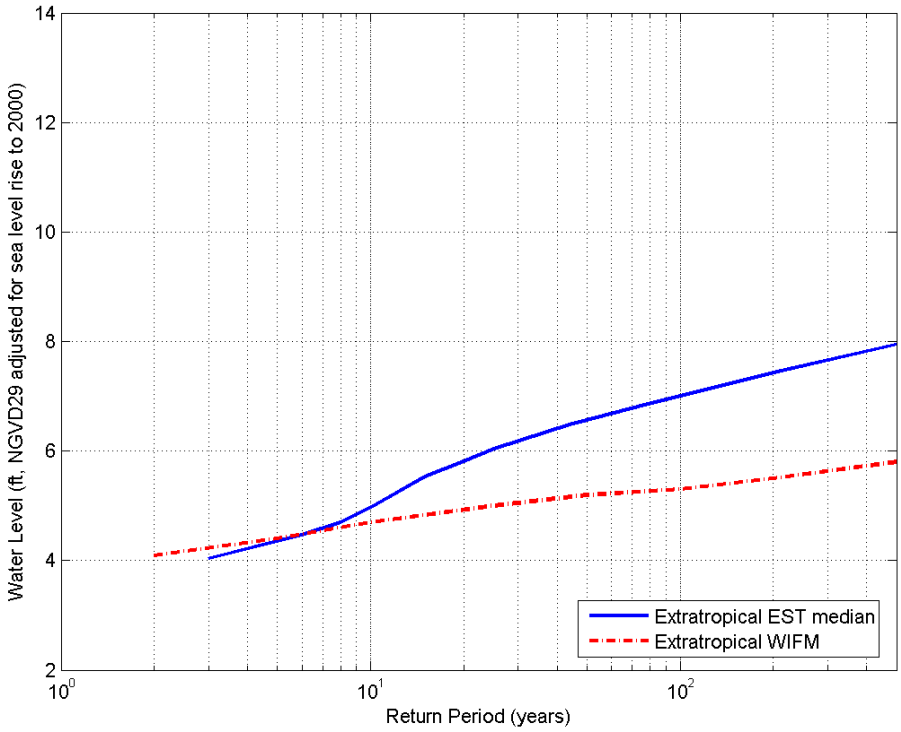

Figure 13-13. Comparison between new and past extratropical stage-frequency curves at Napeaque Beach (station 64).

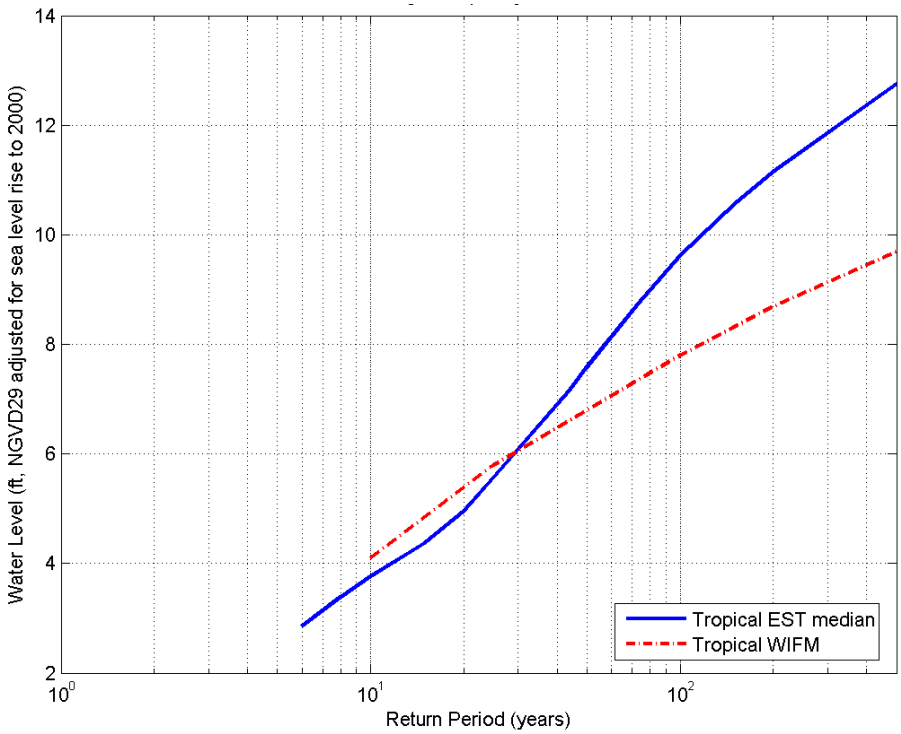

Figure 13-14. Comparison between new and past tropical stage-frequency curves at Napeaque Beach (station 64).

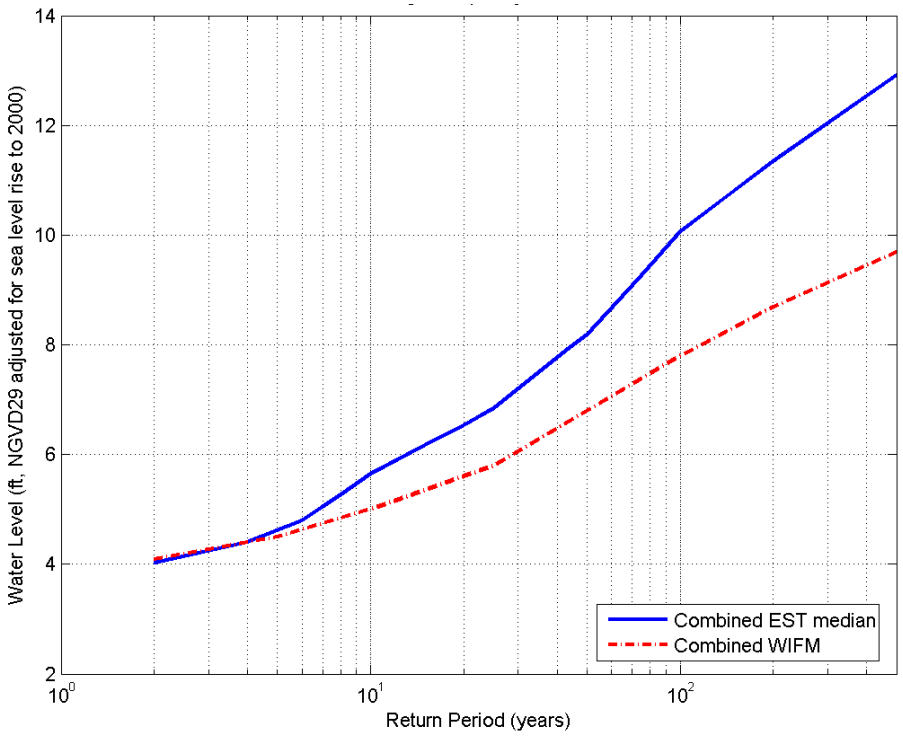

Figure 13-15. Comparison between new and past combined stage-frequency curves at Napeaque Beach (station 64).

14. Conclusions

This report detailed the numerical modeling and statistical approaches used to develop stage-frequency relationships within the FIMP project area. The numerical modeling inputs, numerical modeling tools, and their method of application for this project, are state-of-the-art, and their application here is an improvement over past modeling efforts. These numerical models and their input were tested, calibrated, and validated against all available qualified data with successful results. Furthermore, the modeling approach, EST methods, and a calibration and validation were rigorously checked and endorsed by the Technical Review Panel, led by Dr. Henry Bokuniewicz.

The statistical approach for developing stage-frequency relationship for this study is flexible for all types of probabilistic distributions as it employs nonparametric approaches. Furthermore, the statistical EST method was improved to incorporate, and appropriately weight, the effects of accidental tide phasing with storm surge thus allowing for this probable physical variation and resulting in a smooth water level transition alongshore. Comparisons between the EST-based stage-frequency relationships and measurement-based stage frequency relationships demonstrated that the stage-frequency relationships for this study do represent the historical storm record.

Additional work on the FIMP project included the development of stage-frequency relationships for future with and without project scenarios and for baseline conditions with localized (bay and ocean) wave setup. Additional frequency relationships were developed for morphological storm responses including barrier island breaching, berm recession, dune lowering, and other cross-shore morphological response variables. Results from these additional efforts are summarized in the FIMP Engineering Appendix. These additional numerical modeling and statistical analyses efforts, along with those presented in this report, served as the foundation for all upcoming economic, environmental, planning, and design decisions for the FIMP project.

REFERENCES

Bates, R.L., and Jackson, J.A. (ed) 1987. Glossary of geology, 3rd Ed. American Geological Institute, Alexandria, VA.788p.Cardone, V. J., H. C. Graber, R. E. Jensen, S. Hasselmann, M. J. Caruso, 1995. In search of the true surface wind field in SWADE IOP-1: Ocean wave modelling perspective. The Global Atmosphere and Ocean System, 3, 107-150.Gravens et al., 1999.

Ackers, P., and W. R. White, 1973. Sediment Transport: New Approach and Analysis, Journal of the Hydraulics Division, ASCE, Vol. 99, HY11(2041-2060).

Ang, A., H-S., and W. H. Tang, 1975, Probability concepts in engineering planning and design, John Wiley and Sonds, New York, NY, p.37.

Borgman, 2003. Background and Recommendations: Efficient Selection of Storm Surge Computer Runs to Enhance Empirical Simulation Analysis, Interim Draft report prepared for the U.S. Army Corps of Engineers, New York District.

Butler, H. L. and M. D. Prater, 1983. "Fire Island to Montauk Point storm surge study, interim report," US Army Corps of Engineers, Waterways Experiment Station, Vicksburg, MS.

Cardone, V. J., H. C. Graber, R. E. Jensen, S. Hasselmann, M. J. Caruso. In search of the true surface wind field in SWADE IOP-1: Ocean wave modelling perspective. The Global Atmosphere and Ocean System, 3, 107-150.

Garratt, 1977. Review of drag coefficients over oceans and continents. Monthly Weather Review, 104, 418-442.

Harris, D.L., 1963. Characteristics of the Hurricane Storm Surge, Technical Paper No. 48, United States Weather Bureau, Washington, D.C., 139 p.

Holthuijsen, L.H., Booij, N. and T.H.C Herbers, 1989: A prediction model for stationary, short-crested waves in shallow water with ambient currents. Coastal Engineering, 13, 23-54.

Keulegan, G.H. and Hall, J.V. (1950). "A formula for the calculation of tidal discharge through an inlet," U.S. Army Corps of Engineers, Beach Erosion Board Bulletin, 4, 15-29.

Kraus and Wise, 1993. Simulation of January 4, 1992 Storm Erosion at Ocean City, Maryland, Shore and Beach, 61(1), 34-31.

Larson and Kraus, 1989. SBEACH: Numerical Model for Simulating Storm-Induced Beach Change; Report 1, Empirical Foundation and Model Development. TR CERC-89-9, USACE.

Larson, Kraus, and Byrnes, 1990. SBEACH: Numerical Model for Simulating Storm-Induced Beach Change; Report 2, Numerical Formulation and Model Tests, RT CERC-89-9, USACE.

Leatherman, S.P., 1981. Barrier Beach Development: A Perspective on the Problem. SHORE AND BEACH, V. 49, p. 2-9.

Lillycrop, W. J., Parson, L. E., and Irish, J. L., 1996. Development and operation of the SHOALS airborne lidar hydrographic system, SPIE: Laser Remote Sensing of Natural Waters - From Theory to Practice, 2964(26-37).

Luettich, R.A., Jr., J.J. Westerink, and N.W. Scheffner, 1992, ADCIRC: an advanced three-dimensional circulation model for shelves coasts and estuaries, report 1: theory and methodology of ADCIRC-2DDI and ADCIRC-3DL, Dredging Research Program Technical Report DRP-92-6, U.S. Army Engineers Waterways Experiment Station, Vicksburg, MS, 137p.

Militello, A., and Kraus, N.C.., 2001. Shinnecock Inlet, New York, site investigation, Report 4, Evaluation of Flood and Ebb Shoal Sediment Source Alternatives for the West of Shinnecock Interim Project, New York," Technical Report CHL-98-32, U.S. Army Waterways Experiment Station, Vicksburg, MS.

Mukai A.Y., J.J. Westerink, R.A. Luettich Jr., and D. Mark, 2002, "Eastcoast 2001: a tidal constituent database for the western North Atlantic, Gulf of Mexico and Caribbean Sea", US Army Engineer Research and Development Center, Coastal and Hydraulics Laboratory, Technical Report, ERDC/CHL TR-02-24, September 2002, 201p.

OCTI/Oceanweather, 2002. Wind Field Development for theFire Island to Montauk Point Reformulation Study.

Partheniades, E. (1965). "Erosion and deposition of cohesive soils," J. Hydraulic Eng., 91(1), 105-139.

Powell, 2003.Reduced drag coefficient for high wind speeds in tropical cyclones. Nature, 422, 279-283.

Powell, M.D. and PG. Black, 1989: The relationship of hurricane reconnaissance flightlevel wind measured by NOAA's oceanic platforms. 6th National Conference on Wind Engineering.

Ris, R.C., (1997). Spectral Modelling of Wind Waves in Coastal Areas. Ph.D. Dissertation Delft University of Technology), also Communications on Hydraulic and Geotechnical Engineering, report No. 97-4, Delft, the Netherlands

Sallenger, A. H., Krabill, W., Swift, R., and J. Brock, 2001. Quantifying hurricane-induced coastal changes using topographic lidar, *Proceedings, Coastal Dynamics 2001*, American Society of Civil Engineers, Lund, Sweden (1007-1016).

Scheffner, N. W., Clausner, J. E., Militello, A.,Borgman, L. E., Edge, B. L., and Grace, P. J. 1999. "Use and Application of the Empirical Simulation Technique: User's Guide," Technical Report CHL-99-21, Engineer Research and Development Center, Corps of Engineers, Vicksburg, MS.

Scheffner, N. W. and R. A. Wise, 2001. Fire Island to Montauk Point Reformulation Storm Surge Study, Draft Report, USACE, Engineer Research and Development Center.

Swail, V.R. and A.T. Cox, 1999. On the use of NCEP/NCAR reanalysis surface marine wind fields for a long term North Atlantic wave hindcast. J. Atmos. Ocean. Technology.

Thompson, E. F. and V. J. Cardone. Practical modeling of hurricane surface wind fields. ASCE J. of Waterway, Port, Coastal and Ocean Engineering. 122, 4, 195-205.

Topometrics, 1982. "Map series and reference data for historical mapping – hurricanes 1938, Carol, Donna and northeasters November 1950, March 1962," Maps and Reports Series, Contract DACW51-80-C-0011, US Army Corps of Engineers, New York District, New York, NY.

U.S. Army Corps of Engineers, 1947. "Beach Erosion Study at Long Island (South Shore), New York," Report of Chief of Engineers, U.S. Army and Beach Erosion Board.

U.S. Army Corps of Engineers, 1995. "Breach Contingency Plan, Fire Island Inlet to Montauk Point, Long Island, New York, Reformulation Study," U.S. Army Corps of Engineers, New York District.

U.S. Army Corps of Engineers, 1995. . "Breach Contingency Plan, Fire Island Inlet to Montauk Point, Long Island, New York, Reformulation Study," U.S. Army Corps of Engineers, New York District.

U.S. Army Corps of Engineers. 2002. Coastal Engineering Manual. Engineer Manual 1110-2-1100, U.S. Army Corps of Engineers, Washington, D.C. (in 6 volumes).

U.S. Army Corps of Engineers, 2005. Fire Island to Montauk Point Reformulation Study, Inlet Modification. Draft Report, U.S. Army Corps of Engineers, New York District.

Van Rijn, L.C., 1993. Principles of Sediment Transport in Rivers, Estuaries and Coastal Seas. Aqua Publications, Amsterdam.

van Kessel, T., Roelvink, J.A. (June 2002). Modelling of barrier island response to Storms.

Visser, P.J. (1998). Breach growth in sand dikes. Ph.D.-thesis Delft University of Technology, the Netherlands.

Wilby, F.B., G.R. Young, C.H. Cunningham, A.C. Lieber, Jr., R.K. Hale, T. Saville and M.P. O'brien, 1939. Inspection of Beaches in Path of the Hurricane of September 21, 1938. Shore and Beach 7:43-47.

Wise and Kraus, 1993. Simulation of Beach Fill Response to Multiple Storms, Ocean City, MD, Proc. Coastal Zone '93, ASCE, 133-147.

Wise, Smith, and Larson, 1996. SBEACH: Numerical Model for Simulating Storm-Induced Beach Change; Report 4, USACE.

Zelen and Severo, 1964. Probability functions, Handbook of mathematical functions, Abramowitz, M. and Stegun, I., eds., National Bureau of Standards Applied Mathematics Series 55, Government Printing Office, Washington, D.C., pp.925-995.

STORM SURGE MODELING AND STAGE-FREQUENCY TECHNICAL TEAM

Santiago Alfageme	Moffatt & Nichol
Lynn Bocamazo	New York District, Engineering Division
Leon Borgman	L. E. Borgman, Inc.
Rafael Canizares	Moffatt & Nichol
Vince Cardone	Oceanweather, Inc.
Bruce Ebersole	Coastal and Hydraulics Laboratory
Mark Gravens	Coastal and Hydraulics Laboratory
William Grosskopf	Offshore and Coastal Technologies, Inc.
Jennifer Irish	New York District, Engineering Division
Bobby Khonder	Moffatt & Nichol
David Mark	Coastal and Hydraulics Laboratory
Adele Militello	Coastal Analysis LLC
Donald Resio	Coastal and Hydraulics Laboratory
Edward Thompson	Coastal and Hydraulics Laboratory
Brian Williams	New York District, Engineering Division

APPENDIX

This appendix includes draft stage-frequency relationships for extratropical-alone, tropical-alone, and combined storms at all ocean and bay stations.